Los Alamos
NATIONAL LABORATORY
EST. 1943

Environmental Programs
P.O. Box 1663, MS J591
Los Alamos, New Mexico 87545
(505) 606-2337/FAX (505) 665-1812

National Nuclear Security Administration
Los Alamos Site Office, MS A316
Environmental Restoration Program
Los Alamos, New Mexico 87544
(505) 667-4255/FAX (505) 667-5948

Date: September 14, 2007
Refer To: EP2007-0542

James P. Bearzi, Bureau Chief
Hazardous Waste Bureau
New Mexico Environment Department
2905 Rodeo Park Drive East, Building 1
Santa Fe, NM 87505-6303

Subject: Submittal of the Fate and Transport Modeling Report for Chromium Contamination from Sandia Canyon

Dear Mr. Bearzi:

Enclosed please find two hard copies with electronic files of the "Fate and Transport Modeling Report for Chromium Contamination Originating from Sandia Canyon." The report is being submitted pursuant to a requirement of the New Mexico Environment Department's (NMED's) March 5, 2007, approval with direction of the Sandia Canyon and Cañada del Buey investigation work plan addendum. The addendum was resubmitted on April 6, 2007, and included changes made following from NMED's approval with direction.

This report advances the Los Alamos National Laboratory's current conceptual understanding of the fate and transport of chromium (and related) contaminants from the suspected source in upper Sandia Canyon to the regional groundwater. This model along with other information will guide the next phase of the Sandia Canyon (chromium) investigation to further understand the nature and extent of contamination and chromium behavior and to better inform future decisions. Recommendations for the next investigation phase are included in this report.

If you have any questions, please contact Danny Katzman at (505) 667-6333 (katzman@lanl.gov) or Mat Johansen at (505) 665-5046 (mjohansen@doeal.gov).

Sincerely,

Susan G. Stiger, Associate Director
Environmental Programs
Los Alamos National Laboratory

Sincerely,

David R. Gregory, Project Director
Environmental Operations
Los Alamos Site Office

SGS/DRG/TBA/DK:sm

Enclosures: 1) Two hard copies with electronic files - Fate and Transport Modeling Report for Chromium Contamination from Sandia Canyon (EP2007-0542)

Cy: (w/enc.)
Neil Weber, San Ildefonso Pueblo
Mat Johansen, DOE-LASO, MS A316
Danny Katzman, EP-LWSP, MS M992 (plus 20 copies)
EP-LWSP File, MS M992
RPF, MS M707 (with two CDs)
Public Reading Room, MS M992

Cy: (Letter and CD only)
Laurie King, EPA Region 6, Dallas, TX
Steve Yanicak, NMED-OB, White Rock, NM
Peggy Reneau, EP-ERSS, MS M992

Cy: (w/o enc.)
Tom Skibitski, NMED-OB, Santa Fe, NM
Bonita Eichorst, DOE-LASO (date-stamped letter emailed)
Susan G. Stiger, ADEP, MS M992
Carolyn A. Mangeng, ADEP, MS M992
Alison M. Dorries, ERSS-DO, MS M992
Tina Behr-Andres, EP-LWSP, MS M992
IRM-RMMSO, MS A150

LA-UR-07-6018
September 2007
EP2007-0542

Fate and Transport Modeling Report for Chromium Contamination from Sandia Canyon

Los Alamos
NATIONAL LABORATORY
EST.1943

Prepared by the Environmental Programs Directorate

LA-UR-07-6018
EP2007-0542

Fate and Transport Modeling Report for Chromium Contamination from Sandia Canyon

September 2007

Responsible project leader:

Responsible project leader:

Printed Name	Signature	Title	Organization	Date
Danny Katzman		Project Leader	Environmental Programs	9.10.07

Responsible LANS representative:

Printed Name	Signature	Title	Organization	Date
Susan G. Stiger		Associate Director	Environmental Programs	9/14/07

Responsible DOE representative:

Printed Name	Signature	Title	Organization	Date
David R. Gregory		Project Director	DOE-LASO	9-14-07

EXECUTIVE SUMMARY

This fate and transport report presents the results of investigations implemented as part of the "Addendum to the Sandia Canyon and Cañada del Buey Work Plan" (LANL 2007, 095454). The addendum was submitted to New Mexico Environment Department (NMED) on April 6, 2007. This report is part of an ongoing investigation that addresses the chromium (Cr) and other contaminants detected in surface water and groundwater beneath Sandia and Mortandad Canyons. This report is the latest in a series of Cr-investigation related documents prepared by Los Alamos National Laboratory (LANL or the Laboratory) to meet the requirements of the March 1, 2005, Compliance Order on Consent between the U.S. Department of Energy (DOE), the Regents of the University of California, and NMED. Initial investigations of Cr contamination were presented in the "Interim Measures Investigation Report for Chromium Contamination in Groundwater" (LANL 2006, 094431). The "Addendum to the Sandia Canyon and Cañada del Buey Work Plan" (LANL 2007, 095454) was prepared to address key uncertainties in the Cr mass balance and its fate and transport based on the interim measures report.

This report is one of three reports that are being submitted concurrently by the Laboratory to NMED. One of the reports addresses the sediment contamination in Sandia Canyon, "Summary of Sandia Canyon Phase 1 Sediment Investigations" (LANL 2007, 098127). The other report addresses the drilling and completion of two regional wells, "Completion Report for Regional Aquifer Wells R-35a and R-35b" (LANL 2007, 098129). Submittal of these three reports before the final investigation report for Sandia Canyon is submitted in December 2008 is required by NMED and ensures the protection of drinking water while the remainder of the Sandia Canyon investigation is implemented.

The investigations reported herein were conducted in 2007 to further characterize the nature, extent, and concentrations of Cr in surface water, alluvial groundwater, perched intermediate groundwater, and regional groundwater in the Sandia and Mortandad Watersheds. These data are used to evaluate spatial and temporal trends in Cr contamination, including variations in contaminant concentration and stable isotopes of Cr along the flow path at increasing distances from the source areas and as a function of time since cessation of Cr releases.

The ongoing review of archival records and interviews continue to highlight the cooling towers associated with the Technical Area (TA) 03 power plant (TA-03-22) at the head of Sandia Canyon as the main source of Cr contamination at the Laboratory. Potassium dichromate usage for the TA-03 power plant from circa 1956 to 1972 resulted in an estimated total release of approximately 31,000 to 72,000 kg of Cr(VI) into the south fork of upper Sandia Canyon. Effluent averaging from 7 to 18 mg/L Cr(VI) was discharged to Sandia Canyon at a rate of 379 to 1090 m^3/d (100,000 to 288,000 gal./d). Other sources of Cr(VI) include the cooling tower at the Omega West reactor (TA-02) in Los Alamos Canyon and release sites at TA-3, TA-35, and TA-48 in the Mortandad Watershed. The total Cr mass released and effluent discharge volumes in Sandia Canyon were more than an order of magnitude greater than those released in Los Alamos and Mortandad Canyons.

Ongoing monitoring of surface and groundwater was expanded to include analyses for stable isotopes of Cr (δ^{53}Cr) to determine if isotopic variations in δ^{53}Cr occur along surface water and groundwater flow paths within the Sandia and Mortandad Watersheds. The purpose of this special sampling is to test a hypothesis of possible isotope fractionation of Cr as Cr(VI) reduces to Cr(III) along surface-water and groundwater flow paths. The majority of water samples have δ^{53}Cr values indicative of approximately 18% to 26% reduction of Cr(VI) to Cr(III). Chromium(VI) reduction is not large at R-11 and R-28, based on low δ^{53}Cr values near or at unity. More than 50% reduction of Cr(VI) has occurred along the groundwater flow path(s) to perched intermediate groundwater (well MCOI-5) within the Cerros del Rio basalt beneath Mortandad Canyon. Currently, there are no data for Cr(VI) reduction in the unsaturated zone of Sandia Canyon, but a similar rate of Cr reduction is expected and results are pending.

An expanded water-balance investigation included the installation of two temporary gaging stations in upper Sandia Canyon to better define surface-flow infiltration losses to bedrock units. New data from permanent and temporary stream gages indicate that a relatively small amount of surface water infiltrates deeply into bedrock units beneath the Sandia Canyon wetland. A small volume of surface water is first lost from the wetland via infiltration into shallow bedrock, but then apparently migrates laterally, reemerging into the stream channel to the east of the wetland. Most of the surface-water loss occurs in areas farther downcanyon where porous nonwelded Bandelier Tuff underlies the canyon bottom. The new water-balance data were used in conjunction with data reported in the "Interim Measures Investigation Report for Chromium Contamination in Groundwater" (LANL 2006, 094431) to constrain infiltration locations and fluxes in numerical models of contaminant transport through the vadose zone.

An evaluation of monitoring-well network efficiency was conducted to assess whether existing and planned monitoring wells are adequately located to detect potential migration of Cr from the area that is known to be contaminated in the vicinity of monitoring wells R-11 and R-28. The assessment treated the Cr contamination in the area around R-11 and R-28 as a source with concentrations similar to those at R-28. The simulations indicate that the monitoring-well network is more than 95% effective in detecting potential Cr migration before reaching downgradient supply wells or the Laboratory boundary.

The fate and transport evaluation of Cr and molybdenum (Mo) detected in surface and groundwater in the Sandia and Mortandad Watersheds was performed using a probabilistic groundwater modeling approach, incorporating both conceptual model and parameter uncertainty. The conceptual model was developed with input from the Northern New Mexico Citizen's Advisory Board (NNMAB) and NMED and is captured in the conceptual model "matrix" presented in Appendix D. This includes descriptions of pathways, assumptions about features and processes that affect the fate and transport of contaminants, numerical model assumptions used in representing pathways and conceptual models, and parameters and their probability distributions. The conceptual model elements were then used to guide the construction of vadose zone and regional aquifer models of contaminant transport. The weighting of simulation results based on their agreement with observed contaminant concentrations further tied the modeling results to existing measurements. The numerical models provide results that are consistent with key aspects of the conceptual model of Cr transport through the vadose zone and regional aquifer. However, it is apparent that additional refinement to both conceptual and numerical models is needed to improve the convergence of the probabilistic assessment of nature and extent of contaminants with observations from monitoring wells.

CONTENTS

Figures

Tables

Appendixes

Acronyms and Abbreviations

AOC	area of concern
CME	corrective measures evaluation
COPC	chemical of potential concern
Cr	chromium
DOE	Department of Energy [U.S.]
DOC	dissolved organic carbon
ET	exposure time
FEHM	Finite Element Heat and Mass [transfer code]
HFO	hydrous ferric oxide
ICP-MS	inductively coupled plasma-mass spectroscopy
IFWGMP	Interim Facility-Wide Groundwater Monitoring Plan
LANL	Los Alamos National Laboratory [Laboratory is preferred to LANL]
Mo	molybdenum
MCL	maximum contaminant level [EPA]
NIST	National Institute of Standards and Technology
NMED	New Mexico Environment Department [before 1991: New Mexico Environmental Improvement (NMEID) Division]
NNMCAB	Northern New Mexico Citizens' Advisory Board
NPDES	National Pollutant Discharge Elimination System
PAH	polycyclic aromatic hydrocarbon [interchangeable with polynuclear aromatic hydrocarbon]
PCB	polychlorinated biphenyl
RPF	Records Processing Facility
SME	subject matter expert
SOM	solid organic material
SWMU	solid waste management unit
SWWS	Sanitary Wastewater System
TA	technical area
TD	total depth

1.0 INTRODUCTION

This fate and transport report presents the results of investigations implemented as part of the "Addendum to the Sandia Canyon and Cañada del Buey Work Plan" (LANL 2007, 095454). The addendum was submitted to New Mexico Environment Department (NMED) on April 6, 2007. The report is part of an ongoing investigation that addresses the chromium (Cr) and other contaminants detected in surface water and groundwater beneath Sandia and Mortandad Canyons (Figure 1.0-1). This report is the latest in a series of documents prepared by Los Alamos National Laboratory (LANL or the Laboratory) to meet the requirements of the March 1, 2005, Compliance Order on Consent (hereafter, Consent Order) between the U.S. Department of Energy (DOE), the Regents of the University of California, and the NMED. Initial work on Cr contamination was begun in response to a letter from NMED dated December 29, 2005 (NMED 2005, 091683) that required the Laboratory to submit an interim measures work plan pursuant to Section VII.B.2 of the Consent Order. The Laboratory submitted the "Interim Measures Work Plan for Chromium Contamination in Groundwater" (LANL 2006, 091987) on March 31, 2006, and NMED approved the work plan with modifications on May 5, 2006 (NMED 2006, 092543). Results of investigations conducted under the interim measures work plan were presented in the "Interim Measures Investigation Report for Chromium Contamination in Groundwater" (LANL 2006, 094431). The "Addendum to the Sandia Canyon and Cañada del Buey Work Plan" (LANL 2007, 095454) was prepared to address key uncertainties in the Cr mass balance and fate and transport based on the interim measures investigation report. NMED's approval of the "Addendum to the Sandia Canyon and Cañada del Buey Work Plan" (LANL 2007, 095454) with modifications required the installation of a regional groundwater well (R-35). A work plan for R-35 was submitted to NMED on July 3, 2006 (LANL 2006, 093388), and it was approved by NMED on July 24, 2006 (NMED 2006, 093530).

This report is one of three key reports that are being submitted concurrently by LANL to NMED before the final investigation report for Sandia Canyon is submitted in December 2008. The other two reports address the sediment contamination in Sandia Canyon (LANL 2007, 098127) and drilling and completion of regional well R-35a and R-35b (LANL 2007, 098129).

The purpose of this report is to present the results of a numerical model developed to inform and enhance the understanding of the fate and transport of Cr and related contaminants from their source at the TA-03 power-plant outfall (Consolidated Unit 03-012(b)-00) to the regional groundwater where contaminants have been detected at several existing monitoring wells.

The primary objective of this fate and transport modeling work is to provide a probabilistic depiction of the nature and extent of Cr contamination along the flow path from the source to the regional groundwater. Development of the fate and transport model helps refine the conceptual model of how various physical, hydrological, and geochemical elements lead to the present-day distribution of Cr and its future fate and transport. This model is used in conjunction with other data presented in this report to guide the next phase of the investigation as presented in section 6. The proposed investigations are necessary to support subsequent evaluation of potential corrective measures.

The report presents results for other elements of the work plan addendum, including an update of the archival research activity, the water-balance investigation, ongoing surface-water and groundwater sampling, and the Phase 1 sediment investigation that is presented as a separate report (LANL 2007, 098127). The infiltration investigation expands on the investigation conducted as part of the "Interim Measures Work Plan for Chromium Contamination in Groundwater" (LANL 2006, 091987) to better constrain the areas and amounts of surface water and alluvial groundwater loss in the narrow bedrock-dominated portion of Sandia Canyon (Appendix B). Data from the archival investigation further constrain the mass of Cr and volume of effluent released to Sandia Canyon (Appendix A). The ongoing monitoring

of surface and groundwater was expanded to include analyses for stable isotopes of Cr (δ^{53}Cr) to determine if isotopic variations in δ^{53}Cr occur along surface water and groundwater flow paths within the Sandia and Mortandad Watersheds; such variations may be used to evaluate reduction of Cr(VI) to Cr(III) along transport pathways (Appendix C).

2.0 METHODOLOGY

The fate and transport evaluation of Cr and molybdenum (Mo) detected in surface and groundwater beneath Sandia and Mortandad Canyons was performed using a probabilistic groundwater modeling approach, incorporating both conceptual model and parameter uncertainty.

The source term was assessed through a combination of assembling existing records and seeking new source history through archival research and personal interviews with subject matter experts (SMEs) who are knowledgeable about the cooling tower operations at the power plant (Appendix A).

The conceptual model (section 3) was developed in an inclusive process that brought together the theoretical and conceptual knowledge of all involved Laboratory scientists, input from the Northern New Mexico Citizen's Advisory Board (NNMCAB), and NMED. This input was captured in the conceptual model "matrix" described in Appendix D and included on the CD included with this report. The conceptual model matrix in Appendix D includes descriptions of pathways, assumptions about features and processes that affect the fate and transport of contaminants, numerical model assumptions used in representing pathways and conceptual models, and parameters and their probability distributions.

The conceptual model was then used to guide the vadose zone and regional aquifer modeling of contaminant migration (section 4). This modeling was done by translating the elements of the conceptual model matrix into the numerical model setup and parameter distributions. The conceptual uncertainty is captured through a series of alternative equally probable numerical models, yielding a range of possible answers instead of a single deterministic result. The parameter uncertainty is represented through a series of parameter distributions for the input parameters of numerical models. A stratified form of Monte Carlo sampling, Latin Hypercube Sampling, was used to minimize the number of samples required to cover the full range of parameter uncertainty. The explicit simulation of multiple conceptual models captures the effects of conceptual model uncertainty. The calibration and weighting of results based on their agreement with contaminant measurements further tied the modeling results to existing measurements.

The result of this approach is a probabilistic depiction of spatial distribution of Cr contamination (nature and extent). These probabilistic results form the basis of a quantitative assessment of the value of future characterization. The value of additional data is assessed in light of potential remedial solutions. Future characterization activities may include new wells, vadose zone or surface water sampling, sediment analyses, etc. The probabilistic results also give insight into potential remedies to consider in the later corrective measures evaluation (CME) phase of the program. Finally, an additional product of this approach is the quantitative information necessary to establish optimal locations for groundwater monitoring needed to ensure protection of current production wells and the detection of contaminant migration prior to crossing the Laboratory boundary.

3.0 SUMMARY OF PHYSICAL SYSTEM CONCEPTUAL MODEL

This section summarizes the main elements of the physical system conceptual model that was first presented in the "Interim Measures Investigation Report for Chromium Contamination in Groundwater" (LANL 2006, 094431). In this report, elements of that conceptual model have been revised or expanded based on new data and information collected for this investigation. The primary focus of this section is to summarize the source(s) of Cr and other key contaminants found in the regional groundwater at R-11 and R-28. A discussion of the physical, chemical, and hydrologic processes that govern the fate and transport of Cr and associated contaminants, including Mo, nitrate, sulfate, chloride, and phosphate is also presented in this section. Figure 3.0-1 illustrates key aspects of the physical system conceptual model. The conceptual model forms the basis for identifying pathways, defining model assumptions, and bounding parameters in the Conceptual Model Matrix (Appendix D).

3.1 Source Regions

A review of archival records and interviews with operators identified the cooling towers associated with the Technical Area (TA) 03 power plant (TA-3-22) at the head of Sandia Canyon as the main source of Cr contamination at the Laboratory (Figures 1.0-1 and 3.0-1). Chromium usage for the TA-03 power plant appears to have averaged 16.3 kg/d (35.9 lb/d) from circa 1956 to 1972, resulting in an estimated total release of approximately 31,000 to 72,000 kg of Cr(VI) into the south fork of upper Sandia Canyon (Appendix A). Effluent averaging from 7 to 18 mg/L Cr(VI) was discharged to Sandia Canyon at a rate of 379 to 1090 m^3/d (100,000 to 288,000 gal./d).

Other sources of Cr(VI) include the cooling tower at the Omega West Reactor (TA-02) in Los Alamos Canyon and solid waste management units (SWMUs) and areas of concern (AOCs) at TA-03, TA-35, and TA-48 in the Mortandad Watershed (Figure 1.0-1). In Los Alamos Canyon, the cooling tower at the Omega West reactor released an estimated 2000 to 9100 kg (5000 to 20,000 lb) of Cr(VI) from 1957 to 1973, including stack emissions and blowdown. Effluent discharges from the Omega West reactor cooling tower were approximately 12,000 to 57,000 L/d (3100 to 15,000 gal./d), 5 days a week. TA-03, TA-35, and TA-48 sites in the Mortandad Watershed included small cooling towers and electroplating facilities. These sites are thought to be relatively small sources of Cr releases compared to sites in Sandia and Los Alamos Canyons, both in terms of total Cr mass released and associated discharge volumes that might have served as a hydrologic driver. Sediment investigations indicate that TA-48 at the head of the Effluent Canyon tributary was the primary source of Cr contamination in the Mortandad Watershed, and the downcanyon extent of residual Cr contamination in sediment is limited spatially (LANL 2006, 094161).

The total Cr mass released and effluent discharge volumes in Sandia Canyon were more than an order of magnitude greater than those released in Los Alamos and Mortandad Canyons. Nonetheless, data from archival core show that Cr(III) occurs above background concentrations in the upper vadose zone, indicating vertical migration of Cr in all three canyons (LANL 2006, 094431). Elevated concentrations of dissolved Cr(VI) in perched intermediate groundwater beneath Mortandad Canyon provide additional evidence that this metal is being transported within the vadose zone at that site. Thus, while Sandia Canyon is the hypothesized primary source of Cr(VI) observed at R-11 and R-28, contributions of Cr from Los Alamos and Mortandad Canyons' sources cannot be ruled out for these or other wells.

The remaining discussion in this section focuses on the fate and transport of contaminants released from the TA-03 power plant at the head of Sandia Canyon (Figure 1.0-1). Many elements of the conceptual model discussed below also apply to the fate and transport of Cr in Los Alamos and Mortandad Canyons.

3.2 Surface Water and Sediment Transport

Initially, dissolved Cr(VI) was released from the TA-03 power plant. Some Cr(VI) was adsorbed onto soils and sediments near the outfall, but most was transported by surface flow down the south fork drainage at the head of Sandia Canyon to the wetland located just below the confluence of the south and north forks (Figure 1.0-1). At the time of the initial releases, the wetland was not at its current size, but it is known to have been substantial in size (LANL 1999, 064617). At all stages of its evolution, the wetland contained abundant solid organic matter (SOM) that served as both a chemical reductant and adsorbent, and as a result, Cr(VI) was reduced to its trivalent state. The reduced Cr precipitated as $Cr(OH)_3$ and/or was adsorbed onto SOM, hydrous ferric oxide (HFO), and clay minerals as Cr(III). Evidence for this process is based on elevated concentrations of Cr(III) in sediments found within the wetland and low concentrations of dissolved Cr(VI) in present-day alluvial groundwater within the wetland. Additionally, present-day surface water (filtered samples) entering the wetland contains higher concentrations of Cr(VI) than does surface water exiting the wetland (filtered samples, see Figure 3.0-1). Thus, the wetland is an effective geochemical sink that inhibits the migration of Cr, and a significant portion of the Cr released to the canyon likely remains within the sediments there. A companion report to this document, "Summary of Sandia Canyon Phase I Sediment Investigations" (LANL 2007, 098127) provides a mean estimate of 15,000 kg of Cr stored in sediments of the wetland, almost entirely (~99.8%) as Cr(III). This represents approximately 84% of the Cr stored in canyon-floor sediments and 21% to 49% of the total estimated Cr mass released to Sandia Canyon (Appendix A); however, large uncertainties are associated with these values. The source report provides for a discussion of uncertainties associated with the estimate of Cr inventory in sediments (LANL 2007, 098127).

It is apparent that not all Cr(VI) discharged from the power plant was immobilized within the wetland. Stream concentrations of 2.4 to 7.3 mg/L (as chromate) were reported below the wetland from 1969 to 1971 (Purtymun 1975, 011787), indicating that significant amounts of Cr were transported downcanyon by surface flow, probably both as a dissolved phase and adsorbed onto suspended material. Cr(VI) has also been detected in sediment samples downcanyon as far as reach S-5E, immediately west of New Mexico State Road 4, although at low concentrations (Figures 1.0-1 and 3.0-1) (LANL 2007, 098127).

Redistribution of Cr by surface water, sediment transport, and groundwater is an ongoing process within the Sandia Watershed. Once adsorbed onto SOM and sediment particles in the wetland, Cr-bearing sediments are transported downcanyon by floods that erode headcuts along the channel, scour the streambed, and mobilize the bed sediment. These floods also erode banks in historical floodplains where much of the Cr in sediment deposits is stored in downcanyon reaches (Figure 3.0-1). Data reported in the "Summary of Sandia Canyon Phase I Sediment Investigations" indicate Cr concentrations of up to 22.5 mg/kg (or approximately twice background) occur as far east as reach S-5E at State Road 4. Reoxidation of Cr(III) to Cr(VI) associated with suspended material and stream sediments could be significant in the absence of chemical reductants as surface water moves from the organic-rich environment of the wetland to less reducing conditions in downcanyon reaches. Reoxidation may account for the observed increase of dissolved Cr concentrations in surface water at the eastern terminus of surface water flow relative to surface water exiting the wetland near gaging station E123 (Figures 1.0-1 and 3.0-1).

The transport of contaminants by surface water is facilitated where thin alluvium overlies relatively impermeable bedrock in the stream channel, limiting the amount of infiltration along the stream channel and resulting in greater movement of surface water downcanyon (Figure 3.0-1). The downcanyon extent of surface water flow varies with discharge from the TA-03 power plant, treated sewage effluent discharge rates, runoff from storm events and snowmelt, and previous moisture conditions along the channel. The effects of these variables were highlighted in changing infiltration patterns deduced from gaging data collected in July and August of 2007 (Appendix B).

Based on surface water data from 2007, an estimated 3 to 46 acre-ft/yr, consisting primarily of effluent, infiltrates deeply into bedrock units beneath the wetland (Figure 3.0-1 and Appendix B). An additional volume of surface water is first lost from the wetland via infiltration into shallow bedrock but then apparently migrates laterally, reemerging into the stream channel east of the wetland and west of gaging station D123.6. The canyon floor between gages E123 and D123.6 is underlain by relatively impermeable Bandelier Tuff, unit Qbt 2 (Figure 3.0-1). Uppermost Qbt 2 is the most compacted and welded part of the unit, possibly inhibiting infiltration by porous flow into the rock matrix. However, the brittle nature of upper Qbt 2 probably results in a greater density of fractures from both tectonism and cooling contraction, compared to underlying less welded tuffs. These fractures may facilitate shallow infiltration, particularly where splays of the Rendija Canyon fault zone cross the eastern end of the wetland area, and also lateral flow. Nonetheless, these faults and fractures are probably, at best, secondary pathways for deep infiltration because the volume of potential deep infiltration beneath the wetland is much smaller than that infiltrating east of D123.6 where nonwelded Bandelier Tuff underlies the canyon bottom. Possibly the fractures become filled by secondary minerals with depth, or they die out in less brittle tuffs below. Hydrographs for upper Sandia Canyon indicate that much of the water infiltrating the wetland is rapidly returned to the stream channel downcanyon, suggesting a role for fractures as lateral pathways rather than vertical pathways (Appendix B).

Much of the remaining effluent flow infiltrates bedrock units between gaging stations D123.6 and D123.8. This part of the canyon is steep and has a narrow canyon bottom where the stream incises through increasingly less welded tuffs in the lower part of Qbt 2 and then through the nonwelded units Qbt 1v and Qbt 1g (Figure 3.0-1). During July 2007, when effluent releases were smaller than in 2006 and before summer runoff saturated the alluvium, flow only made it past D123.8 for several hours per day, with most of the effluent infiltrating into bedrock farther upcanyon. The remaining effluent is lost over a short canyon segment (300 to 700 m [900 to 2300 ft]) below gaging station D123.8 (Figure 3.0-1). This portion of the canyon is characterized by rapidly thickening alluvium as the canyon floor widens eastward, resulting in greater alluvial groundwater storage (Figure 3.0-1). Runoff from storm events and snowmelt sometimes causes ephemeral flow and episodic infiltration to occur through the remaining portion of Sandia Canyon on Laboratory property, and possibly as Far East as the Rio Grande, but these events are infrequent.

3.3 Vadose Zone Transport

The infiltration of water near the eastern limit of surface flow recharges alluvial groundwater that generally accumulates in the lower part of the alluvial deposits, most often perching on or within shallow bedrock units. This alluvial groundwater is a major pathway for additional downcanyon transport of soluble Cr and mobile constituents including nitrate, sulfate, Mo, and chloride. In Sandia Canyon, the thickest, most persistent perched alluvial groundwater occurs between alluvial wells SCA-2 and SCA-5 (Figure 3.0-1). The region between these two alluvial wells is identified by water-level measurements as contributing to alluvial groundwater loss to bedrock units beneath the canyon floor. This interpretation is supported by downward pressure gradients and high seepage velocities measured at nested piezometers. High infiltration rates in this area are also supported by core measurements at SCC-2 through SCC-4 that show the Otowi Member is characterized by relatively high moisture contents and that moisture contents are relatively higher in the western-most coreholes (LANL 2006, 094431). The western boundary of the main zone of bedrock infiltration is uncertain, but it possibly extends to the area between gaging stations D123.6 and D123.8 (Figure 3.0-1).

Infiltration of alluvial groundwater to bedrock units results in the vertical transport of mobile contaminants into suballuvium bedrock units. Movement of moisture and contaminants probably occurs as gravity and moisture-gradient-driven porous flow. Transport of contaminants to these deeper zones is generally limited to soluble constituents such as Cr(VI), Mo(VI), nitrate, chloride, and sulfate. The results reported in

the “Interim Measures Investigation Report for Chromium Contamination in Groundwater” (LANL 2006, 094431) suggest that most of the dissolved Cr beneath the middle reaches of the canyon has been flushed out of the upper 122 m (400 ft) of the vadose zone by Cr-free water following cessation of the releases. Residual concentrations of Cr are observed in pore water and adsorbed onto mineral surfaces within the unsaturated zone, but the concentrations are generally low (<0.050 mg/L) and the occurrence of elevated concentrations (>0.1 mg/L) is sporadic. Molybdenum and phosphate are also observed in pore water and adsorbed onto mineral surfaces within the unsaturated zone (LANL 2006, 094431).

A thin zone of perched intermediate groundwater occurs within the Puye Formation atop the Cerros del Rio basalt between SCC-1 and SCC-4 (Figure 3.0-1). This perched system appears to thicken westwards, and it probably is recharged by percolation of moisture from the overlying rocks. Contaminant concentrations in screening samples for this perched zone are slightly elevated with respect to background. These data, combined with the generally low concentrations of contaminants in the overlying pore waters, suggest that years of recharge and high hydraulic fluxes have flushed most soluble contaminants out of the upper vadose zone and into deeper sections of the vadose zone. Most likely, moisture carrying these dissolved contaminants percolated into the lower vadose zone with some portion entering the regional groundwater system, which lies approximately 253 m (830 ft) below the canyon floor at R-11 (Figure 3.0-1).

Dipping strata may divert moisture along geologic contacts or internal bedding features as water travels through the vadose zone, possibly affecting the distribution of contaminants in the vadose zone and the location of the entry point of contaminants into the regional aquifer (Appendix H). The basal contact of the Guaje Pumice Bed dips south to southwest and that of the Cerros del Rio basalt dips south to south-southeast beneath the zone of maximum infiltration. The upper contact of the Cerros del Rio basalt dips primarily to the west and southwest. Near the water table, Miocene sedimentary rocks dip primarily to the south and southwest. Although there are large uncertainties, these relationships suggest that vadose zone pathways might include southerly and southwesterly to moderately southeasterly components. The effects of medium anisotropy might also be influenced by transients in recharge becoming more pronounced during high infiltration events.

3.4 Transport in the Regional Aquifer

Dissolved-phase contaminants including Cr(VI), nitrate, perchlorate, sulfate, chloride, and tritium, are detected only near the regional water table beneath Mortandad and Sandia Canyons. Dissolved concentrations of Cr, nitrate, perchlorate, and tritium have increased over time at R-11. The presence of nitrate, tritium, and perchlorate strongly suggests that mixing with Mortandad Canyon groundwater is taking place at R-11. Concentrations of Cr, tritium, and perchlorate are also increasing at R-15, and this well is most likely influenced by TA-50 discharges, based on chemical and isotope signatures. Differences in nitrogen isotopic ratios for some wells (e.g., R-28 vs. R-11) indicate that contamination in regional groundwater beneath Sandia Canyon includes contributions from mixed-source areas including Mortandad Canyon. The major ion chemistry of groundwater at R-28 is very similar to that of well MCOI-6 completed within the Cerros del Rio basalt upgradient of R-28, suggesting that perched intermediate groundwater has recharged the regional aquifer in the vicinity of R-28. Tritium concentrations (180 pCi/L) measured at R-28 provide additional evidence for Mortandad Canyon-derived contaminants at the well. Preliminary screening data from newly installed wells R-35a and R-35b (Figure 1.0-1) indicate that Cr is at or below background concentrations in the vicinity of water supply well PM-3 (LANL 2007, 098129). The first groundwater monitoring samples for these two wells were collected on August 29 and 30, 2007, and analytical results will be available through the Laboratory’s periodic monitoring reports.

Analytical results for stable isotopes of Cr (δ^{53}Cr) show that various fractions of Cr(VI) have been reduced to Cr(III) in surface water and groundwater within Sandia and Mortandad Canyons. At well MCOI-5, δ^{53}Cr ratios for Cr(VI) indicate that up to 50% of Cr(VI) has been reduced to Cr(III), most likely within the Cerros del Rio basalt. Solid organic matter in wetlands and ferrous iron within the Cerros del Rio basalt are thought to be the two most important reductants for Cr(VI). The wetlands and Cerros del Rio basalt contribute to natural attenuation of Cr to a greater extent than does the regional aquifer at R-11 and R-28. Variations in δ^{53}Cr ratios of Cr(VI) in perched intermediate groundwater and the regional aquifer are controlled by groundwater mixing, groundwater flow paths, groundwater residence times, kinetics of Cr(VI) reduction, and the reductive capacity of aquifer material.

The regional aquifer is a complex, heterogeneous system that includes confined and unconfined zones. The degree of hydraulic communication between these zones is thought to be spatially variable. The shallow portion of the regional aquifer (near the water table) is predominantly under phreatic (unconfined) conditions and has limited thickness (approximately 30 to 50 m [98 to 164 ft]). Groundwater flow and contaminant transport directions in this zone generally follow the gradient of the regional water table; the flow is generally east/southeastward. The direction and gradient of flow at the regional water table are predominantly controlled by areas of recharge (e.g., the Sierra de los Valles and variably within some Pajarito Plateau canyons) and discharge (White Rock Canyon springs and the Rio Grande).

The deep portion of the regional aquifer is predominantly under confined conditions, and it is stressed by Pajarito Plateau water-supply pumping. The pumping likely has a small impact on the flow directions in the phreatic zone because of poor hydraulic communication (see Appendix E). Capture of contaminants by supply well PM-3, which is screened approximately 56 to 536 m (183 to 1759 ft) below the regional water table, seems unlikely because of this poor vertical hydraulic communication. This interpretation is supported by the contrasting water-level responses observed in R-35a and R-35b during pumping of PM-3 (LANL 2007, 098129). The water level in R-35a, which has a well screen opposite the upper part of louvers in PM-3, responds rapidly to pumping at PM-3 (as well as at O-4), whereas R-35b, which is screened near the water table, shows either no or a very small response. Therefore, the pumping at PM-3 does not seem to affect the hydraulic gradients in the phreatic zone of the regional aquifer intercepted by R-28, R-11, and R-35b. As a result, it can be expected that contaminant migration follows the water-table gradients rather than diverting toward the pumping well (PM-3).

Poor hydraulic communication does not preclude the possibility that some contaminant migration may occur between the shallow and deep zones. Between the two zones, the hydraulic gradient has a downward vertical component because of water-supply pumping, creating the possibility that downward contaminant flow may occur along “hydraulic windows.”

In the regional aquifer, the advective flow paths of contaminant migration might not be perpendicular to the equipotential water-table lines. Deviations from the flownet conformity rule might occur because of the anisotropy/heterogeneity of aquifer materials. Flow- and head-gradient vectors do not coincide in an anisotropic medium when the flow gradient is not coincident with the principal directions of the permeability tensor (Freeze and Cherry 1979, 088742, Chapter 5). As a result, the south-southwest dips of aquifer rock units in this area may influence the flow vectors. Large-scale permeability along the sedimentary layering is expected to be 1 to 4 orders of magnitude higher than large-scale permeability perpendicular to the layering.

4.0 MODEL IMPLEMENTATION

Flow and transport simulations are used to predict the migration of Cr and Mo from their source at the outfall through the unsaturated zone and through the regional aquifer. The simulations consider transport in surface water, alluvial groundwater, the unsaturated zone and the regional aquifer. The effects of geochemical interactions of contaminants with wetland materials and with rocks along the flow paths are also included. Monte Carlo simulations that represent uncertainty in input parameters are run to determine the range of likely transport behavior. The implementation of assumptions, boundary conditions and parameter distributions made in the models honor the conceptual model described above and in the more comprehensive conceptual model matrix described in Appendix D.

The following items describe the source and pathway components included in the modeling study. Specifically, the simulations calculate the transport of Cr and Mo through the unsaturated zone (excluding the shallow alluvial system) and then through the regional aquifer. The unsaturated zone and regional models are separate in this study. The sources of water and contaminants and subsequent distribution to the suballuvial unsaturated zone are calculated and applied as boundary conditions to the unsaturated-zone model. The simulations are run with the Finite Element Heat and Mass (FEHM) Transfer code (Zyvoloski et al. 1997, 070147). Complete descriptions of the models are included in Appendix E.

Water source: The effluent volumes released at National Pollutant Discharge Elimination System (NPDES) outfall 01A-001 into the head of Sandia Canyon are the assumed primary water sources to the canyon. These volumetric flow rates are bounded by discharge records (Appendix A) and include both cooling-tower blowdown and sanitary effluent that are released at the same outfall. The water is distributed down the canyon through lateral surface water and alluvial groundwater flow and assumed to infiltrate into the deeper unsaturated zone in a manner consistent with surface water balances for Sandia Canyon. Two alternative conceptual models of infiltration are included in the modeling study. The first is based on the surface water data collected in October 2006, and presented in the “Interim Measures Investigation Report for Chromium Contamination in Groundwater” (LANL 2006, 094431). The second is a continuation of the first field study and is presented in Appendix B. These two surface water balances yielded different distributions of assumed infiltration along the length of the canyon and are included as alternative conceptual models to determine the results on contaminant nature and extent. Volumetric flux to the unsaturated zone as a function of both location and time is calculated based on uncertain parameters describing time-varying effluent release to the canyon and the distribution of that flow along the length of the canyon. These spatially and temporally varying water fluxes are applied as boundary conditions to the unsaturated-zone model runs.

Contaminant source: This study considers the migration of both Cr and Mo from Sandia Canyon. The two chemicals were used at different times as cooling tower additives in the TA-03 power plant cooling towers, Cr from approximately June 1956 to April 1972 and Mo from 1993 to 2001 (LANL 2006, 094431). More Mo than Cr was detected in the upper unsaturated zone in the Sandia Canyon characterization core holes (SCC) drilled in 2006 because of its later release (LANL 2006, 094431); therefore, the Mo data are useful for model calibration. Chromium and Mo released from the TA-03 power plant cooling towers reacted with wetland sediments and SOM resulting in lower surface water concentrations than the original effluent concentrations. Because surface water is the source of unsaturated-zone water, reported surface water concentrations are used to define mass fluxes for Cr and Mo that are used as boundary conditions for the unsaturated-zone simulations.

Unsaturated zone model: The unsaturated zone is modeled using 18 one-dimensional vertical columns (grids) that span the length of the canyon from the wetland area to the location of core hole SCC-6 (Figure 4.0-1). The columns represent the strata that lie between the base of the alluvium (if present, otherwise from the ground surface) to the water table, except that one column represents the Rendija Canyon fault zone in SW1. In the simulations, the strata are assigned hydrologic properties that are represented by parameter distributions. Geochemical reactions affecting contaminant transport are accounted for through either reversible or irreversible adsorption. Irreversible sorption of Cr is expected to occur onto basalt (Appendix E).

The columns are linked to the four surface water segments described in the conceptual model and shown in Figure 3.0-1. In addition, each column has a surface area that represents the area over which infiltration is likely to occur. This area is determined either by the approximate channel width (in the upper three canyon segments) or by the approximate width of the perched-alluvial groundwater body that exists in SW4. Water and contaminant mass fluxes are applied as boundary conditions to these columns and the resultant unsaturated-zone flow and transport is calculated. The results of these simulations are time-dependent contaminant mass fluxes exiting the bottom of each of the 18 columns. These mass fluxes are applied as input boundary conditions to the regional model. Other important predictions are travel times to the regional aquifer and contaminant mass distributions in the different sections of the vadose zone.

Regional aquifer model: The regional aquifer is simulated using a two-dimensional numerical model that characterizes the groundwater flow and contaminant transport along the regional water-table. As discussed in Appendixes C and E, two major conceptual models describe regional hydrogeology. However, most of the recent information from drilling, such as water-level and geochemistry data for R-35 and R-17 (Kleinfelder 2006, 092493; LANL 2007, 098129) and groundwater stable-isotope analyses (Longmire et al. 2007, 096660), supports a conceptual model in which the primary migration paths are shallow and the focus is on the phreatic zone for contaminant migration. Therefore, the numerical model is implemented to account for this predominantly shallow migration. In this model, pumping at the water-supply wells on the Pajarito Plateau has a minor or negligible influence on contaminant flow directions. However, the model allows for contaminants to be captured at the water-supply wells by vertical flow from the shallow phreatic zone into deep, and otherwise confined, aquifer zones through hydraulic windows. Such hydraulic windows have not been observed in the field but are expected to occur, possibly where medium heterogeneity yields areas with higher relative vertical permeability. Water-table maps define the hydraulic gradients in the numerical model. The contaminant-transport simulations include the effects of dispersion, dilution, and adsorption.

A predominant portion of the simulated Cr transport near Sandia Canyon occurs in the Puye Formation. In this hydrostratigraphic unit, a high probability exists that highly permeable channels exist rather than discrete faults or fractures. Borehole geophysical logs (Formation Microimager) indicate that channeling in sediments of the saturated zone is pervasive and has a general southerly to southwest direction, and studies of volcanic-derived sediments comparable to the Puye Formation (e.g., Lin and Oguchi 2004, 098050) provide some constraints on likely channel density. The potential for preferential flow along such heterogeneity-based features are incorporated into the model using geostatistical techniques.

The main predictions made by these simulations are spatial contaminant distributions in the regional aquifer (including predictions of uncertainties, breakthrough curves at the wells, and probability of exceeding maximum contaminant level [MCL]) and travel times for contaminant migration.

5.0 MODELING RESULTS

The modeling results presented below represent an important milestone in a modeling process that will develop in an iterative fashion. The simulation results are considered preliminary. The modeling results are consistent with key aspects of the conceptual model of Cr transport through the vadose zone and regional aquifer, but identify components of the model that need refinement. Additionally, the models provide a tool for assessing the sensitivity of parameters that control Cr fate and transport.

Key observations from these preliminary simulations appear to overestimate Cr concentrations in the regional aquifer. The model also overstates the area affected by Cr contamination in the regional aquifer, indicating its presence at monitoring wells that contain background concentrations. Finally, the relative distribution of Cr concentrations does not match the observed concentration gradients in the monitoring wells (e.g., concentrations in R-11 vs. R-28). To address the lack of convergence with site data, ongoing refinement of the numerical models will incorporate additional elements of the conceptual model such as potential lateral transport along dipping units in the unsaturated zone and the heterogeneous structure of the regional aquifer.

The following discussion presents the preliminary model results because they are generally useful for describing system behavior. However, the probabilistic assessment of nature and extent requires additional refinement and calibration to match Cr observations from monitoring wells.

5.1 Unsaturated-Zone Modeling Results

The unsaturated-zone model was used to calculate the current-day distribution of Cr and Mo in the unsaturated zone and the arrival of these contaminants as a function of time at the regional aquifer. Two sets of results are presented in detail in Appendix E, and these show the difference in transport behavior predicted by using the two different infiltration scenarios. Infiltration Model 1, which is based on the 2006 surface water balance, yields simulated results that better match unsaturated-zone field data than do the results for Infiltration Model 2.

Summary results for the current-day distributions of Cr mass in the unsaturated zone predicted by the two infiltration models are shown in Tables 5.1-1 and 5.1-2. The summary includes the mass of Cr that entered the unsaturated zone and the amount that was predicted to have exited to the regional aquifer to date. These distributions are shown for the entire canyon and for the four canyon segments. In addition, the distributions are further segregated into two sections by depth. The first section (UZ1) is the upper portion of the unsaturated zone that lies between the base of the alluvium (or the surface if no alluvium is present) and the base of the Guaje Pumice Bed. The second section (UZ2) is the lower portion of the unsaturated zone that lies between the base of the Guaje Pumice Bed and the regional water table. Further detail for these distributions describes the media where the contaminant resides, either porewater, adsorbed onto non-basalt units, or reacted with the Cerros del Rio basalt. The level of detail given here helps define the accessibility of the contaminant and may provide information to guide further site characterization or define remediation options.

The following observations are based on these summaries.

- Cr mass input to the unsaturated-zone simulations ranges from 9,600 to 69,000 kg. The estimated initial Cr release is 31,000 to 72,000 kg (Appendix A), and the sediment investigation estimates that approximately 15,000 kg of Cr is currently present in the wetland sediments (LANL 2007, 098127). Simulations using the higher range of input Cr mass have a higher groundwater-related source term than is consistent with the archival source and sediment investigations.

- For Infiltration Model 1, the majority of the Cr enters SW4 (54% for mean values). For Infiltration Model 2, the majority of Cr enters SW3 (64% for mean values). Corresponding water volumes entering these segments are proportional to these Cr masses.
- In both cases, more Cr has exited the unsaturated zone (67% and 78% for the mean values for infiltration Models 1 and 2, respectively) than is retained there. For Infiltration Model 1, the majority of the Cr exits from SW4. For Infiltration Model 2, the majority of the Cr exits from SW3 (64% for mean values).
- For Infiltration Model 1, the Cerros del Rio basalt located in SW4 retains the greatest mass of Cr that is present in the unsaturated zone, which is 4800 kg or approximately 13% of the source for the mean values. For Infiltration Model 2, the combined media in SW4 retain the greatest mass of Cr that is present in the unsaturated zone, which is approximately 3800 kg or 10% of the source for the mean values. However, Infiltration Model 2 calculates slow infiltration rates for SW4 and yields residual Cr porewater concentrations that are not consistent with data in many simulations.
- The porewater and adsorbed-phase Cr mass in the column representing the wetland in SW1 are greater than for those phases in the remainder of the unsaturated zone. However, the Cr mass retained there is less than approximately 8% of the total assumed mass for the mean values.
- For Infiltration Model 1, the fault is modeled as a fast path although not a large mass of Cr enters there. The simulations predict that all Cr entering the fault has exited to the regional aquifer. For Infiltration Model 2, the hydrologic properties of the fault are modeled identically as for Infiltration Model 1. However, only a small quantity of water (equivalent to 50 mm/yr infiltration rate) and Cr enter. The result is small but rapid breakthrough with no Cr mass retained in the fault. For both infiltration models, the fault zone is predicted to contain an insignificant mass of Cr.
- SW2 is a narrow segment of the canyon. For Infiltration Model 1, 5% to10% of the water entering the canyon infiltrates SW2. This produces a high enough infiltration rate, given the small surface area of the canyon segment, that the Cr is predicted to be flushed from the unsaturated zone in this segment. Conversely, for Infiltration Model 2, virtually no water or Cr enters SW2. Therefore, for both infiltration models, the unsaturated zone in the SW2 segment is predicted to contain an insignificant mass of Cr.
- Transport in SW3 is significantly different for the two infiltration models. For Infiltration Model 1, 25% to 30% of the water entering the canyon infiltrates SW3. This produces infiltration rates that are not high enough to fully flush Cr out of the unsaturated zone. Some Cr remains throughout the unsaturated zone in porewater or is retained within the basalt. For Infiltration Model 2, a large fraction of the incoming water and Cr (64% for the mean values) infiltrates SW3, producing high enough infiltration rates to flush most of the Cr from the porewater and absorbed phases, although some retention by basalt occurs.

5.2 Regional Aquifer Modeling Results

The saturated-zone model was used to calculate the current-day distribution of Cr and Mo in the regional aquifer. The predicted distributions of Cr mass in the regional aquifer (Figures 5.2-1 and 5.2-2) are based on breakthrough from the unsaturated zone model assuming Infiltration Models 1 and 2, respectively (Appendix E). These numerical results predict the average Cr concentrations in the regional aquifer obtained for the 100 model realizations. The snapshots represent 1967, 1977, 1987, 1997 and 2007 predictions.

In the case of Infiltration Model 1 (Figure 5.2-1), the initial contamination arrives in the regional aquifer under the upper section of Sandia Canyon (SW1 and SW2). The maximum Cr concentration occurs in 1977 and declines thereafter because the Cr source was removed in 1972 and ambient regional groundwater flow dilutes the remaining mass. By 1987, the average concentrations in this section of the regional aquifer are substantially less. In 1987, breakthrough occurs in the middle and lower sections of the canyon (SW3 and SW4) and impacts the regional aquifer. However, the predicted concentrations substantially exceed the field observations from monitoring wells (Figure G-11, Appendix G). Therefore, it can be assumed that either the Cr was flushed out of the unsaturated zone faster than predicted or it remains there. Nearly all the simulations predict high Cr concentrations at R-35, and higher Cr concentrations at R-11 than at R-28. Both of these results are not supported by existing field data.

In the case of Infiltration Model 2 (Figure 5.2-2), the initial contamination arrives in the middle section of Sandia Canyon (SW3). Small quantities reach the regional aquifer in the other canyon sections. As a result, the Cr plume in the regional aquifer migrates predominantly toward R-6. However, the low concentrations observed at R-6 contradict these model predictions.

In their present form, the coupled unsaturated/saturated transport models do not match observed well data and need refinement before producing reliable predictions of nature and extent. Therefore, a different approach was used to determine the network efficiency of the existing monitoring wells to detect Cr in the area of Sandia Canyon. Using only the regional aquifer model, the efficiency of the regional monitoring network is evaluated to detect Cr plumes originating in the area of R-28 and R-11. The goal of the analysis is to evaluate the capability of the downgradient monitoring wells to detect potential contaminant transport towards offsite locations and to water-supply wells. The analysis includes R-36, which is a well planned for the monitoring network that is not installed yet.

The numerical model is applied to predict the spatial distribution of the Cr plume assuming a uniform constant concentration source of 450 ppb throughout the source area (shown as a red square in Figure 5.2-3). The source area encompasses R-11 and R-28. The assumption about source concentration is conservative because it assumes that the R-28 Cr concentration is found at similarly high concentrations over a large source area within the aquifer. Actual measured concentrations of Cr measured at R-11 are much lower (~30 ppb). The source concentrations are also assumed to be persistent in time. Model predicted Cr concentrations are shown in Figure 5.2-3. The simulations demonstrate that most Cr migration may be toward R-36, which is located between R-28 and R-12. Tables 5.2-1 and 5.2-2 summarize the network efficiency and the efficiency of individual wells, respectively. The network efficiency meets the 95% confidence level for detection of Cr from the R-28/R-11 source area.

6.0 RECOMMENDATIONS

The following recommendations identify additional work to address key uncertainties in the conceptual model for contaminant fate and transport in Sandia Canyon and to select CME alternatives. The table below presents the recommended actions and their rationale. These recommendations are made to address key uncertainties in the ability to answer the following questions.

- What is the nature and extent of contamination released by Laboratory operations in Sandia Canyon; in particular, what is the distribution of Cr mass in all affected media?
- What are the pathways for contaminant transport by surface water, surface sediment, alluvial groundwater, the vadose zone, and the regional aquifer?
- Do the existing groundwater monitoring wells provide adequate detection of contaminants moving towards municipal water-supply wells and the Laboratory boundary?

- What data are needed to assess CME remediation alternatives?

The fate and transport model presented in this report is a preliminary step for identifying the scope of additional investigation work necessary to support recommendations for monitoring and potential remedial options. These modeling results are used to improve the conceptual model of flow and transport and are used in conjunction with other characterization data to assess future characterization needs. The preliminary status of this modeling initiative implies that further refinement is needed to better match modeling results to observed data in monitoring wells. Additional assessment of modeling results is ongoing, and the Laboratory intends to engage NMED and DOE over the next few months to define characterization activities that will yield the most valuable information with respect to groundwater monitoring and remediation.

The recommendations listed below are the remaining activities needed to complete the Sandia Canyon investigation. Results of the investigations described below will be incorporated into the Sandia Canyon investigation report in December 2008.

Scope	Work Description	Rationale
Sediment Investigation	Phase 1 sediment investigations were recently completed and are reported in a companion report entitled "Summary of Sandia Canyon Phase I Sediment Investigations" (LANL 2007, 098127). Recommendations for Phase 2 of the sediment investigation from that report are summarized below. Details about proposed reaches, sample numbers, and analyte suites can be found in Table 6 of the Phase 1 sediment investigation report (LANL 2007, 098127). (1) Reaches S-6W and S-6E are proposed for investigation in Phase 2 to determine the downcanyon extent of chemicals of potential concern (COPCs) in Sandia Canyon sediment deposits and potential inputs to the Rio Grande. The proposed analytical suites include all COPCs identified in S-5E during Phase 1. Because S-6W and S-6E are on San Ildefonso Pueblo land, investigation of these reaches is contingent on approval from the Pueblo. (2) Additional sample collection is proposed for reaches S-1N and S-1S, and the proposed Phase 2 analytical suite includes all COPCs identified in reaches S-1N, S-1S, or S-2 during the Phase 1 investigation. (3) Collection of additional samples for pesticides and polycyclic aromatic hydrocarbons (PAHs), as well as metals and PCBs is proposed for in reach S-3W.	Proposed Phase 2 sediment investigations in Sandia Canyon focus on evaluating the extent of COPCs and on improving estimates of average concentrations of COPCs that are important for evaluating potential human health risk. (1) The easternmost reach investigated during Phase 1, S-5E, contains Laboratory-derived COPCs, and the downcanyon extent of these COPCs has not been determined. Reaches S-6 West (S-6W) and S-6 East (S-6E) were proposed in section 7.1.2.3 of the work plan as contingency reaches to be investigated contingent on results in S-5E (LANL 1999, 064617, pp. 7-13 and 7-14). (2) Relatively few samples from well defined geomorphic contexts have been colled in Reaches S-1N and S-1S. Additional data are needed to define the nature and extent of contamination in the areas proximal to contaminant outfalls. (3) Phase 1 sampling in reach S-3W only included metals and polychlorinated biphenyls (PCBs), which have been previously identified as including the most important COPCs upcanyon in S-2. Additional analyses will be required from S-3W to provide data for a human health risk assessment. In addition to metals and PCBs, data on pesticides and PAH are potentially needed to evaluate the carcinogenic risk endpoint.

Scope	Work Description	Rationale
Water Balance Investigation	This ongoing activity will constrain the location and amount of surface water and alluvial groundwater loss in Sandia Canyon between surface-water gaging stations E121/122 and E124. The infiltration investigation conducted for this report and the "Interim Measures Work Plan for Chromium Contamination in Groundwater" (LANL 2006, 091987) will be extended to include two additional time periods (October and November 2007 and April to June 2008). Streambed infiltration losses for four segments of Sandia Canyon are determined by comparing discharge data from outfalls and flow data from the existing network of permanent and temporary stream gages.	Areas of surface water and alluvial groundwater loss probably coincide with those parts of the canyon floor that contributed recharge to deeper perched zones and to the regional aquifer during and after the period of Cr release from the TA-03 power plant. Periods of lower than normal effluent discharge during 2007 may have shifted the focus of streambed infiltration losses west of areas identified in the "Interim Measures Work Plan for Chromium Contamination in Groundwater" (LANL 2006, 091987). To further reconcile the differences between the 2006 and the 2007 results, additional gage data will be collected. The emphasis of the additional data will be to collect gage data during long periods with little or no precipitation. This approach is expected to provide a data set that can be used in ongoing modeling efforts to further refine the vadose-zone infiltration pathways as necessary to support potential remedy selection.
Surface Water and Groundwater Sampling	Analytical suites for ongoing sampling conducted in Sandia Canyon are described in the Interim Facility Groundwater Monitoring Plan (IFGMP). The routine analytical suite is modified to include analyses for stable isotopes of Cr (δ^{53}Cr) by the University of Illinois at Urbana-Champaign. Isotope fractionation of Cr(VI) (δ^{53}Cr) was observed to a varying degree in surface water samples and groundwater samples collected from alluvial, perched intermediate, and regional aquifer wells. Residual Cr(VI) contained δ^{53}Cr ratios ranging from 0.3 to 2.93 per mil corresponding to 0 to 53% reduction of Cr(VI).	Chemical and isotopic data have been shown to fingerprint potential contaminant sources and improve geochemical and hydrologic-transport numerical models that quantify processes controlling fate and transport of Cr and other contaminants of relevance (arsenic, Mo, and zinc). Ultimately, these data support the evaluation of potential remedial options for contaminated sediments and alluvial, perched intermediate, and regional aquifer groundwater. Use of δ^{53}Cr ratios for environmental decision-making regarding fate and transport and remediation options for Cr are endorsed by state and federal regulatory agencies and academia.

Scope	Work Description	Rationale
Surface Water and Groundwater Sampling (cont.)	The following modifications are made to Cr isotope sampling based on the results of the initial sample data reported herein. Wells MCOI-5, MCOI-6, MCO-7.5, R-1, R-10, R-10a, R-11, R-13, R-15, R-16r, R-28, and R-34 will be sampled for three more quarters in the Sandia Watershed and as approved in the next IFGMP for Mortandad Canyon. Depending on water availability, wells SCA-1, SCA-3, SCA-5, and SCI-1 in Sandia Canyon will be sampled for four quarters for δ^{53}Cr. Well R-12 (screens 1 and 2), MCOI-4, and MCOBT-4.4 will also be sampled for δ^{53}Cr for four quarters. New wells R-35a and R-35b and planned deep wells (R-36 and others) within Sandia and Mortandad Watersheds will be sampled for δ^{53}Cr for four quarters. Wells MCO-0.6, MCO-4B, MCO-5, R-14, and R-33 will not be sampled for δ^{53}Cr, based on analytical difficulty resulting from dissolved organic matter and/or spectral interference by dissolved iron or the well location not critical for determining the nature and extent of Cr contamination. Surface water stations E123, at terminus of persistent baseflow, and E123.4 will continued to be sampled for δ^{53}Cr for three more quarters. Surface water in Mortandad Canyon below Effluent Canyon and E-1FW will not be sampled for δ^{53}Cr because of spectral interferences resulting from the presence of dissolved iron and organic carbon during analysis.	Analytical results for δ^{53}Cr have provided quantitative information on the fate and transport and natural attenuation of Cr in surface water and groundwater environments within Sandia and Mortandad Canyons. Ratios of δ^{53}Cr provide a quantitative approach for evaluating the reductive capacities of Cr(VI) within strata in the vadose zone and in the regional aquifer. Analytical results for Cr isotopes could not be obtained for some samples because of the presence of dissolved organic carbon in the sample or very low Cr concentrations. Further analysis of Cr isotopes will focus on the locations along the flow path that have been shown to be suitable for this analytical approach.

Scope	Work Description	Rationale
Adsorption of Cr(VI)	This activity includes measurement of Cr(VI) adsorption constants (distribution coefficients, K_d) for key stratigraphic units. Batch and/or column experiments will be conducted using aquifer material. Representative groundwater collected from the perched intermediate zone and the regional aquifer will be used in the adsorption experiments. Adsorption experiments will be conducted using Laboratory-specific aquifer material. It is anticipated that the adsorption experiments will be conducted using three different concentrations of Cr(VI) including 5, 50, and 500 μg/L. The experiments will be conducted following detailed procedures developed by the Laboratory for the Yucca Mountain Project. Mineralogical characterization of aquifer material will be conducted if the information is not available from previous studies. Details of the experimental procedures, analytical methods, and the approach for evaluating measured K_d values for Cr(VI) will be documented.	Laboratory-specific adsorption constants (K_d) are required for continued refinement of the fate and transport modeling of Cr within the vadose zone and regional aquifer. Groundwater chemical and stable isotope data show that Cr interacts with SOM and aquifer material to a varying extent. Literature-derived K_d values for Cr(VI) may not be representative of conditions at the Laboratory. Laboratory-specific adsorption data for Cr(VI) have direct application to: (1) determining the nature and extent of Cr contamination, (2) quantifying the long-term fate of Cr, and (3) evaluating the most effective and efficient remedial option for Cr.
Fate and Transport Modeling	This activity includes the ongoing refinement of the groundwater-flow and contaminant-transport models for historical Cr sources in the Sandia, Mortandad, and Los Alamos Watersheds. The models will consider existing water-supply wells in the vicinity of these canyons (PM-3 and O-4), and new groundwater data (e.g., Cr, Mo, and other related constituents) from R-35 (a and b) and R-36. Model advancements will include coupling the vadose zone and regional aquifer in a three-dimensional framework and use other available data such as results from zonal sampling at PM-3, the R-28 sampling test, and the R-35 pumping test. The model will include detailed documentation of key input parameters and conceptual models and address uncertainties in the model results. The Laboratory will seek input from NMED in incorporation of aspects of the conceptual model and plausible ranges and distributions for model input parameters. Model results will be compared to available monitoring data as well as to estimates of the total mass of Cr in the system. If necessary, simulation results will be weighted based on agreement between simulated and measured concentrations.	Numerical models are useful tools for integrating available knowledge about the fate and transport of Cr. Combining a quantitative treatment of all uncertainties with calibration of results based on their agreement with Cr measurements provides a defensible approach to finding quantitative answers to key questions including the following. (1) What is the nature and extent of Cr? (2) What is the uncertainty in the nature and extent of Cr? (3) Is the current monitoring-well network capable of intercepting all potential Cr pathways? (4) What is the long-term fate of Cr in the vadose zone and regional aquifer? (5) What is the most effective and efficient remedial option for Cr? (6) What additional characterization is necessary to reduce model uncertainty sufficient to allow the selection of a remedial option?

Scope	Work Description	Rationale
R-28 Testing	R-28 will be pumped for at least 30 hr at a constant rate of approximately 5 gal./min. while water levels, chemical constituents, and other indicator parameters are measured. In addition, water levels will be monitored continuously in R-35 (a and b), R-11, R-13, R-15, and R-8A during the test. The 30-hr test duration should produce water that is currently located outside the "zone of influence" of the potential residual drilling fluids. The Laboratory will work with NMED before the test to define a set of potential test responses, in terms of water levels, contaminant concentrations, and indicator parameters. These potential responses will be based on conceptual models of flow and transport such as one model assuming that the Cr concentrations are affected by drilling fluids and another model assuming they are not affected. These hypothetical responses will seek to identify unique responses of each conceptual model and ensure test design and sampling protocols that can observe these unique responses. Water samples will be collected at R-28 before pumping and during pumping at the following frequency: every hour during 0 to 12 hr; every 4 hr from 12 to 24 hr; and at 30 hr at the end of pumping. Field parameters including oxidation-reduction potential, temperature, pH, turbidity, specific conductance, and dissolved oxygen will be measured during pumping and sampling. For all samples collected, filtered waters will be analyzed for metals and anions (including perchlorate), and nonfiltered waters will be analyzed for metals, total organic carbon, acetone, and 2-proponal (isopropyl alcohol). In addition, at the 4- and 6-hr intervals, filtered water samples will be analyzed for stable isotopes of nitrogen, and nonfiltered waters will be analyzed for low-level tritium (using electrolytic enrichment at the University of Miami) and stable isotopes of oxygen and hydrogen. To evaluate Cr reduction by potential residual drilling fluids, stable isotopes of Cr will be analyzed in samples collected at 0, 2, 4, 8, 12, 18, 24, and 30 hr.	This test will evaluate the effects of possible residual drilling fluid contamination on measured Cr concentrations, provide insight into the nature of the Cr plume, and provide information on aquifer parameters to be used in conceptual and numerical models of Cr fate and transport.

Scope	Work Description	Rationale
PM-3 Zonal Sampling	The Los Alamos County Utilities Department informed the Laboratory that access to PM-3 will not be granted until at least the fall of 2007.	Zonal sampling may provide insights into depth-dependant variations in the quality of water entering the well screen at PM-3. The Laboratory proposes that the need for zonal sampling at PM-3 be assessed after results for the R-35 and numerical modeling activities are evaluated.
Regional Aquifer Well	The Laboratory plans to install a new single-screen regional groundwater-monitoring well in Mortandad Canyon near corehole MCOBT-8.5. A conceptual location for this well is shown in Figure 1.0-1. The specific location will be determined in consultation with NMED and presented in a well-specific work plan.	Placement of this well will help identify the groundwater pathways for the Cr contamination and provide a test of the regional flow and transport model predictions. This well will also help to constrain the nature and extent of Cr contamination in regional groundwater and provide information about the relative contributions of Cr contamination from Sandia and Mortandad Canyons.
Intermediate Well SCI-2	The Laboratory plans to install a new single-screen perched intermediate well in Sandia Canyon near SCC-2. A conceptual location for this well is shown in Figure 1.0-1. A specific location will be determined in consultation with NMED and presented in a well-specific work plan.	The objective of this well is to determine if significant perched intermediate water exists on or within the basalt as has been observed beneath Mortandad Canyon. If present, deep perched intermediate groundwater may be an important groundwater pathway for Cr and other contaminants, and it will provide a monitoring point for assessing the potential for ongoing Cr migration in the vadose zone over time. This location may also help resolve the conceptual model element that indicates that dips in the basalt may divert perched intermediate water southward from beneath Sandia Canyon. If installed, the intermediate well will be cored from the top of basalt to total depth (TD) (first significant water or base of basalt) to characterize Cr distributions in the vadose zone below the depth of existing core data from SCC-2.

7.0 REFERENCES

The following list includes all documents cited in this report. Parenthetical information following each reference provides the author(s), publication date, and ER ID number. This information is also included in text citations. ER ID numbers are assigned by the Environmental Programs Directorate's Records Processing Facility (RPF) and are used to locate the document at the RPF and, where applicable, in the master reference set.

Copies of the master reference set are maintained at the NMED Hazardous Waste Bureau; the U.S. Department of Energy–Los Alamos Site Office; the U.S. Environmental Protection Agency, Region 6; and the Directorate. The set was developed to ensure that the administrative authority has all material needed to review this document, and it is updated with every document submitted to the administrative authority. Documents previously submitted to the administrative authority are not included.

Freeze, R.A., and J.A. Cherry, January 1979. *Groundwater*, Prentice-Hall, Inc., Englewood Cliffs, New Jersey. (Freeze and Cherry 1979, 088742)

Kleinfelder, May 2006. "Final Completion Report, Characterization Well R-17," report prepared for Los Alamos National Laboratory, Project No. 49436, Albuquerque, New Mexico. (Kleinfelder 2006, 092493)

LANL (Los Alamos National Laboratory), September 1999. "Work Plan for Sandia Canyon and Cañada del Buey," Los Alamos National Laboratory document LA-UR-99-3610, Los Alamos, New Mexico. (LANL 1999, 064617)

LANL (Los Alamos National Laboratory), March 2006. "Interim Measures Work Plan for Chromium Contamination in Groundwater," Los Alamos National Laboratory document LA-UR-06-1961, Los Alamos, New Mexico. (LANL 2006, 091987)

LANL (Los Alamos National Laboratory), June 2006. "Drilling Work Plan for Regional Aquifer Wells R-35a and R-35b," Los Alamos National Laboratory document LA-UR-06-3964, Los Alamos, New Mexico. (LANL 2006, 093388)

LANL (Los Alamos National Laboratory), October 2006. "Mortandad Canyon Investigation Report," Los Alamos National Laboratory document LA-UR-06-6752, Los Alamos, New Mexico. (LANL 2006, 094161)

LANL (Los Alamos National Laboratory), November 2006. "Interim Measures Investigation Report for Chromium Contamination in Groundwater," Los Alamos National Laboratory document LA-UR-06-8372, Los Alamos, New Mexico. (LANL 2006, 094431)

LANL (Los Alamos National Laboratory), April 2007. "Addendum to the Work Plan for Sandia Canyon and Cañada del Buey, Revision 1," Los Alamos National Laboratory document LA-UR-07-2186, Los Alamos, New Mexico. (LANL 2007, 095454)

LANL (Los Alamos National Laboratory), September 2007. "Summary of Sandia Canyon Phase 1 Sediment Investigations," Los Alamos National Laboratory document LA-UR-07-6019, Los Alamos, New Mexcio. (LANL 2007, 098127)

LANL (Los Alamos National Laboratory), September 2007. "Completion Report for Regional Aquifer Wells R-35a and R-35b," Los Alamos National Laboratory document LA-UR-07-5342, Los Alamos, New Mexcio. (LANL 2007, 098129)

Lin, Z., and T. Oguchi, 2004. "Drainage Density, Slope Angle, and Relative Basin Position in Japanese Bare Lands from High-Resolution DEMs," *Geomorphology,* Vol. 63, pp. 159-173. (Lin and Oguchi 2004, 098050)

Longmire, P., M. Dale, D. Counce, A. Manning, T. Larson, K. Granzow, R. Gray, and B. Newman, July 2007. "Radiogenic and Stable Isotope and Hydrogeochemical Investigation of Groundwater, Pajarito Plateau and Surrounding Areas, New Mexico," Los Alamos National Laboratory report LA-14333, Los Alamos, New Mexico. (Longmire et al. 2007, 096660)

NMED (New Mexico Environment Department), December 29, 2005. "Interim Measures Work Plan Requirement, Groundwater Contaminants Detected in the Regional Aquifer at R-28," New Mexico Environment Department letter to M. Johansen (DOE LASO) and D. McInroy (LANL) from J.P. Bearzi (NMED-HWB), Santa Fe, New Mexico. (NMED 2005, 091683)

NMED (New Mexico Environment Department), May 5, 2006. "Approval with Modifications for the 'Interim Measures Work Plan for Chromium Contamination in Groundwater'," New Mexico Environment Department letter to M. Johansen (DOE LASO) and D. McInroy (LANL) from J.P. Bearzi (NMED-HWB), Santa Fe, New Mexico. (NMED 2006, 092543)

NMED (New Mexico Environment Department), July 24, 2006. "Approval for the Drilling Work Plan for Regional Aquifer Wells R-35a and R-35b," New Mexico Environment Department letter to M. Johansen (DOE LASO) and D. McInroy (LANL) from J. Young (NMED-HWB), Santa Fe, New Mexico. (NMED 2006, 093530)

Purtymun, W.D., December 1975. "Geohydrology of the Pajarito Plateau with Reference to Quality of Water, 1949-1972," Informal Report, Los Alamos Scientific Laboratory document LA-UR-02-4726, Los Alamos, New Mexico. (Purtymun 1975, 011787)

Zyvoloski, G.A., B.A. Robinson, Z.V. Dash, and L.L. Trease, July 1997. "Summary of the Models and Methods for the FEHM Application — A Finite-Element Heat- and Mass-Transfer Code," Los Alamos National Laboratory report LA-13307-MS, Los Alamos, New Mexico. (Zyvoloski et al. 1997, 070147)

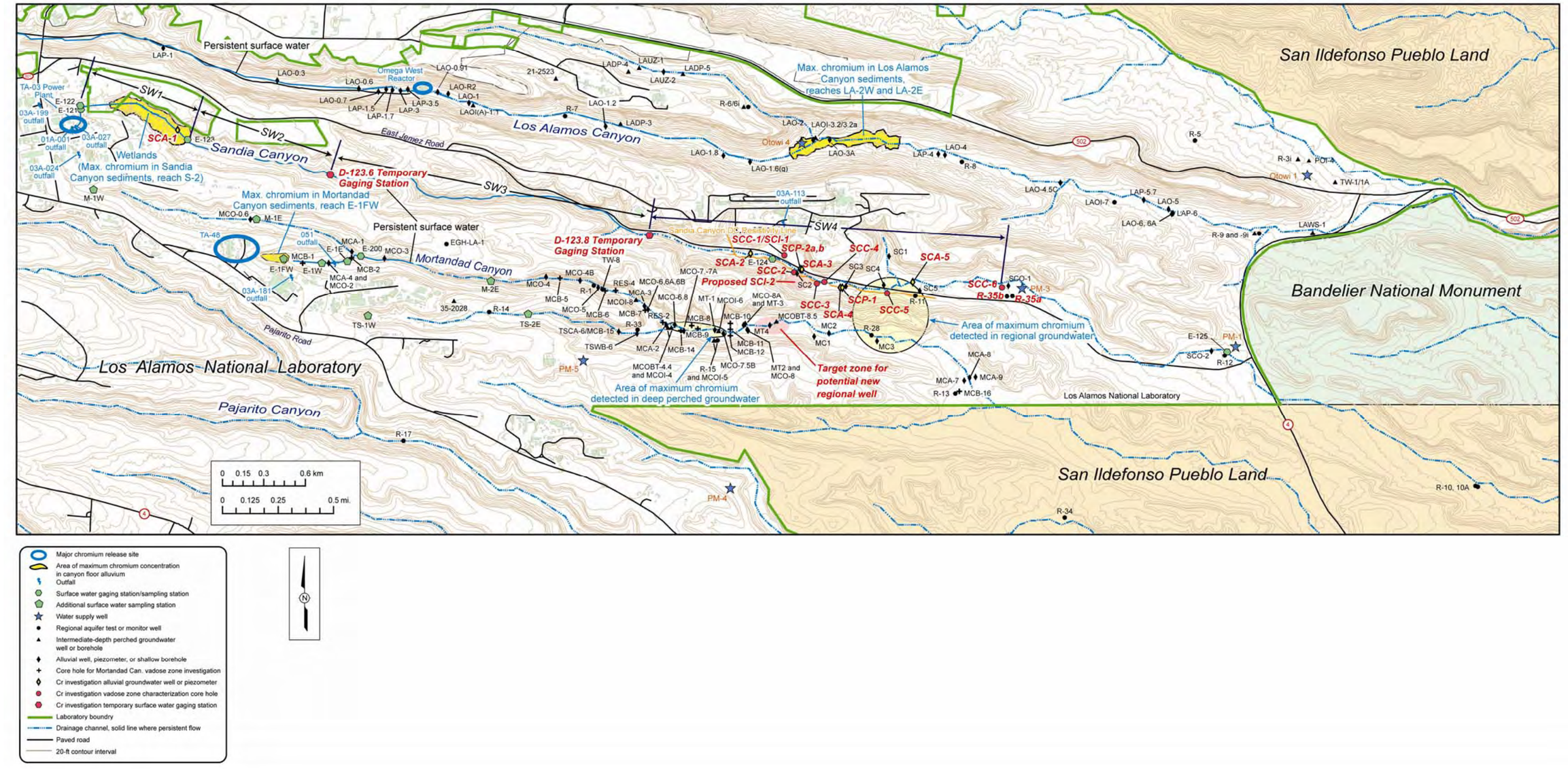

Figure 1.0-1 Location of Sandia, Los Alamos, and Mortandad Canyons showing major chromium release sites, stream-flow gages, infiltration reaches, boreholes and wells, and conceptual locations of proposed wells

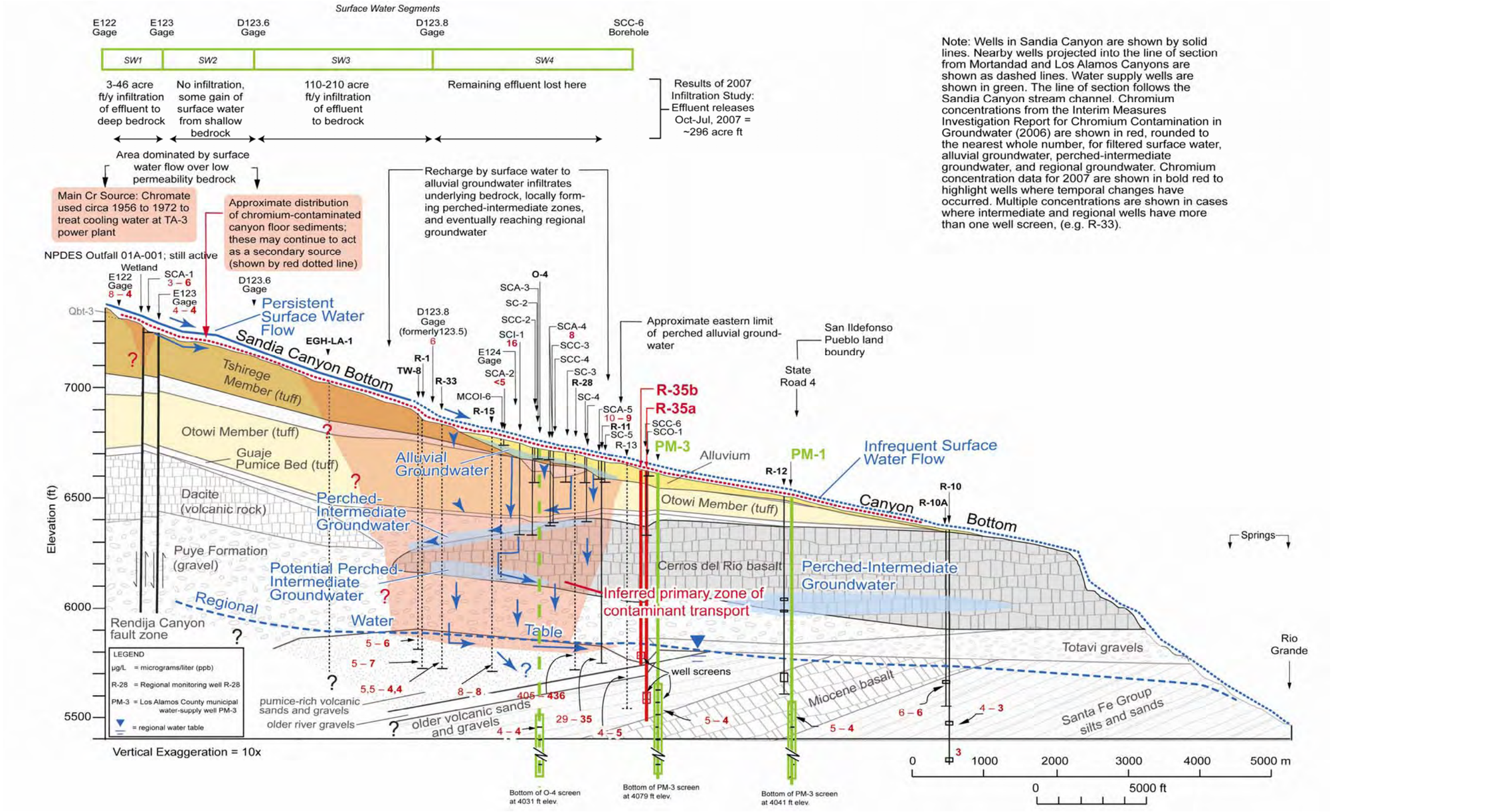

Note: Wells in Sandia Canyon are shown by solid lines. Nearby wells projected into the line of section from Mortandad and Los Alamos Canyons are shown as dashed lines. Water supply wells are shown in green. The line of section follows the Sandia Canyon stream channel. Chromium concentrations from the Interim Measures Investigation Report for Chromium Contamination in Groundwater (2006) are shown in red, rounded to the nearest whole number, for filtered surface water, alluvial groundwater, perched-intermediate groundwater, and regional groundwater. Chromium concentration data for 2007 are shown in bold red to highlight wells where temporal changes have occurred. Multiple concentrations are shown in cases where intermediate and regional wells have more than one well screen, (e.g. R-33).

Figure 3.0-1 Conceptual hydrogeologic cross section showing potential chromium transport pathways and dissolved hexavalent chromium for surface water, monitoring wells, and water supply wells in the vicinity of Sandia Canyon

Note: Red numbers indicate values of chromium, in units of µg/L, for 2006 (unbolded) and 2007 (bolded).

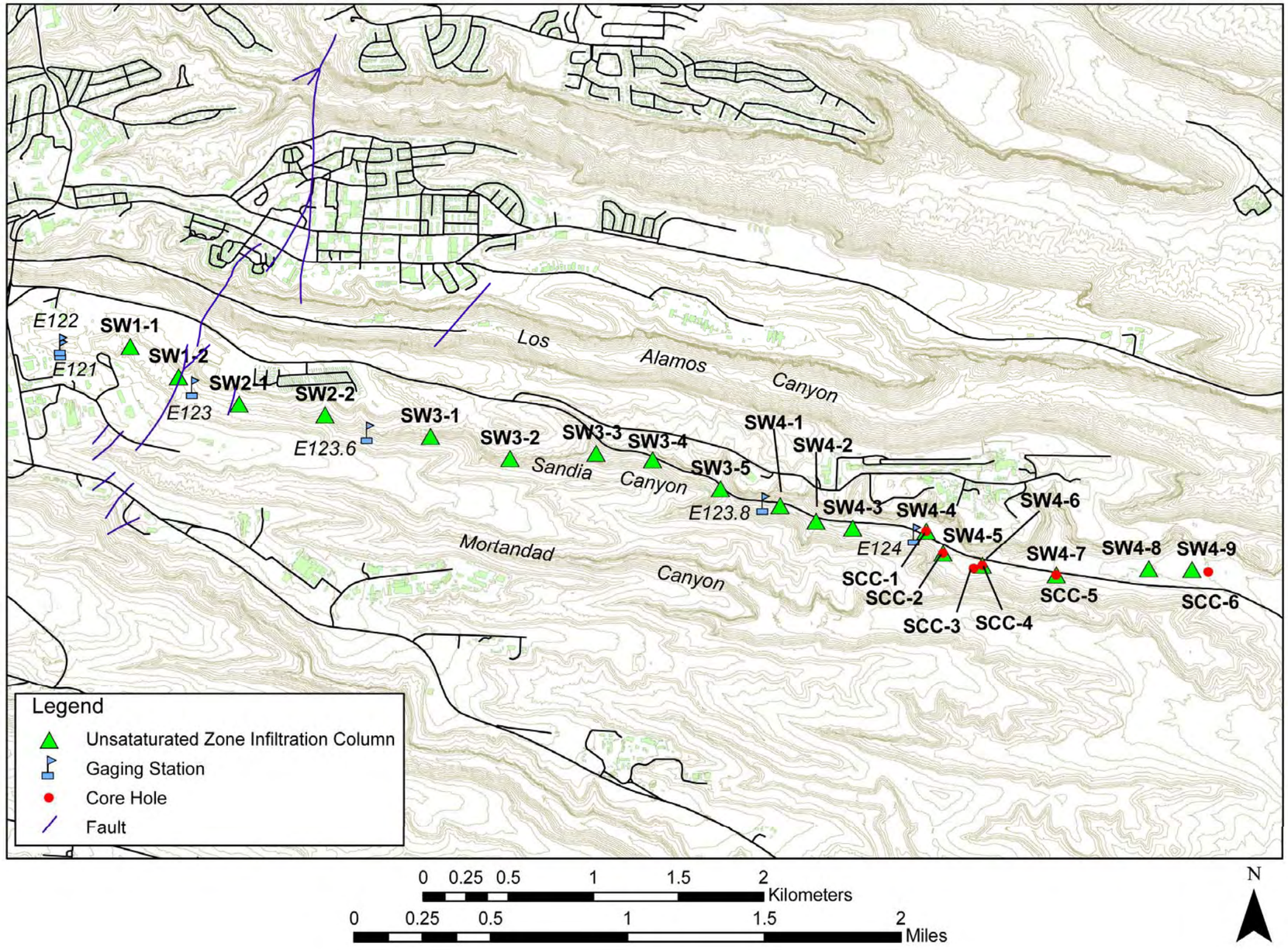

Figure 4.0-1 Locations of the 18 one-dimensional columns used in the unsaturated-zone flow and transport model

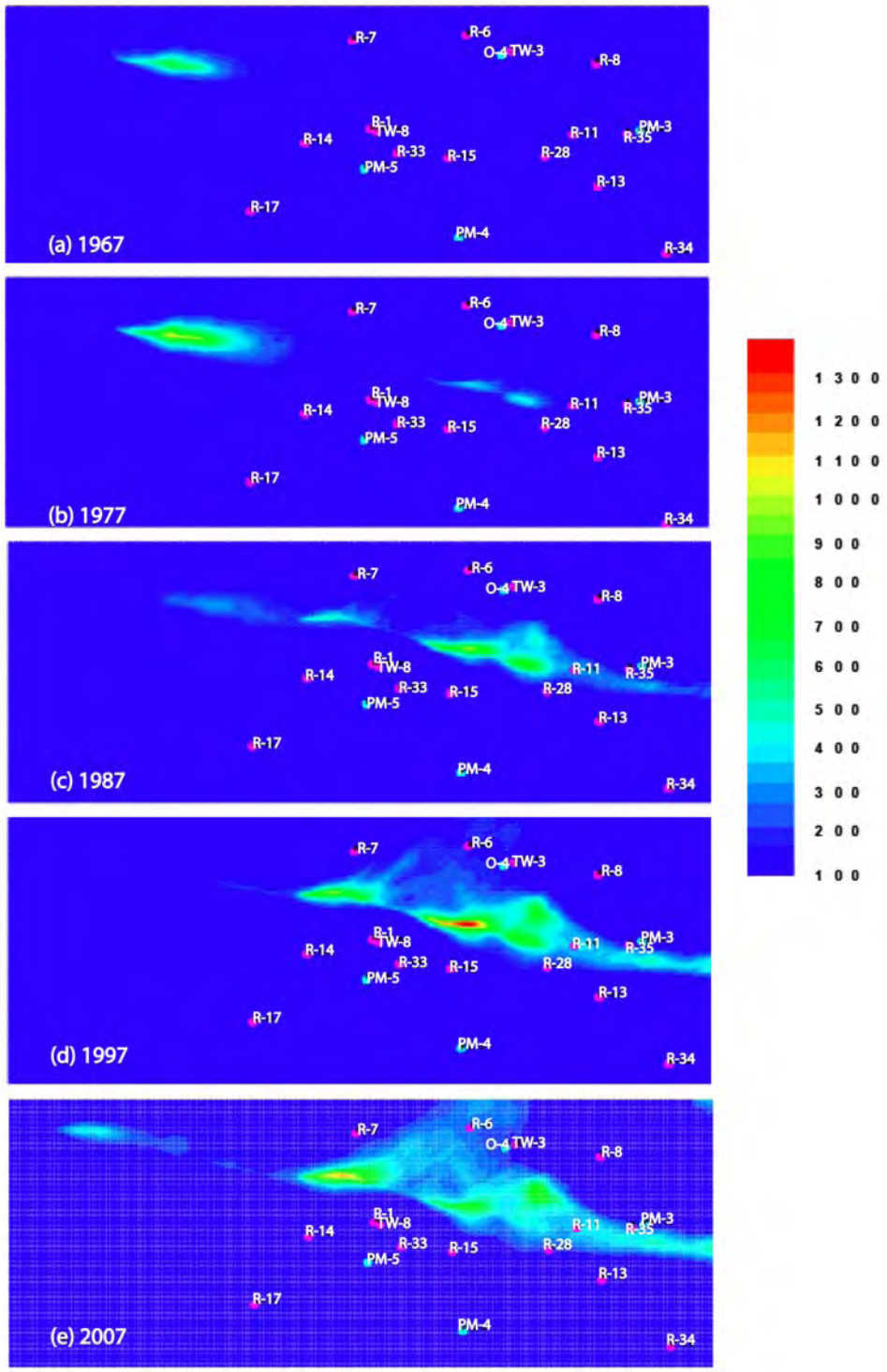

Figure 5.2-1 Numerical model predictions of average chromium concentrations in the regional aquifer based on Infiltration Model 1. Snapshots define 1967, 1977, 1987, 1997 and 2007 predictions

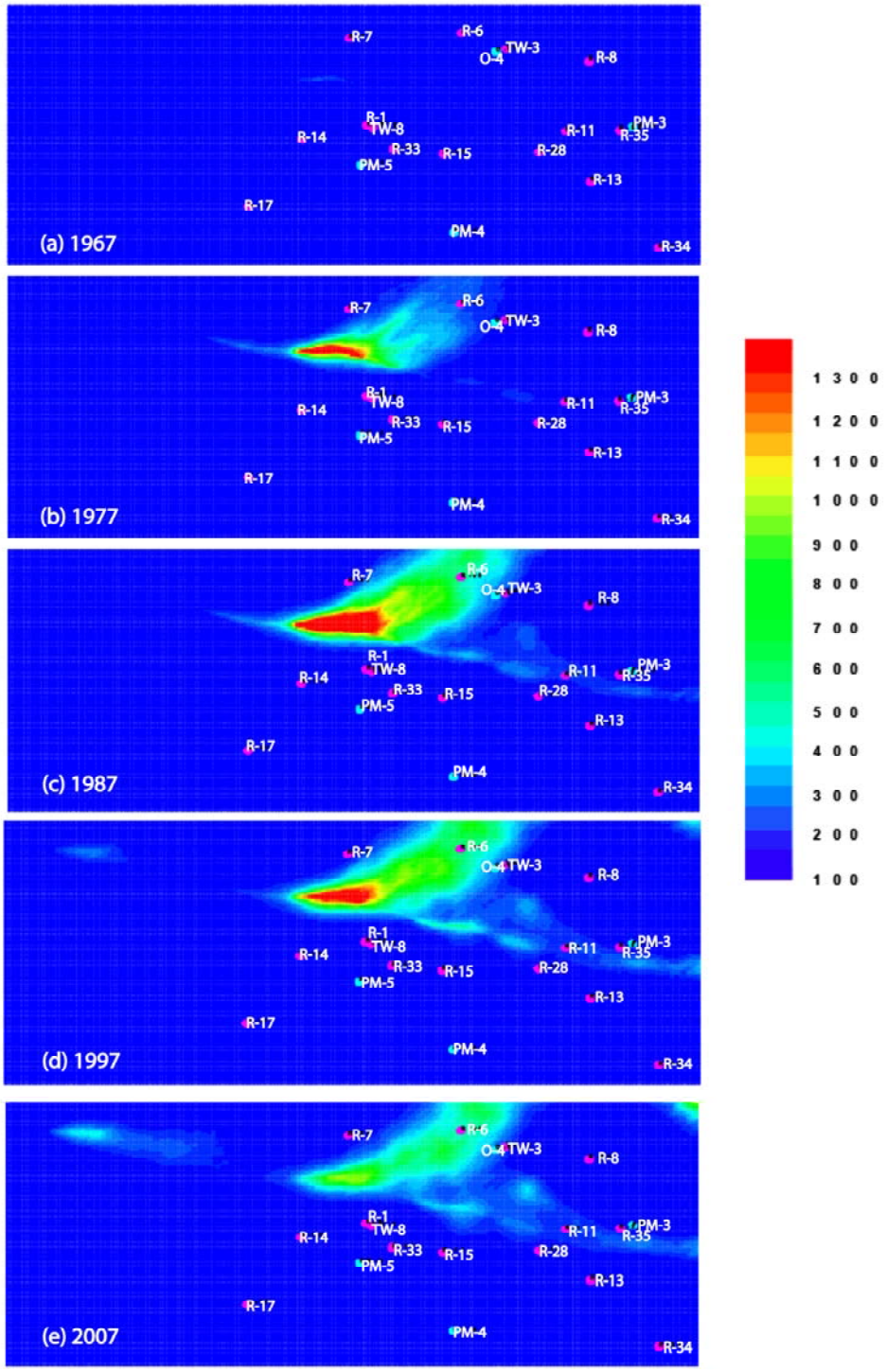

Figure 5.2-2 Numerical model predictions of average chromium concentrations in the regional aquifer based on Infiltration Model 2. Snapshots define 1967, 1977, 1987, 1997 and 2007 predictions

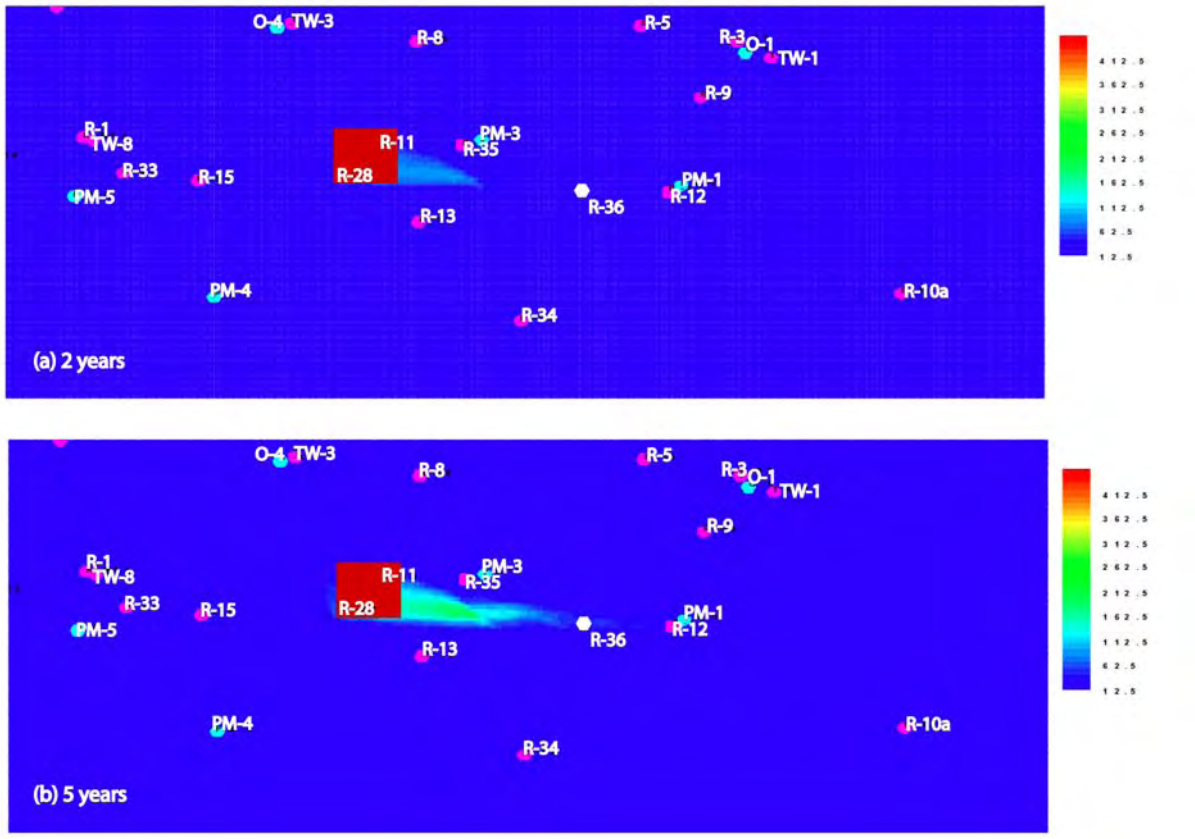

Figure 5.2-3 Spatial distribution of Cr concentrations [ppb] 2 (a) and 5 (b) years from now predicted using the numerical model assuming uniform constant concentration source of 450 ppb throughout the source areas (shown as red square)

Table 5.1-1
Simulated Present-Day Distribution of Cr(VI) [kg] in the Vadose Zone Assuming Conceptual Infiltration Model 1

Cr(VI) (kg)	Total Mean [Minimum-Maximum]	SW1 Wetland Mean [Minimum-Maximum]	SW1 fault Mean [Minimum-Maximum]	SW2 Mean [Minimum-Maximum]	SW3 Mean [Minimum-Maximum]	SW4 Mean [Minimum-Maximum]
Input	35879 [9640-69046]	3730 [995-6914]	413 [3.7-1332]	2666 [638-6879]	9856 [2720-17835]	19215 [4821-36439]
Output to Regional Aquifer	24027 [5504-48255]	877 [0-5956]	413 [3.7-1332]	2665 [638-6878]	6768 [173-15350]	13303 [2517-30173]
UZ1 Porewater	1803 [47-5311]	1479 [29-4084]	0	0.34 [0-3.8]	245 [0.9-2140]	79 [1-1364]
UZ1 Adsorbed	1042 [2-4644]	837 [1-2699]	0	0.1 [0-2]	156 [0-1757]	50 [0-983]
UZ2 Porewater	1175 [52-4289]	223 [0.5-904]	0 [0-0.03]	0.1 [0-1.65]	677 [0.6-3000]	277 [0.4-2580]
UZ2 Adsorbed (Non-basalt)	2529 [9-15204]	318 [2-1243]	0	0.2 [0-4.7]	1527 [0.2-7405]	683 [0-7794]
Cerros del Rio Basalt	5282 [1442-13433]	0	0	0	459 [2.7-1308]	4823 [2189-5990]

Table 5.1-2
Simulated Present-Day Distribution of Cr(VI) [kg] in the Vadose Zone Assuming Conceptual Infiltration Model 2

Cr(VI) (kg)	Total Mean [Minimum-Maximum]	SW1 Wetland Mean [Minimum-Maximum]	SW1 fault Mean [Minimum-Maximum]	SW2 Mean [Minimum-Maximum]	SW3 Mean [Minimum-Maximum]	SW4 Mean [Minimum-Maximum]
Input	36026 [9650-69141]	3695 [334-10425]	13 [4-23]	9 [3-16]	23197 [5840-48878]	9111 [147-36538]
Output to Regional Aquifer	28124 [6411-49554]	1009 [0-6199]	13 [4-23]	0	21778 [5565-46841]	5324 [0-25595]
UZ1 Porewater	1937 [261-6194]	1350 [51-3429]	0	6 [1-13]	8 [0-36]	574 [1-3681]
UZ1 Adsorbed	1086 [4-6201]	728 [4-2463]	0	3 [0-9]	3 [0-18]	351 [0-4722]
UZ2 Porewater	641 [1-3104]	225 [0-1217]	0 [0-2]	0	37 [0-498]	380 [0-2604]
UZ2 Adsorbed (Non-basalt)	1138 [1-5201]	387 [0-2800]	0	0	78 [0-1035]	673 [0-4294]
Cerros del Rio Basalt	3105 [401-11350]	0	0	0	1293 [273-2001]	1812 [0-10100]

Table 5.2-1
Efficiency of the Regional Monitoring Network
to Detect Plumes Originating in the Area of R-28 and R-11
Before Being Observed Offsite or at the Water-Supply Wells

O-1	O-4	PM-1	PM-2	PM-3	PM-4	PM-5	Offsite	Comment
1	1	0.999	1	0.98	1	1	0.975	Total-breakthrough test
1	1	1	1	1	1	1	0.981	Maximum-concentration test
1	1	0.999	1	0.98	1	1	0.996	First-arrival test

Table 5.2-2
Details about Efficiency of Individual Regional Monitoring Network
to Detect Plumes Originating in the Area R-28 and R-11

Well	Detected Plumes	Success		Failure		False Positive	
		Supply Well	Offsite	Supply Well	Offsite	Supply Well	Offsite
R-12	954	549	761	374	141	31	52
R-13	404	123	24	280	373	1	7
R-15	34	0	0	34	34	0	0
R-35	881	755	162	94	654	32	65
R-36	974	766	383	164	517	44	74

Appendix A

Update of Archival Work on Source Term

A-1.0 INTRODUCTION

The "Interim Measures Investigation Report for Chromium Contamination in Groundwater" (LANL 2006, 091987) presented an estimate for a hexavalent chromium (Cr) [Cr(VI)] source of 26,000 to 105,000 kg (58,000 to 230,000 lb) to upper Sandia Canyon (LANL 2006, 094431, Table 2.0-2). The Cr(VI) was released in effluent from the Technical Area (TA) 03 power plant cooling towers from approximately 1956 to 1972. This mass estimate was based on archival research conducted through late 2006 using four primary references: Reinig (1972, 003848); Zia (1972, 003855); Birdsell (2006, 091685); and Kennedy (1971, 033896). Information in this appendix further refines the Cr(VI) source and accompanying cooling tower outfall volumes based on continued archival research conducted to date and now includes nine primary references.

Table A-1 summarizes information on effluent volumes and Cr(VI) mass or concentration used to refine the Cr(VI) source. The first five entries in this table are data that pertain directly to Cr releases and discharge volumes while Cr(VI) was used at the cooling towers. The last three entries relate to discharge volumes that occurred later, from 1975 through 1983. These volumes are relevant because the power plant is thought to have produced power at approximately the same capacity from 1975 to 1983 as it did previously towards the end of the period of Cr(VI) release. That is, all three generators continuously operated, and cooling needs would have been similar (Birdsell 2006, 098048). These new data then yield ranges in discharge rates of 379 to 1091 m^3/day (100,000 to 288,000 gal./d) and in average discharge Cr(VI) concentrations of 7 to 18 mg/L, with a potential maximum of 34 mg/L.

Table A-2 lists approximate daily blowdown volumes from the TA-03 power plant cooling towers for 1959 and 1960. These volumes are derived from weekly data recorded by the Zia Company on sewage effluent volumes used as cooling water at the power plant (Zia Company 1959-1960, 098051) as follows.

- In the early 1970s, the Zia Company reported that sewage effluent had supplied over 75% of the cooling-system water makeup to the power plant over its history. Potable water was added to meet the full demand (Birdsell 2006, 098048). Because the sewage effluent was used as cooling water during Cr use at the cooling towers, the blowdown (or discharge water) from the cooling towers was primarily recycled sewage effluent; this represented the main source of anthropogenic water to Sandia Canyon. This dilution factor is used to calculate the quantity of water that entered the cooling towers.

- Cooling towers rely on evaporative cooling, and over a third of the cooling water was lost to the atmosphere by evaporation or entrainment of water droplets (windage) (Reinig 1972, 003848; LANL 2007, 095787). Therefore, blowdown volumes are significantly less than the water volumes entering the towers.

Once dilution and evaporation were accounted for, a factor of 0.8 times the sewage volume coming into TA-03 was estimated as being released at the outfall as blowdown water. The range of daily blowdown volumes in Table A-2 spans the outfall volumes listed in Table A-1. Also, the mean of the blowdown volumes based on the Zia Company sewage effluent, 652 m^3/d (172,000 gal./d), closely agrees with the mean of the six other reported values listed in Table A-1 (excluding the Zia 1960 reference) of 679 m^3/d (179,000 gal./d). Therefore, the blowdown volumes and the associated distribution given in Table A-2 are considered to represent a likely range of discharge volumes at the outfall during and following Cr(VI) usage. This distribution is used to define the input water volume to Sandia Canyon in the flow and transport simulations presented in this report, as described in Appendix E.

Finally, the original estimated Cr(VI) source to upper Sandia Canyon of 26,000 to 105,000 kg (58,000 to 230,000 lb) (LANL 2006, 094431) represents the full range of the potential source. This range has not changed substantially based on the expanded archival information. However, the additional archival information is used to refine the source by estimating "a more likely" Cr mass. First, the most likely average range of outfall volumes is taken as the mean in Table A-2 plus and minus one standard deviation, yielding a likely range of 538 to 761 m^3/d (143,000 to 201,000 gal./d). The most likely range of outfall Cr(VI) concentrations is considered to be that range reported by at least two of the references in Table A-1, 10 to 16 mg/L. These two ranges together applied over an assumed release period of 5814 days (June 1956 to April 1972) then yield a likely released Cr(VI) mass to Sandia Canyon of 31,000 to 72,000 kg (69,000 to 160,000 lb). This value agrees well with the mass estimated using the chromate (CrO_4^{2-}) use rate of 35.9 lb/d (Reinig 1972, 003848), which yields a value of 43,000 kg (94,000 lb).

Based on this update archival review, the most likely Cr(VI) mass released into upper Sandia Canyon from the TA-03 power plant cooling towers is considered to range from 31,000 to 72,000 kg (69,000 to 160,000 lb).

A-2.0 REFERENCES

The following list includes all documents cited in this appendix. Parenthetical information following each reference provides the author(s), publication date, and ER ID number. This information is also included in text citations. ER ID numbers are assigned by the Environmental Programs Directorate's Records Processing Facility (RPF) and are used to locate the document at the RPF and, where applicable, in the master reference set.

Copies of the master reference set are maintained at the New Mexico Environment Department Hazardous Waste Bureau; the U.S. Department of Energy–Los Alamos Site Office; the U.S. Environmental Protection Agency, Region 6; and the Directorate. The set was developed to ensure that the administrative authority has all material needed to review this document, and it is updated with every document submitted to the administrative authority. Documents previously submitted to the administrative authority are not included.

Birdsell, K., March 23, 2006. "Documentation of Discussions with Various People Concerning LANL and Zia Operations Specific to Cooling Towers and the Use of Chromium," Los Alamos National Laboratory memorandum to File from K. Birdsell, Los Alamos, New Mexico. (Birdsell 2006, 091685)

Birdsell, K., May 2006. "TA-3 Cogeneration Plant Operations, Interview with Bob Prindle and Joe Ortiz," Los Alamos, New Mexico. (Birdsell 2006, 098048)

Dunne, W.M., November 2, 1976. "Updated List of Waste Sources," Los Alamos Scientific Laboratory memorandum (H7-76-530) to H.S. Jordan (H-DO) from W.M. Dunne (H-7), Los Alamos, New Mexico. (Dunne 1976, 098049)

Kennedy, W.R., May 13, 1971. Los Alamos Scientific Laboratory letter (enclosing tables of radiochemical and chemical analyses of water completed July through December 1970) to W.E. Hale (District Chief/USGS) from W.R. Kennedy (H-8 Associate Group Leader), Los Alamos, New Mexico. (Kennedy 1971, 033896)

LANL (Los Alamos National Laboratory), March 2006. "Interim Measures Work Plan for Chromium Contamination in Groundwater," Los Alamos National Laboratory document LA-UR-06-1961, Los Alamos, New Mexico. (LANL 2006, 091987)

LANL (Los Alamos National Laboratory), November 2006. "Interim Measures Investigation Report for Chromium Contamination in Groundwater," Los Alamos National Laboratory document LA-UR-06-8372, Los Alamos, New Mexico. (LANL 2006, 094431)

LANL (Los Alamos National Laboratory), April 2007. "Evaluation of the Suitability of Wells Near Technical Area 16 for Monitoring Contaminant Releases from Consolidated Unit 16-021(c)-99," Los Alamos National Laboratory document LA-UR-07-2370, Los Alamos, New Mexico. (LANL 2007, 095787)

Ortiz, J.V., November 13, 2006. "History of Water Treatment Chemicals Used at the TA-03 Power Plant from 1951 through November, 2006," information compiled by J. Ortiz (power plant chemist) for K. Birdsell, Los Alamos National Laboratory, Los Alamos, New Mexico. (Ortiz 2006, 094153)

Purtymun, W.D., December 1975. "Geohydrology of the Pajarito Plateau with Reference to Quality of Water, 1949-1972," Informal Report, Los Alamos Scientific Laboratory document LA-UR-02-4726, Los Alamos, New Mexico. (Purtymun 1975, 011787)

Reinig, L.P., March 7, 1972. "Preliminary Report - Chromate Problem," Los Alamos Scientific Laboratory memorandum (ENG-353) from L.P. Reinig, Los Alamos, New Mexico. (Reinig 1972, 003848)

Zia Company, 1959-1960. "Weekly Water Reports, 9-30-59 through 4-26-60," Utilities and Engineering Division, Zia Company, Los Alamos, New Mexico. (Zia Company 1959-1960, 098051)

Zia Company, February 1, 1972. "Conceptual Design Report for Chemical Reduction System, TA-3 Power Plant, Los Alamos, New Mexico," Los Alamos, New Mexico. (Zia Company 1972, 003855)

Table A-1
Volumetric Discharges and Reported Cr(VI) Releases
at the TA-03 Power Plant Cooling Towers and/or Outfall 01A-001

Reference	Outfall Volume m^3/day (gal./day)	Concentration Cr(VI) Released mg/L	Notes
Reinig (1972, 003848)	485 (128,000)	15 to 18	Report on Cr(VI) usage at power plant while replacement process was being considered; Total CrO_4^{2-} used: 16.3 kg/day (35.9 lb/day). Windage loss: 5.4 kg/day (12 lb/day).
Zia (1972, 003855)	1091 (288,000)	7 to 15 (max up to 34)	Report on Cr(VI) usage at power plant while replacement process was being considered.
Birdsell (2006, 091685)	947 (250,000)	13 to 15	Report on Cr(VI) usage at power plant while replacement process was being considered and discussion with Bill Radzinski.
Kennedy (1971, 033896)		9.6 $\pm$ 0.3 to 16.3 $\pm$ 0.3	Measured effluent Cr concentration, three samples - December, 1968 through February, 1969.
Zia (1959-1960, 098051); Ortiz (2006, 094153)	652 (172,000)		Weekly discharge volumes recorded during 1959 and 1960 (see Table A-2); estimate that sewage effluent supplied >75% cooling system water makeup to power plant.
Purtymun (1975, 011787)	625 (165,000)		Discharge volume in approximately 1975, combined release of sewage treatment and power plant.
Birdsell (2006, 098048)	557 (147,000)		Detailed daily records from 1983 of power plant make-up water, blowdown, and calculated evaporation (277 m^3/day [73,000 gal./day]); Joe Ortiz, power plant operator, stated that power generation in 1983 was close to that during Cr(VI) use.
Dunne (1976, 098049)	379 (100,000)		Estimates of Los Alamos National Laboratory (LANL, or the Laboratory)-wide effluent volumes generated during initial NPDES permit application, circa 1976, Table III, p. 11.
	Summary of Range 379 to 1091 (100,000 to 288,000)	**Summary of Range 7 to 18**	

Table A-2
Weekly Volumetric Sewage Effluent to TA-03 during 1959 and 1960
and Resultant Estimated Power Plant Daily Blowdown Volumes

Week	Weekly Gal. Effluent Water to TA-03	Daily Average Sewage Effluent to Power Plant (gal.)	Daily Average Estimated Blowdown from Power Plant (gal.)
28-Apr-59	1.80E+06	2.57E+05	2.05E+05
7-May-59	1.78E+06	2.55E+05	2.04E+05
14-May-59	1.63E+06	2.32E+05	1.86E+05
20-May-59	1.74E+06	2.48E+05	1.99E+05
30-May-59	1.61E+06	2.31E+05	1.84E+05
3-Jun-59	1.66E+06	2.36E+05	1.89E+05
10-Jun-59	1.64E+06*	2.35E+05	1.88E+05
17-Jun-59	1.89E+06*	2.71E+05	2.16E+05
23-Jun-59	1.50E+06*	2.14E+05	1.71E+05
2-Jul-59	1.70E+06*	2.43E+05	1.94E+05
7-Jul-59	1.20E+06*	1.72E+05	1.37E+05
15-Jul-59	1.90E+06*	2.71E+05	2.17E+05
22-Jul-59	1.80E+06*	2.57E+05	2.06E+05
30-Jul-59	1.30E+06*	1.86E+05	1.49E+05
5-Aug-59	1.29E+06*	1.85E+05	1.48E+05
20-Aug-59	1.80E+06*	2.57E+05	2.06E+05
28-Aug-59	1.73E+06*	2.47E+05	1.97E+05
2-Sep-59	1.43E+06*	2.04E+05	1.63E+05
10-Sep-59	1.98E+06*	2.83E+05	2.26E+05
14-Sep-59	1.50E+06*	2.14E+05	1.71E+05
23-Sep-59	1.80E+06*	2.57E+05	2.06E+05
30-Sep-59	1.77E+06	2.53E+05	2.03E+05
8-Oct-59	1.53E+06	2.19E+05	1.75E+05
14-Oct-59	1.50E+06	2.14E+05	1.71E+05
21-Oct-59	1.47E+06	2.10E+05	1.68E+05
29-Oct-59	1.53E+06	2.19E+05	1.75E+05
4-Nov-59	1.40E+06	2.00E+05	1.60E+05
12-Nov-59	1.39E+06	1.99E+05	1.59E+05
18-Nov-59	1.33E+06	1.90E+05	1.52E+05
25-Nov-59	1.44E+06	2.06E+05	1.65E+05
1-Dec-59	1.31E+06	1.87E+05	1.50E+05
9-Dec-59	1.29E+06	1.84E+05	1.47E+05
17-Dec-59	1.26E+06	1.79E+05	1.43E+05
22-Dec-59	1.24E+06	1.78E+05	1.42E+05
30-Dec-59	1.18E+06	1.68E+05	1.35E+05

Table A-2 (continued)

Week	Weekly Gal. Effluent Water to TA-03	Daily Average Sewage Effluent to Power Plant (gal.)	Daily Average Estimated Blowdown from Power Plant (gal.)
6-Jan-60	1.19E+06	1.69E+05	1.35E+05
20-Jan-60	1.18E+06	1.69E+05	1.35E+05
3-Feb-60	1.24E+06	1.78E+05	1.42E+05
9-Feb-60	1.22E+06	1.74E+05	1.39E+05
18-Feb-60	1.17E+06	1.68E+05	1.34E+05
23-Feb-60	1.23E+06	1.76E+05	1.41E+05
3-Mar-60	2.23E+06	3.19E+05	2.55E+05
10-Mar-60	1.25E+06	1.79E+05	1.43E+05
17-Mar-60	1.28E+06	1.83E+05	1.47E+05
23-Mar-60	1.51E+06	2.16E+05	1.73E+05
31-Mar-60	1.10E+06	1.57E+05	1.26E+05
6-Apr-60	1.56E+06	2.23E+05	1.78E+05
14-Apr-60	1.63E+06	2.32E+05	1.86E+05
21-Apr-60	1.61E+06	2.29E+05	1.84E+05
28-Apr-60	1.65E+06	2.36E+05	1.89E+05
	Average (gal./d)	2.15E+05	1.72E+05
	Std Dev (gal./d) = 17%	36565.6737	2.93E+04
	Max (gal./d)	3.19E+05	2.55E+05
	Min (gal./d)	1.57E+05	1.26E+05
	Median (gal./d)		1.71E+05

Source: (Zia Company 1959-1960, 098051)

*Print in original record is blurred. Values in this table are best estimates of recorded values.

Appendix B

Surface Water Balance

B-1.0 INTRODUCTION

This appendix summarizes results from the investigations of potential surface water loss in Sandia Canyon that were conducted as part of the implementation of the "Addendum to the Work Plan for Sandia Canyon and Cañada del Buey" (LANL 2007, 095060, p. 3), which was approved by the New Mexico Environment Department (NMED) (NMED 2007, 095486). This expands on work conducted under the "Interim Measures Work Plan for Chromium Contamination in Groundwater" (LANL 2006, 091987) and previously reported in the "Interim Measures Investigation Report for Chromium Contamination in Groundwater" (LANL 2006, 094431), revising the conceptual model of surface water loss presented therein.

Investigations focused on potential water loss in three areas with perennial or common surface water supplied from effluent discharges: (1) the approximately 0.6 km (0.4 mi) long Sandia wetland, Reach S-2, between the confluence of the south fork and the north fork of Sandia Canyon (gaging stations E121 and E122, respectively) and the east end of the wetland (gaging station E123) (Katzman 2000, 064349); (2) an approximately 0.9 km (0.6 mi) section of canyon east of the wetland, between gaging stations E123 and D123.6; and (3) an approximately 2.6 km (1.6 mi) section of canyon between gaging stations D123.6 and D123.8. Gaging station locations are shown in Figures B-1 and Figure 1.0-1 of this report.

The Sandia wetland is located in a broad, relatively low gradient area that is upcanyon of exposures of resistant unit Qbt 2 of the Bandelier Tuff (Gardner et al. 1999, 063492). The nonwelded lower part of unit Qbt 3 probably underlies most of the wetland, and down-to-the-west splays of the Rendija Canyon fault also cross Sandia Canyon in this area. The second downcanyon investigation area is steeper and has a narrower canyon bottom where the stream incises through the most welded upper part of unit Qbt 2. The third downcanyon investigation area also has a narrow canyon bottom, and the stream here incises through the less-welded lower part of Qbt 2 and the nonwelded underlying units Qbt 1v and Qbt 1g (Gardner et al. 1999, 063492; Lavine et al. 2003, 092527). Drainage areas are 234 acres (0.95 km^2), 358 acres (1.45 km^2), and 824 acres (3.33 km^2), respectively, above the lower ends of the three investigation areas.

Gaging station D123.6 is a new station installed in 2007 to evaluate if water loss was occurring into fractures in the welded part of unit Qbt 2 east of the wetland. D123.6 consists of a portable 6-in. Parshall flume and is shown in Figure B-2. Water level (stage) in the Parshall flume was recorded with a Milltronics ultrasonic level monitor between July 18 and August 26, 2007, (Table B-1). The accuracy of Parshall flumes is ±3% (Dodge 1990, 094146, p. 3).

Parshall flumes were also used extensively in 2007 to improve the quality of discharge measurements at other gaging stations in Sandia Canyon. Rating curves at the preexisting upcanyon stations (E121, E122, and E123) were all checked or refined using Parshall flumes, and the eastern station in this investigation from 2006, D123.8 (formerly D123.5 in LANL 2006, 094431), was replaced with a Parshall flume. The evaluation of surface water hydrology in upper Sandia Canyon was also improved by the use of three additional precipitation stations installed in 2007 (Figure B-1): E121.9 (start date of May 2), E196 (start date of May 1), and E200.5 (start date of August 2).

Comparison of available outfall data with discharge data immediately below the wetland, at D123 or E123, from summer 2007 indicates a net surface water loss through the wetland, which is consistent with the observations from 2006 (LANL 2006, 094431, pp. 11-12). However, examination of the discharge record at the new downstream station, D123.6, yielded unexpected results. Whereas it was expected that there would be either no loss or small losses into welded unit Qbt 2, discharge records from July 26 to August 26, 2007, consistently indicate a net gain between the wetland and D123.6. Figures B-3 and B-4

are example hydrographs from intervals within this period, showing the higher baseflow at D123.6. A hypothesis to explain this net gain is that some of the water that infiltrated the lower nonwelded part of unit Qbt 3 in the wetland entered fractures in underlying Qbt 2 and moved laterally downgradient, emerging in the stream channel between E123 and D123.6. Comparison of discharge upgradient of the wetland with that at D123.6 during this period shows that the total daily flow at D123.6 is less than at the outfalls, indicating that only some of the water infiltrating into bedrock beneath the wetland reemerges before D123.6. The remainder of the wetland losses, above that attributable to evapotranspiration (ET), are inferred to represent infiltration into deeper bedrock units.

Estimated net daily losses between the outfalls and D123.6 on select days in summer 2007 are shown in Table B-2. Days were chosen when discharge at both stations was considered to be reliable and not significantly affected by precipitation events. The difference between average daily discharge at these stations, subtracting ET, is assumed to approximate loss into deeper bedrock. Equivalent annual loss using these daily data ranges from 0 to 51 acre-ft/yr, averaging 21 ± 18 acre-ft/yr. This average is considered to represent a lower bound for actual annual losses into deeper bedrock because ET should only be significant during the growing season, mid-March to mid-November. An upper bound for annual losses of approximately 46 acre-ft/yr can be estimated by assuming no ET from mid-November to mid-March and considering the uncertainty in daily loss (0.03 ± 0.02 cubic feet per second [cfs], or an upper estimate of 0.05 cfs).

Comparison of discharge records at D123.6 and D123.8 consistently indicate net loss downstream through this canyon segment in summer 2007, which was expected based on the data from 2006 (LANL 2006, 094431, p. 12). Hydrographs from D123, D123.6, and D123.8 for 1 day are shown in Figure B-5 as an example. One difference between 2006 and 2007 is that there was continuous flow past D123.8 in 2006, whereas in July 2007 flow was discontinuous; however, by August 2007 surface flow was again continuous past D123.8. This difference indicates complete infiltration into alluvium and underlying bedrock upstream of D123.8 under baseflow conditions early in the summer, and saturation of the alluvium later in the summer. It is notable that outfall discharges in 2007 were significantly less than in 2006 (Table B-3), consistent with the greater downcanyon extent of saturation and continuous stream flow in 2006.

Estimated net daily surface water losses between the D123.6 and D123.8 on select days in summer 2007 are shown in Table B-4. Days were chosen when discharge at both stations was considered to be reliable and not significantly affected by precipitation events. Total loss from alluvium into bedrock between D123.6 and D123.8 for these days averages 110 acre-ft/yr, which is considered to be a lower bound because of the reduced outfall discharges in 2007 relative to 2006. The maximum result from the days shown in Table B-4, 210 acre-ft/yr, is considered to represent a reasonable upper bound for losses between these gaging stations.

Flow is ephemeral at the next downcanyon gaging station, E124 (Shaull et al. 2006, 093735), located approximately 0.9 km (0.6 mi) downcanyon from E123.8, and indicates complete infiltration of the remaining effluent into alluvium in this reach. Only stormwater, estimated as about 19% of the total flow in water year 2006 (October 2005 to September 2006), based on data from E123, extends downcanyon past E124 in some events.

B-2.0 REFERENCES

The following list includes all documents cited in this appendix. Parenthetical information following each reference provides the author(s), publication date, and ER ID number. This information is also included in text citations. ER ID numbers are assigned by the Environmental Programs Directorate's Records Processing Facility (RPF) and are used to locate the document at the RPF and, where applicable, in the master reference set.

Copies of the master reference set are maintained at the NMED Hazardous Waste Bureau; the U.S. Department of Energy–Los Alamos Site Office; the U.S. Environmental Protection Agency, Region 6; and the Directorate. The set was developed to ensure that the administrative authority has all material needed to review this document, and it is updated with every document submitted to the administrative authority. Documents previously submitted to the administrative authority are not included.

Dodge, R.A., February 1990. "Effects of Mountain Stream Topography on the Accuracy of Small Parshall Flumes," U.S. Department of the Interior Bureau of Reclamation report R-90-03, Denver, Colorado. (Dodge 1990, 094146)

Gardner, J.N., A. Lavine, G. WoldeGabriel, D. Krier, J., D.T. Vaniman, F.A. Caporuscio, C.J. Lewis, M.R. Reneau, E.C. Kluk, and M.J. Snow, March 1999. "Structural Geology of the Northwestern Portion of Los Alamos National Laboratory, Rio Grande Rift, New Mexico: Implications for Seismic Surface Rupture Potential from TA-3 to TA-55," Los Alamos National Laboratory report LA-13589-MS, Los Alamos, New Mexico. (Gardner et al. 1999, 063492)

Katzman, D., February 2000. "Summary Status of Environmental Restoration Project Investigations in Upper Sandia Canyon," Los Alamos National Laboratory document LA-UR-00-777, Los Alamos, New Mexico. (Katzman 2000, 064349)

LANL (Los Alamos National Laboratory), March 2006. "Interim Measures Work Plan for Chromium Contamination in Groundwater," Los Alamos National Laboratory document LA-UR-06-1961, Los Alamos, New Mexico. (LANL 2006, 091987)

LANL (Los Alamos National Laboratory), November 2006. "Interim Measures Investigation Report for Chromium Contamination in Groundwater," Los Alamos National Laboratory document LA-UR-06-8372, Los Alamos, New Mexico. (LANL 2006, 094431)

LANL (Los Alamos National Laboratory), January 30, 2007. "Submittal of the Addendum to the Work Plan for Sandia Canyon and Cañada del Buey," Los Alamos National Laboratory letter (EP-2007-0059) to J.P. Bearzi from A. Phelps (LANL) and D. Gregory (DOE-LASO), Los Alamos, New Mexico. (LANL 2007, 095060)

Lavine, A., C.J. Lewis, D.K. Katcher, J.N. Gardner, and J. Wilson, June 2003. "Geology of the North-central to Northeastern Portion of Los Alamos National Laboratory, New Mexico," Los Alamos National Laboratory report LA-14043-MS, Los Alamos, New Mexico. (Lavine et al. 2003, 092527)

NMED (New Mexico Environment Department), March 5, 2007. "Approval with Direction for the Addendum to the Work Plan for Sandia Canyon and Cañada del Buey," New Mexico Environment Department letter to D. Gregory (DOE LASO) and D. McInroy (LANL) from J.P. Bearzi (NMED-HWB), Santa Fe, New Mexico. (NMED 2007, 095486)

Shaull, D.A., D. Ortiz, M.R. Alexander, and R.P. Romero, May 2006. "Surface Water Data at Los Alamos National Laboratory: 2005 Water Year," Los Alamos National Laboratory report LA-14239-PR, Los Alamos, New Mexico. (Shaull et al. 2006, 093735)

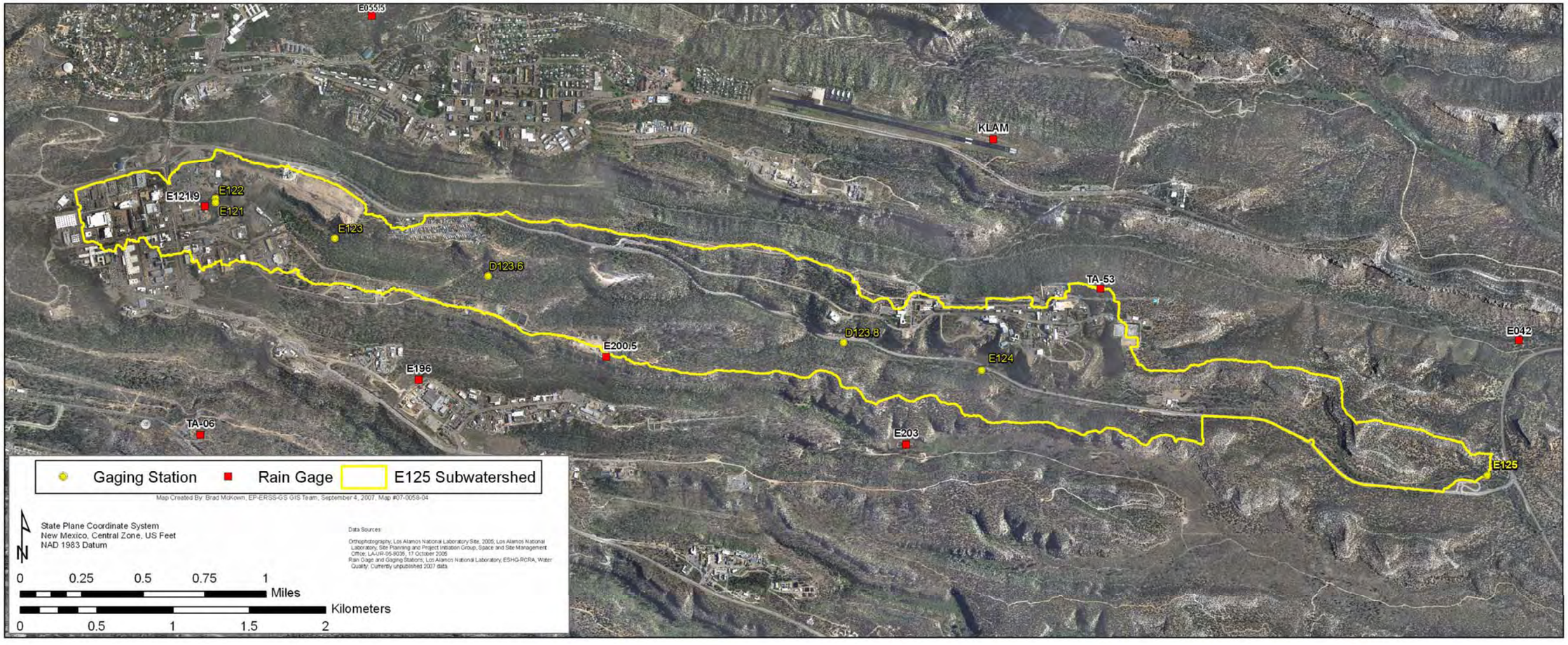

Figure B-1 Orthophotograph of Sandia Canyon on Laboratory land showing locations of gaging stations and precipitation stations used in this appendix and the extent of the drainage basin upcanyon from gaging station E125

Figure B-2 Photograph of gaging station D123.6, a portable Parshall flume, looking upstream

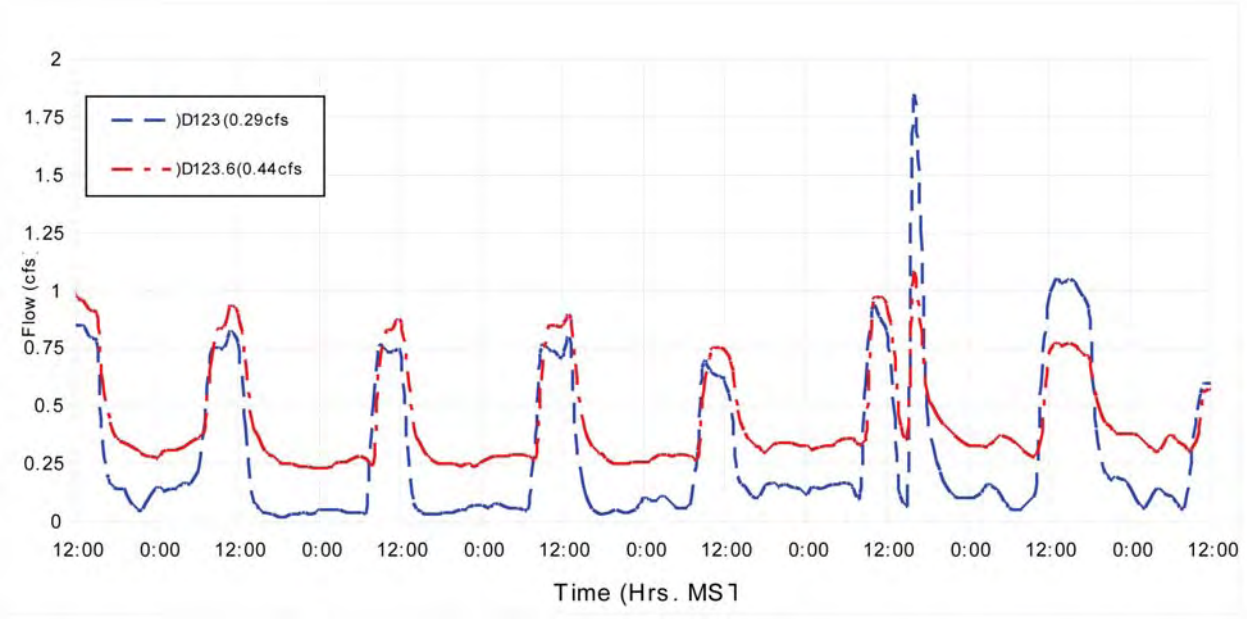

Figure B-3 **Hydrographs from gaging stations D123 and D123.6 from noon 8/8/07 to noon 8/14/07; time of D123.6 hydrograph shifted by 1 hr to better show relationship with D123; average daily discharge shown in parentheses.**

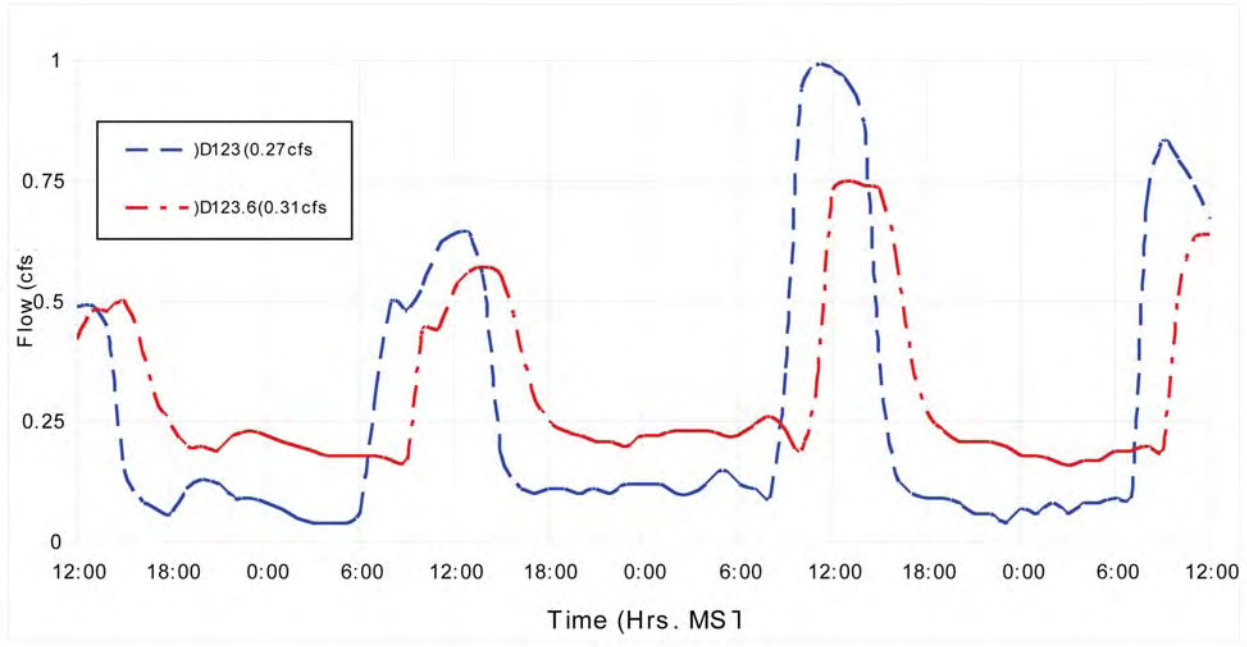

Figure B-4 **Hydrographs from gaging stations D123 and D123.6 from noon 8/20/07 to noon 8/24/07; average daily discharge shown in parentheses**

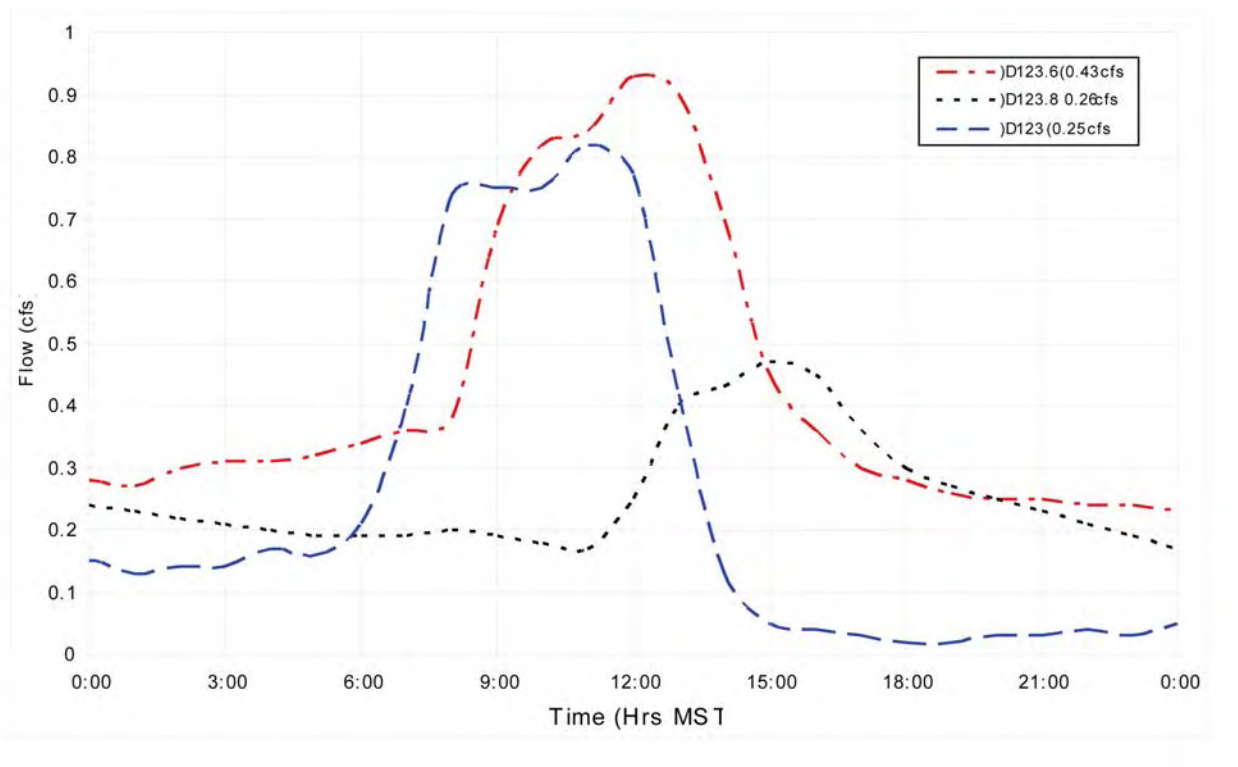

Figure B-5 **Hydrographs from gaging stations D123, D123.6, and D123.8 on 8/8/07; average daily discharge shown in parentheses**

Table B-1
Field Data Collection at Temporary Gaging Stations in Sandia Canyon, 2007

Gaging Station[a]	Period of Record	Number of Missing Days	Comments
D123.6	July 18 - August 26 (39 d)	8 – no data 7 – partial[b] record 1 – poor[c] data	Stormwater runoff impacts to flume affect completeness of record
D123.8	July 20 - August 26 (37 d)	5 – no data 5 – partial record 8 – poor data	Stormwater runoff impacts to flume affect completeness of record; difficult to maintain installation integrity
D123	August 7 - August 26 (19 d)	5 – no data 6 – partial record	Equipment (logger) malfunctions affect completeness of record[d]

[a] To guarantee low flow accuracy, 6-in. Parshall flumes were used with a maximum useable stage of 1.75 ft (~4.6 cfs). During five or more stormwater events, the temporary flumes below E123 were overtopped and needed either maintenance or reinstallation to provide accurate data.

[b] Less than 24 hr of recorded values.

[c] Data quality such that if/when data are used, some estimated adjustments are necessary.

[d] Equipment problems also resulted in some data gaps at stations E121 and E123.

Table B-2
Estimated Losses between Outfalls and Gaging Station D123.6 for Select Days in Summer 2007

Date	Estimated Average Daily Discharge from Outfalls (cfs)	Estimated Average Daily Discharge at D123.6 (cfs)	Estimated Daily Loss to ET (cfs)[a]	Estimated Net Loss to Bedrock Between Outfalls and D123.6 (cfs)[b]	Equivalent Annual Loss Rate (acre-ft/yr)[c]
July 25	0.41	0.29	0.05	0.07	51
July 27	0.33	0.29	0.05	0	0
July 28	0.36	0.29	0.05	0.02	14
July 29	0.40	0.32	0.05	0.03	22
August 8	0.37	0.43	0.04	0	0
August 21	0.37	0.29	0.04	0.04	29
August 23	0.36	0.28	0.04	0.04	29
Average	**0.37**	**0.31**	**0.04**[d]	**0.03 ± 0.02**	**21 ± 18**

[a] ET based on monthly evaporation pan data from Santa Fe (downloaded from http://weather.nmsu.edu/Pan_Evaporation/santa_fe_evap.htm) and assumption that ET is 70% of pan evaporation (LANL 2006, 094431, p. 11).

[b] Negative values replaced by zero.

[c] Daily loss extended to 365 days; average daily loss in cfs x 1.984 = average daily loss in acre-ft.

[d] Average from mid-March to mid-November.

Table B-3
Outfall Discharges into Upper Sandia Canyon, Water Years 2006 and 2007

Month	Monthly Discharge, 2006 (acre-ft)	Monthly Discharge, 2007 (acre-ft)	Difference (WY 2007 –2006) (acre-ft)	Average Daily Discharge, 2006 (cfs)	Average Daily Discharge, 2007 (cfs)
October	36.6	35.8	-0.8	0.60	0.60
November	32.2	34.4	2.2	0.54	0.56
December	35.3	30.6	-4.7	0.57	0.50
January	39.3	34.6	-4.7	0.64	0.56
February	31.8	28.5	-3.3	0.57	0.51
March	38.4	32.0	-6.4	0.62	0.52
April	33.1	28.2	-5.0	0.56	0.54
May	34.4	28.9	-5.4	0.56	0.47
June	33.6	21.5	-12.1	0.56	0.36
July	36.5	21.0	-15.5	0.59	0.34
August	40.4	25.6	14.8	0.66	0.42
September	34.4	n/a*	n/a	0.56	n/a

* n/a = not available

Table B-4
Estimated Surface Water Losses Between Gaging Stations D123.6 and D123.8 for Select Days in Summer 2007

Date	Average Daily Discharge at D123.6 (cfs)	Average Daily Discharge at D123.8 (cfs)	Average Daily Surface Water Loss between D123.6 and D123.8 (cfs)	Equivalent Annual Loss Rate (acre-ft/year)[a]
July 23–24	0.22	0.01	-0.21	152
July 25	0.29	0.01	-0.23	164
July 26	0.36	0.02	-0.29	210
August 8	0.43	0.26	-0.17	123
August 9	0.37	0.21[b]	-0.16	116
August 10	0.41	0.22[b]	-0.19	138
August 11	0.39	0.22[b]	-0.17	123
August 23	0.28	0.16	-0.12	87
August 24	0.58	0.51	-0.07	51
August 25	0.34	0.23	-0.11	80
August 26	0.91	0.84	-0.07	51
August 27	0.54	0.53	-0.01	7
August 28	0.34	0.16	-0.18	130
Average	**0.42**	**0.26**	**-0.15**	**110**

[a] Daily loss extended to 365 days; average daily loss in cfs x 1.984 = average daily loss in acre-ft.

[b] Estimated value.

Appendix C

Chromium Isotope Investigation

C-1.0 INTRODUCTION

Samples of surface water in Mortandad and Sandia Canyons and groundwater beneath Sandia, Mortandad, Los Alamos Canyons, and Cañada del Buey were collected and analyzed for stable isotopes of chromium (Cr) (^{52}Cr and ^{53}Cr, δ^{53}Cr). The purpose of this special sampling is to test a hypothesis of possible fractionation of Cr(VI) to Cr(III) due to reduction along surface water and groundwater flow paths. Stable isotopes of Cr may provide quantitative information on biological and/or chemical conditions that control the extent of Cr(VI) reduction in surface and subsurface environments. Key reductants include solid organic matter (SOM) (especially abundant in the Sandia Canyon wetland) and ferrous iron [Fe(II)] concentrated in reactive minerals and glass, which is particularly abundant at depth within the Cerros del Rio basalt. Analyses of δ^{53}Cr in water samples should enhance the geochemical conceptual model for chromium, including reduction of Cr(VI), followed by adsorption of Cr(III) onto ferric (oxy)hydroxide, and precipitation of insoluble $Cr(OH)_3$.

C-2.0 CHROMIUM ISOTOPE FRACTIONATION

Chromium has four stable isotopes, ^{50}Cr (4.35%), ^{52}Cr (83.8%), ^{53}Cr (9.50%), and ^{54}Cr (2.37%). Ratios of ^{53}Cr to ^{52}Cr have been demonstrated to reflect the degree of reduction of dissolved Cr(VI) to Cr(III) along surface water and groundwater flow paths (Ellis et al. 2002, 098081; Kitchen et al. 2004, 098088; Sikora et al. 2004, 098101). During both abiotic and biotic reduction of Cr(VI) to Cr(III), there is a kinetic isotope effect in which the lighter isotope, ^{52}Cr, reacts preferentially, leaving the remaining dissolved Cr(VI) pool enriched in the heavier isotope, ^{53}Cr.

This process is represented mathematically as follows (Ellis et al. 2002, 098081):

Equation C-1

$$\delta^{53}Cr=[(\delta^{53}Cr_{ini} + 10^3)f^{(\alpha-1)}]-10^3$$

where: δ^{53}Cr is the isotopic composition of the residual dissolved Cr(VI) pool and f is the fraction of Cr(VI) remaining.

In Equation C-1, alpha(α) is the instantaneous fractionation factor, and a range of values from 0.9953 (i.e., an instantaneous fractionation of 4.7‰) to 0.9974 (i.e., an instantaneous fractionation of 2.6‰), depending on the mechanism of reduction (Ellis et al. 2002, 098081; Kitchen et al. 2004, 098088; Sikora et al. 2004, 098101). The isotopic fractionation factor for oxidation of Cr(III) to Cr(VI), typically accompanying the reduction of manganese(IV) oxides, is not well understood, but there may be some isotopic fractionation (Bain and Bullen 2004, 098074). Fractionation factors for other potential oxidizing agents including nitrate and dissolved oxygen, are also unknown. Chromium isotopes are not fractionated significantly by adsorption processes (Ellis et al. 2004, 098086).

$\delta^{53}Cr_{ini}$ is the initial Cr isotope composition of the dissolved chromate before reduction. Ellis et al. (2002, 098081) have suggested that most industrial sources of chromium have δ^{53}Cr values of approximately 0.3‰, the value assumed herein. This value may not apply to natural background sources of chromate at Los Alamos, New Mexico. The isotopic composition of background chromate may vary depending on the amount of Cr oxidation for which fractionation factors are poorly constrained (Bain and Bullen 2004, 098074) relative to Cr(VI) reduction occurring in perched intermediate zones and different parts of the regional aquifer. Before any reduction of Cr(VI), f will be equal to 0, and δ^{53}Cr will be equal to $\delta^{53}Cr_{ini}$.

The delta (δ) notation is as follows:

Equation C-2

$$\delta^{53}Cr = \{[(^{53}Cr/^{52}Cr_{sample})/(^{53}Cr/^{52}Cr_{standard})-1)]*1000\},$$

in units of per mil (‰) or parts per thousand.

The standard used in this study was National Institute of Standards and Technology (NIST) SRM 979, a chromium nitrate compound sold by the NIST as an isotopic standard.

C-3.0 SAMPLE COLLECTION AND PRESERVATION

A total of 32 surface water samples and groundwater samples were collected in 1-L high-density polypropylene bottles for Cr isotope analyses. The nonacidified samples were filtered through 0.45-micrometer membranes. The chromium isotope analyses were conducted at the University of Illinois, Department of Geology.

C-4.0 SAMPLE PREPARATION

The sample preparation process consisted of purifying Cr and removing interfering elements such as titanium (Ti), vanadium (V), and Fe. A measured amount of the $^{50}Cr+^{54}Cr$ double isotope spike solution (explained below) was added and thoroughly mixed with an aliquot of the water. Chromium(VI) was separated from the sample matrix and purified using an anion exchange process. Chromium(VI) was adsorbed onto an anion exchange resin, sample matrix species were rinsed from the resin with hydrochloric acid, the Cr was converted to Cr(III) form, and Cr(III) was eluted from the resin.

With most of the samples containing less than 30 μg/L of Cr, some Fe was not fully separated from Cr in the purification process described above. It is possible that the Fe occurred as complex ions bound to dissolved and suspended organic species. Excessive Fe was removed using a second ion exchange step in which Fe was adsorbed onto anion exchange resin as $FeCl_4^-$ and Cr passed through.

C-4.1 Double Isotope Spike

Multicollector inductively coupled plasma-mass spectrometer (ICP-MS) instruments impart a large bias to the measured ratios; measured $^{53}Cr/52Cr$ ratios differ from true ratios by approximately 3%. This measurement bias was determined precisely and corrected for using the double isotope spike approach. A solution containing ^{50}Cr and ^{54}Cr in a known ratio was added to each sample and mixed thoroughly with it. When the sample-spike mixture was analyzed, the measured $^{50}Cr/^{54}Cr$ ratio was used to determine the measurement bias. The measured $^{53}Cr/^{52}Cr$ was then corrected for this bias. Any isotopic fractionation that occurred during sample preparation after addition of the double spike was corrected for as part of the overall bias. More detail about the double spike approach can be found in recent publications (Beard and Johnson 1999, 098076; Johnson et al. 1999, 098087) and references therein.

C-4.2 Mass Spectrometry

Isotopic ratios for Cr were determined using a Nu Plasma HR multicollector ICP-MS. The argon (Ar)-based inductively coupled plasma generates ArC+, ArN+ and ArO+ ions with masses close to, but slightly greater than, those of ^{52}Cr, ^{53}Cr, ^{54}Cr, and ^{56}Fe. The instrument is operated in a high-resolution mode that allows measurement of ^{50}Cr, ^{52}Cr, ^{53}Cr, ^{54}Cr, and ^{56}Fe while excluding ArC+, ArN+, and ArO+. Interferences from ^{54}Fe, ^{50}Ti, and ^{50}V were corrected for by measuring ^{56}Fe, ^{49}Ti, and ^{51}V; calculating the ^{54}Fe, ^{50}Ti, and ^{50}V interference intensities using natural $^{54}Fe/^{56}Fe$, $^{50}Ti/^{49}Ti$, and $^{50}V/^{51}V$ ratios; and subtracting the calculated interference intensities from the measured Cr isotope intensities. A thoroughly

tested calculation routine was used to correct for interferences, determine the instrumental bias, mathematically subtract the double spike Cr from the sample Cr, and calculate a final $^{53}Cr/^{52}Cr$ result.

Because the measured changes in the $^{53}Cr/^{52}Cr$ ratios are small (<1%), the isotopic composition is reported in δ notation. $\delta^{53}Cr$ expresses the parts-per-thousand (per mil or ‰) deviation of a measured isotope ratio relative to the NIST SRM 979 standard (see Equation C-2).

C-4.3 Quality Control and Uncertainty of Method

Standard solutions were run through the sample preparation procedure along with batches of samples. The results from these four prepared standards all differed from unprocessed standards by less than 0.1‰ and show no statistically significant offset from unprocessed standards. Ten samples were prepared in duplicate. Offsets between results of the duplicate pairs were always less than 0.2‰. The root-mean-square difference for all the pairs was 0.08‰.

C-5.0 ANALYTICAL STATUS

Table C-1 provides a summary of the Cr isotope analytical results received to date. Several samples were not analyzed because of the presence of dissolved organic carbon (DOC) and Fe, rendering the samples difficult to analyze. These samples were collected from Mortandad Canyon below Effluent Canyon, MCO-0.6, MCO-4B, and MCO-5. Additionally, because of low concentrations of Cr(VI), the samples could not be analyzed using this method. Additional sample collection and analysis will be conducted under ongoing monitoring in the Sandia and Mortandad Watersheds and reported in the Sandia Canyon investigation report, due to the New Mexico Environment Department (NMED) in December 2008.

C-6.0 RESULTS AND DISCUSSION

The analytical results provided in Table C-1 are listed by watershed, generally organized from upgradient to downgradient along the flow path within intermediate zones (MCOI-5 and MCOI-6) and the regional aquifer (R-10, R-10a, R-11, R-13, R-14, R-15, R-16r, R-28, R-33, and R-34). Well MCO-7.5 is completed within the alluvium in Mortandad Canyon. The fraction of Cr(VI) reduced versus $\delta^{53}Cr$ values is shown in Figure C-1.

The $\delta^{53}Cr$ values in surface water samples collected in Sandia Canyon are variable, depending on the extent to which Cr(VI) reacts with SOM present within the wetland. Surface water at the eastern end of the Sandia Canyon wetland (gaging station E-123) shows some evidence of Cr(VI) reduction, based on a $\delta^{53}Cr$ value of 1.43‰ (Table C-1). A surface water sample collected farther to the east at the terminus of persistent baseflow in Sandia Canyon, however, shows no evidence of Cr(VI) to Cr(III) reduction, based on a $\delta^{53}Cr$ value of 0.3‰ (Table C-1 and Figure C-1). It is possible that this water did not significantly react with SOM within the Sandia Canyon wetland. Surface water at E-123.4 has a $\delta^{53}Cr$ value of 1.59‰ (Table C-1), indicating a Cr(VI) reduction of approximately 31% (Figure C-1). Reoxidation of Cr(III) to Cr(VI) in surface water east of the wetland is potentially viable in the presence of dissolved oxygen and manganese(IV) solids under turbulent flow conditions.

A groundwater sample collected at alluvial well MCO-7.5 in Mortandad Canyon shows approximately 28% reduction of Cr(VI) (Figure C-1) with a corresponding $\delta^{53}Cr$ value of 1.47‰ (Table C-1). Solid organic matter present within the alluvium in Sandia and Mortandad Canyons is believed to be the most important reductant enhancing partial reduction of Cr(VI).

Alluvial groundwater provides recharge to perched-intermediate zones within the Puye Formation and Cerros del Rio basalt. Groundwater samples collected from perched intermediate wells MCOI-5 and MCOI-6, completed in the Cerros del Rio basalt, have δ^{53}Cr values of 2.93 and 1.60‰, respectively (Table C-1). These two samples are indicative of the highest degree of Cr(VI) reduction, with the sample collected from MCOI-5 exceeding 50% (Figure C-1). It is hypothesized that Fe(II) within the Cerros del Rio basalt is an important reductant for Cr(VI) at these locations. The net reduction of Cr(VI) observed at MCOI-5 and MCOI-6 is probably the sum of reduction occurring in the alluvial system and in the Cerros del Rio basalt along groundwater flow paths recharging the perched-intermediate zones.

Several regional aquifer wells, including R-16r, R-1, R-10, R-13, and R-34, currently show background concentrations of total dissolved Cr. Reduction of Cr(VI) to Cr(III) under natural, background conditions within the regional aquifer is plausible in the presence of magnetite, amphiboles, biotite, and pyroxenes. These minerals contain Fe(II), a known reductant for Cr(VI). Under background conditions within the regional aquifer, variability in the amount of Cr(VI) is expected based on varying concentrations of Fe(II) minerals. A groundwater sample collected from R-16r shows only about 12% reduction of naturally occurring Cr(VI) (Figure C-1), with a δ^{53}Cr value of 0.74‰ (Table C-1). A groundwater sample collected from R-1 is characterized by a δ^{53}Cr value of 1.24‰, with a Cr(VI) reduction of approximately 23%. Well R-10, consisting of two screens, shows about 24% and 26% reduction of Cr(VI) with δ^{53}Cr values of 1.26 and 1.37‰, respectively. Well R-13 is characterized by a δ^{53}Cr value of 1‰ and shows approximately 18% reduction of Cr(VI). A groundwater sample collected from R-34 shows about 22% reduction of naturally occurring Cr(VI), with a δ^{53}Cr value of 1.18‰.

Calculated percentage reduction for background locations assumes that natural Cr has a $\delta^{53}Cr_{ini}$ value of 0.3‰, which is similar to that of anthropogenic sources. Natural Cr derived from igneous rock sources is not likely to undergo much fractionation during purification (Ellis et al. 2002, 098081). Moreover, three basalt standards measured by Ellis et al. (2002, 098081) have δ^{53}Cr values close to 0‰. Therefore, assuming little isotope fractionation during oxidation of rock sources of Cr(III) to Cr(VI) in natural systems, both natural and anthropogenic sources of chromate are likely to have similar values, close to 0‰. Oxidation experiments using local aquifer materials need to be carried out to verify this assumption.

Alluvial and perched intermediate groundwater provides recharge to the regional aquifer in Sandia and Mortandad Canyons, based on the occurrence of chromate, perchlorate, nitrate, chloride, sulfate, and/or tritium at regional aquifer wells (LANL 2006, 094161). Mixing of native regional aquifer groundwater with recharge water occurs at varying portions, which would be expected to have significant influence on δ^{53}Cr values of mixed groundwater. Longmire et al. (2007, 096660) have shown that native groundwater in the regional aquifer at R-15 and R-28 is the major fraction mixing with recharge water derived from surface water and alluvial and perched-intermediate groundwater. Mixing processes also influence concentrations of conservative solutes including chloride, tritium, boron, nitrate, perchlorate, and sulfate, in addition to stable isotopes of nitrogen (δ^{15}N), hydrogen (δ^{2}H), and oxygen (δ^{18}O). Therefore, concentrations of Cr(VI) and δ^{53}Cr values are expected to vary along groundwater flow paths within intermediate zones and the regional aquifer as a result of both groundwater mixing and reduction of Cr(VI).

Wells R-11, R-15, and R-28 contain Laboratory-derived contaminants including perchlorate, chromate, tritium, and nitrate (LANL 2006, 094431). Groundwater samples collected at these three wells have δ^{53}Cr values ranging from 1‰ to 1.18‰, which are analytically indistinguishable. Based on the measured δ^{53}Cr values at R-15, R-11, and R-28, additional reduction of Cr(VI) has not taken place to a significant extent (i.e., not greater than 25% reduction; Table C-1). In the case of R-15 and R-11, which contain total dissolved concentrations of Cr of approximately 7 μg/L and 34 μg/L respectively, it is very likely that the measured δ^{53}Cr values result from groundwater mixing. It is possible that a small fraction of reduced Cr(VI) having a heavier δ^{53}Cr value is significantly diluted by groundwater characterized by a lighter δ^{53}Cr

value at the regional water table. Background concentrations of total dissolved Cr within the regional aquifer range from 4 to 6 μg/L (see Table C-1). Mixing, however, is unlikely to be the primary cause for relatively low δ^{53}Cr values in R-28, given that the Cr concentrations are 2 orders of magnitude higher than background. In this case, anthropogenic chromate clearly dominates any mixing that occurs. The relatively low percentage reduction observed at R-28 likely reflects the location of this well screen near the center of mass of a Cr plume. The core of a plume will show less Cr isotopic fractionation and lower percentage of Cr reduction because of the mass of Cr relative to available reductant, much of which may already have been consumed (Ellis et al. 2002, 098081). Significant percentage reduction of Cr(VI) and enrichment of ^{53}Cr is more likely to occur at the edges of plumes. Increased residence time in the presence of reductants will also tend to increase δ^{53}Cr of residual chromate. The δ^{53}Cr value of 1.32‰ at R-10a (Table C-1) indicates approximately 25% reduction of Cr(VI) (Figure C-1).

Groundwater samples collected from screens 1 and 2 at R-33 have δ^{53}Cr values of 1.79 and 1.36‰, respectively. Well R-33 shows about 35% and 26% reduction of Cr(VI) for screens 1 and 2, respectively (Figure C-1). Reduction of Fe(III) solids has taken place at R-33, based on analytical data for dissolved and total Fe (LANL 2007, 096330). Chromium(III) is the dominant form of Cr under Fe-reducing conditions, which is consistent with measured δ^{53}Cr values at the well. Well R 33 is not significantly impacted by residual drilling effects, and analytical results for Cr are considered to be reasonably representative of pre-drilling conditions, excluding Fe reduction (LANL 2007, 096330).

C-7.0 SUMMARY

Surface water in Mortandad and Sandia Canyons and groundwater beneath Sandia, Mortandad, and Los Alamos Canyons, and Cañada del Buey were analyzed for stable isotopes of Cr (δ^{53}Cr) to evaluate isotope fractionation resulting from Cr(VI) reduction. Isotope fractionation of Cr(VI) is occurring to a varying degree within surface and subsurface environments, based on analytical results. The highest δ^{53}Cr values, indicative of the greatest degree of Cr(VI) reduction, appear to be to occurring under the following conditions:

1. where the dissolved mass of Cr(VI) is small relative to the available SOM and reactive Fe(II) in sediments and aquifer material, and

2. when groundwater-travel times are such that Cr(VI) remains in Fe(II)-bearing strata (Cerros del Rio basalt) sufficiently long that a significant portion of the dissolved Cr(VI) pool can be reduced.

The majority of water samples have δ^{53}Cr values indicative of approximately 18% to 26% reduction of Cr(VI) to Cr(III) (Figure C-1). Based on an analytical uncertainty (2σ) of ±0.2‰, this latter group of samples could be considered to have undergone a similar degree of biotic or abiotic reduction. Chromium(VI) reduction is not large at R-11 and R-28, based on low δ^{53}Cr values near or at unity. Concentrations of total dissolved Cr are approximately 30 and 440 μg/L at R-11 and R-28, respectively. Significant reduction of Cr(VI) has occurred along the groundwater flow path(s) to MCOI-5, completed within the Cerros del Rio basalt. Reduction of Cr(VI) likely occurred both within the alluvial system and the Cerros del Rio basalt, based on δ^{53}Cr values of samples collected from MCO-7.5 and MCOI-5.

Groundwater mixing is an important process that influences δ^{53}Cr values of samples collected from intermediate zones and the regional aquifer. Longmire et al. (2007, 096660) have shown that native groundwater in the regional aquifer at R-15 and R-28 is the major fraction mixing with recharge water derived from surface water and alluvial and intermediate groundwater. It is entirely consistent that variation in δ^{53}Cr values in samples collected from different aquifers occurs in Sandia and Mortandad Canyons. Use of chloride and other conservative tracer helps to quantify components contributing to groundwater mixing.

Chromium isotope variation, along with total dissolved Cr concentration data, can be used to define spatial variation of Cr(VI) reduction in contaminant plumes. High dissolved concentrations of Cr coupled with low levels of Cr(VI) reduction at R-28 are suggestive of a location near where Cr might be entering the regional aquifer. At that location, high Cr concentrations in groundwater overwhelm the ability of aquifer solids to reduce much of the Cr(VI).

C-8.0 REFERENCES

The following list includes all documents cited in this appendix. Parenthetical information following each reference provides the author(s), publication date, and ER ID number. This information is also included in text citations. ER ID numbers are assigned by the Environmental Programs Directorate's Records Processing Facility (RPF) and are used to locate the document at the RPF and, where applicable, in the master reference set.

Copies of the master reference set are maintained at the NMED Hazardous Waste Bureau; the U.S. Department of Energy–Los Alamos Site Office; the U.S. Environmental Protection Agency, Region 6; and the Directorate. The set was developed to ensure that the administrative authority has all material needed to review this document, and it is updated with every document submitted to the administrative authority. Documents previously submitted to the administrative authority are not included.

Beard, B.L., and C.M. Johnson 1999. "High Precision Iron Isotope Measurements of Terrestrial and Lunar materials." *Geochim. Cosmochim. Acta* 63: 1653-60 (Beard and Johnson 1999, 098076)

Bain, D.J., and T.D. Bullen, 2004. "Experimental Determination of Isotopic Fractionation of Chromium(III) During Oxidation by Manganese Oxides," *Eos Transactions, American Geophysical Union*, Vol. 85, No. 47, Fall Meeting Supplement, Abstract H42C-03. (Bain and Bullen 2004, 098074)

Beard, B.L., and C.M. Johnson, 1999. "High Precision Iron Isotope Measurements of Terrestrial and Lunar Materials," *Geochimica et Cosmochimica Acta,* Vol. 63, 11/12, pp. 1653-1660. (Beard and Johnson 1999, 098076)

Ellis, A.S., T.M. Johnson, and T.D. Bullen, March 15, 2002. "Chromium Isotopes and the Fate of Hexavalent Chromium in the Environment," *Science,* Vol. 295, pp. 2060-2062. (Ellis et al. 2002, 098081)

Ellis, A.S., T.M. Johnson, and T.D. Bullen, 2004. "Using Chromium Stable Isotope Ratios to Quantify Cr(VI) Reduction: Lack of Sorption Effects," *Environmental Science & Technology,* Vol. 38, No. 13, pp. 3604-3607. (Ellis et al. 2004, 098086)

Johnson, T.M., M.J. Herbel, T.D. Bullen, and P.T. Zawislanski, 1999. "Selenium Isotope Ratios as Indicators of Selenium Sources and Oxyanion Reduction," *Geochimica et Cosmochimica Acta,* Vol. 63, No. 18, pp. 2775-2783. (Johnson et al. 1999, 098087)

Kitchen, J.W., T.M. Johnson, and T.D. Bullen, 2004. "Chromium Stable Isotope Fractionation During Abiotic Reduction of Hexavalent Chromium," *Eos Transactions, American Geophysical Union*, Vol. 85, No. 47, Fall Meeting Supplement, Abstract V51A-0519. (Kitchen et al. 2004, 098088)

LANL (Los Alamos National Laboratory), October 2006. "Mortandad Canyon Investigation Report," Los Alamos National Laboratory document LA-UR-06-6752, Los Alamos, New Mexico. (LANL 2006, 094161)

LANL (Los Alamos National Laboratory), November 2006. "Interim Measures Investigation Report for Chromium Contamination in Groundwater," Los Alamos National Laboratory document LA-UR-06-8372, Los Alamos, New Mexico. (LANL 2006, 094431)

LANL (Los Alamos National Laboratory), May 2007. "Well Screen Analysis Report, Revision 2," Los Alamos National Laboratory document LA-UR-07-2852, Los Alamos, New Mexico. (LANL 2007, 096330)

Longmire, P., M. Dale, D. Counce, A. Manning, T. Larson, K. Granzow, R. Gray, and B. Newman, July 2007. "Radiogenic and Stable Isotope and Hydrogeochemical Investigation of Groundwater, Pajarito Plateau and Surrounding Areas, New Mexico," Los Alamos National Laboratory report LA-14333, Los Alamos, New Mexico. (Longmire et al. 2007, 096660)

Sikora, E.R., T.M. Johnson, and T.D. Bullen, 2004. "Chromium Stable Isotope Fractionation During Bacterial Reduction of Hexavalent Chromium," *Eos Transactions, American Geophysical Union*, Vol. 85, No. 17, Joint Assembly Supplement, Abstract H43E-05. (Sikora et al. 2004, 098101)

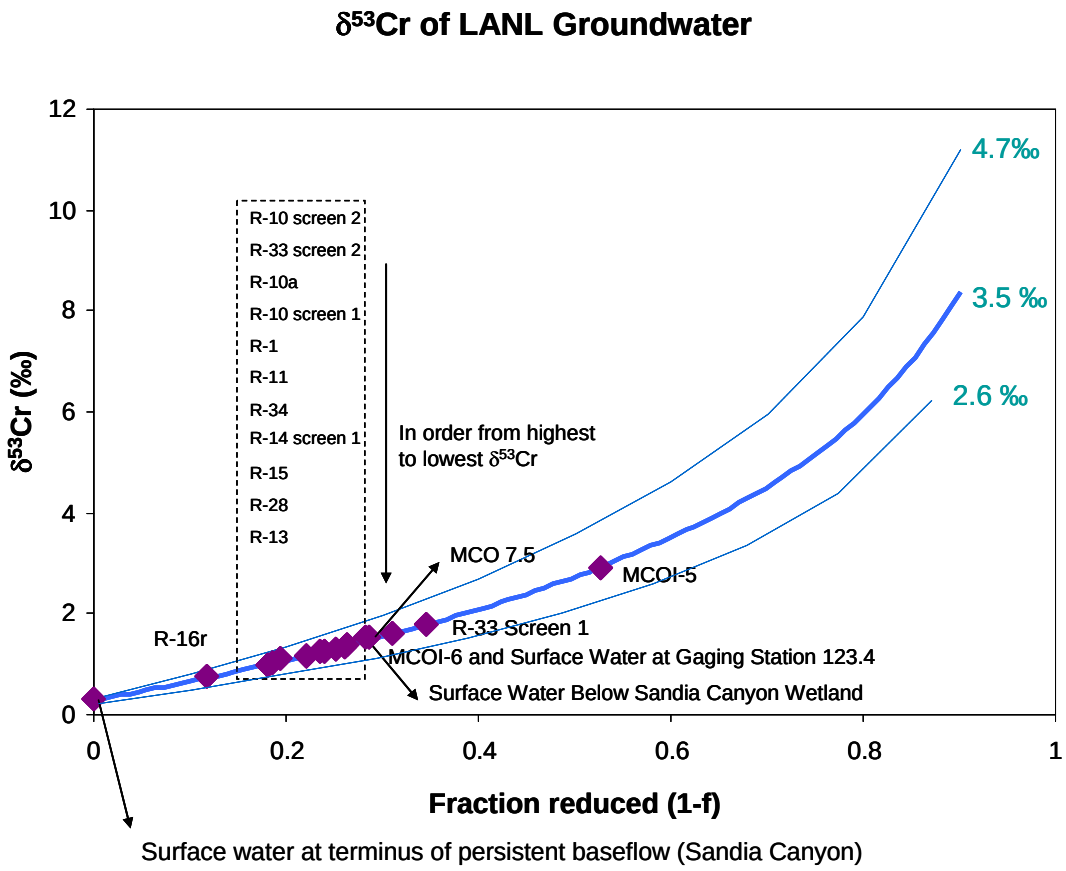

Figure C-1 **Chromium isotope results from Sandia and Mortandad Canyons surface water and groundwater samples for a range of fractionation factors. The solid line is for a fractionation factor of 3.5‰, a typical fractionation factor approximately in the middle of the range of observed abiotic fractionation (Ellis et al. 2002, 098081).**

Table C-1
Chromium Isotope Results from Sandia and Mortandad Canyons and Cañada del Buey Surface Water and Groundwater Samples

Sample ID	Sample Location	Total Dissolved Cr (μg/L)	δ^{53}Cr (‰)	Fraction Remaining (f)*	Fraction Reduced (1-f)[a]
Mortandad Canyon					
UF07020PWF1E01	E-1FW	38.8	NA	Not calculated	Not calculated
UF070200P20001	Surface water[b]	6	NA	Not calculated	Not calculated
UF070200GM0601	MCO-0.6	2.5	NA	Not calculated	Not calculated
UF070200G4BM01	MCO-4B	1.1	NA	Not calculated	Not calculated
UF070200G4BM20	MCO-4B	1.1	NA	Not calculated	Not calculated
UF070200G01R01	R-1	4.6	1.24	0.765	0.235
UF070200G5CM01	MCO-5	1, U	NA	Not calculated	Not calculated
UF070200G57M01	MCO-7.5	2.4	1.47[c]	0.716	0.284
UF07020G14R101	R-14 (screen 1)	2.4	1.11	0.794	0.206
UF07020G14R201	R-14 (screen 2)	No results	NA	Not calculated	Not calculated
UF07020G33R101	R-33 (screen 1)	No results	1.79	0.654	0.346
UF07020G33R201	R-33 (screen 2)	No results	1.36	0.739	0.261
UF070200GMC601	MCOI-6	29.4	1.6	0.690	0.310
UF070200GMC620	MCOI-6	30.3	Pending	Not calculated	Not calculated
UF070200GMC501	MCOI-5	5, U	2.93	0.472	0.528
UF070200G15R01	R-15	7.5	1.02	0.814	0.186
UF070200G28R01	R-28	446	1	0.819	0.181
UF070200G28R20	R-28	425	Pending	Not calculated	Not calculated
UF070200G13R01	R-13	3.8	1	0.819	0.181
UF070200G34R01	R-34	5	1.18	0.779	0.221
Sandia Canyon					
UF070200P12301	Surface water[d]	2.7	1.43	0.724	0.276
UF070200PMSC01	Surface water[e]	7.6	0.3	1	0
UF0702E123.401	Surface water at E-123.4	3.3	1.59	0.692	0.308
UF0702E123.420	Surface water at E-123.4	No results	Pending	Not calculated	Not calculated
UF070200G11R01	R-11	33.2	1.18	0.778	0.222
UF070200G11R20	R-11	34.9	Pending	Not calculated	Not calculated
UF07020GR10A01	R-10a	5.6	1.32	0.747	0.253
UF07020GR10101	R-10 (screen 1)	2.7	1.26	0.760	0.240
UF07020GR10201	R-10 (screen 2)	2.7	1.37	0.737	0.263

Table C-1 (contined)

Sample ID	Sample Location	Total Dissolved Cr (μg/L)	δ^{53}Cr (‰)	Fraction Remaining (f)*	Fraction Reduced (1-f)[a]
Cañada del Buey					
UF07020GR16A01	R-16r	6.3	0.74	0.882	0.118
UF07020GR16A20	R-16r	6.4	Pending	Not calculated	Not calculated

*NA means not analyzed for δ^{53}Cr due to Cr(VI) concentration less than detection and/or iron, particulate, or dissolved organic matter interfering with isotope analysis. U means not detected. Pending means analytical results not received from the University of Illinois. No results mean results from Los Alamos National Laboratory are not available. Fractions of Cr(VI) remaining and reduced were not calculated because δ^{53}Cr were not measured for several samples.

[a] These calculations assume a fractionation factor of 3.5‰ (see Figure C-1).

[b] Surface water in Mortandad Canyon below Effluent Canyon.

[c] Sample from MCO-7.5 has a 2σ error of ±0.5 per mil with the rest of the samples having a 2σ error of ±0.2 per mil.

[d] Surface water below Sandia Canyon wetland.

[e] Surface water at terminus of persistent baseflow in Sandia Canyon.

Appendix D

Conceptual Model Matrix

D-1.0 INTRODUCTION

The main body of this report describes the conceptual model shown in Figure 3.0-1. This appendix describes a new process for specifying the details of the conceptual model as it relates to fate and transport pathways, assumptions that govern contaminant transport, assumptions that relate the conceptual model assumptions to numerical model implementation, and parameters and their uncertainties that control the rates and direction of contaminant transport.

The change in process was to include a wide range of Los Alamos National Laboratory (LANL or the Laboratory) technical experts in open meetings to define pathways, assumptions, and parameters. The goal was not to reach a consensus but to define alternative sets of conceptual models and parameters that reflect the range of possibilities that are consistent with available data. This process was then presented to the Northern New Mexico Citizen's Advisory Board (NNMCAB), the public, and New Mexico Environment Department (NMED) to widen the range of perspectives about how chromium (Cr) contamination could reach and travel in the regional aquifer.

The change in documentation was to use an interaction matrix to capture and communicate the resulting pathways, assumptions, and parameters. This interaction is herein called the Conceptual Model Matrix. The complete interaction matrix for Sandia Canyon is captured in an EXCEL spreadsheet found on the CD included with this report. The EXCEL spreadsheet contains the following worksheets:

1. General Pathways
2. Pathways Assumptions
3. Groundwater Model Assumptions
4. Groundwater Model Justification of Assumptions
5. Model References
6. Parameters

A small segment of the Conceptual Model Matrix is shown in Figure D-1. The matrix is first meant to show all major pathways from the contaminant source to the regional aquifer. Physical media are shown along the diagonal of the matrix (e.g., air, surface water, and groundwater). The off-diagonal terms define the processes by which the contaminant moves between the various media. An interaction matrix is read clockwise. For example, in Figure D-1, one of the processes that moves the contaminant source from plants to the first surface water segment, SW1, is biomass decay. Contaminants can then move from surface water to plants via plant uptake. The media boxes, the diagonals, also contain descriptions of the media (see SW1).

It is important to point out that the interaction matrix is meant to capture all major pathways but not all of these pathways end up in the numerical model of fate and transport. For example, the air to sediment pathway is not explicitly modeled. Instead, contamination on sediments is assumed to wash into surface water and Cr concentrations in surface water are input to the model. The Groundwater Model Assumptions spreadsheet defines how the various pathways and processes are either implicitly or explicitly included in the groundwater model.

A brief summary of the key components of the Conceptual Model Matrix is presented below. Included are descriptions of the pathways, model assumptions adopted, and groundwater model justifications for the fate and transport analysis done for Sandia Canyon due to potential sources released from the

Laboratory. The Conceptual Model Matrix provides lists of parameters for each modeled media and process; however, it does not include the probability distributions used to define plausible parameter values. These distributions are found in the last section of this appendix.

D-2.0 PATHWAYS ASSUMPTIONS FOR THE SANDIA CANYON ANALYSIS

Contaminant Source

The main discharges released into Sandia Canyon came from the cooling towers associated with the Technical Area (TA) 03 power Plant (TA-3-22). The major components of this discharge are CrO_4, MoO_4, PO_4, NO_3, SO_4 and zinc. In addition, Cr was released into Mortandad and Los Alamos Canyons.

The source-air interaction consists of direct releases and resuspension particulates.

The source-surface water interaction occurs within the first segment of the Sandia Canyon (SW1); the assumption for this case is that 100% of the effluent becomes surface water.

Air

Releases of Cr to the air likely settled within about 1 km after being released. At the TA-03 power plant, drift losses constituted about 20% of the Cr releases. These releases were likely to be dispersed fairly uniformly across about a 1-km radius. A fraction of the Cr mass is then assumed to fall onto neighboring mesas and canyons as well as in the Sandia Watershed.

At the Omega West reactor, drift losses were likely deposited into Los Alamos Canyon because of the steep canyon sides.

The air-plant interaction and the air-surface water Segment 1 (SW1) interaction consisted of historical direct depositions. The air-sediment interaction consists in direct deposits.

Vegetation

Biomass uptake and decay process interact with surface water Segment 1, sediments, and alluvial groundwater.

Surface Water

The surface water was divided in four segments (see Figure 1.0-1 in the main body of this report).

- Segment 1: the first segment begins at the source outfall and extends to the eastern edge of the wetland – the E123 gaging station.
- Segment 2: SW2 starts at gaging station E123 and ends at gaging station E123.6.
- Segment 3: this segment starts at gaging station E123.6 and ends at gaging station E123.8.
- Segment 4: this segment starts at gaging station E123.8 and ends at the Rio Grande.

Surface Water Segment 1

This segment is perennial. Sources of surface water and contaminants include direct discharge from the power plant, runoff, and precipitation within the watershed. In the lower portion of this segment surface water flow is spread across the entire valley floor within the wetland; some percentage of surface water is evaporated.

The interactions of this segment with other media are as follows.

- Air
    - ❖ Some percentage of water is evaporated.
- Plants
    - ❖ Uptake of dissolved contaminants from surface water into plants.
- Surface Water Segment 2
    - ❖ Water and soluble contaminants migrate downstream.
    - ❖ Adsorbed contaminants on sediments are transported downstream.
- Sediments
    - ❖ Dissolved phase contaminants infiltrate and variably adsorb onto and react with sediment particles.
    - ❖ Adsorbed phase contaminants are transported in floods and deposited in the channel and on floodplains
- Alluvial groundwater
    - ❖ Surface water infiltrates and recharges alluvium.
    - ❖ Contaminants are transported from surface water to the alluvium depending on their solubility and adsorption characteristic
- Unsaturated zone
    - ❖ Surface water Segment 1 has a thick base of alluvium with alluvial groundwater present.
    - ❖ Direct infiltration of surface water to the unsaturated zone does not occur.

Surface Water Segment 2

This segment is perennial. Additional sources of surface water and contaminants include runoff and precipitation within the watershed. This segment is characterized by thin, discontinuous alluvium over welded tuff in a steep narrow canyon.

The interactions of this segment with other media are as follows.

- Surface water Segment 3
    - ❖ Water and soluble contaminants migrate downstream (to SW3).
    - ❖ Adsorbed contaminants on sediments are transported downstream.
- Sediments
    - ❖ Dissolved-phase contaminants infiltrate and variably adsorb onto and react with sediment particles.
    - ❖ Adsorbed phase contaminants are transported in floods and deposited in the channel and on floodplains.
- Alluvial groundwater
    - ❖ Surface water infiltrates and recharges alluvium.

- ❖ Contaminants are transported from surface water to the alluvium depending on their solubility and adsorption characteristics.

- Unsaturated zone
  - ❖ Some surface water may locally infiltrate and recharge along fractures into the unsaturated zone.
  - ❖ Contaminants may be transported from surface water to the unsaturated zone depending on their solubility and adsorption characteristics.

Surface Water Segment 3

This segment is perennial. Additional sources of surface water and contaminants include runoff and precipitation within the watershed. This segment is characterized by eastward thickening and widening alluvium over nonwelded tuff. The western part of this segment may have discontinuous alluvium in the steep and narrow part of the canyon.

The interactions of this segment with other media are as follows.

- Surface water Segment 4
  - ❖ Water and soluble contaminants migrate downstream (to SW4).
  - ❖ Adsorbed contaminants on sediments are transported downstream.
- Sediments
  - ❖ Dissolved phase contaminants infiltrate and variably adsorb onto and react with sediment particles.
  - ❖ Adsorbed phase contaminants are transported in floods and deposited in the channel and on floodplains.
- Alluvial groundwater
  - ❖ Surface water infiltrates and recharges alluvium.
  - ❖ Contaminants are transported from surface water to the alluvium as functions of solubility and adsorption.
- Unsaturated zone
  - ❖ Some surface water may locally infiltrate and recharge along fractures and/or into the rock matrix of the unsaturated zone.
  - ❖ Contaminants could be transported from surface water to the unsaturated zone depending on their solubility and adsorption characteristics.

Surface Water Segment 4

This segment is ephemeral. This segment includes continuous alluvium of variable thickness to gaging station 125, locally discontinuous alluvium to the major canyon pour off, and variable thick alluvium from the pour off to the Rio Grande. The source of surface water and contamination is runoff.

The interactions of this segment with other media are as follows.

- Sediments
    - ❖ Dissolved phase contaminants infiltrate and variably adsorb onto and react with sediment particles.
    - ❖ Adsorbed phase contaminants are transported in floods and deposited in the channel and on floodplains.
- Alluvial groundwater
    - ❖ Surface water infiltrates and recharges alluvium.
    - ❖ Contaminants are transported from surface water to the alluvium depending on their solubility and adsorption characteristics.
- Unsaturated zone
    - ❖ Some surface water may locally infiltrate and recharge along fractures and/or into the rock matrix of the unsaturated zone.
    - ❖ Contaminants may be transported from surface water to the unsaturated zone depending on their solubility and adsorption characteristics.

Sediment

Sediment includes secondary phases such as organic matter and iron oxides.

Sediment deposits in the canyon bottom act as a storage medium for soluble and adsorbed contaminants.

The geochemical environment in the sediments affects contaminant speciation and mobility

The sediment interactions with other media include the following.

- The sediment interacts with the air via eolian transport of contaminated particles.
- The sediment/plant interaction is through uptake of dissolved contaminants from soil moisture.
- The sediment/surface water interaction in all the segments is due to the storm runoff that erodes stream banks and floodplains thereby mobilizing contaminants.
- The sediment/alluvium interaction consists of flood water infiltration and fluctuating alluvial groundwater levels that can mobilize contaminants.

Alluvial Groundwater

Soluble contaminants migrate downgradient. The geochemical environment in the alluvial groundwater affects contaminant speciation and mobility. Some percentage of the alluvial groundwater is evapotranspired.

Interactions of the alluvial water with other media include the following.

- Air
    - ❖ Water could evaporate from alluvial groundwater to air but would not contain contaminants of interest.

- Plants
    - ❖ The uptake process is the main process for mobilizing contaminants.
- Surface water Segment 1
    - ❖ Alluvial groundwater discharges locally to surface water and may contain contaminants.
- Sediment
    - ❖ Fluctuating alluvial groundwater levels can result in geochemical interaction with sediment particles.
- Unsaturated zone
    - ❖ Alluvial groundwater infiltrates into the vadose zone variably along the length of the canyon.
    - ❖ Contaminants are transported into vadose zone as a function of solubility and adsorption. For example, transport of contaminants to deeper zones is generally limited to soluble constituents such as Cr(VI), molybdenum(VI), nitrate, and sulfate.

Unsaturated Zone

Soluble contaminants and colloids migrate downgradient in the unsaturated zone. Adsorption and precipitation reactions occur in this zone.

The unsaturated zone interactions with other media include the following.

- Interaction with the alluvial groundwater via return flow or Cr transport from the unsaturated zone back to the alluvium.
- Percolation of vadose zone pore water may carry contaminants to intermediate perched zones and the regional aquifer.

Perched Water

Perched intermediate groundwater occurs in the Cerros del Rio basalt and the Puye Formation.

Other as yet undetected perched zones may occur.

Soluble contaminants and colloids may migrate laterally or be fairly stagnant within the perched intermediate groundwater due to stratigraphic control. Adsorption and precipitation reactions occur in these zones.

Perched water interactions with other media include the following.

- Interaction between plants and perched water result from uptake at the springs.
- Lateral migration of perched water may carry contaminants to surface water in Segments 3 and 4, and to alluvial groundwater.
- Percolation of perched water may carry contaminants to the underlying unsaturated zone.
- Perched water may carry contaminants that directly enter the regional groundwater system.

Regional Aquifer

Two alternative conceptual models are considered for regional aquifer flow:

- Model A

  The regional aquifer may be locally confined or unconfined and affected by water-supply pumping.

- Model B

  The shallow portion of the regional aquifer (along the water table) is predominantly under phreatic (unconfined) conditions and has limited thickness. The deep portion of the regional aquifer is predominantly under confined conditions, and it is stressed by water-supply pumping, but the shallow zone of contaminant transport is unaffected by water-supply pumping.

Transport of contaminants is generally limited to soluble constituents such as Cr(VI), molybdenum(VI), nitrate, and sulfate. Geochemical interactions may control mobility.

D-3.0 MODEL ASSUMPTIONS FOR THE SANDIA CANYON ANALYSIS

Contaminant Source

The source of Cr considered for this study will be that released into Sandia Canyon from the TA-03 power plant (between 26,000 to 105,000 kg Cr[VI]). Sources released into Los Alamos Canyon or Mortandad Canyon will not be included. MoO_4 fate and transport released into Sandia Canyon after Cr releases ceased will also be modeled.

The source-air interaction pathway will not be explicitly modeled. Drift releases of Cr at TA-03 to the air likely settled within about a 1-km radius after being released between 1956 and the mid 1970s. The resultant mass of Cr dispersed in air to the Sandia Canyon Watershed will be estimated based on surface water concentrations. This mass will be treated as a surface water source with no time lag.

All Cr released from the TA-03 cooling towers will be assumed to go directly to surface water Segment 1. However, the mass of Cr in surface water is less than the original mass released by the power plant cooling towers due to uptake through other processes (wetland adsorption, drift losses to other watersheds). Therefore, a combination of historical surface water concentrations, current sediment and wetland concentrations, and original source estimates will be used to constrain the Cr(VI) mass available for downstream surface water and groundwater transport.

Surface water volumes and evaporation rates will be estimated based on recorded outfall volumes and gage data.

Air Media

The air pathway, as well as the interactions of air/plants, air/surface water Segment 1, air/sediment, and air/unsaturated zone will not be explicitly modeled.

Vegetation

Plants, as well as the interactions of plants/air, plants/surface water Segment 1, plants/sediment, plants/alluvial groundwater, and plants/unsaturated zone will not be explicitly modeled. However, any Cr(VI) in plants is already accounted for in surface water Cr concentrations measurements.

Surface Water

The surface water was divided in the four segments listed below.

- Segment 1
    - ❖ The first segment begins in the source outfall and goes to the eastern of the wetland, E123 gaging station.
- Segment 2
    - ❖ The second segment starts at the gaging station Gage E123 and ends at gaging station Gage E123.6.
- Segment 3
    - ❖ This segment starts at gaging station E123.6 and ends at gaging station E123.8.
- Segment 4
    - ❖ This segment starts at gaging station E123.8 and ends at borehole SCC-6.

Surface Water Segment 1

Surface water flow and transport is not explicitly modeled. Instead, it provides a boundary condition for vadose zone flow and transport simulations. Based on gage data, the modeled water volume infiltrating in this segment is 10% to 13% of the total flow. Chromium mass for this segment will be estimated using gage data, mass balance estimates, and surface water concentrations. Information on this surface water volume will ultimately constrain the volume and rate of infiltration into the underlying alluvium and tuff units and the surface water available for Segment 2.

The interactions of surface water Segment 1 with air, plants, and sediments will not be explicitly modeled.

The interaction between surface water Segments 1 and 2 will be modeled by transferring water and Cr between these segments with the amount of transfer estimated by using gage data, mass balance information, and historical surface water Cr concentrations.

Alluvial groundwater Cr concentrations are assumed to equal surface water concentrations in this segment.

Surface Water Segment 2

Surface water flow and transport is not explicitly modeled. Instead surface water flow and contaminant concentrations provide boundary conditions for vadose zone flow and transport simulations.

Based on gage data, 35% of the flow will be split between this segment and the next (SW3). Chromium mass for this segment will be estimated using gage data, mass balance estimates, and surface water concentrations. The volume of surface water available to this segment will ultimately constrain the volume and rate of infiltration into the underlying alluvium or bedrock, and the volume available for surface water Segment 3.

The interactions of this segment with sediments and alluvial groundwater will not be explicitly modeled.

The interaction between this segment and surface water Segment 3 is modeled by transferring water and Cr between these segments with the amount of transfer estimated by using gage data, mass balance information, and historical surface water Cr concentrations.

Infiltration of surface water directly into the vadose zone along this length of the canyon will be modeled as an upper boundary condition for the fate and transport model. Based on gage data, 35% of the flow will be split between this segment and the next (SW3) for infiltration. If available, field observations of moisture and contaminant profiles may also help constrain infiltration rates.

This segment will be represented with two 1-d unsaturated zone columns. These columns will be 5 m wide based on the very narrow stream channel.

A plausible range of Cr(VI) mass entering the unsaturated zone (as a boundary condition) beneath this surface water segment will be estimated using measured surface water concentrations. This mass will be the expected Cr(VI) available after passing through the wetland environment and a partitioning between the water volume that infiltrates the unsaturated zone beneath this surface water segment and the volume that flows into the next surface water segment.

Surface Water Segment 3

Surface water flow and transport is not explicitly modeled. Instead, surface water contaminant concentrations and water volumes provide boundary conditions for vadose zone flow and transport simulations.

Based on gage data, 35% of the flow will be split between this segment and the previous (SW2) for infiltration. This approach will constrain the volume and rate of infiltration into the underlying alluvium or bedrock as well as a constraint on the volume of surface water available for Segment 4.

The interactions of this segment with sediments and unsaturated zone won't be explicitly modeled.

The infiltration below this segment will be represented with five 1-d unsaturated zone columns. These columns will be 10 m wide based on the narrow stream channel.

Surface Water Segment 4

Surface water flow and transport is not explicitly modeled. Instead, surface water contaminant concentrations and water volumes provide boundary conditions for vadose zone flow and transport simulations.

Based on gage data, 52% to 55% of the assumed effluent volume will infiltrate in this segment.

The interactions of this segment with sediments, alluvial groundwater and unsaturated zone will not be explicitly modeled. It is assumed that there is no connection between this segment and the alluvial water.

The infiltration of this segment to the unsaturated zone will be represented by a minimum of six unsaturated zone columns. Column widths will be set based on the estimated alluvial groundwater body width perpendicular to the stream channel along this segment.

Sediment

Sediment transport is not explicitly modeled; instead, it provides a boundary condition to the vadose zone model. Estimates of the Cr mass in sediments will be used to constrain the amount of Cr entering the vadose zone.

The sediment interactions with the air; plants; surface water Segments 1, 2, and 3; and alluvial groundwater will not be modeled.

Alluvial Groundwater

Flow and transport within the alluvial groundwater system will not be explicitly modeled. Water and Cr in alluvial groundwater is transported downcanyon based on conservation of mass. At a given location in the alluvial system, water and Cr may enter from surface water or upstream alluvial groundwater and exit to downstream alluvial groundwater or to the underlying unsaturated zone with infiltrating water.

Plant uptake from alluvial groundwater, resurfacing of alluvial groundwater to surface water and interaction with sediments will not be modeled.

Infiltration of alluvial groundwater into the vadose zone along the length of the canyon will be distributed nonuniformly. The infiltration rates will be uncertain and depend on an alluvial groundwater balance (which, in turn, depends on the surface water balance) that is done outside the fate and transport simulation. Also, a range in infiltration rates will be constrained and calibrated based on field observations of moisture and contaminant profiles. Vadose zone beneath the wetland area (SW1 segment) will be represented with two 1-d columns. The first will be segmented by strata; the second will represent a continuous fault zone so some simulations may include the possibility of rapid flow along a fault zone. This zone will be 150 m wide perpendicular to the stream channel and based on wetland width. Chromium(VI) from the alluvial groundwater will be the source of Cr(VI) to the unsaturated zone. The alluvial groundwater concentrations will be assumed to be equal to surface water concentrations, using an uncertain distribution of time-dependent concentrations derived from field data and constrained by estimates of the initial Cr mass. The source concentration will be estimated outside the actual fate and transport simulation and applied as a boundary condition.

Unsaturated Zone

The Finite Element Heat and Mass (FEHM) computer code will be used to simulate unsaturated flow and the transport of Cr and molybdenum. Van Genuchten hydraulic characteristic curves will describe hydrologic properties; saturated hydraulic conductivities, Van Genuchten alpha and porosity will be uncertain parameters. The advection-dispersion equation will be used to model transport. At least some of the simulations will consider faulting and fractures, especially beneath the uppermost surface water segment (SW1).

The unsaturated zone pathway will be the uppermost pathway that is modeled explicitly. This zone will be modeled with a series of 1-d columns that run along the axis of Sandia Canyon and are linked to the four surface water segments. The columns will represent the strata that lie between the base of the alluvium (if present, otherwise from the surface) to the water table, except for one column that represents a fault zone in SW1 segment. Each column will have a surface area that represents the area over which infiltration is likely to occur.

Mass balances for water, Cr(VI), and molybdenum will be calculated external to the simulations and provide sources (boundary conditions) to the fate and transport simulations. It is assumed that Cr(III) is not mobile enough to enter the upper boundary of the unsaturated zone; that is, Cr entering the unsaturated zone is hexavalent. However, some reduction of Cr(VI) to Cr(III) may occur along the flow path and result in a loss of Cr(VI).

Interaction with surface water Segments 3 and 4, and return flow or Cr transport from the unsaturated zone back to the alluvium groundwater will not be modeled.

Some unsaturated-zone flow paths will be assumed to contain intermediate perched zones. Flow and transport within the perching layer will not be explicitly modeled. Also, the simulated unsaturated-zone travel times are assumed to not be affected by the perching horizons. Rather, the perched zone is assumed to affect the location where contaminants reach the regional aquifer. That is, the vadose zone contaminant breakthrough curve for a given location in Sandia Canyon will be calculated as though no translocation occurs. Then the saturated zone model will input that breakthrough curve to a location between the two canyons, as defined by a parameter that controls lateral migration.

Percolation of unsaturated-zone pore water to the regional groundwater will be modeled. Breakthrough curves of Cr(VI) mass versus time will be applied as an upper boundary condition to the regional model and the breakthrough location will depend on the location of the original 1 d unsaturated-zone column and then any displacement caused by assumed lateral flow along perching layers.

Perched Water

A thin zone of perched intermediate groundwater occurs within the Puye Formation atop the Cerros del Rio basalt between SCC-1 and SCC-4. This layer may cause some lateral flow toward the south or southwest. The simulations will account for lateral migration in the perched zones by translocating vadose zone flow paths from beneath Sandia Canyon toward Mortandad Canyon using an uncertain parameter. Observations of perching layers in Sandia and Mortandad Canyons as well as the water chemistry of these perched zones will help to define that uncertain parameter. Some simulations will assume that no lateral transport occurs.

The major geochemical process affecting transport in the perched intermediate groundwater occurring in basalt is precipitation of amorphous $Cr(OH)_3$.

Plant uptake at the springs won't be modeled. Interaction with surface water Segments 3 and 4 and with alluvial groundwater will not be modeled.

No direct pathways occur between this zone and the regional aquifer because observed perching layers are well above regional water table. However, lateral flow along perching layers is represented by transferring the breakthrough point for the vadose zone breakthrough curve laterally such that the mass flux entering the regional groundwater model is moved toward Mortandad Canyon.

Regional Aquifer

The regional aquifer is a complex, heterogeneous system that includes confined and unconfined zones. The degree of hydraulic communication between these zones is thought to be spatially variable. The model assumptions for both models are detailed below.

- Model A

  No hydraulic separation occurs between shallow and deep (pumped) aquifer zones, which allows pumping drawdown to reach the water table. Hydraulic gradients in the phreatic zone are directly affected by the pumping, and contaminants are drawn toward water-supply wells. Resistance to downward flow is caused by anisotropic permeability structure (horizontal permeability greater than vertical permeability). All contaminants that enter the well's capture zone are expected to arrive at water-supply wells under these conditions.

- Model B

  There is a phreatic zone that has weak hydraulic connection to the rest of the regional aquifer. Hydraulic separation occurs between the shallow (phreatic aquifer; water table) and deep (regional aquifer; pumped) zones that minimizes pumping drawdown at the water table. Contaminants are expected to largely bypass the water-supply wells and arrive at the springs near the Rio Grande.

For both models, the major geochemistry process affecting transport of Cr(VI) in the regional groundwater is sorption.

The regional groundwater interaction with the source is not explicitly modeled.

It is assumed that no connection exists between groundwater and perched intermediate groundwater.

D-4.0 GROUNDWATER MODEL JUSTIFICATION FOR THE SANDIA CANYON ANALYSIS

Contaminant Source

The Cr released into Sandia Canyon from the TA-03 power plant cooling towers is thought to be the largest Cr source at the Laboratory. It likely exceeds the Cr released to Los Alamos Canyon from cooling towers at the Omega West Reactor by at least a factor of 10, and no evidence was found of large Cr releases into Mortandad Canyon. Also, the Sandia Canyon release location is closer to the elevated regional aquifer wells that show elevated Cr(VI) concentrations (primarily, R-28 and R-11).

The contribution of the air pathway to groundwater is reflected in surface water and sediment measurements.

Measured surface water concentrations at Segment 1 are generally less than effluent concentrations. These surface water concentrations reflect Cr losses resulting from interactions with the wetland environment, sediments, and other processes that can reduce Cr(VI) concentrations. This reduced surface water concentration then becomes the source concentration for further waterborne transport of Cr(VI).

Air Media

Drift releases of Cr to the air will be considered a surface water source with no time lag because the time scale for air deposition is short compared to groundwater fate and transport.

The air/sediment interaction has a short time scale in terms of Cr fate and transport.

No direct connection exists between air and unsaturated zone.

Vegetation

The net effect of any contribution of plants to surface water is captured in the historic surface water concentrations and current information about Cr in the wetland and the sediment-plants interaction has a short time scale in terms of Cr fate and transport. Additionally, plants are not likely to contribute Cr directly to alluvial groundwater.

There’s no direct connection between plants and the unsaturated zone

Surface Water

The surface water was divided in the four segments that are listed below.

- Segment 1
    - ❖ The first segment begins in the source outfall and goes to the eastern of the wetland, E123 gaging station.
- Segment 2
    - ❖ This segment starts at the gaging station Gage E123 and ends at gaging station Gage E123.4.
- Segment 3
    - ❖ This segment starts at gaging station E123.4 and ends at gaging station E124.
- Segment 4
    - ❖ This segment starts at gaging station E124 and ends at the Rio Grande.

Surface Water Segment 1

Surface water in this segment acts as a direct and indirect source to the vadose zone that is modeled.

The net effect of any contribution of surface water to plants is captured in the historic surface water concentrations as plants die and decay and is captured in current information about Cr in the wetland.

Mass conservation is assumed between Segments 1 and 2 and is based on the surface water measurements.

The net effect of Cr loss from surface water to sediment is captured in the historical surface water concentrations. The surface water concentration bounds the alluvial groundwater concentration in the absence of historical groundwater data.

Surface Water Segment 2

Surface water in this segment acts as a direct and indirect source to the vadose zone that is modeled.

The approach conserves mass between Segments 2 and 3 and is based on the surface water measurements.

The net effect of Cr loss from surface water to sediment is captured in the historical surface water concentrations.

Surface water infiltrates the unsaturated zone directly in this segment because bedrock is present at the surface, and very little alluvial groundwater is present at this location. Water entering the unsaturated zone here has Cr concentrations equal to surface water concentrations.

Surface Water Segment 3

Surface water in this segment acts as a direct and indirect source to the vadose zone that is modeled.

The approach conserves mass between Segments 3 and 4 and is based on the surface water measurements.

The net effect of Cr loss from surface water to sediment is captured in the historical surface water concentrations.

The surface water concentration bounds the alluvial groundwater concentration in the absence of historical groundwater data.

Input to unsaturated zone at this location is assumed to come from alluvial groundwater.

Surface Water Segment 4

Surface water in this segment acts as a direct and indirect source to the vadose zone that is modeled.

The net effect of Cr loss from surface water to sediment is captured in the historical surface water concentrations.

Surface water flow in this segment is infrequent, and alluvial groundwater in this segment is recharged by upstream groundwater.

Input to unsaturated zone at this location is assumed to come from alluvial groundwater.

Sediment

Regional groundwater concentrations are not sensitive to sediment transport other than its effect on surface water Cr concentrations.

The sediment/plant interaction has no direct connection with the groundwater pathway.

Redistribution of Cr from sediment back to all segments of surface water may be captured by nonzero tail in surface water concentration following Cr use.

All Cr(VI) associated with sediment is assumed to be transported by surface water and does not directly interact with alluvial groundwater.

Alluvial Groundwater

Alluvial groundwater is not modeled but it acts as a direct and indirect source of both water and Cr to the vadose zone that is modeled.

Most plant activity is in the wetlands where plants are assumed to be in direct contact with surface water.

The dominant pathway for alluvial groundwater in surface water Segment 1 is to the vadose zone.

Alluvial groundwater is the main source of water to the unsaturated zone along much of the length of Sandia Canyon.

Unsaturated Zone

Water flow and contaminant transport through the unsaturated zone controls the breakthrough of contaminants to the regional aquifer. Migration of Cr(VI) in groundwater above the basalts is documented in the literature and shown to be affected by sorption.

Chromium is not expected to migrate upward to the alluvial groundwater.

Perched intermediate groundwater containing Cr is observed in both Sandia and Mortandad Canyons. It is not known if these perched zones between the two canyons are continuous or discontinuous. However, the intermediate perching units in Sandia Canyon appear to have a southerly dip, and lateral flow toward Mortandad Canyon is possible.

Numerical modeling based on available data will bound potential infiltration rates and yield expected nature and extent of various contaminant distributions such as Cr.

Perched Water

Thermodynamic calculations show that $Cr(OH)_3$ should precipitate from solution based on oxidation of olivine containing ferrous iron. The mineral olivine is concentrated within the Cerros del Rio basalt. Olivine oxidizes to $Fe(OH)_3$ as CrO_4^{-2} reduces to Cr(III) and precipitates as $Cr(OH)_3$.

Concentrations of total Cr in nonfiltered samples are much higher than total dissolved Cr in filtered samples collected from the Cerros del Rio basalt. These concentrations suggest that a fraction of total Cr is associated with suspended material that could be partly present as $Cr(OH)_3$. Stable isotopes of Cr suggest that approximately 25% of Cr(VI) has been reduced to Cr(III) at MCOI-6, possibly resulting in the precipitation of $Cr(OH)_3$.

The interaction between plants and perched water occurs from uptake at the springs; however spring Cr concentrations are low.

The interaction of perched water to surface water in Segments 3 and 4 is likely to be a minor or absent flow path.

No connection exists between perched intermediate groundwater and alluvial groundwater.

Intermediate perched groundwater containing Cr is observed in both Sandia and Mortandad Canyons. It is not known if these perched zones between the two canyons are continuous or discontinuous. However, the intermediate perching units (strata) in Sandia Canyon appear to have a southerly dip, and lateral flow toward Mortandad Canyon is possible.

Numerical modeling based on available data will bound potential infiltration rates to the regional groundwater and yield expected nature and extent of various contaminant distributions such as Cr.

Regional aquifer

Two possibilities are considered for the regional aquifer flow and contaminant transport.

- Model A

  Hydraulic communication between the upper phreatic aquifer and the deeper confined aquifer is supported by the presence of molybdenum in the deeper screen of well R-35. Additionally, the influence of pumping in production wells (deep portion of the aquifer) over monitoring regional wells located in the shallow phreatic aquifer was detected.

- Model B

  Various hydrostratigraphic units can provide large-scale confinement. Some tests data collected during pumping of wells PM-2 and PM-4 suggest that the deeper portion of the aquifer is essentially confined.

Migration of Cr(VI) in groundwater is documented in the literature and shown to be affected by sorption.

Regional groundwater used in laboratory facilities (i.e., TA-03), and discharged into Sandia Canyon is not a significant source of contaminants.

Both conceptual models A and B will be simulated in defining the potential nature and extent of Cr in the regional aquifer.

D-5.0 PARAMETER DISTRIBUTIONS

The treatment of uncertainty is a key to providing an accurate assessment of the nature and extent of Cr contamination beneath Sandia Canyon. One component of uncertainty is found in the conceptual models defined in the previous section. Another component is uncertainty in the parameter values that control the rate and direction of contaminant transport. This section provides brief descriptions of the probability distributions for each uncertain parameter used in fate and transport modeling. These distributions are based on statistical analysis of available data, physical constraints, and expert judgment.

A list of the parameters and their distributions is presented in this section.

D-5.1 Parameters for the Sandia Canyon Analysis

Contaminant Source

The parameters for the contaminant source are

- surface water concentration of Cr(VI) during release in mg/L,
- pre-April 1972 Cr(VI) concentrations in surface water in mg/L,
- current Cr concentrations in µg/L, and
- average effluent discharge rate in gallons per day.

Air Media

No parameters are related with this media.

Vegetation

No parameters are related with vegetation.

Surface Water

No parameters are related with this media.

Sediment

No parameters are involved in this media.

Alluvial Groundwater

The infiltration rate into the vadose zone is used as a parameter for the interaction between alluvial groundwater and unsaturated zone.

Unsaturated Zone

The following parameters will be used for the unsaturated zone.

- Vadose zone longitudinal dispersivity,
- Hydraulic conductivity for
    - ❖ Guaje Pumice bed
    - ❖ Unit 1g of the Bandelier Tuff
    - ❖ Bandelier Tuff, Otowi Member
    - ❖ Cerro Toledo interval
    - ❖ Tsankawi Pumice Bed
    - ❖ Cerros del Rio basalt rubble
    - ❖ Puye fanglomerates
    - ❖ Fault zone
- Porosity for
    - ❖ Guaje Pumice Bed
    - ❖ Unit 1g of the Bandelier Tuff
    - ❖ Bandelier Tuff, Otowi Member
    - ❖ Cerro Toledo interval
    - ❖ Tsankawi Pumice Bed
    - ❖ Cerros del Rio basalt rubble
    - ❖ Puye fanglomerates
    - ❖ Fault zone
- van Genuchten α for
    - ❖ Guaje Pumice Bed
    - ❖ Unit 1g of the Bandelier Tuff
    - ❖ Bandelier Tuff, Otowi Member
    - ❖ Cerro Toledo interval
    - ❖ Tsankawi Pumice Bed
    - ❖ Fault zone
- Other hydrogeologic properties for the same units using single values
- K_d (distribution coefficients)

Hydrogeological properties and dispersivities from Mortandad Canyon will be used for the interaction between the unsaturated zone and the perched intermediate groundwater and the interaction with the regional groundwater.

Perched Water

The following parameters will be used for the perched water

- Vadose zone longitudinal dispersivity

- Hydraulic conductivity for
    - ❖ Guaje Pumice Bed
    - ❖ Unit 1g of the Bandelier Tuff
    - ❖ Bandelier Tuff, Otowi Member
    - ❖ Cerro Toledo interval
    - ❖ Tsankawi Pumice Bed
    - ❖ Cerros del Rio basalt rubble
    - ❖ Puye fanglomerates
- Porosity for:
    - ❖ Guaje Pumice Bed
    - ❖ Unit 1g of the Bandelier Tuff
    - ❖ Bandelier Tuff, Otowi Member
    - ❖ Cerro Toledo interval
    - ❖ Tsankawi Pumice Bed
    - ❖ Cerros del Rio basalt rubble
    - ❖ Puye fanglomerates
- van Genuchten α for
    - ❖ Guaje Pumice Bed
    - ❖ Unit 1g of the Bandelier Tuff
    - ❖ Bandelier Tuff, Otowi Member
    - ❖ Cerro Toledo interval
    - ❖ Tsankawi Pumice Bed
- Other hydrogeologic properties for the same units using single values
- Mass transfer for basalt as a percentage of Cr entering this layer
- Fractioning (%)

Hydrogeological properties from Mortandad Canyon will be used for the interaction between perched intermediate groundwater and the unsaturated zone.

Regional Aquifer

The following parameters will be used for the regional aquifer.

- Longitudinal dispersivity of the regional aquifer (aL)
- Permeability factors for Santa Fe fanglomerate (fTf) and pumiceous Puye (fTpp)
- Anisotropy factors for Santa Fe Group (aTf) and Puye (aTp)

- Hydraulic conductivities and porosities for units
    - ❖ Galisteo Group (kTgs)
    - ❖ Santa Fe Group (kTsf)
    - ❖ Totavi (kTpt)
    - ❖ Puye (kTp)
    - ❖ Keres Group (nTk)
    - ❖ Tschicoma (nTt)
    - ❖ Older basalts (nTb1)
    - ❖ Bayo Canyon basalts (nTb2)
    - ❖ Cerros del Rio basalts (nTb4)
- Porosities for units
    - ❖ Galisteo Group (kTgs)
    - ❖ Santa Fe Group (kTsf)
    - ❖ Totavi (kTpt)
    - ❖ Puye (kTp)
    - ❖ Keres Group (nTk)
    - ❖ Tschicoma (nTt)
    - ❖ older basalts (nTb1)
    - ❖ Bayo Canyon basalts (nTb2)
    - ❖ Cerros del Rio basalts (nTb4)
- Ri = Capture radius for contamination
- Range of correlation lengths in X, Y and Z directions
- K_d (coefficient distributions)
- Fractioning (precipitation) of Cr (%)

D-5.2 Parameter Distributions

Monte Carlo methods were used to capture and propagate parameter uncertainty in the vadose zone and regional aquifer models. The following table provides descriptions of each of the probability distributions that were treated as uncertain in modeling. These distributions are based on a combination of statistical analyses and expert opinion.

Parameter: 1991–2001 Molybdenum SW Concentration in µg/L

Uniform distribution with parameters:

Minimum 100.00

Maximum 400.00

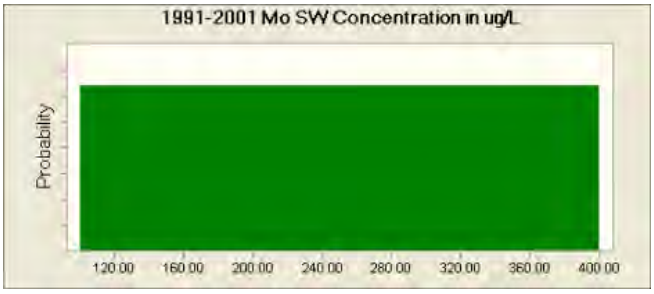

Parameter: Anisotropy Factors for Santa Fe Group and Puye

Uniform distribution with parameters:

Minimum 1.00

Maximum 5.00

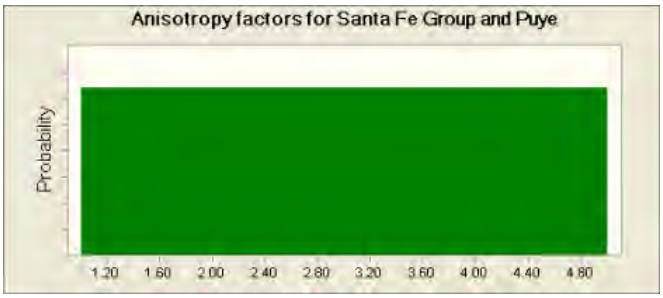

Parameter: Bandelier Tuff, Otowi Member Alpha (1/cm)

Lognormal distribution with parameters:

Mean 6.84E-3

Std. Dev. 3.03E-3

Selected range is from 2.90E-3 to 1.73E-2

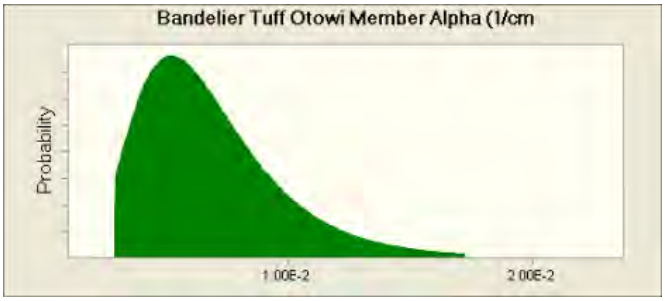

Parameter: Bandelier Tuff Otowi Member Hydraulic Conductivity (cm/s)

Lognormal distribution with parameters:

Mean 6.66E-4

Std. Dev. 1.56E-3

Selected range is from 1.10E-5 to 7.80E-3

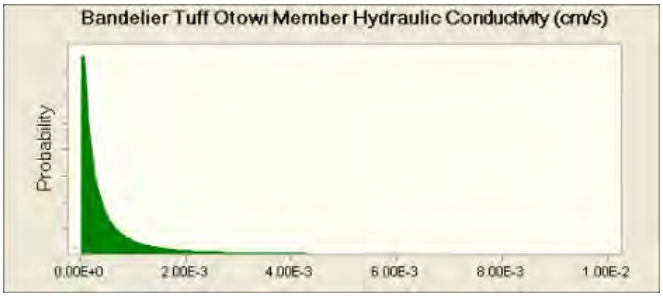

Parameter: Bandelier Tuff, Otowi Member Porosity

Normal distribution with parameters:

Mean 0.48

Std. Dev. 0.05

Selected range is from 0.31 to 0.54

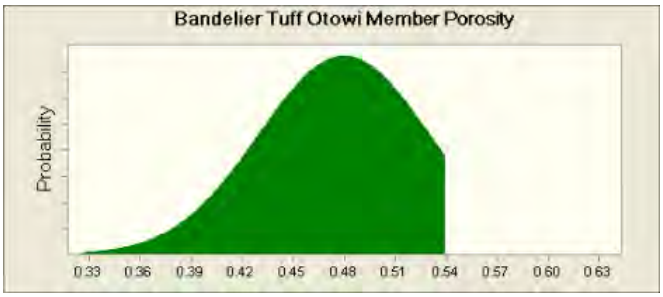

Parameter: Bandelier Tuff Unit 1g Alpha (1/cm)

Lognormal distribution with parameters:

Mean 3.59E-2

Std. Dev. 9.43E-2

Selected range is from 5.00E-4 to 2.31E-1

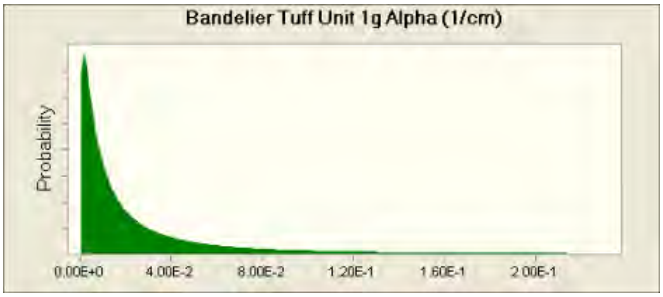

Correlated with: Bandelier Tuff Unit 1g Hydraulic Conductivity (cm/s)

Coefficient 0.53

Parameter: Bandelier Tuff Unit 1g Hydraulic Conductivity (cm/s)

Lognormal distribution with parameters:

Mean 9.68E-4

Std. Dev. 2.60E-3

Selected range is from 4.70E-5 to 4.30E-3

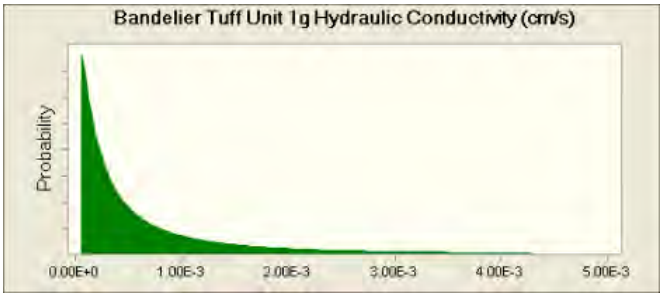

Correlated with: Bandelier Tuff Unit 1g Alpha (1/cm)

Coefficient 0.53

Parameter: Bandelier Tuff Unit 1g Porosity

Lognormal distribution with parameters:

Mean 0.53

Std. Dev. 0.05

Selected range is from 0.48 to 0.66

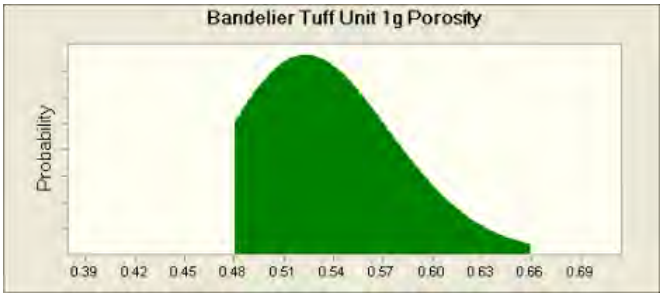

Parameter: Bayo Canyon Basalts - Log of Effective Porosity

Normal distribution with parameters:

Mean -4.50

Std. Dev. 0.75

Selected range is from -6.00 to -3.00

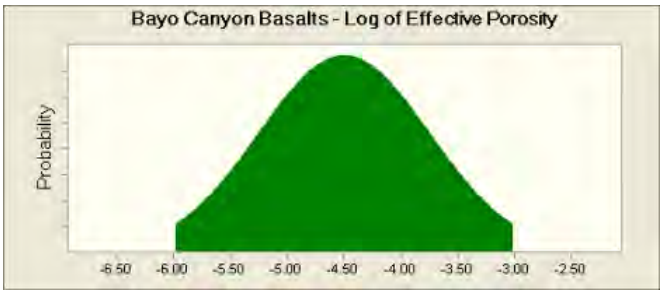

Parameter: Bayo Canyon Basalts - Log of Hydraulic Conductivity (cm/s)

Normal distribution with parameters:

Mean -11.50

Std. Dev. 1.00

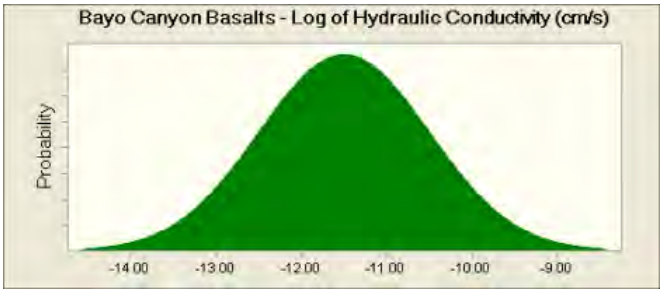

Parameter: Capture Radius Index

Uniform distribution with parameters:

Minimum 0.00

Maximum 1.00

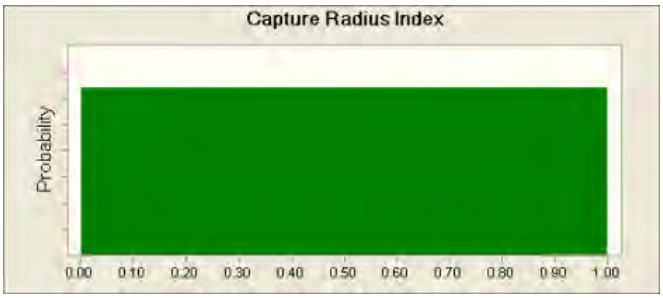

Parameter: Cerro Toledo Alpha (1/cm)

Lognormal distribution with parameters:

Mean 1.75E-3

Std. Dev. 3.31E+0

Selected range is from 6.86E-3 to 2.80E-2

Correlated with: Cerro Toledo Hydraulic Conductivity (cm/s)

Coefficient 0.67

Parameter: Cerro Toledo Hydraulic Conductivity (cm/s)

Lognormal distribution with parameters:

Mean 2.34E-4

Std. Dev. 5.47E+0

Selected range is from 6.00E-5 to 2.80E-4

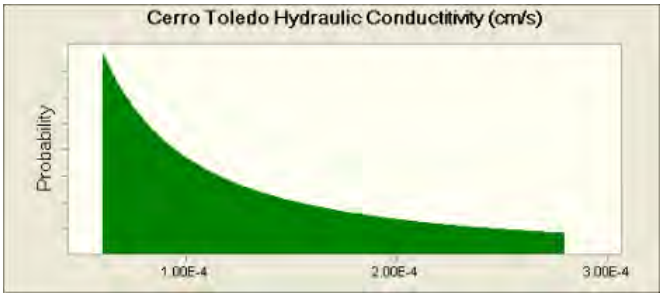

Correlated with: Cerro Toledo Alpha (1/cm) Coefficient 0.67

Parameter: Cerro Toledo Porosity

Normal distribution with parameters:

Mean 0.48

Std. Dev. 0.02

Selected range is from 0.47 to 0.50

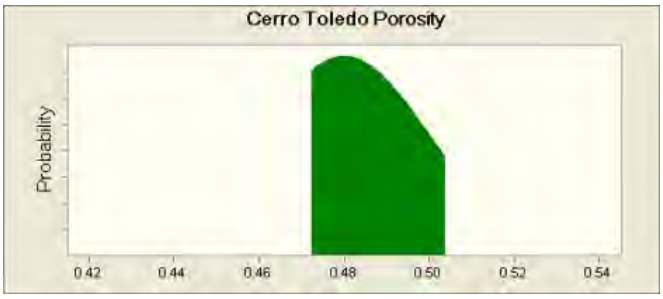

Parameter: Cerros del Rios Basalt Rubble Log Permeability (m2)

Normal distribution with parameters:

Mean -1.05E+1

Std. Dev. 1.00E+0

Selected range is from -1.20E+1 to -9.00E+0

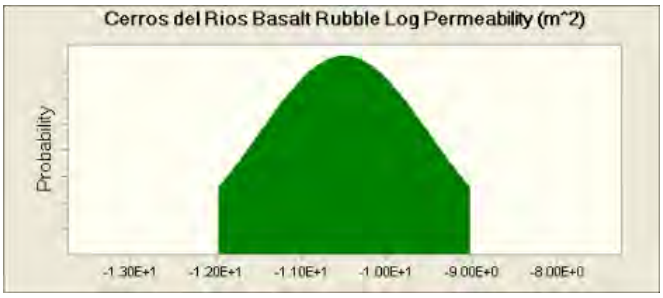

Correlated with: Cerros del Rios Basalt Rubble Total Porosity

Coefficient 0.90

Parameter: Cerros del Rios Basalt Rubble Total Porosity

Uniform distribution with parameters:

Minimum 0.10

Maximum 0.30

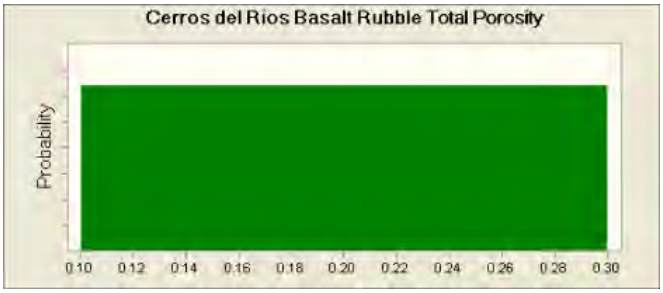

Correlated with: Cerros del Rios Basalt Rubble Log Permeability (m^2)

Coefficient 0.90

Parameter: Cerros del Rios Basalts - Log of Effective Porosity

Uniform distribution with parameters:

Minimum -4.00

Maximum -2.00

Parameter: Cerros del Rios Basalts - Log of Permeability (m2)

Normal distribution with parameters:

Mean -11.50

Std. Dev. 1.00

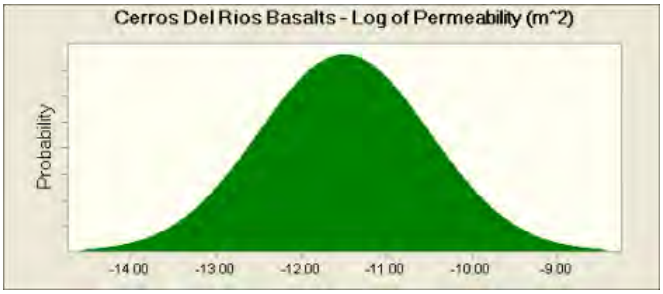

Parameter: Cr-1 1956-1972 SW Concentration in mg/L

Normal distribution with parameters:

Mean 7.03

Std. Dev. 3.71

Selected range is from 1.90 to 12.00

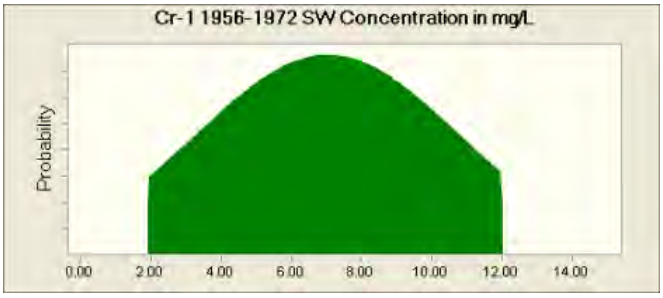

Correlated with:

Cr2 1972–1990 SW Concentration in µg/L	Coefficient	0.90
Current Chromium Concentrations in µg/L	Coefficient	0.90

Parameter: Cr2 1972–1990 SW Concentration in µg/L

Uniform distribution with parameters:

Minimum 10.00

Maximum 60.00

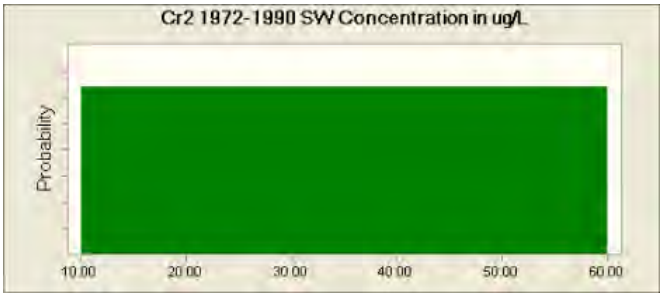

Correlated with: Cr-1 1956–1972 SW Concentration in mg/L

Coefficient 0.90

Parameter: Current Chromium Concentrations in µg/L

Beta distribution with parameters:

Minimum 0.13

Maximum 31.49

Alpha 1.0213

Beta 8.9

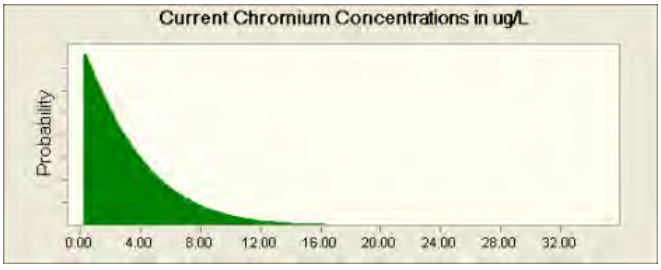

Correlated with: Cr-1 1956–1972 SW Concentration in mg/L

Coefficient 0.90

Parameter: Effective Porosity of the Puye Fanglomerate

Uniform distribution with parameters:

Minimum 0.02

Maximum 0.10

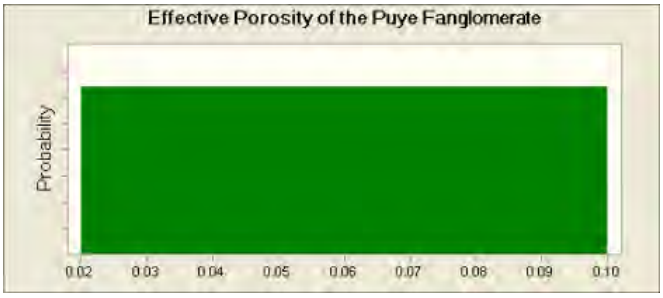

Parameter: Effluent Discharge Rate beginning 1992 (gal./d)

Maximum Extreme distribution with parameters:

Likeliest 2.60E+5

Scale 1.60E+5

Selected range is from 1.00E+5 to 6.00E+5

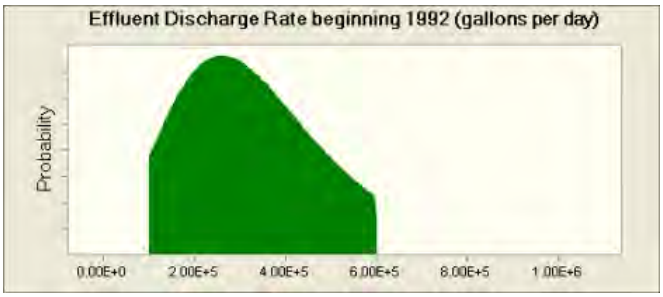

Parameter: Effluent Discharge Rate from 1950 to 1991 (gal./d)

Beta distribution with parameters:

Minimum 1.456E+5

Maximum 3.566E+5

Alpha 2.155

Beta 4.36

Selected range is from 1.570E+5 to 3.190E+5

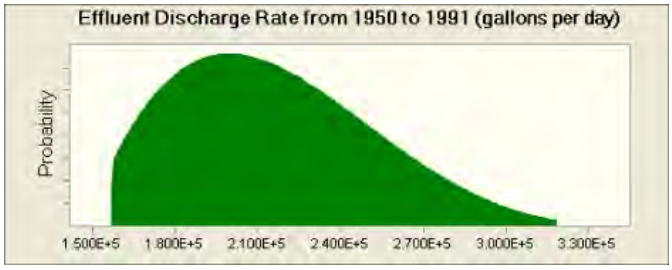

Parameter: Fault Percentage

Uniform distribution with parameters:

Minimum 0.00

Maximum 0.20

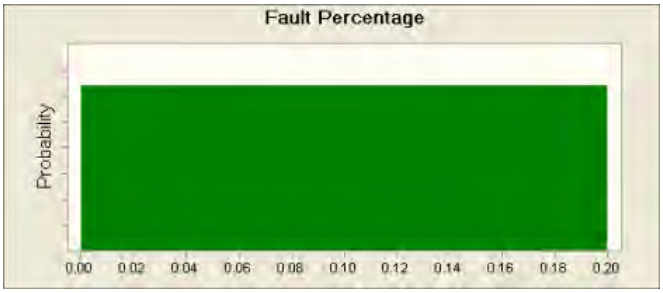

Parameter: Fault Zone Alpha (1/cm)

Uniform distribution with parameters:

Minimum 0.00

Maximum 0.23

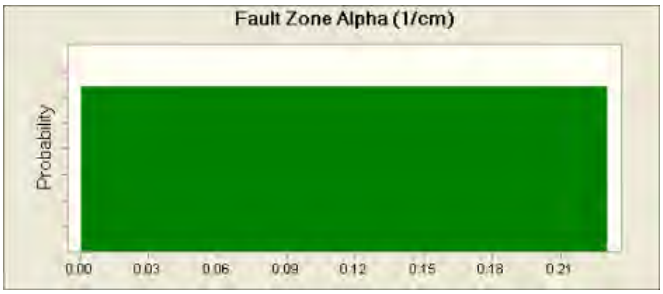

Parameter: Fault Zone Hydraulic Conductivity (cm/s)

Uniform distribution with parameters:

Minimum 1.00E-5

Maximum 7.80E-3

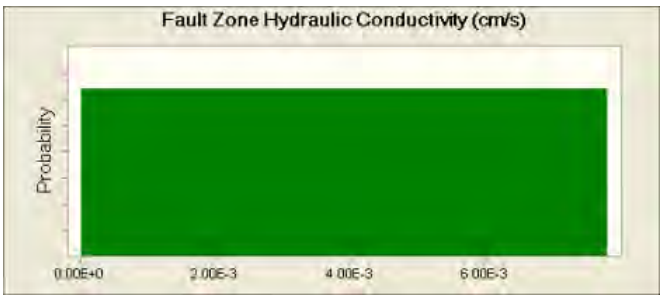

Correlated with: Fault Zone Porosity

Coefficient 0.95

Parameter: Fault Zone Porosity

Uniform distribution with parameters:

Minimum 0.02

Maximum 0.70

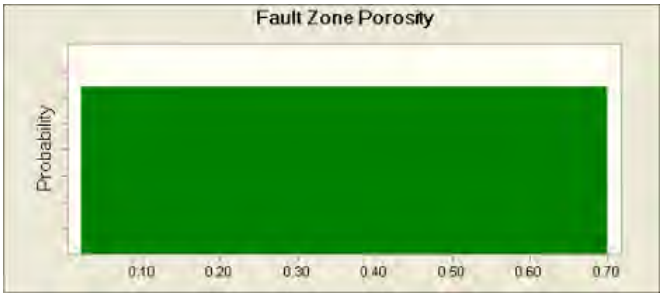

Correlated with: Fault Zone Hydraulic Conductivity (cm/s)

Coefficient 0.95

Parameter: Galisteo Group - Log of Effective Porosity

Normal distribution with parameters:

Mean -1.50

Std. Dev. 0.75

Selected range is from -3.00 to -0.60

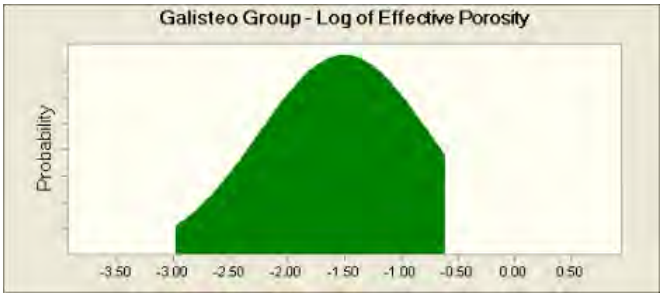

Parameter: Galisteo Group - Log of Hydraulic Conductivity (cm/s)

Normal distribution with parameters:

Mean -12.50

Std. Dev. 0.50

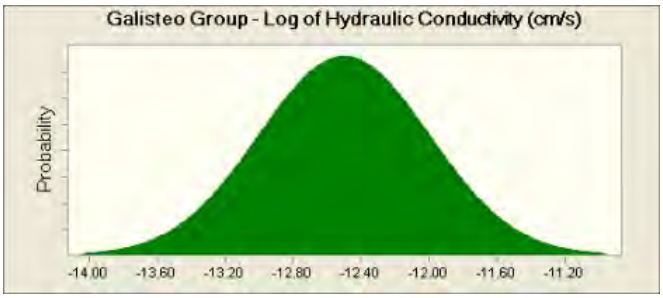

Parameter: Guaje Pumice Bed - Log of Alpha (1/cm)

Normal distribution with parameters:

Mean -3.09

Std. Dev. 0.40

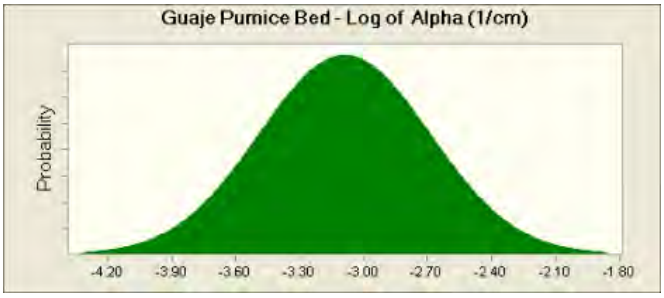

Parameter: Guaje Pumice Bed Hydraulic Conductivity (cm/s)

Normal distribution with parameters:

Mean -3.82

Std. Dev. 0.50

Selected range is from -4.80 to infinity

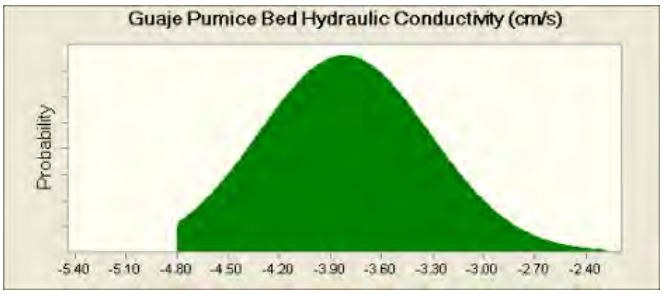

Parameter: Guaje Pumice Bed Porosity

Normal distribution with parameters:

Mean 0.50

Std. Dev. 0.02

Selected range is from 0.45 to 0.55

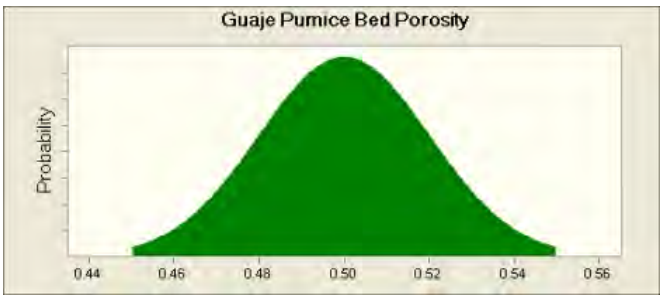

Parameter: K_d - Vadose Zone Above and Below the Basalt in mL/g

Uniform distribution with parameters:

Minimum 0.00

Maximum 0.30

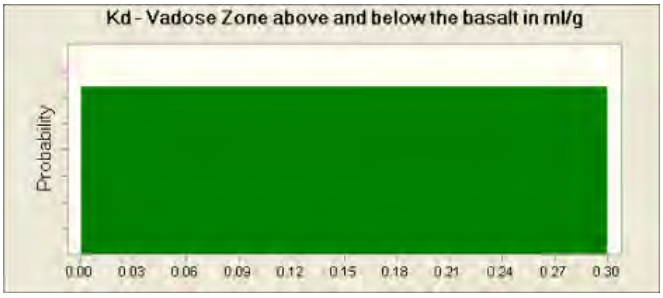

Parameter: Keres Group - Log of Effective Porosity

Normal distribution with parameters:

Mean -4.00

Std. Dev. 0.75

Selected range is from -6.00 to -3.00

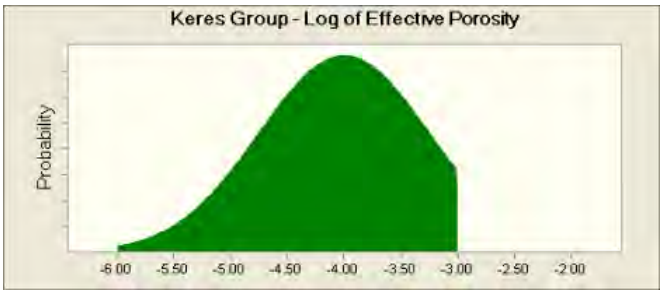

Parameter: Keres Group - Log of Hydraulic Conductivity (cm/s)

Normal distribution with parameters:

Mean -10.50

Std. Dev. 0.50

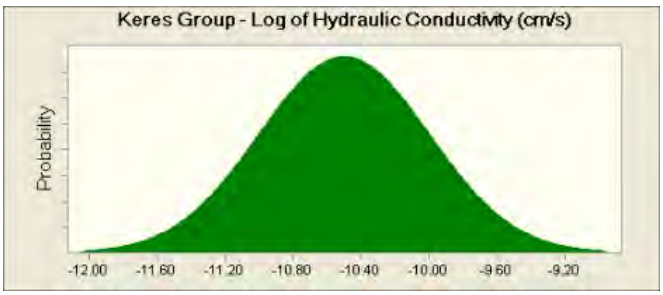

Parameter: Longitudinal Dispersivity (m)

Uniform distribution with parameters:

Minimum 50.00

Maximum 150.00

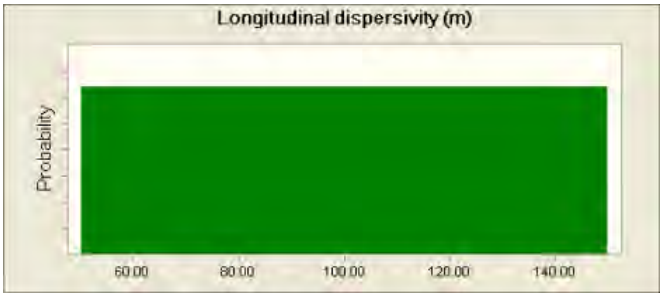

Parameter: Mass Transfer for Basalt as a Percentage of the Chromium Exiting a vz Column

Uniform distribution with parameters:

Minimum 0.00

Maximum 64.00

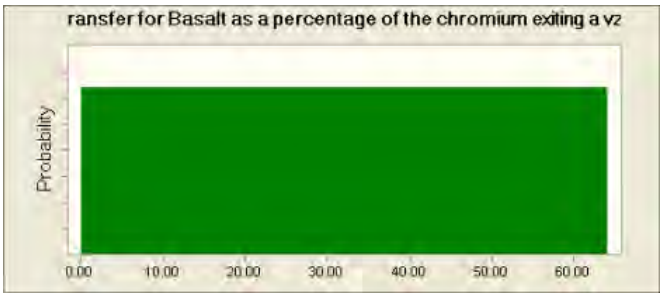

Parameter: Older Basalts - Log of Effective Porosity

Normal distribution with parameters:

Mean -4.50

Std. Dev. 0.75

Selected range is from -6.00 to -3.00

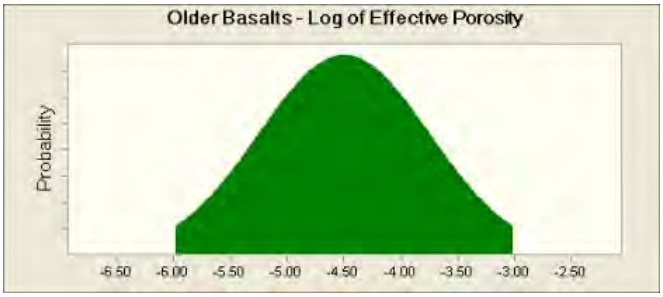

Parameter: Older Basalts - Log of Hydraulic Conductivity (cm/s)

Normal distribution with parameters:

Mean -11.50

Std. Dev. 1.00

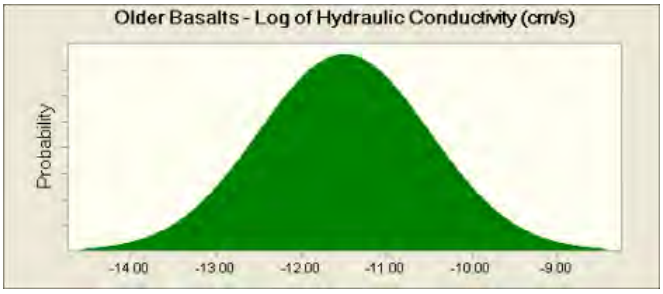

Parameter: Permeability Factors for Santa Fe Fanglomerate and Pumiceous Puye

Uniform distribution with parameters:

Minimum 0.00

Maximum 3.00

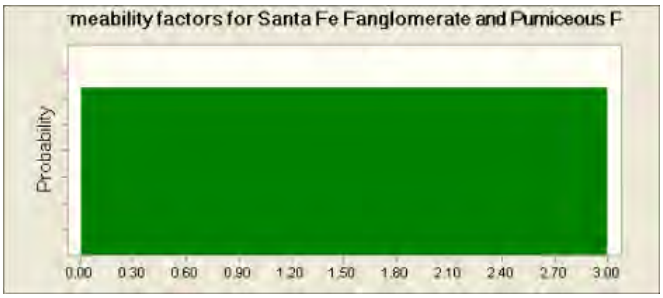

Parameter: Pumiceous Puye Hydraulic Conductivity (cm/s)

Lognormal distribution with parameters:

Mean 9.77E-4

Std. Dev. 3.16E+0

Selected range is from 5.00E-4 to 1.00E-2

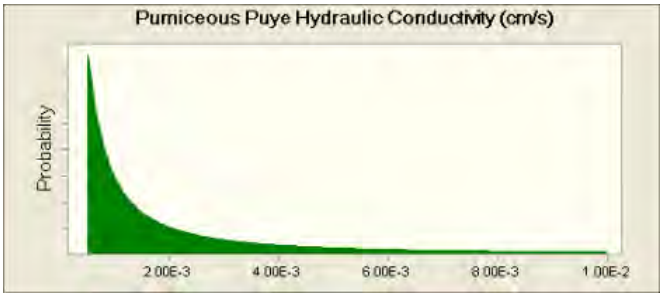

Parameter: Pumiceous Puye Total Porosity

Uniform distribution with parameters:

Minimum 0.10

Maximum 0.30

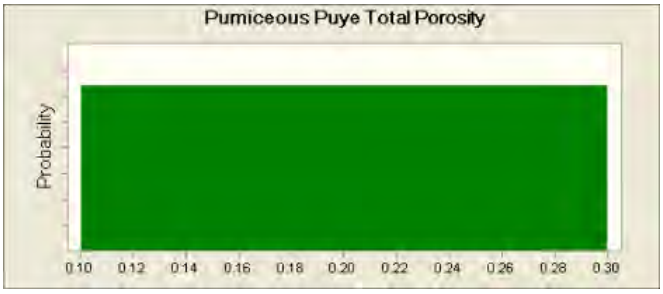

Parameter: Puye - Log of Effective Porosity

Normal distribution with parameters:

Mean -1.00

Std. Dev. 1.00

Selected range is from -3.00 to -0.30

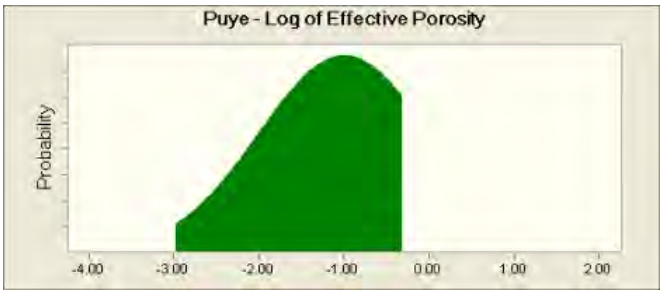

Parameter: Puye Fanglomerate Hydrologic Conductivity (cm/s)

Lognormal distribution with parameters:

Mean 9.77E-4

Std. Dev. 3.16E+0

Selected range is from 5.00E-4 to 1.00E-2

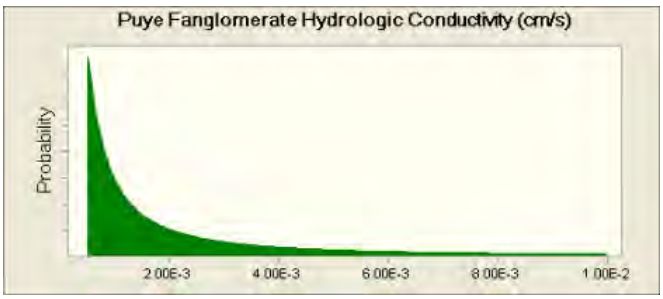

Parameter: Puye Fanglomerate Log Alpha (1/cm)

Uniform distribution with parameters:

Minimum 0.01

Maximum 0.05

Selected range is from 0.01 to 0.05

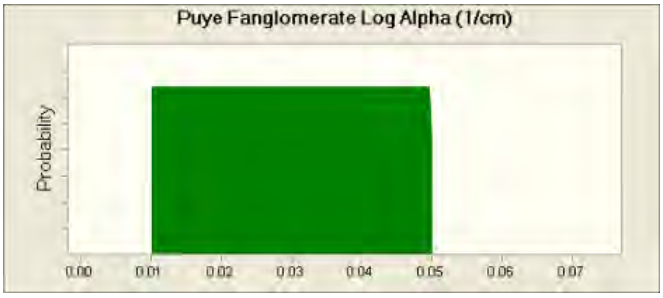

Parameter: Puye Fanglomerate Total Porosity

Uniform distribution with parameters:

Minimum 0.10

Maximum 0.30

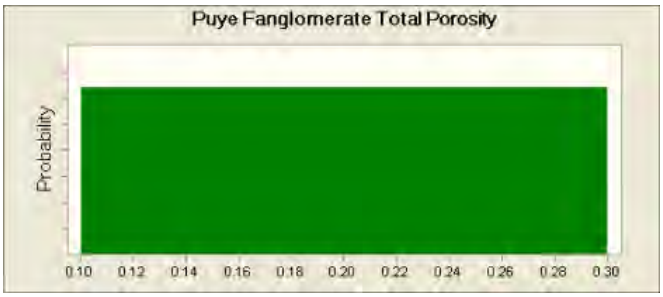

Parameter: Puye Hydraulic - Log of Hydraulic Conductivity (cm/s)

Normal distribution with parameters:

Mean -11.00

Std. Dev. 0.50

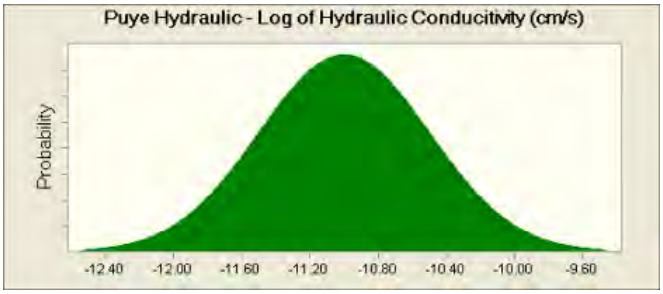

Parameter: QSW1

Uniform distribution with parameters:

Minimum 0.00

Maximum 1.00

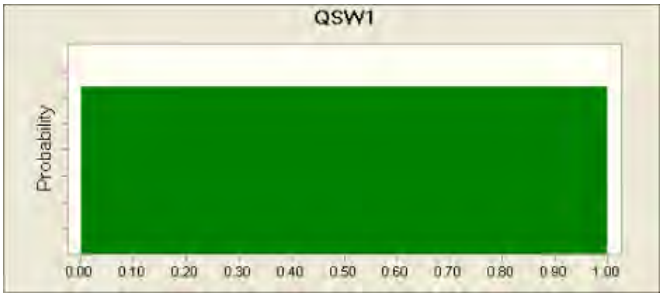

Parameter: QSW3

Uniform distribution with parameters:

Minimum 0.00

Maximum 1.00

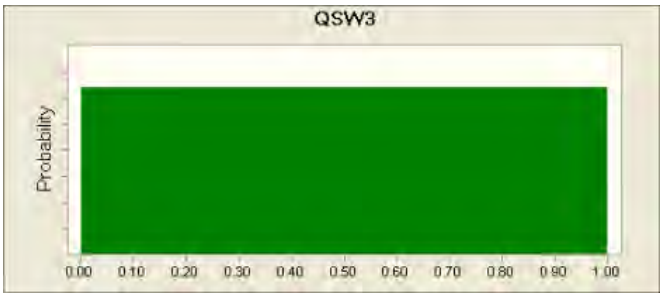

Parameter: Santa Fe Group - Log of Effective Porosity

Normal distribution with parameters:

Mean -1.50

Std. Dev. 0.75

Selected range is from -3.00 to -0.60

Parameter: Santa Fe Group - Log of Hydraulic Conductivity (cm/s)

Normal distribution with parameters:

Mean -12.50

Std. Dev. 0.50

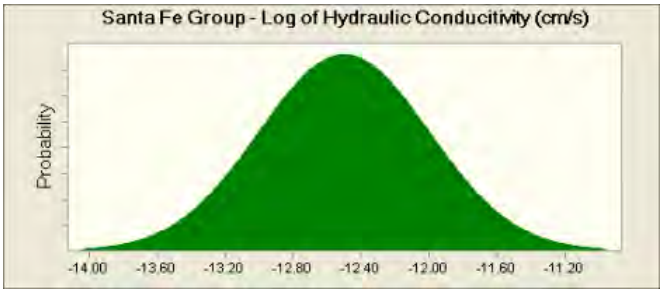

Parameter: Sorption for the Regional Aquifer

Uniform distribution with parameters:

Minimum 0.00

Maximum 0.30

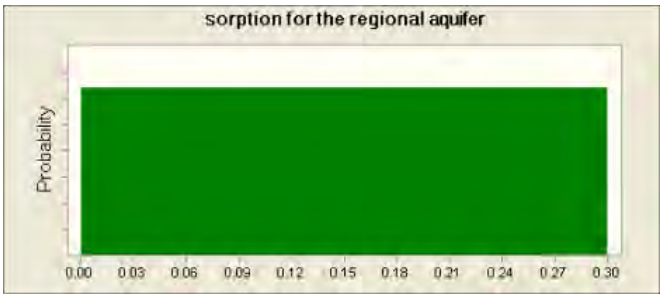

Parameter: SW1 Infiltration Percentage

Uniform distribution with parameters:

Minimum 0.10

Maximum 0.13

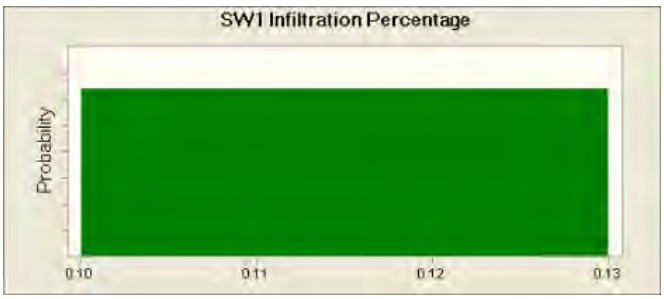

Parameter: SW2 Infiltration Percentage

Uniform distribution with parameters:

Minimum 0.05

Maximum 0.10

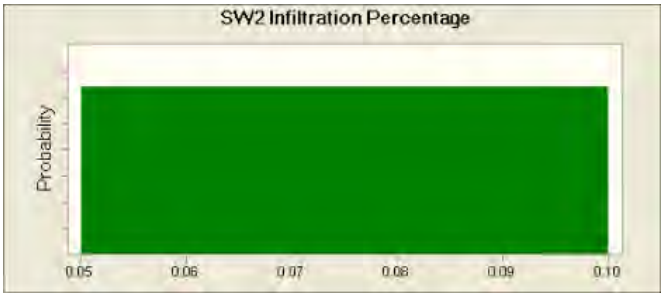

Parameter: SW3 Infiltration Percentage

Uniform distribution with parameters:

Minimum 0.25

Maximum 0.30

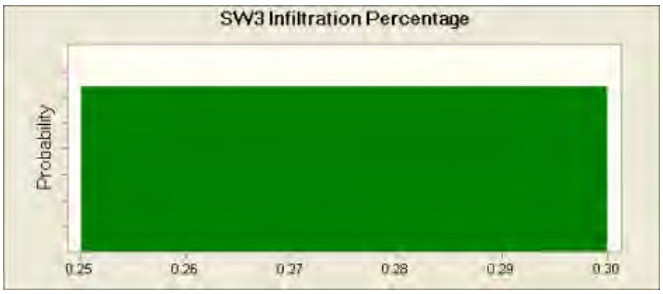

Parameter: TF Hydrologic Conductivity (cm/s)

Lognormal distribution with parameters:

Mean 9.77E-4

Std. Dev. 3.16E+0

Selected range is from 5.00E-4 to 1.00E-2

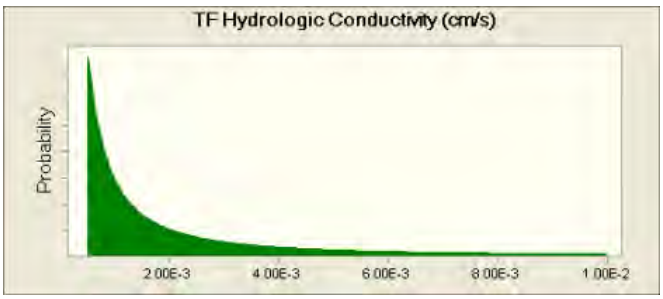

Parameter: TF Total Porosity

Uniform distribution with parameters:

Minimum 0.10

Maximum 0.30

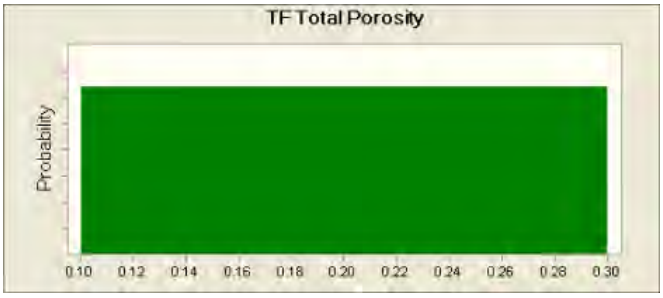

Parameter: Totavi - Log of Effective Porosity

Normal distribution with parameters:

Mean -1.25

Std. Dev. 0.75

Selected range is from -2.00 to -0.60

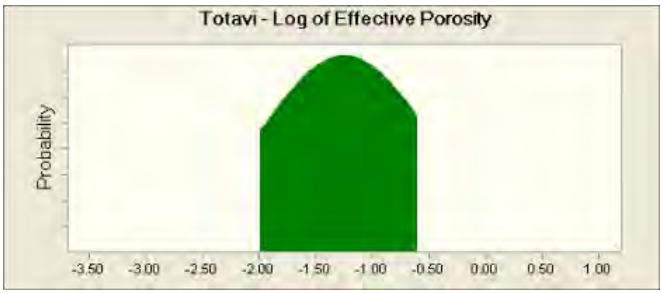

Parameter: Totavi - Log of Hydraulic Conductivity (cm/s)

Normal distribution with parameters:

Mean -11.00

Std. Dev. 0.33

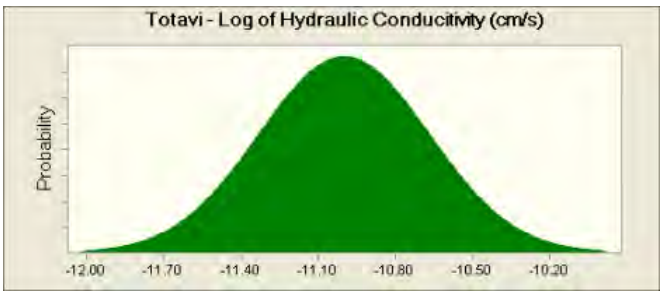

Parameter: Tsankawi Pumice Alpha (1/cm)

Pareto distribution with parameters:

Location 3.76E-3

Shape 1.46649

Selected range is from 3.90E-3 to 4.96E-2

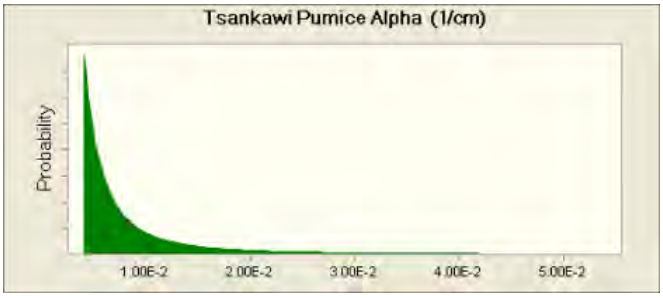

Correlated with: sankawi Pumice Hydraulic Conductivity (cm/s)

Coefficient 0.67

Parameter: Tsankawi Pumice Hydraulic Conductivity (cm/s)

Lognormal distribution with parameters:

Mean 3.88E-4

Std. Dev. 6.69E-4

Selected range is from 2.20E-5 to 2.50E-3

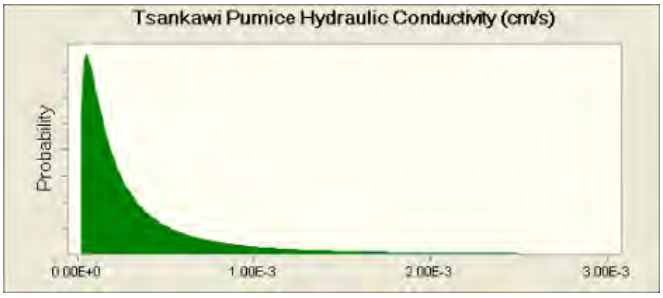

Correlated with: sankawi Pumice Alpha (1/cm)

Coefficient 0.67

Parameter: Tsankawi Pumice Porosity

Normal distribution with parameters:

Mean 0.48

Std. Dev. 0.02

Selected range is from 0.45 to 0.52

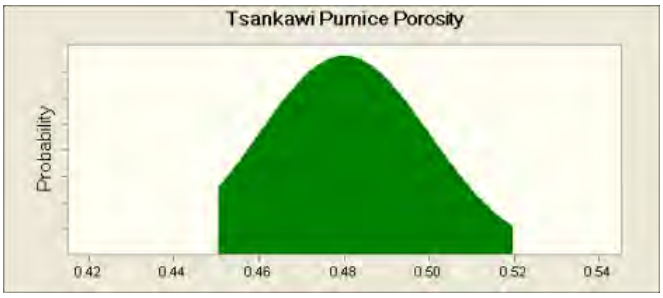

Parameter: Tschicoma - Log of Effective Porosity

Normal distribution with parameters:

Mean -4.50

Std. Dev. 0.75

Selected range is from -6.00 to -3.00

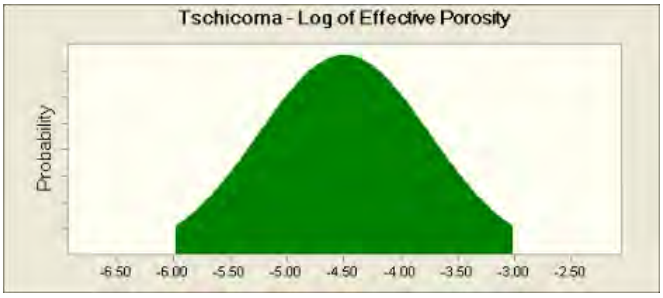

Parameter: Tschicoma - Log of Permeability (m^2)

Normal distribution with parameters:

Mean -10.50

Std. Dev. 0.50

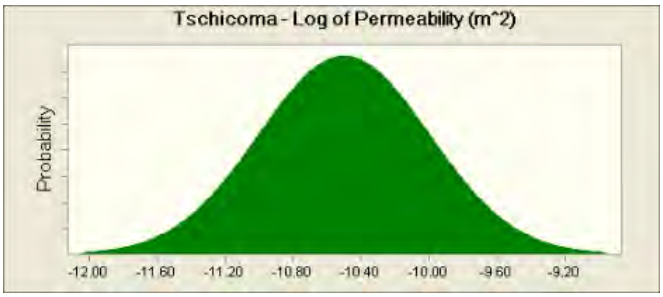

Parameter: Tschicoma Dacite Log of Total Porosity

Uniform distribution with parameters:

Minimum -4.00

Maximum -2.00

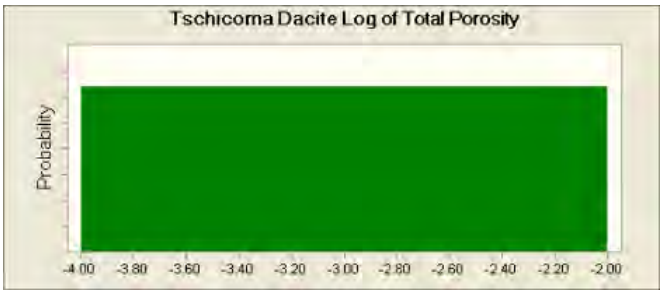

Parameter: Tshirege Unit 1v - Alpha

Lognormal distribution with parameters:

Mean 4.96E-3

Std. Dev. 3.42E-3

Selected range is from 1.20E-3 to 1.54E-2

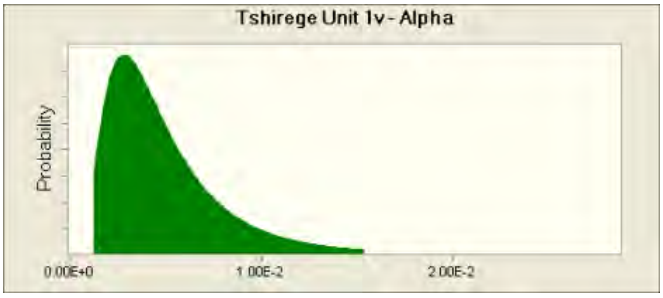

Parameter: Tshirege Unit 1v - Porosity

Lognormal distribution with parameters:

Mean 0.53

Std. Dev. 0.07

Selected range is from 0.41 to 0.60

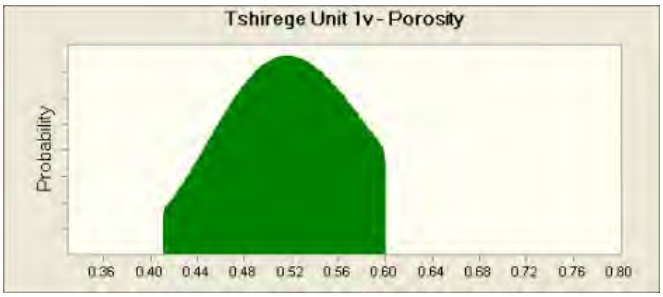

Parameter: Tshirege Unit 1v Log of K_{sat} (cm/s)

Normal distribution with parameters:

Mean -3.88

Std. Dev. 0.45

Selected range is from -4.50 to -2.64

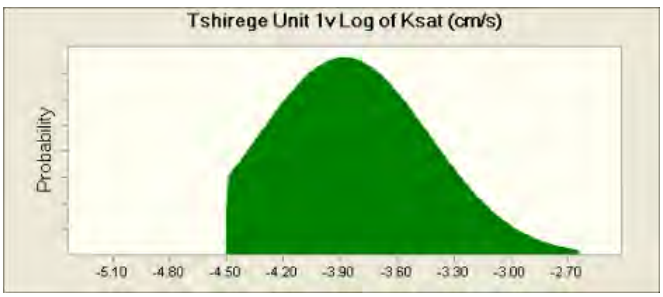

Parameter: Tshirege Unit 2 - Alpha (1/cm)

Lognormal distribution with parameters:

Mean 4.39E-3

Std. Dev. 3.09E-3

Selected range is from 8.00E-4 to 1.46E-2

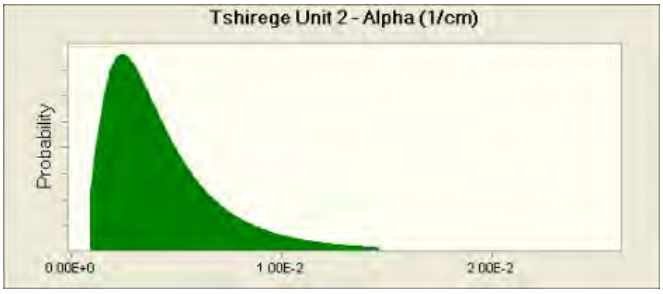

Parameter: Tshirege Unit 2 - Log of K_{sat}(cm/s)

Normal distribution with parameters:

Mean -3.99

Std. Dev. 0.59

Selected range is from -4.72 to -3.29

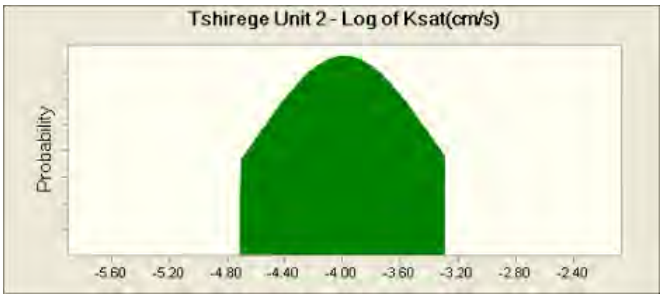

Parameter: Tshirege Unit 2 - Porosity

Student's t distribution with parameters:

Midpoint 0.44

Scale 0.05

Deg. Freedom 2

Selected range is from 0.26 to 0.60

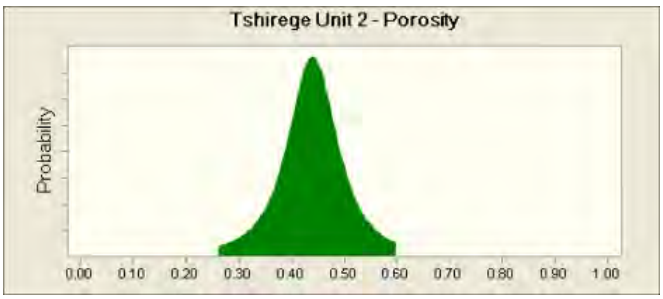

Parameter: Vadose Zone Longitudinal dispersivity (m)

Uniform distribution with parameters:

Minimum	0.50
Maximum	5.00

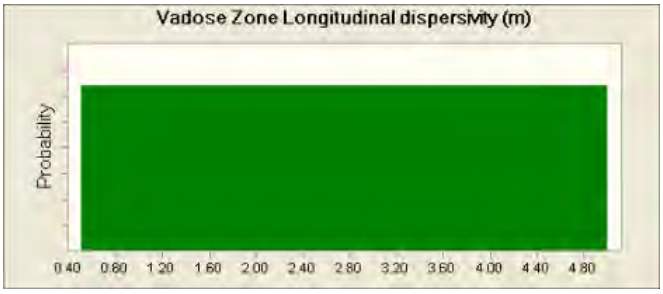

	Plants	SW1
Plants	Plants	Plants/SW1 Interaction Biomass Decay, direct contact, exudates
SW1	SW1/Plants Interaction Uptake of dissolved contaminants from surface water into plants.	Sandia Surface Water Segment to E123 From the outfall to the eastern end of the wetland (E123 gaging station) This segment is perennial. Additional sources of surface water and contaminants include runoff and precipitation within the watershed. In the lower portion of this segment, surface water flow is expressed across the entire valley floor within the wetland Some percentage of the surface water is evaporated

Figure D-1 Sample segment of the Conceptual Model Matrix

Appendix E

Numerical Evaluation of Chromium Transport in the Unsaturated Zone and Regional Aquifer Near Sandia Canyon

E-1.0 INTRODUCTION

Numerical flow and transport models of the unsaturated zone and the regional aquifer in the Sandia Canyon area are developed to inform and enhance the understanding of the fate and transport of chromium (Cr) in the environment. The goals of the Los Alamos National Laboratory (LANL or the Laboratory) study are to develop groundwater flow and contaminant transport models and to use the models to predict future contaminant concentrations and contaminant transport times to monitoring and municipal supply wells. This appendix describes the current state for the development of these models and discusses preliminary results. Further model development and calibration are required before the simulations can be used to predict the nature and extent of Cr contamination or assess the monitoring well network for Sandia Canyon contaminants. However, the modeling results are consistent with key aspects of the conceptual model of Cr transport through the vadose zone and regional aquifer, and the results provide a tool for assessing the sensitivity of parameters that control Cr fate and transport.

Flow and transport simulations are used to predict the migration of Cr from its source at the outfall through the regional aquifer. The simulations consider transport in surface water, alluvial groundwater, the unsaturated zone, and the regional aquifer. The effects of geochemical interactions of contaminants with wetland materials and with rocks along the flow paths are also included. Monte Carlo simulations that include uncertainty in input parameters are run to determine the range of likely transport behavior. The implementation of assumptions, boundary conditions, and parameter distributions made in the models honors the conceptual model described in section 3 of this report and in the more comprehensive Conceptual Model Matrix presented in Appendix D. In addition, section E-3 outlines the assumptions and Laboratory's interpretation of the site-scale and basin-scale flow in the Los Alamos region.

Sodium molybdate was used from 1993 to 2001 in the Technical Area (TA) 03 power plant cooling towers and released with effluent to Sandia Canyon. Molybdenum (Mo) is observed in Sandia Canyon characterization coreholes (SCC) in the upper portion of the unsaturated zone and provides useful data for model calibration. Therefore, simulations of Mo transport are also developed and presented.

The following items describe the source and pathway components that are included in the modeling study. Specifically, the simulations calculate the transport of Cr and Mo through the unsaturated zone (excluding the shallow alluvial system) and then through the regional aquifer. In this study, the unsaturated-zone and regional models are separate. The sources of water and contaminants and subsequent distribution to the suballuvial unsaturated zone are calculated and applied as boundary conditions to the unsaturated-zone model.

The simulations are run with the Finite Element Heat and Mass Transfer code (FEHM) (Zyvoloski et al. 1996, 054421; Zyvoloski et al. 1997, 070147). FEHM was developed by researchers at the Laboratory and is capable of simulating three-dimensional, time-dependent, multiphase, nonisothermal flow and multi-component reactive groundwater transport through porous and fractured media. FEHM has been used in a wide variety of applications. The software is mature, has users throughout the world, and has been certified through the Yucca Mountain Project Software Quality Assurance Program. FEHM is available to the public and operates under various operating systems.

E-2.0 UNSATURATED-ZONE FLOW AND TRANSPORT MODEL

The numerical model for unsaturated-zone flow and transport includes components that define the water source to Sandia Canyon and the spatial distribution of infiltration along the canyon floor resulting from this source. In addition, Cr and Mo sources are included as part of the unsaturated zone.

E-2.1 Model Setup

Water source: The effluent volumes released at National Pollutant Discharge Elimination System (NPDES) Outfall 01A-001 into the head of Sandia Canyon are the assumed primary water source to the canyon. These volumetric flow rates are bounded by discharge records and include both cooling tower blowdown and sanitary effluent that were released at the same outfall. In the simulations, two time periods are used to describe the historical discharges into upper Sandia Canyon.

- The first period is from 1951 to 1991 when the cooling towers used treated sewage effluent as their primary water source. Outfall volumes during that time were dominated by cooling tower effluent, and effluent volumes are assumed to be described by the range of values presented in Appendix A, Table A-2. This data set has a mean value of 650 m^3/d (172,000 gal./d) and ranges between 480 and 970 m^3/d (126,000 and 255,000gal./d). The data set is described by the parameter distribution "Effluent Discharge Rate from 1950 to 1991" in Appendix D. For a given Monte Carlo simulation, a single value from this distribution is chosen and applied for the entire period from 1951 to 1991. That is, the effluent volume is assumed to be steady and that volume enters the canyon as surface-water flow that in turn infiltrates into the unsaturated zone. Transient flow is not included, but the uncertainty in the effluent volume discharged to the canyon is captured in the set of Monte Carlo numerical simulations.
- The second period is from 1992 to 2007. The Laboratory's TA-46 Sanitary Wastewater System (SWWS) came online in 1992. This system consolidates Laboratory-wide sanitary waste treatment and releases to the head of Sandia Canyon at Outfall 01A-001. In general, the sanitary effluent was not used as cooling water, and effluent volumes increased in 1992. Outfall volumes for the period from 1999 to 2006 were used to estimate the distribution for this second time period. This data set has a mean value of 980 m^3/d (260,000 gal./d) and ranges between 380 and 2300 m^3/d (100,000 and 600,000 gal./d). It is described by the parameter distribution "Effluent Discharge Rate beginning 1992" in Appendix D. For a given Monte Carlo simulation, a single value from this distribution is chosen and applied to the entire time period from 1992 to 2007. As with the first time period, the effluent volume is assumed to be steady and results in infiltration into the unsaturated zone. Uncertainty in the effluent volume is captured by the set of Monte Carlo simulations.

Infiltration Models 1 and 2: Water discharged to the canyon is distributed down the canyon through lateral surface water and alluvial groundwater flow and is assumed to infiltrate the deeper unsaturated zone, consistent with two surface water balances performed in the canyon. The canyon is described using four surface water segments named SW1, SW2, SW3, and SW4 (Figures 1.0-1 and 3.0-1). SW1 is the wetland area at the head of the canyon and includes the Rendija Canyon fault zone. SW2 is a narrow section of the canyon that has a bedrock base and is located between gages E-123 and D-123.6. SW3 is another narrow canyon segment that has a bedrock base and some alluvium in the canyon floor. SW3 is located between gages D-123.6 and D-123.8. Finally, SW4 is the broadest segment in the canyon located east of gage D-123.8. This segment has a substantial thickness of alluvium that houses a perched alluvial aquifer atop unsaturated bedrock. Infiltration patterns differ across these four segments because of topographic and hydrologic controls.

- The two infiltration models used in the simulations assume that the spatial distribution of surface-water losses control infiltration patterns.

- Infiltration Model 1 is based on the Sandia Canyon surface water balance performed in 2006 (see Figure 2.0-1 in LANL 2006, 094431). In that study, surface water losses were presented as percentages of the canyon surface-water balance with approximately 10% to 13% lost in SW1, approximately 35% lost in the combined SW2 and SW3 segments, and approximately 50% lost in SW4. Infiltration Model 1 assumes the following ranges in percentages to account for uncertainty in the infiltration model: 10% to 13% lost in SW1, with 0% to 20% of this SW1 volume infiltrating into the Rendija Canyon fault; 5% to 10% lost in SW2; 25% to 30% lost in SW3; and the remainder (47% to 60%) lost in SW4. A single value for each of these percentages is chosen using Monte Carlo sampling (Appendix D) and is fixed for a given simulation.
- Infiltration Model 2 is based on the more recent Sandia Canyon surface water balance performed in the summer of 2007 and presented in Appendix B. A temporary gage (D-123.6) was installed at the eastern end of SW2 to estimate surface water losses in that steep, narrow canyon segment. Results of the study indicate that losses in SW1 and SW3 are fairly steady rather than being a percentage of the surface water present. Some of the water lost in SW1 emerges in SW2, indicating that SW2 is considered to be a gaining reach rather than an infiltration zone. Finally, flow to SW4 is transient and depends on antecedent conditions, effluent discharge volumes, and precipitation. Based on this updated study, Infiltration Model 2 uses the following volumetric flows to define infiltration rates in the different canyon segments: 10 to 150 m^3/d (3 to 46 acre-ft/yr) in SW1 and 370 to 710 m^3/d (110 to 210 acre-ft/yr) in SW3. Any remaining water, as defined by the water sources described above, that has not infiltrated in SW1 and SW3 infiltrates SW4. If the water source entering the canyon cannot satisfy the combined specified fluxes in SW1 and SW3, the water flux to SW3 is decreased to satisfy the water balance and no flow continues to SW4. However, the simulations do assume a minimum infiltration rate of 50 mm/yr in the Rendija Canyon fault zone in SW2 and in SW4 as a lower bound.
- When two infiltration models are used, volumetric water flux to the unsaturated zone as a function of both location and time is calculated based on uncertain parameters describing time-varying effluent release to the canyon and the distribution of that flow along the length of the canyon. These spatially and temporally varying water fluxes are applied as boundary conditions to the unsaturated-zone model runs. The unsaturated-zone model uses a series of 18 one-dimensional vertical columns (grids) to describe the unsaturated zone beneath Sandia Canyon. The center location of the columns is shown in Figure 4.0-1 of this report. Partitioning of water flux to a column depends first on the surface-water segment where it is located, as described above. In addition, each column has a surface area that represents the area over which infiltration is likely to occur. This area is determined by the spacing between the one-dimensional columns and an approximate channel width, which is defined either by the topographic width of the channel in the narrow sections or by the estimated width of the perched-alluvial groundwater body that is thought to exist at the base of the alluvium at that location. Table E-2.1-1 gives the location, length, width, and resulting areas for the 18 columns. For a given surface water segment, the water flux is applied using area weighting, which results in identical infiltration rates for all columns in a given surface water segment. The simulations start in 1951, the approximate time when effluent releases to the canyon began, using an initial steady flow condition that sets a 50 mm/yr infiltration rate along the entire canyon. The increased water flux is superimposed upon this steady condition, which has little effect on simulation results.

Contaminant source: Cr(VI) and Mo released from the TA-03 power plant cooling towers reacted with wetland sediments and organic matter resulting in lower surface-water concentrations than the original effluent concentrations. Because surface water is the source of unsaturated-zone water, reported surface-water concentrations are used to define mass fluxes for Cr and Mo are then used as boundary conditions for the unsaturated-zone simulations.

- Historical Cr releases are described using three time periods based on measured surface-water concentrations. The first historical release took place from June 1956 to April 1972, which is the active period of Cr use at the power plant (LANL 2006, 094431). During that time, surface water concentrations averaged 7 mg/L and ranged from 1.9 to 12 mg/L. The second period extends from April 1972 to 1990. It reflects decreased concentrations in response to discontinued Cr use and concentrations range uniformly between 10 to 60 μg/L. The third period is from 1991 to 2007, and concentrations range between 0.1 and 31 μg/L. The distributions used for these three variables are provided in Appendix D and are called "Cr1 1956-1972 SW Concentration, Cr2 1972-1990 SW Concentration and Current Chromium Concentrations," respectively.
- Historical Mo releases are described using only one period based on measured surface water concentrations. Mo was reportedly used at the power plant from 1993 to 2001 (LANL 2006, 094431). However, elevated levels of Mo were detected in Sandia Canyon surface water between 1991 and 2001. During that time, surface-water concentrations averaged from 100 to 400 μg/L, and a uniform distribution in this range is used to define the Mo source ("1991-2001 Mo SW Concentration" in Appendix D).
- To calculate contaminant mass flux, the time-dependent surface-water concentration is multiplied by the appropriate time-dependent water flux. The contaminant mass flux at each location is then applied as a time-varying boundary condition to the corresponding one-dimensional unsaturated zone column. For a given simulation, a single value is determined for each of the concentration ranges (and time periods) described above and fixed for that particular simulation. Therefore, the simulations grossly account for transients in contaminant releases as defined by the release time periods, but within a specified release period the surface water concentration is fixed. Uncertainty is captured through the Monte Carlo simulations.

Unsaturated-zone model: As described above, the unsaturated zone is modeled using 18 one-dimensional vertical columns (grids) that span the length of the canyon from the wetland area to the location of Corehole SCC-6 (Figure 4.0-1 of this report and Table E-2.1-1 of this appendix). Several of the columns in SW4 are located at SCC coreholes to easily compare model results to data from the coreholes. The columns represent the strata that lie between the base of the alluvium (if present, otherwise from the surface) to the water table, excluding the second column in SW1, which represents the Rendija Canyon fault zone. The grids use an updated Sandia Canyon stratigraphic framework model to define the one-dimensional unsaturated-zone columns. In the simulations, the strata are assigned hydrologic properties that are represented by parameter distributions, which are described in Appendix D. The hydrologic properties of the fractured Cerros del Rio basalt are used to represent flow in the fault zone so water flows quickly through this area, particularly for Infiltration Model 1. An important feature of the geology is that the Cerros del Rio basalt is present in the eastern portion of the canyon (Figure 3.0-1 of this report) corresponding to the locations of column SW3-5 and all of SW4 (Figure 4.0-1 of this report).

- Geochemical interactions of Cr and Mo with unsaturated-zone bedrock units are included in the model. Cr is assumed to adsorb onto all units (except for the treatment of the Cerros del Rio basalt described below) with an adsorption coefficient (K_d) of from 0 to 0.3 ml/g (Appendix D, parameter "K_d–Vadose Zone above and below the basalt"). Mo is assumed to adsorb onto all units with K_d of 0 to 0.1 mL/g that is perfectly correlated with the K_d for Cr. Adsorption is reversible and acts to delay the transport of Cr and Mo as they migrate through the unsaturated zone. Adsorption is explicitly modeled in the numerical simulations. A fraction of the mobile Cr(VI) is expected to be reduced to Cr(III) in the eastern portion of the canyon where the Cerros del Rio basalt is present. At those locations, the Cr reacts with and is permanently retained by the Cerros del Rio basalt. This reaction is not explicitly modeled in the transport simulations. Rather, the appropriate fractional reduction is accounted for by reducing the simulated mass flux exiting each

unsaturated zone column that contains basalt by a factor of 0% to 64% (Parameter "Mass Transfer for Basalt as a Percentage of the Cr Exiting a VZ Column" in Appendix D. Note that this parameter originally ranged from 0% to 52% but was rescaled in the simulations to cover the correct range).

- Water fluxes and contaminant mass fluxes are applied as boundary conditions to the 18 one-dimensional columns using the assumptions described above. The resultant unsaturated-zone flow and transport are calculated with FEHM using a Richard's equation solution for flow and the advection-dispersion equation for transport (Zyvoloski et al. 1996, 054421; Zyvoloski et al. 1997, 070147). The main outputs of these simulations are breakthrough curves that depict the time-dependent contaminant mass fluxes to the regional aquifer for each of the 18 columns. The mass fluxes are applied as a boundary condition to the regional model and is described in section E-3. For this modeling exercise, 100 transport simulations for Cr and for Mo were run for each infiltration model.

E-2.2 Unsaturated-Zone Flow and Transport Model Results

Chromium breakthrough to the regional aquifer: The primary results for the unsaturated-zone transport models are breakthrough curves of Cr and Mo as a function of time for the 18 one-dimensional columns to the regional aquifer. Realization 60 was determined to be a typical simulation for Infiltration Model 1. The predicted Cr breakthrough curves for Realization 60 are presented for Infiltration Models 1 and 2 in Figures E-2.2-1 and E-2.2-2, respectively. This example illustrates the transport behaviors that result from the two infiltration models. The results are very different given that the majority of the input parameters (hydrologic properties, K_ds, water source, and input Cr concentrations) are identical for the two runs. The difference in the two simulations is the distribution in the assumed infiltration pattern along the canyon floor.

- Results for Infiltration Model 1 (Figure E-2.2-1) show near-immediate breakthrough along the Rendija Canyon fault zone as evidenced by the green curve that terminates in the early 1970s. The infiltration model was designed to provide this type of behavior to determine the sensitivity of a preferential unsaturated-zone transport pathway on regional aquifer results. In the remainder of the surface-water segments, the relative travel times are determined by the ratio of the percentage of the water volume that infiltrates in a segment (as defined by Infiltration Model 1) compared to its relative area over which infiltration occurs (last column in Table E-2.1-1). For example, rapid transport is calculated for SW2 because this canyon segment receives a comparatively large percentage of the total flow (5% to 10%) given its small relative surface area of less than 2% of the canyon (Table E-2.1-1). Arrival of the contaminants at the water table from SW3 (25% to 30% of water over 25% of the area) lags behind SW4. Chromium arrives next at the water table in SW4 because most (47% to 60%) of the water infiltrates in this segment which makes up 51% of the infiltration area in the canyon. Finally, Cr arrives last at the water table in SW1 because a relatively small percentage of the water infiltrates wetland area (10% to 13%) compared to its relatively large relative infiltration area of 23%. The magnitude of the Cr fluxes from SW4 and SW3 are higher because more contaminated water enters (and exits) these segments because of their greater surface areas. For Realization 60 in the year 2007, peak breakthrough of Cr has already occurred in the fault (SW2) and SW4. Near-peak breakthrough occurs in SW3, and almost no breakthrough occurs at SW1. This result agrees well with the summary discussion of Table 5.1-1 presented in section 5 of this report.
- Results for Realization 60 using Infiltration Model 2 (Figure E-2.2-2) show breakthrough only in SW3 and SW4. The infiltration model was designed to have virtually no flow along the fault or in SW2. In most realizations, the water volume infiltrating SW3 is higher than for SW4 and

breakthrough occurs at SW3 first. Many realizations show significantly delayed transport in SW4 relative to this example. In addition, many realizations show more rapid transport in SW1 than is depicted here because Realization 60 defines a relatively low flow of 45 m^3/dy (14 acre-ft/yr) to the wetland area. For Realization 60 in the year 2007, peak breakthrough of Cr has already occurred in both SW3 and SW4, but no Cr has arrived at the water table from SW1. This result concurs with the results for SW3 and SW1 presented in summary Table 5.1-2 presented in section 5 of this report. However, the summary results show greater retention in the unsaturated zone in SW4 than is indicated by Realization 60 because of low water volumes.

Comparisons to field data: It is useful to compare modeled concentrations to field data to determine whether the model set up and parameter distributions recreate the system behavior. Porewater concentration data for Cr and Mo collected in the unsaturated zone in the SCC coreholes are compared to the unsaturated-zone simulation results for Column SW4-5 (Figure 4.0-1 of this report), which is located at SCC-2. Simulated transport at this location is typical for SW4, the only canyon segment for which unsaturated-zone field data are available. Also, the coreholes were drilled just to the top of the Cerros del Rio basalt; therefore, simulated concentration profiles can only be compared to data for the upper 80 to 120 m of the unsaturated zone (LANL 2006, 094431).

- Figures E-2.2-3 and E-2.2-4 compare the 100 simulated Cr porewater concentration profiles as functions of elevation for Infiltration Models 1 and 2, respectively, to the Cr porewater concentrations observed in SCC-1 through SCC-6 (LANL 2006, 094431). The field data were collected in 2006 and simulation results for that same time are shown. The elevations plotted for the SCC data are realigned so that the elevation at the base of the alluvium at each corehole aligns with the base of the alluvium in SCC-2. Only data below the base of the alluvium are compared to the simulated results because the simulations consider transport below this horizon. The filtered samples are for dissolved Cr, which represents Cr(VI). All measured porewater concentrations were less than 0.2 mg/L. In the combined data set presented here, more than half of the samples had concentrations below the Cr detection limit (for more detail, see Figure 5.5-1 in LANL 2006, 094431). For Infiltration Model 1 (Figure E-2.2-3), the majority (>60%) of the simulations predict very low concentrations that agree with much of the field data. However, none of the simulations predict the residual Cr observed at (adjusted) elevations of 2010 to 2030 m in SCC-4 and SCC-5. For Infiltration Model 2 (Figure E-2.2-4), fewer of the realizations predict the very low concentrations observed in the data and predicted by Infiltration Model 1. The Cr concentration profiles remain at high elevations with this model, and many of the simulations have much high concentrations (up to 5 mg/L) than are observed in the data. Infiltration Model 1 yields results that better match the unsaturated-zone Cr field data.
- Figures E-2.2-5 and E-2.2-6 compare the 100 simulated Mo porewater concentration profiles as functions of elevation for Infiltration Models 1 and 2, respectively, to the Mo porewater concentrations observed in SCC-1 through SCC-6 (LANL 2006, 094431). Again, the field data and simulation results are for 2006, and elevations for the SCC data are realigned for better comparison. In the combined data set presented here, most of the Mo concentrations are above its detection limit (for more detail, see Figure 5.5-3 in LANL 2006, 094431). Because Mo profiles are detected, the data set is considered to be useful for model calibration, particularly for determining potential infiltration rates. Both infiltration models predict concentrations that agree well with observed porewater concentrations. However, as for Cr, none of the simulations predict the residual Mo detected at the higher (adjusted) elevations in the coreholes, particularly SCC-2 and SCC-4.

- A statistical comparison between simulated results and the combined Cr and Mo concentrations for the SCC coreholes is provided in Appendix G. Also, a brief discussion of Cr adsorption throughout the unsaturated zone and reaction with the Cerros del Rio basalt is provided in the summary given in section 5 of this report.

E-3.0 NUMERICAL EVALUATION OF GROUNDWATER FLOW IN THE REGIONAL AQUIFER NEAR SANDIA CANYON

E-3.1 Conceptual Model

This section describes the hydrology and geology of both near Sandia Canyon and the Pajarito Plateau region. Particular emphasis is placed on describing regional groundwater flow and assumptions made about how water migrates from the plateau to the regional aquifer and to the Rio Grande.

E-3.1.1 Regional Aquifer

The regional aquifer beneath the Pajarito Plateau is a complex heterogeneous system. The elements of the water balance, properties of the flow medium, and hydrodynamics of the system are discussed in the following sections. The aquifer beneath the Laboratory is a subportion of the basin-scale aquifer associated with the Española Basin. Because the site-scale aquifer dynamic hydraulics are connected with the basin-scale aquifer, some of the characteristics of the Española Basin aquifer that influence the site-scale aquifer are discussed as well.

E-3.1.2 Structure of the Saturated Zone

The top of the saturated zone beneath the Pajarito Plateau is predominantly under phreatic (water table) condition. The regional water table is located approximately 300 to 400 m below ground surface across the Plateau. The spatial distribution of hydrostratigraphic units intersected by the water table is presented in Figure E-3.1-1. From west to east, major hydrostratigraphic units intersecting the regional water table are Keres Group, Tschicoma Formation, Puye Formation, Cerros del Rio basalts, Totavi Lentil, Santa Fe Group, and Bayo Canyon basalts. Near Sandia Canyon the important units that are expected to affect the flow and transport near the water table are the Puye Formation and Cerros del Rio basalts.

The total thickness of the regional aquifer is unknown. It can be assumed that at a minimum the aquifer encompasses the total thickness of the Española Basin fill. The approximate thickness of the fill varies from 300 m at the basin edges to 2000 m in the central portion. The amount of information available about the hydrogeological properties of the regional aquifer diminishes with depth because monitoring wells are not drilled deep into the aquifer. Most of the data relevant for the deep portion of the aquifer come from the water-supply wells and deep monitoring wells. Because of screen lengths, information collected at the supply wells represents a large thickness of the formation (for example, the water levels measured at the supply wells are representative of an average pressure along the entire length of the screen).

The aquifer is composed of stratified sedimentary and volcanic hydrostratigraphic units. The sedimentary units are made up of beds of varying thickness, lateral extent, and permeability. Relatively continuous horizontal zones of high permeability and low porosity are associated with the coarse-grained materials of the Totavi lentil (in the area between the Laboratory and the Rio Grande) and the pumiceous Puye Formation. However, the degree of lateral continuity of low- and high-permeability beds within the sedimentary units is not known because the individual beds cannot be accurately mapped between the existing widely spaced boreholes. However, the existence of multiple low-permeability beds in the Puye

Formation and the Santa Fe Group (Broxton and Vaniman 2005, 090038) potentially produces a large-scale aquitard, which causes the observed large-scale confinement of the deeper portions of the aquifers (Purtymun 1995, 045344).

The groundwater flow medium can be defined as a complex multiaquifer-multiaquitard system. The existing groundwater flow exhibits a complex three-dimensional structure. Uncertainty in the conceptual model is associated with defining groundwater flow and contaminant transport pathways in the regional aquifer. Currently, two alternative conceptual models address this uncertainty (Figure E-3.1-2) as follows.

Conceptual Model A. No hydraulic separation exists between the shallow and deep (pumped) aquifer zones. Pumping drawdowns are manifested at the water table. Near the pumping wells, water-table hydraulic gradients are affected by pumping, and contaminants are drawn toward the supply wells. The shallow and deep aquifer zones have similar hydrodynamic properties and are not hydrodynamically distinct. Potential contaminants in the regional aquifer are expected to be predominantly captured by the water-supply wells. In both the shallow and deep portions of the regional aquifer, flow directions are west (Jemez Mountains) to east (Rio Grande), and groundwater flow is predominantly discharged at the Rio Grande. This conceptual model is close to the classical basin-scale flow structure (Figures E-3.1-3) discussed in previous studies (Freeze and Cherry 1979, 088742; Keating et al. 1999, 088746; Keating et al. 2000, 090188; Keating et al. 2001, 095399; Collins et al. 2005, 092028).

Conceptual Model B. A strong hydraulic separation exists between the shallow (phreatic, water table) and deep (pumped) aquifer zones, which does not allow pumping drawdowns to reach the water table. As a result, hydraulic gradients in the phreatic zone are expected to be unaffected or negligibly affected by pumping from municipal supply wells. The deep portion of the regional aquifer is predominantly under confined conditions. Contaminants are likely to flow predominantly in the phreatic zone, above the well screens of the water-supply wells. Discharge of water from the phreatic zone occurs in springs near the Rio Grande. Nevertheless, because of substantial downward vertical hydraulic gradients between the shallow and deep aquifer zones, some contaminants may reach the water-supply wells by flow through hydraulic windows and potentially along well filter packs (Vesselinov 2005, 090040; Vesselinov 2005, 089753; LANL 2006, 094431). In the shallow portion of the regional aquifer, flow directions are from west (Jemez Mountains) to east (Rio Grande), and groundwater flow predominantly discharges at the Rio Grande. In the deep portion of the regional aquifer, flow directions may not be coincident with the flow directions in the phreatic zone (Figure E-3.1-3). There is uncertainty, but the deep flow directions may have a more dominant southern component based on the basin-scale discharge boundaries to the south (Cochiti Lake, Albuquerque Basin) (Vesselinov 2005, 089753; Vesselinov 2005, 090040).

These alternative models represent two end members for a spectrum of potential flow configurations and therefore capture some aspects of the potential conceptual model uncertainty. The contaminant pathways in the regional aquifer depend strongly on the existence, or lack thereof, of a phreatic zone in the shallow portion of the regional aquifer, which is hydraulically separated from the deep portions of the regional aquifer.

The thickness of the phreatic zone is difficult to characterize based on existing hydrogeological information. Instead, the thickness of the phreatic zone is approximately defined by the water-table response at individual wells. For example, one of the objectives of drilling R-35 in Sandia Canyon is to evaluate vertical stratification of the potential Cr plume (LANL 2006, 091987). Two closely spaced wells with screens vertically are separated by about 165 ft. Based on the recently obtained R-35 data, the screens are hydraulically separated (LANL 2007, 098129). The top screen responds as if located in the phreatic zone, and the deeper screen is impacted by water-supply pumping (e.g., PM-3 and O-4). Similar observations are made at R-19 and R-17 to the west of Sandia Canyon. The top regional screens at these wells are in the phreatic zone, and the deeper screens are impacted by water-supply pumping. The

distance between the screens is 200 ft at R-19 and 44 ft at R-17. At these locations, the thickness of the phreatic zone is some unknown fraction of this distance. Spatial interpolation of phreatic zone thicknesses based on individual well data is even more complicated.

The actual thickness of the phreatic zone may not be that important for contaminant transport predictions. It is much more important to consider the potential for (1) vertical flow from the shallow phreatic into deep confined aquifer zones through hydraulic windows and (2) vertical dispersion of the plume at the top of the regional aquifer. There are no field data to estimate the magnitude of these processes.

Most of the recently collected data (e.g. water-level and geochemistry data for R-35 and R-17 (Kleinfelder 2006, 092493; LANL 2007, 098129) and groundwater stable-isotope analyses (Longmire et al. 2007, 096660), support the conceptual model that focuses on the impacts of water table ("phreatic") zone on contaminant migration. It has been concluded that Conceptual Model B is more appropriate to characterize flow and transport conditions at the site. For the purpose of this report, only simulations based on this conceptual model are performed.

E-3.1.3 Water Table Maps and Flow Directions

Figure E-3.1-4 shows a map of water-table elevation based on the existing water-level data (LANL 2007, 095787). Additional details about contouring process are presented in the "2007 General Facility Information Report" (LANL 2007, 095787). The water table map suggests an influence of groundwater recharge along Los Alamos, Pueblo, Sandia, de Valle and Water Canyons on the shape of the water table. At the water table, horizontal components of the hydraulic head gradient tend to have an easterly/southeasterly direction across the plateau, and the gradients range from 0.0026 to 0.162 m/m. Generally, gradients are higher to the west and lower to the east (Purtymun 1995, 045344).

It should be emphasized that the water table maps do not suggest that the intensive water-supply pumping in the deep zone of the regional aquifer on the Pajarito Plateau impacts the shape of the regional water table. Therefore, it is concluded that hydraulic gradients at the water table near Sandia Canyon are not or negligibly affected by the water-supply pumping.

E-3.2 Numerical Model for the Regional Aquifer

The major objective of the regional aquifer simulations is to determine the likely migration direction for contaminants released along Sandia Canyon in the regional aquifer. Uncertainties in the model predictions are also addressed. In these analyses, it is assumed that contaminant transport through the vadose zone is predominantly vertical and one-dimensional, without lateral divergence as described in Section E1.

The regional aquifer flow simulations are solved using a finite-volume formulation in FEHM (Zyvoloski et al. 1997, 070147). The transport within the regional aquifer is simulated using random-walk, particle-tracking techniques in FEHM (Robinson et al. 2000, 097897; Lichtner et al. 2002, 095397). In this case, a predefined, large number of particles are released within areas at the top of the regional aquifer corresponding to the locations of the one-dimensional unsaturated-zone model columns. The number of particles is selected to be large enough for sufficient characterization of contaminant dispersion in the model domain. The particles' movement is tracked through the model domain to estimate potential spatial migration of contaminants. Specially developed codes for numerical convolution (PlumeConvolute) and computation of plume statistics (PlumeStat) are used to process and analyze FEHM simulation outputs.

The simulations and data processing are computationally highly intensive and produce a considerable amount of output data. The analyses are achieved efficiently through parallelization using the Laboratory's supercomputers. The code MPRUN is used to efficiently execute the Monte Carlo runs in a multiprocessor environment.

E-3.2.1 Regional Aquifer Model Setup

The flow medium is represented in the numerical model as a single continuum. No discrete faults and fractures are explicitly built into the computational grid. The potential for preferential flow heterogeneity-based channels are incorporated into the model through the input parameters.

It is important to note that the hydraulic gradients in the model are constrained based on the water table map (Figure E-3.1-4). The permeabilities of various hydrostratigraphic units are assumed to be geostatistical random variables that vary in predefined ranges. Groundwater flow (Darcy) velocity is equal to the hydraulic gradient times permeability (Freeze and Cherry 1979, 088742, Chapter 5). As a result, high-permeability values may produce groundwater flow velocities that are unexpectedly high when compared with previous estimates. However, this discrepancy can be explained in groundwater flow velocities. The transport velocities simulated in the model are considered to be characteristic only of the fraction of the groundwater flow medium where a dominant portion of contaminant transport occurs. Such a situation may arise in the case of fracture-dominated flow. In this way, the model implicitly accounts for preferential flow through the aquifer, for example, fracture flow. Therefore, the total amount of groundwater flowing through the aquifer may yet be consistent with existing hydrogeological information. In summary, the simulations target the estimation of potential uncertainties associated with contaminant transport velocities rather than groundwater flow velocities.

E-3.2.2 Model Domain and Computational Grid

In the current and future numerical analyses, three different models will be used for different simulation purposes. Each model is based on different model domains and computational grids. The three model domains are shown in Figure E-3.2-1. The domain shown in green is applied to simulate three-dimensional flow and transport in the vicinity close to the potential contaminant source at the regional aquifer. Vadose zone flow and transport above the regional water table can also be simulated using this grid. The two site-scale models (also called "pancake" models) are shown in pink and blue. These models are applied to simulate larger-scale flow and transport in the regional aquifer near Sandia Canyon. For reference purposes, the green domain is termed a "site" model (labeled as Model 1 in Figure E-3.2-1). The pink domain is Model 3—a thick pancake model—and the blue domain is Model 2—a thin pancake model. The thin pancake model was used for the simulations presented in section 5 of this report.

The computational grid of the site model is three-dimensional and predominantly structured but includes zones of telescoping grid refinement. Its thickness is approximately 1200 m (Figure E-3.2-1). The grid cells are not uniform in size. Laterally, the grid cells form squares with sizes varying from 16 to 250 m. Vertically, the thickness of the cell layers varies from 12.5 to 200 m (Figure E-3.2-2).

The grids of the two pancake models (the pink and blue domains in Figure E-3.2-1) extend from the flanks of the Sierra de los Valles on the west to the Rio Grande on the east. The entire Laboratory, as well as all the existing monitoring and Los Alamos County water-supply wells, is within the boundaries of these domains. The tops of both model domains are defined by the shape of the regional water table. The computational grids are structured. Laterally, the size of the grid cells is uniform and equal to 125 ×125 m in the thick pancake model (Figure E-3.2-2) and 25 × 25 m in the thin pancake model (Figure E-3.2-2).

For the thick pancake model, the size of the grid cells is not uniform vertically and varies from 7 to 50 m; vertical refinements are in areas where there are hydrostratigrahic units with limited vertical thickness (e.g., Totavi lentil); the total vertical thickness of the grid is about 500 m below the water table. For the thin pancake model, the thickness of the grid is 50 m and includes a single layer of grid cells.

The total number of nodes and elements in the models are as follows: the site model has 244,048 nodes and 1,394,880 elements; the thick pancake model has980,553 nodes and 5,520,462 elements; and the thin pancake model has 693,948 nodes and 2,072,862 elements. The grids are designed to sufficiently characterize medium heterogeneity, and the total number of nodes does not exceed 1 million; this limitation is caused by the size of the computer memory.

The three-dimensional geologic model (Cole et al. 2006, 095079) defines the spatial distribution of various hydrostratigraphic units that are applied to the numerical grids (Figure E-3.2-3). Table E-3.2-1 lists the hydrostratigraphic units identified in the three models and describes their spatial representation within the model domain.

E-3.2.3 Boundary Conditions

All the boundaries of the thin pancake model domain used for the transport simulations presented in section 5 of this report are defined as no-flow boundaries (Figure E-3.2-4). The existing recharge along the flanks of the Sierra de los Valles, recharge along canyons and mesas of the Pajarito Plateau, and discharge near the Rio Grande (including the White Rock Canyon springs) are not explicitly defined in the model. They are implicitly defined by the shape of the water table, which is affected by these recharge/discharge mechanisms. In this way, for example, the model can still compute contaminant concentrations at the White Rock Canyon springs.

In addition, internal boundary conditions are defined at the pumping of the water-supply wells of Otowi (O-1 and O-4) and Pajarito well fields (PM-1, PM-2, PM-3, PM-4, and PM-5). The contaminant mass fluxes calculated by the 18 one-dimensional unsaturated zone simulations are applied as boundary conditions to the regional model at the source locations shown in Figure E-3.2-4. The wells are assumed to capture contaminants migrating along the phreatic zone by vertical flow through hydraulic windows. The model also accounts for mixing that occurs at the water-supply wells when it computes contaminant concentrations.

E-3.2.4 Medium Properties

Permeability and porosity values of the hydrostratigraphic units are uncertain and are represented as random variables. The permeability and porosity are represented in the numerical model as spatially uniform for most of the hydrostratigraphic units, except the permeability of Puye Formation. The permeability of the Puye Formation is assumed to be spatially correlated with high-permeable channels in northeasterly-southwesterly direction and correlation lengths on the order of 500 m. Sample spatial distributions of permeability heterogeneity in Puye Formation are presented in Figure E-3.2-5.

It is important to note that in the case of contaminant transport near Sandia Canyon, only the flow properties (permeability, porosity) of the Puye Formation (Puye Fanglomerate, Tpf, and Pumiceous Puye) and Cerros del Rio basalts are directly relevant. The flow properties of the other hydrostratigraphic units are not expected to significantly influence the simulated flow and transport.

To represent the dispersion of the contaminant plumes, an axisymmetric form of the dispersion tensor was used (Lichtner et al. 2002, 095397); the longitudinal and transverse dispersivities are defined to characterize the tensor. It is assumed that longitudinal and transverse dispersivities are random variables

with the statistical parameters discussed in Appendix F. Site-specific data supporting these values are not available. Based on data from the literature, the selected range of values is reasonable for the spatial scale of simulated contaminant transport (approximately 100 to1000 m) (Neuman 1990, 090184) and the properties of the flow medium.

E-3.2.5 Model Calibration

Because the water table maps are directly applied to defined hydraulic heads in the models, there is no need to calibrate against existing water-level data. The model predicted concentrations of Cr and Mo are compared against existing data for monitoring wells and municipal supply wells. The model predictions obtained using the implemented ranges of conceptualizations and parameters are ranked weighted based on the matches between the simulated and observed values (Appendix G). This comparison serves as a model validation that allows predictive model simulations to be conducted and assessed with more confidence.

E-3.2.6 Estimation of Uncertainty in the Model Predictions

To estimate uncertainty in the model predictions, a Monte Carlo analysis is performed. A set of 100 uncorrelated, equally probable random realizations are generated using a Latin Hypercube sampling technique with the software Crystal Ball. Each realization includes random variables representing various model parameters that include the permeability and the porosity of the hydrostratigraphic units and the longitudinal and transverse dispersivities.

E-3.2.7 Results

The results of the regional simulations are discussed in section 5 of this report.

E-4.0 REFERENCES

The following list includes all documents cited in this appendix. Parenthetical information following each reference provides the author(s), publication date, and ER ID number. This information is also included in text citations. ER ID numbers are assigned by the Environmental Programs Directorate's Records Processing Facility (RPF) and are used to locate the document at the RPF and, where applicable, in the master reference set.

Copies of the master reference set are maintained at the New Mexico Environment Department Hazardous Waste Bureau; the U.S. Department of Energy–Los Alamos Site Office; the U.S. Environmental Protection Agency, Region 6; and the Directorate. The set was developed to ensure that the administrative authority has all material needed to review this document, and it is updated with every document submitted to the administrative authority. Documents previously submitted to the administrative authority are not included.

Broxton, D.E., and D.T. Vaniman, August 2005. "Geologic Framework of a Groundwater System on the Margin of a Rift Basin, Pajarito Plateau, North-Central New Mexico," *Vadose Zone Journal,* Vol. 4, No. 3, pp. 522–550. (Broxton and Vaniman 2005, 090038)

Cole, G., J.W. Carey, L. Burnette, and T. Miller, 2006. "The 2005 Three-Dimensional Geologic Model of the Pajarito Plateau," Los Alamos National Laboratory document LA-UR-06-3060, Los Alamos, New Mexico. (Cole et al. 2006, 095079)

Collins, K.A., A.M. Simmons, B.A. Robinson, and C.I. Nylander (Eds.), December 2005. "Los Alamos National Laboratory's Hydrogeologic Studies of the Pajarito Plateau: A Synthesis of Hydrogeologic Workplan Activities (1998–2004)," Los Alamos National Laboratory report LA-14263-MS, Los Alamos, New Mexico. (Collins et al. 2005, 092028)

Freeze, R.A., and J.A. Cherry, January 1979. *Groundwater*, Prentice-Hall, Inc., Englewood Cliffs, New Jersey. (Freeze and Cherry 1979, 088742)

Keating, E., E. Kwicklis, M. Witkowski, and T. Ballantine, September 30, 1999. "A Simulation Model for the Regional Aquifer beneath the Pajarito Plateau," Progress Report, Los Alamos National Laboratory document LA-UR-00-1029, Los Alamos, New Mexico. (Keating et al. 1999, 088746)

Keating, E.H., E.M. Kwicklis, V.V. Vesselinov, A.M. Idar, Z. Lu, G.A. Zyvoloski, and M.S. Witkowski, October 31, 2000. "A Regional Flow and Transport Model for Groundwater at Los Alamos National Laboratory," Los Alamos National Laboratory document LA-UR-01-2199, Los Alamos, New Mexico. (Keating et al. 2000, 090188)

Keating, E.H., V.V. Vesselinov, Z. Lu, and E. Kwicklis, 2001. "Annual Report on Regional Aquifer Modeling and Data Analysis," Los Alamos National Laboratory document LA-UR-04-1420, Los Alamos, New Mexico. (Keating et al. 2001, 095399)

Kleinfelder, May 2006. "Final Completion Report, Characterization Well R-17," report prepared for Los Alamos National Laboratory, Project No. 49436, Albuquerque, New Mexico. (Kleinfelder 2006, 092493)

LANL (Los Alamos National Laboratory), March 2006. "Interim Measures Work Plan for Chromium Contamination in Groundwater," Los Alamos National Laboratory document LA-UR-06-1961, Los Alamos, New Mexico. (LANL 2006, 091987)

LANL (Los Alamos National Laboratory), November 2006. "Interim Measures Investigation Report for Chromium Contamination in Groundwater," Los Alamos National Laboratory document LA-UR-06-8372, Los Alamos, New Mexico. (LANL 2006, 094431)

LANL (Los Alamos National Laboratory), April 2007. "Evaluation of the Suitability of Wells Near Technical Area 16 for Monitoring Contaminant Releases from Consolidated Unit 16-021(c)-99," Los Alamos National Laboratory document LA-UR-07-2370, Los Alamos, New Mexico. (LANL 2007, 095787)

LANL (Los Alamos National Laboratory), September 2007. "Completion Report for Regional Aquifer Wells R-35a and R-35b," Los Alamos National Laboratory document LA-UR-07-5342, Los Alamos, New Mexcio. (LANL 2007, 098129)

Lichtner, P.C., S. Kelkar, and B. Robinson, August 17, 2002. "New Form of Dispersion Tensor for Axisymmetric Porous Media with Implementation in Particle Tracking," *Water Resources Research,* Vol. 38, No. 8, pp. 21-1–21-16. (Lichtner et al. 2002, 095397)

Longmire, P., M. Dale, D. Counce, A. Manning, T. Larson, K. Granzow, R. Gray, and B. Newman, July 2007. "Radiogenic and Stable Isotope and Hydrogeochemical Investigation of Groundwater, Pajarito Plateau and Surrounding Areas, New Mexico," Los Alamos National Laboratory report LA-14333, Los Alamos, New Mexico. (Longmire et al. 2007, 096660)

Neuman, S.P., August 1990. "Universal Scaling of Hydraulic Conductivities and Dispersivities in Geologic Media," *Water Resources Research,* Vol. 26, No. 8, pp. 1749-1758. (Neuman 1990, 090184)

Purtymun, W.D., January 1995. "Geologic and Hydrologic Records of Observation Wells, Test Holes, Test Wells, Supply Wells, Springs, and Surface Water Stations in the Los Alamos Area," Los Alamos National Laboratory report LA-12883-MS, Los Alamos, New Mexico. (Purtymun 1995, 045344)

Robinson, B., E. Keating, B. Newman, K. Birdsell, B. Carey, M. Witkowski, Z. Lu, A. Idar, M. Haagenstad, G. Zyvoloski, and V. Vesselinov, October 6, 2000. "Process-Level and Systems Models of Groundwater Flow and Transport Beneath the Pajarito Plateau: Migration of High Explosives from Technical Area 16," Los Alamos National Laboratory document LA-UR-07-5752, Los Alamos, New Mexico. (Robinson et al. 2000, 097897)

Vesselinov, V.V., 2005. "An Alternative Conceptual Model of Groundwater Flow and Transport in Saturated Zone Beneath the Pajarito Plateau," Los Alamos National Laboratory document LA-UR-05-6741, Los Alamos, New Mexico. (Vesselinov 2005, 090040)

Vesselinov, V.V., 2005. "Logical Framework for Development and Discrimination of Alternative Conceptual Models of Saturated Groundwater Flow Beneath the Pajarito Plateau," Los Alamos National Laboratory document LA-UR-05-6876, Los Alamos, New Mexico. (Vesselinov 2005, 089753)

Zyvoloski, G.A., B.A. Robinson, Z.V. Dash, and L.L. Trease, May 20, 1996. "Users Manual for the FEHMN Application," Rev. 1, Los Alamos National Laboratory document LA-UR-94-3788, Los Alamos, New Mexico. (Zyvoloski et al. 1996, 054421)

Zyvoloski, G.A., B.A. Robinson, Z.V. Dash, and L.L. Trease, July 1997. "Summary of the Models and Methods for the FEHM Application — A Finite-Element Heat- and Mass-Transfer Code," Los Alamos National Laboratory report LA-13307-MS, Los Alamos, New Mexico. (Zyvoloski et al. 1997, 070147)

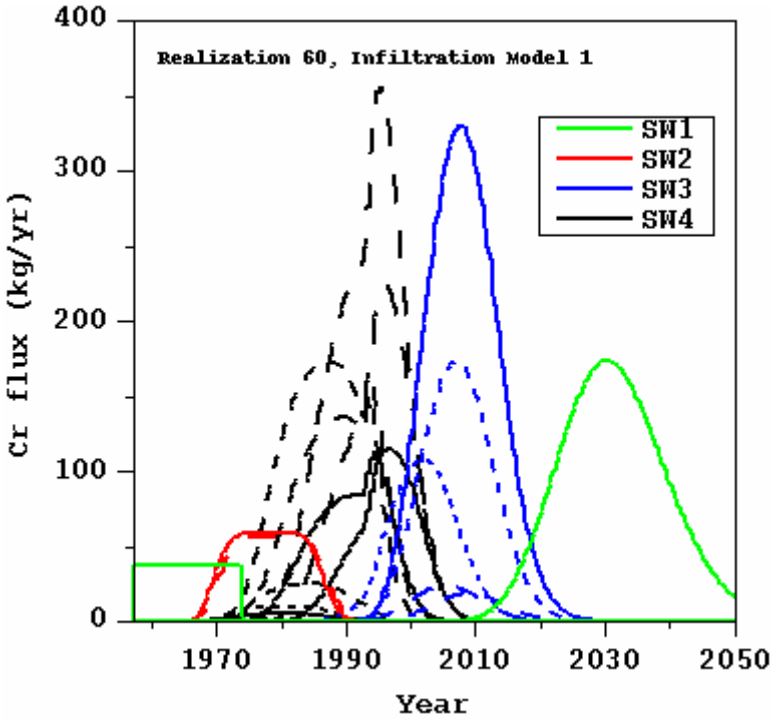

Figure E-2.2-1 Predicted Cr flux (kg/yr) exiting the base of the 18 unsaturated zone columns, Infiltration Model 1 and Realization #60

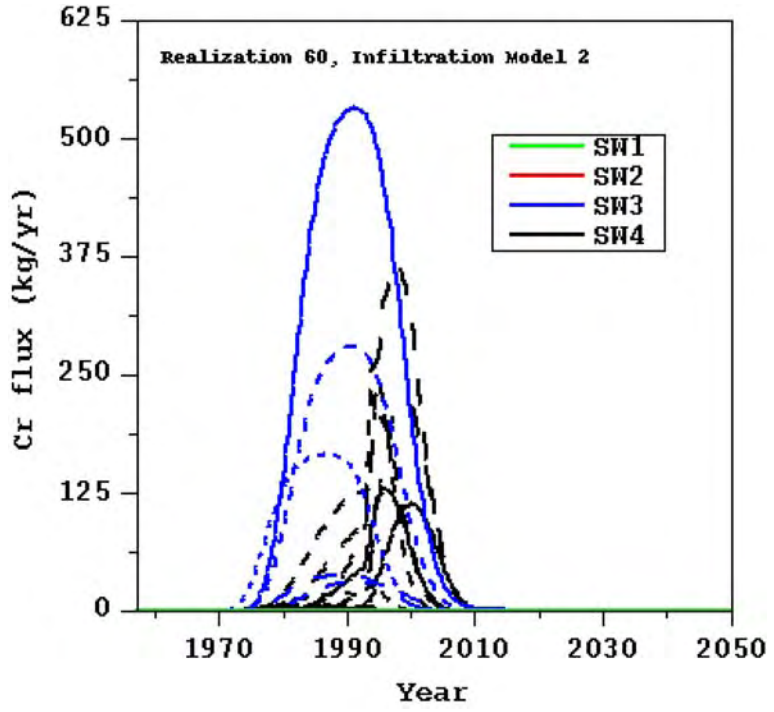

Figure E-2.2-2 Predicted Cr flux (kg/yr) exiting the base of the 18 unsaturated zone columns, Infiltration Model 2 and Realization #60.

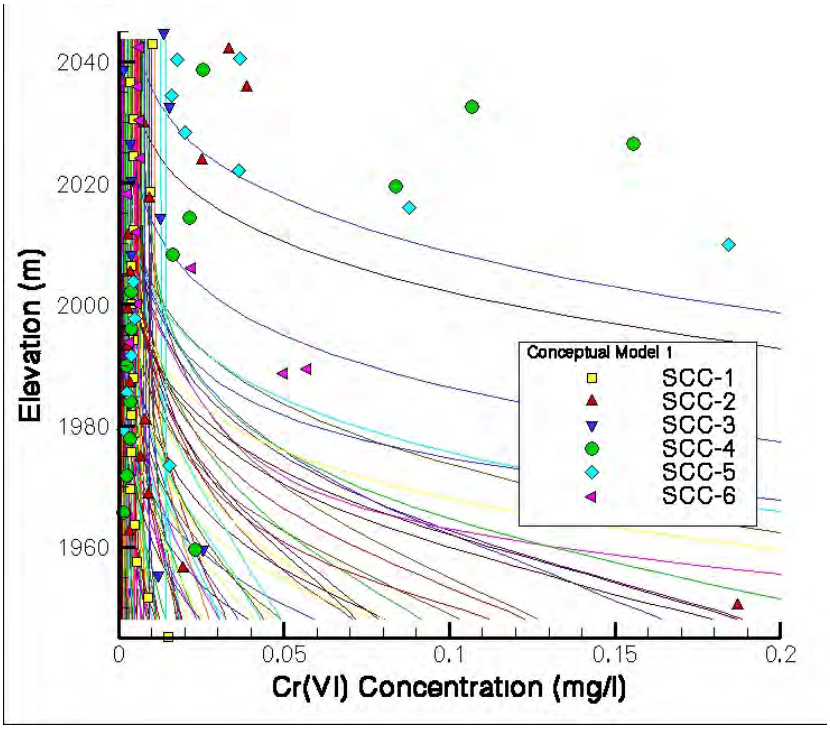

Figure E-2.2-3 Comparison of Cr porewater concentration data from SCC core holes to 100 simulated concentration profiles, Infiltration Model 1

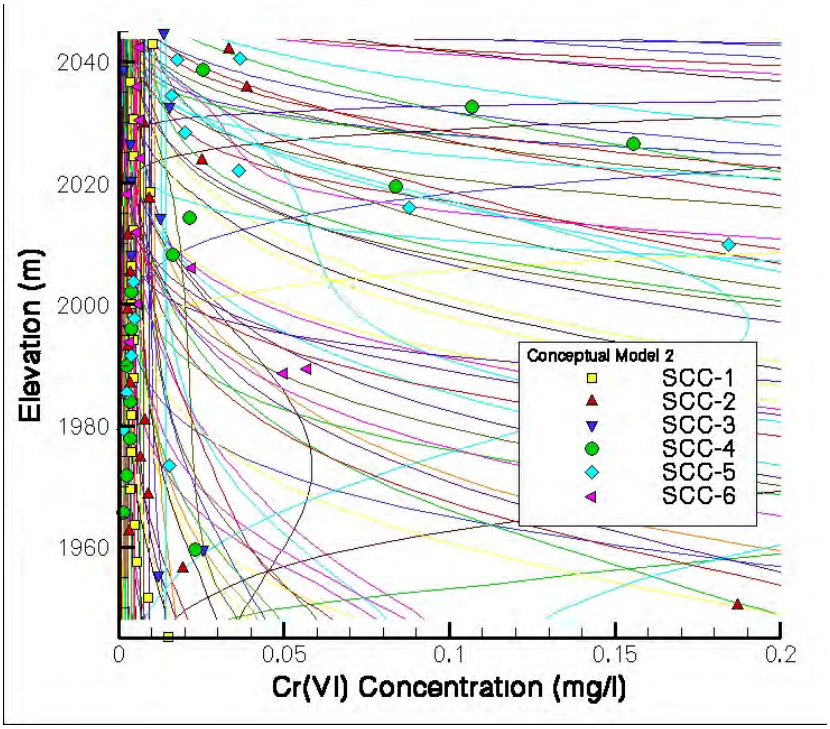

Figure E-2.2-4 Comparison of Cr porewater concentration data from SCC core holes to 100 simulated concentration profiles, Infiltration Model 2

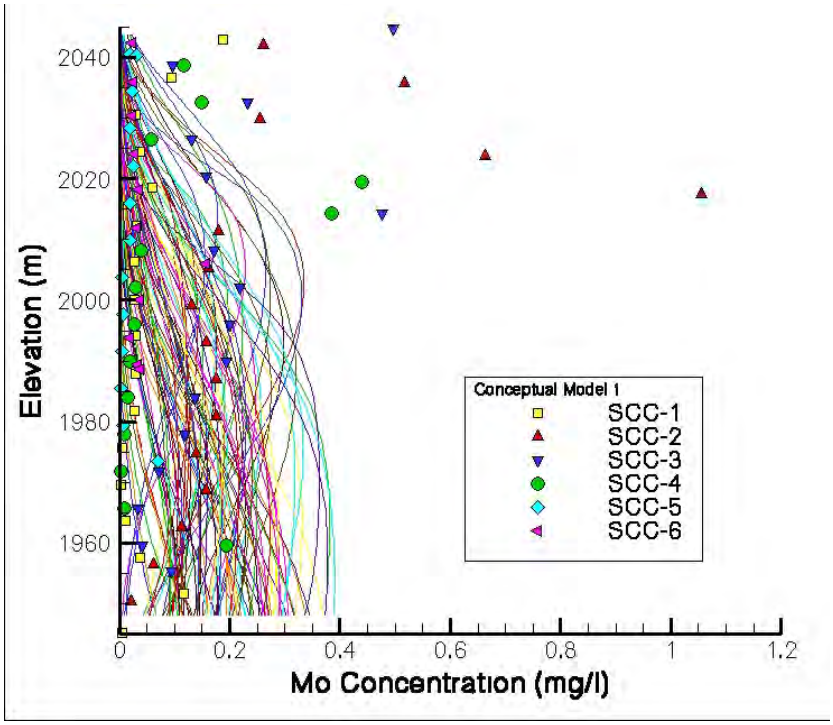

Figure E-2.2-5 Comparison of Mo porewater concentration data from SCC core holes to 100 simulated concentration profiles, Infiltration Model 1

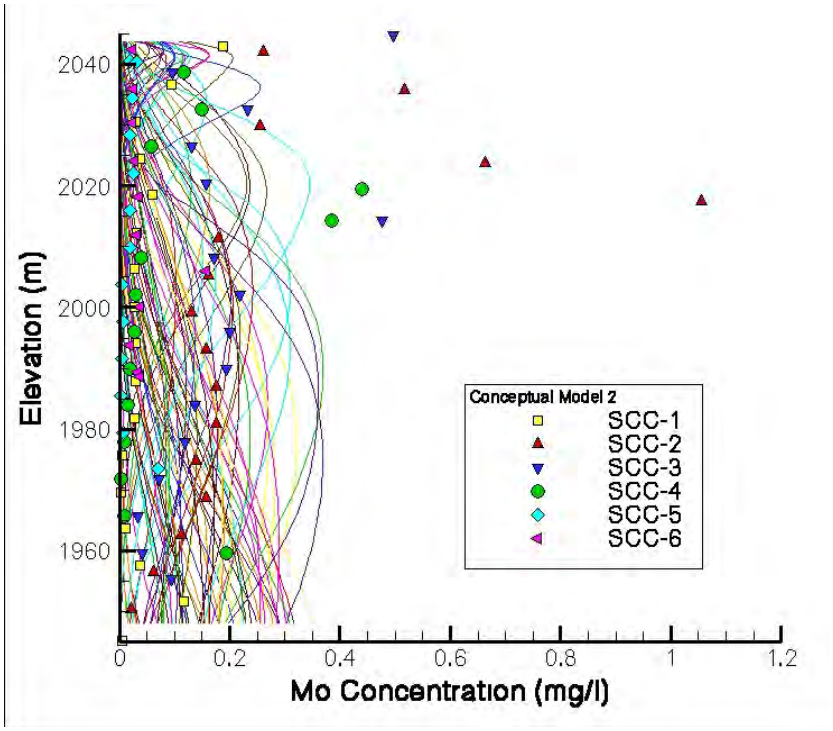

Figure E-2.2-6 Comparison of Mo porewater concentration data from SCC core holes to 100 simulated concentration profiles, Infiltration Model 2

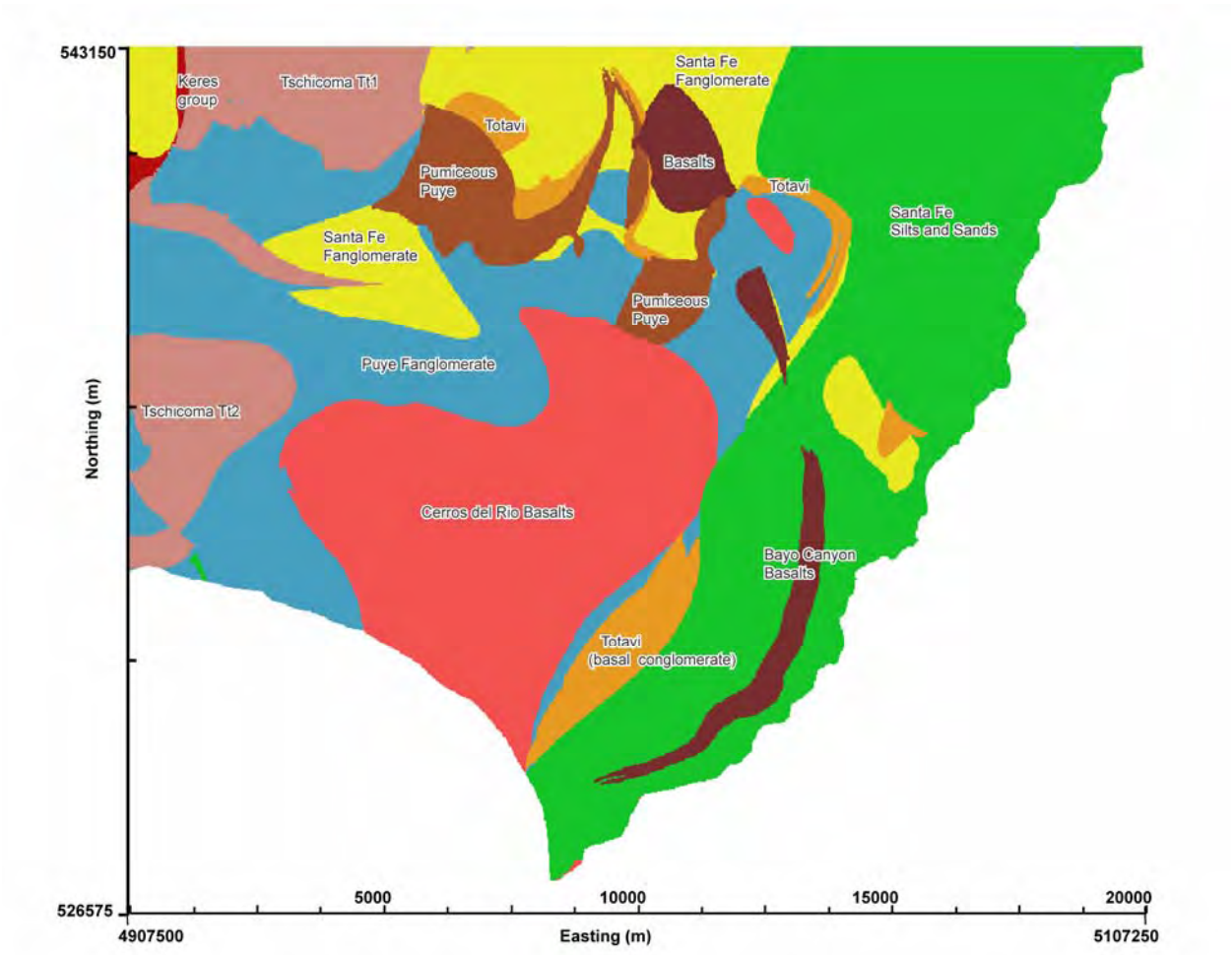

Figure E-3.1-1 Hydrostratigraphy along the water table

Conceptual Model A

Contaminants are expected to primarily migrate toward pumping wells

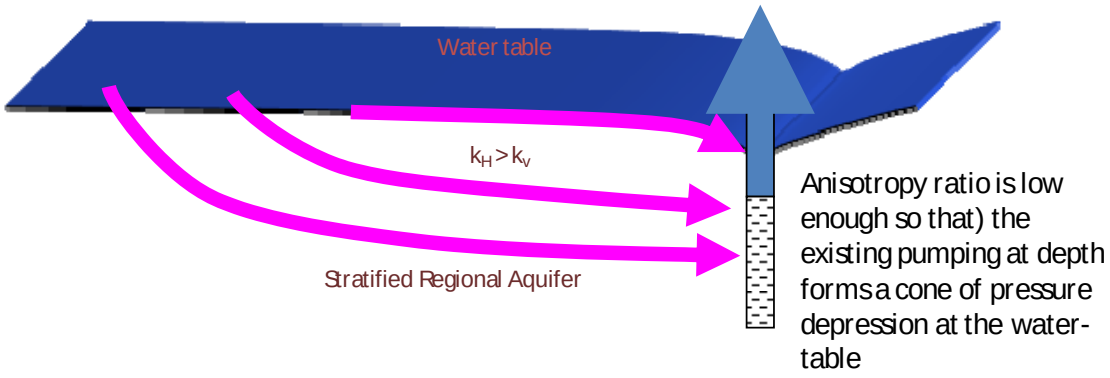

Conceptual Model B

Contaminants are expected to primarily migrate laterally in phreatic zone toward springs and Rio Grande; small portion will migrate toward pumping wells

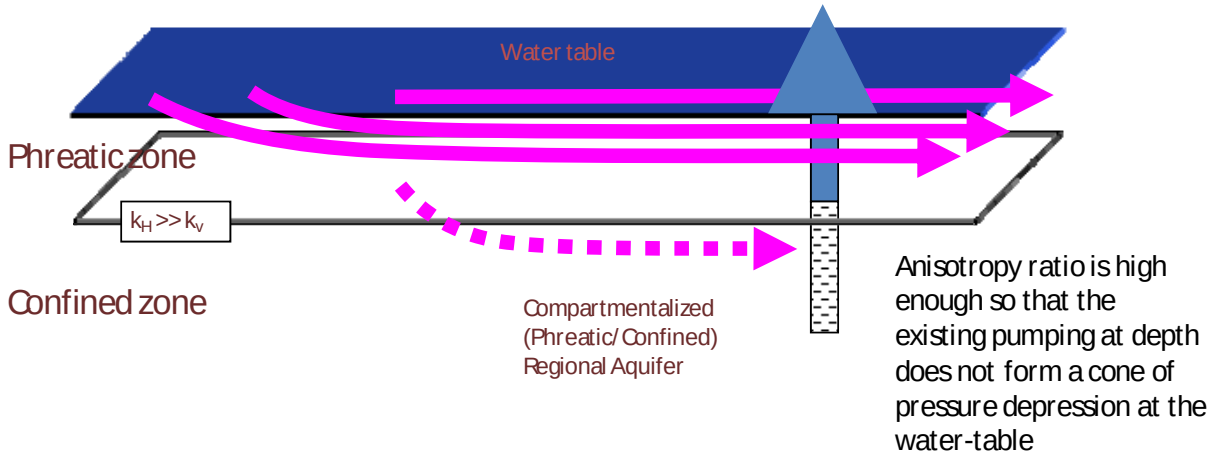

(a)

Figure E-3.1-2 Schematic representation of alternative conceptual models of the flow and transport in the regional aquifer near water-supply wells

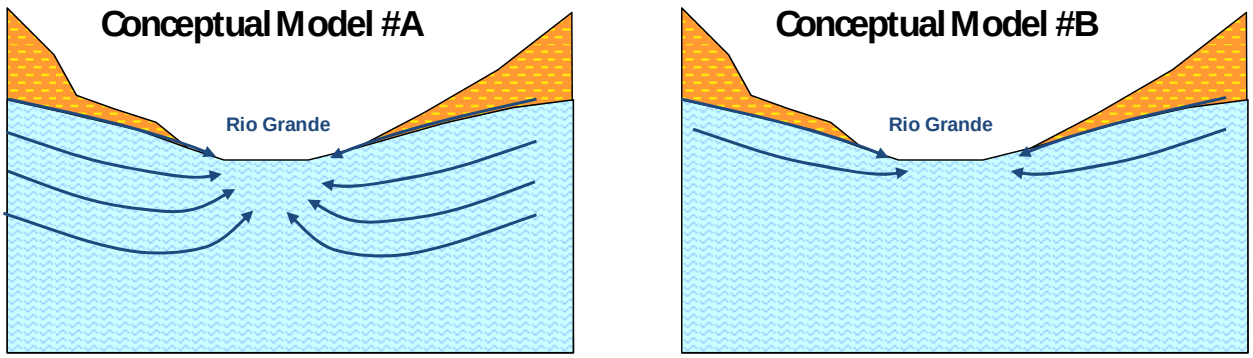

(a)

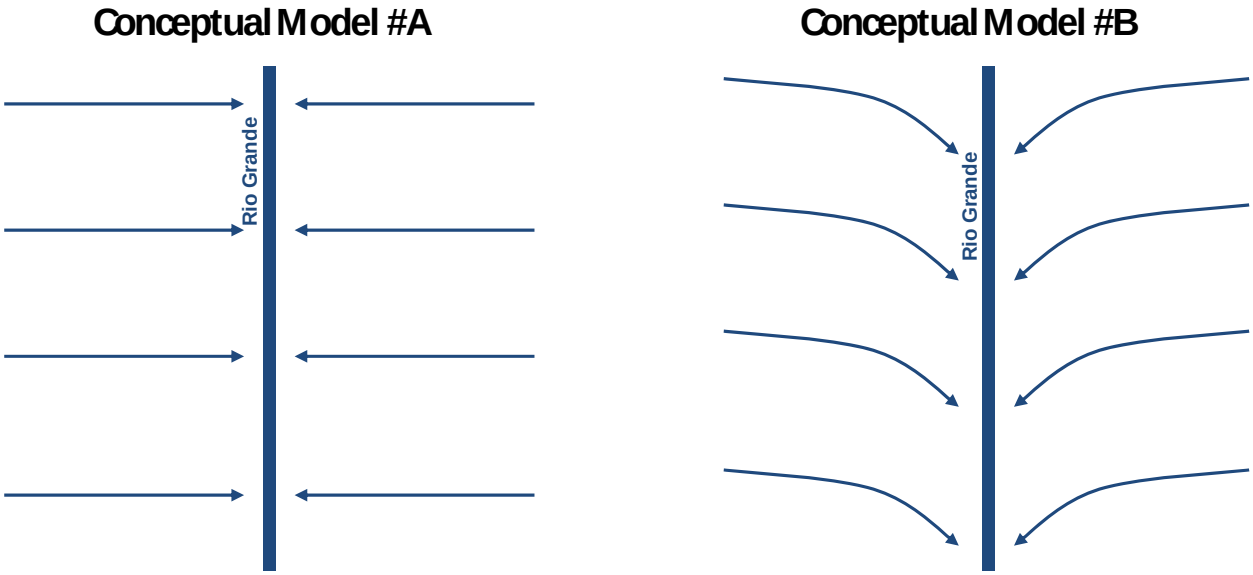

(b)

Figure E-3.1-3 Schematic representation of alternative conceptual models of the flow and transport in the regional aquifer close to the Rio Grande. Plots characterize the three-dimensional aspect of the discharge flow paths through the regional aquifer close to Rio Grande: (a) representation of potential vertical distribution of discharge flow paths close to Rio Grande (for Model B, deep flow vectors are not shown because in three-dimensional space they intersect the cross-section plane); (b) lateral flow paths of aquifer discharge in the deep zone of the regional aquifer close to Rio Grande.

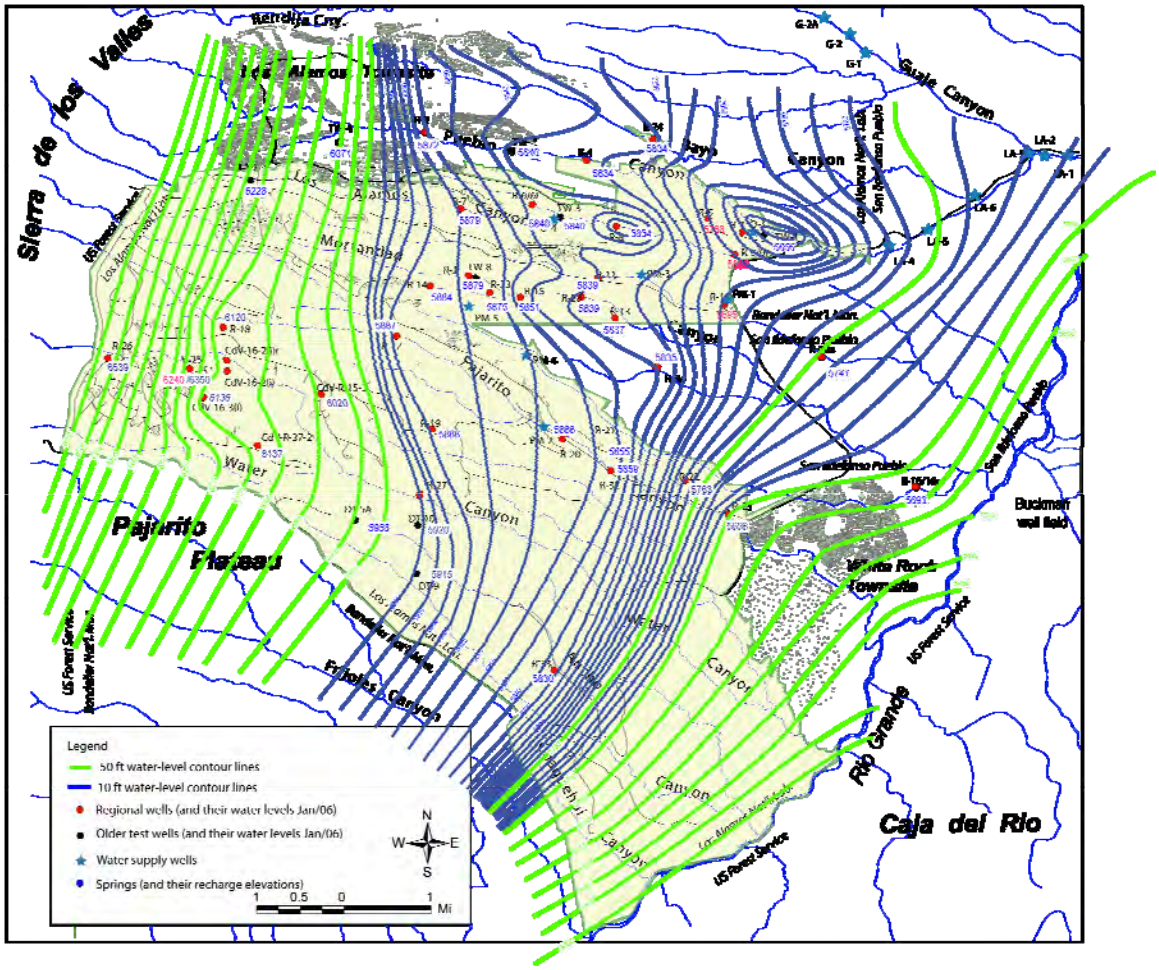

Figure E-3.1-4 Contour maps of average water table elevations in March 2006; it is assumed that water level at R-25 is defined by either Screen 5 (a) or Screen 4 (b). The second map (b) also shows the potential flow directions. In our analysis, data values in pink are uncertain (after LANL 2007, 095787).

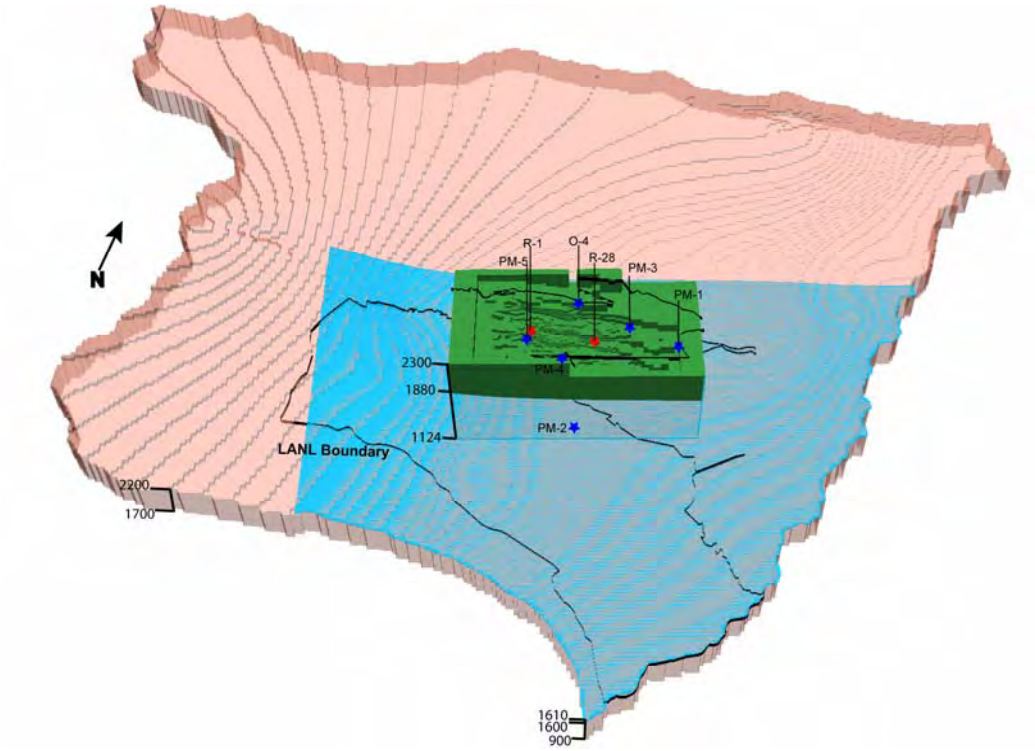

Figure E-3.2-1 Domains associated with the chromium-contamination (1) "site" model (green), (2) thin pancake model (blue), and (3) thick pancake model (pink)

(a)

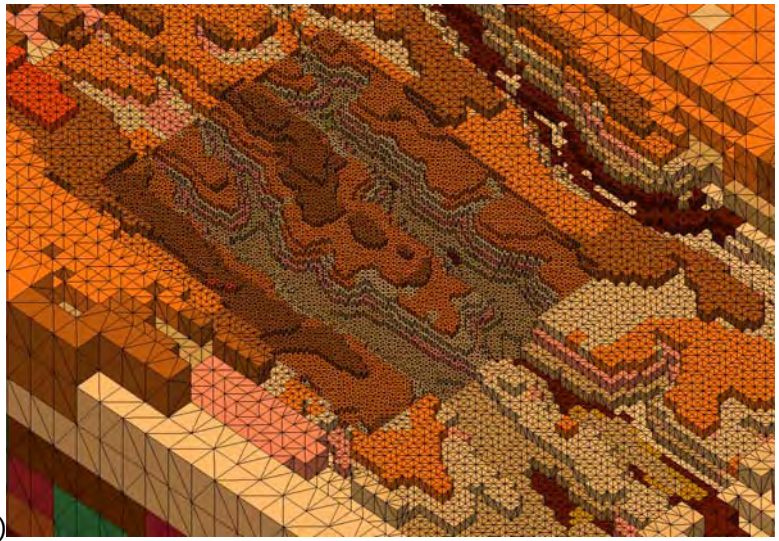

(b)

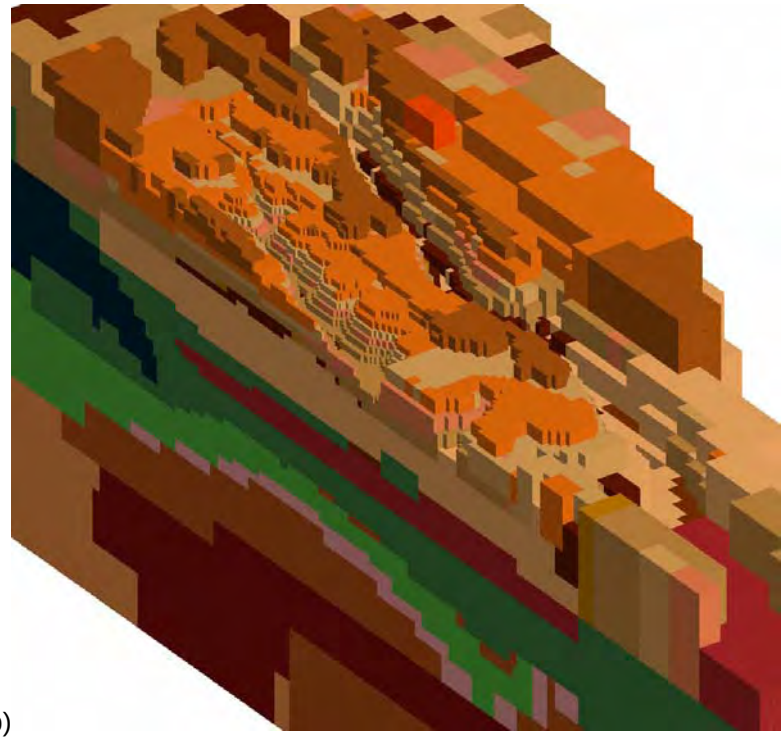

Figure E-3.2-2 Close-up views of the refined site model grid, (a) top view and (b) cut away that is parallel to Sandia Canyon

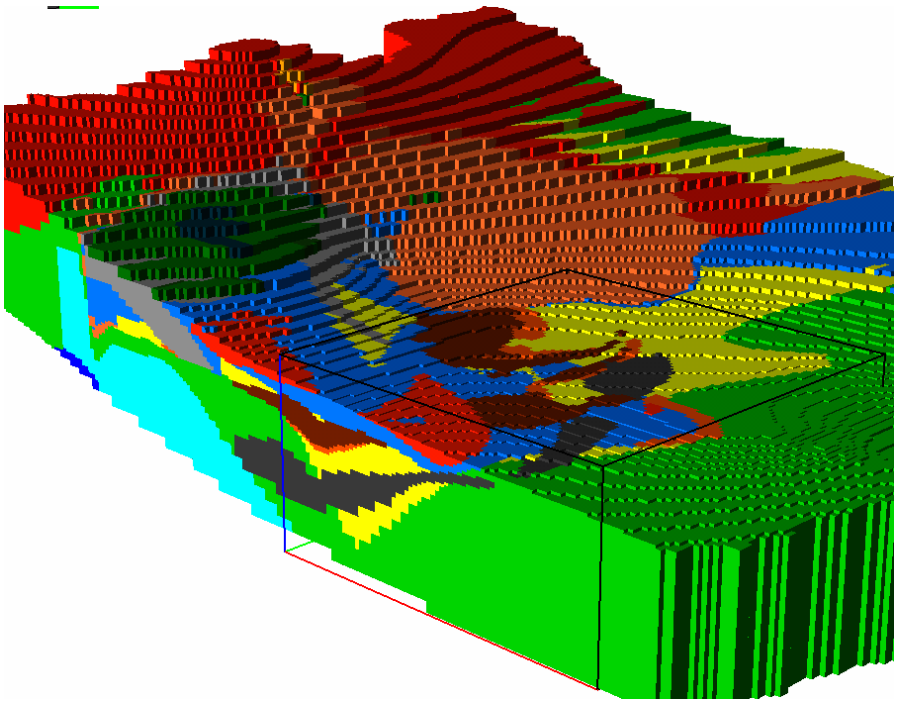

Figure E-3.2-3 Computational grids and representation of hydrostratigraphy in the numerical models

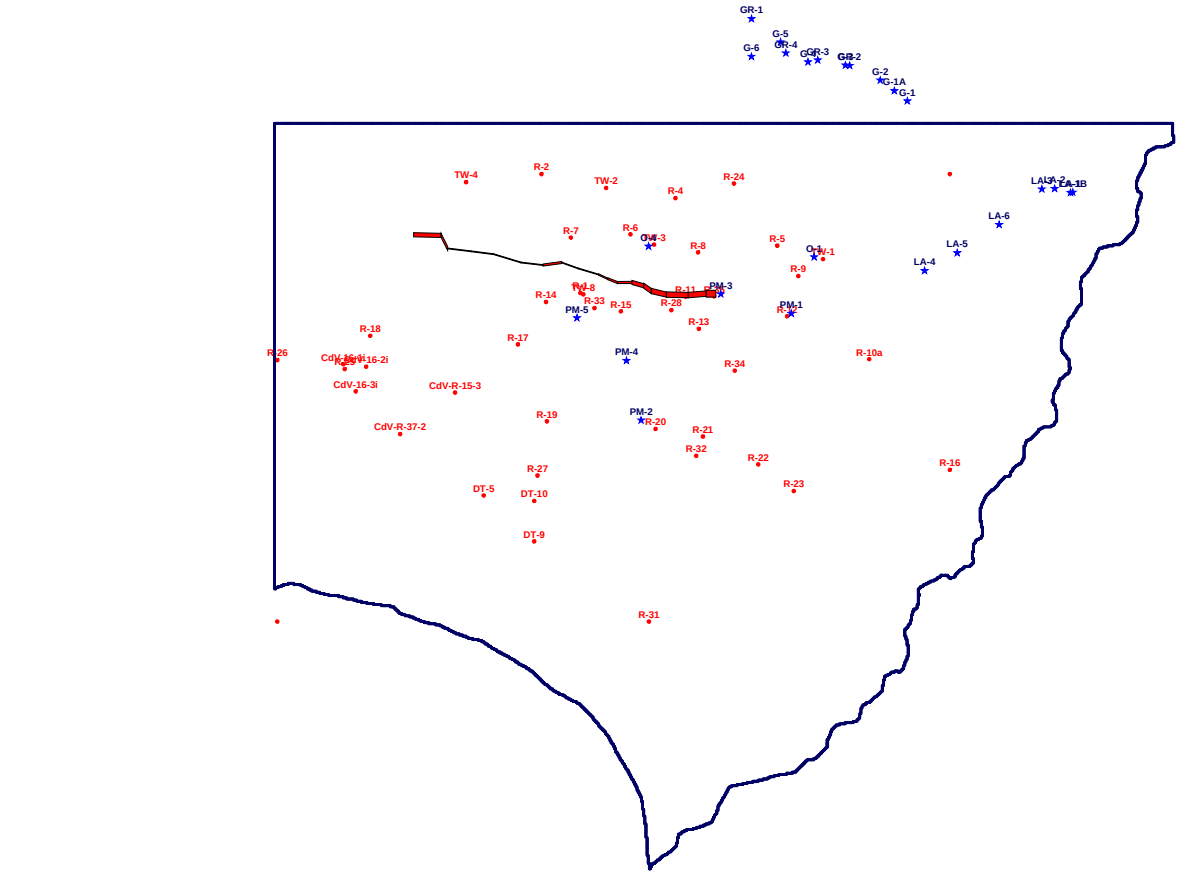

(a)

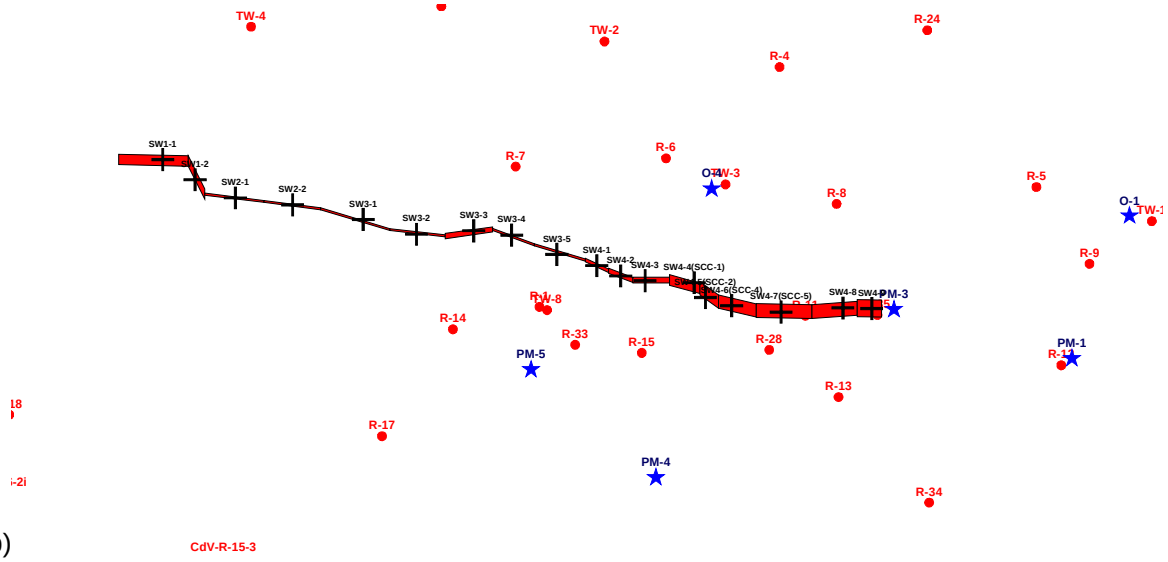

(b)

Figure E-3.2-4 Domain of the "thin pancake" model and zones of contaminant release at the regional aquifer associated with Sandia Canyon. The second graph shows zoom in on the 18 one-dimensional source polygons defined by the unsaturated-zone model along Sandia Canyon.

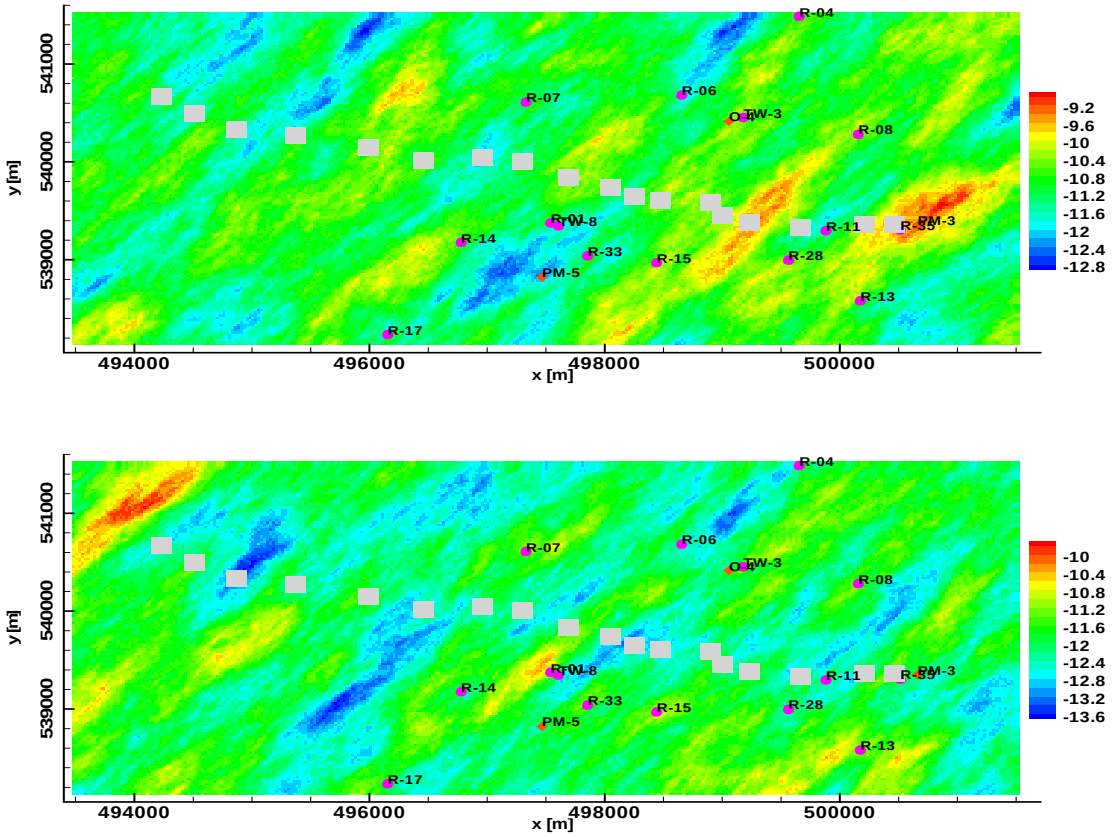

Figure E-3.2-5 Example spatial distributions of permeability heterogeneity in Puye Formation. Locations of 18 unsaturated-zone source polygons along Sandia Canyon are shown as grey squares.

Table E-2.1-1
Locations (State Plane Coordinate System) and Surface Area Information for 18 One-Dimensional Columns Used in the Unsaturated-Zone Flow and Transport Simulations

Column	Easting (ft)	Northing (ft)	Width (ft)	Segment Length (ft)	Area (ft^2)	Area (m^2)	% of Total Canyon Area for Each Column
SW1-1	1621475	1773857	120	2007	240840	22375	20.9
SW1-2	1622405	1773271	50	480	24000	2230	2.1 (23)*
SW2-1	1623574	1772747	5	1713	8565	796	0.7
SW2-2	1625226	1772545	5	1636	8180	760	0.7 (1.5)
SW3-1	1627264	1772128	5	1996	9982.5	927	0.9
SW3-2	1628801	1771698	5	1596	7982.5	742	0.7
SW3-3	1630457	1771800	100	1374	137450	12770	11.9
SW3-4	1631550	1771673	60	1201	72060	6695	6.3
SW3-5	1632859	1771119	40	1481	59260	5505	5.1 (25)
SW4-1	1634007	1770791	75	668	50100	4654	4.3
SW4-2	1634701	1770493	140	699	97860	9091	8.5
SW4-3	1635405	1770354	150	1061	159142	14785	13.8
SW4-4 (SCC-1)	1636823	1770298	100	870	87027	8085	7.6
SW4-5 (SCC-2)	1637145	1769868	100	542	54181	5034	4.7
SW4-6 (SCC-4)	1637906	1769635	100	1093	109303	10155	9.5
SW4-7 (SCC-5)	1639332	1769451	10	1605	16052	1491	1.4
SW4-8	1641117	1769570	5	1310	6549	608	0.6
SW4-9	1641951	1769552	5	698	3490	324	0.3 (51)

* The number given in parentheses is the area of the southwest segment.

Table E-3.2-1
Spatial Representation of Hydrostratigraphic Units Represented in the Three Models

Unit	Short Name	"Site" 3D Model 415327 Nodes		"Thick Pancake" Model 980,553 Nodes		"Thin Pancake" Model 693,948 Nodes	
		Number of Nodes	Percentage in the Model	Number of Nodes	Percentage in the Model	Number of Nodes	Percentage in the Model
Bandelier Tuff	Qb	64350	0.154938	785	0.1%	*	*
Cerro Toldedo Interval	Qct	9839	0.02369	120	0%	*	*
Tschicoma	Tt	5736	0.013811	51187	5.2%	73049	10.5%
Keres Group	Tk	0	0	60723	6.2%	2865	0.4%
Cerros del Rio Basalt	Tb4	0	0	12157	1.2%	97099	14.0%
Bayo Canyon Basalt	Tb2	6534	0.015732	22948	2.3%	24007	3.5%
Older Basalts	Tb1	0	0	13526	1.4%	0	0
Totavi Lentil	Tpt	12085	0.029098	7661	0.8%	22543	3.2%
Pumiceous Puye	Tpp	43449	0.104614	13395	1.4%	29116	4.2%
Puye Fanglomerate	Tpf	72937	0.175613	45270	4.6%	152808	22.0%
Santa Fe Fanglomerate	Tf	5306	0.012775	192275	19.6%	78269	11.3%
Santa Fe Silt and Sands	Ts	0	0	560566	57.2%	214192	30.9%

*Geologic units have been combined. Galisteo is combined with Santa Fe Silt and Sands. Bandelier Tuff and Cerro Toledo members are not expected at these model elevations and are combined with Tschicoma in the thin pancake model.

Appendix F

Sampling Statistics and Convergence

F-1.0 INTRODUCTION

This appendix presents a summary of statistical tests in support of the probabilistic analysis presented in this report along with decision-analysis tools used to relate data collection and decision making.

F-2.0 SAMPLE CONVERGENCE

Monte Carlo techniques, specifically Latin Hypercube Sampling (LHS), were used to generate sets of input files that reflect the uncertainty in model input parameters. LHS is a stratified sampling method that ensures the range of parameter space is covered with a minimum number of samples. However, no absolute proof exists that a given number of samples will cover the full range of parameter values and all possible combinations of parameter values. To ensure that parameter space and combinations of parameters have been adequately covered, sample convergence testing is performed. Convergence testing requires rerunning sets of simulations using more and a greater number of samples. In the case of the Sandia Canyon analysis, insufficient time was available to rerun the integrated vadose-zone regional aquifer simulations. Therefore, a series of convergence tests was performed on components of the overall modeling system. The most sensitive of these tests, and the one most related to the overall model, is the convergence test for vadose zone travel times.

LHS was used repeatedly to generate 10, 25, 50, 75, 100, 200, 300, 400, 500, 750, 1000, 2000, 5000, 10,000 sets of parameter input values or realizations. Figure F-1 shows the distribution of travel times associated with 10,000 sets of input parameters. In this case, the results have converged into a smooth distribution of travel times.

From Figure F-1 it is evident that travel time ranges from slightly less than 10 yr to more than 100 yr. Ninety five percent of the travel times exceed a travel time of about 15 yr and only approximately 5% of the travel times exceed a time of approximately 150 yr.

Next, in Figure F-2, the results 10 realizations are shown along with the results of 10,000 realizations.

Using only 10 samples, the general range of travel times is accurately described; however, individual points along the curve differ significantly from the 10,000 realizations curve.

Figure F-3 shows the vadose zone travel times for 50 realizations along with the 10,000 realizations curve.

The 50 realizations curve captures nearly the complete range of behavior of the system, missing only the very extreme parts of the tails.

Figure F-4 displays the results of 100 realizations along with the results for 10,000 realizations.

This set of 100 realizations produces essentially the same results as 10,000 realizations. The only difference is in the portion of the curve corresponding to the earliest travel times. For approximately 2% of the curve, 100 realizations overestimate the travel time by perhaps 3 yr. If a difference of 3 yr for 2% of the curve were critical for a given application or decision, then additional samples will be needed; however, this event is not likely.

Finally, the curve for 200 realizations is shown along with the curve for 10,000 realizations in Figure F-5. In this case, virtually no discernable difference exists between the curves. Beyond 200 samples the difference was even less, proving that complete convergence had occurred at least by 200 samples.

Another way to look at convergence is to plot the travel time associated with a specific level of confidence to a given number of realizations. Figure F-6 shows the travel times versus the number of realizations at a variety of confidence levels. The travel times at the 5% and 10% confidence limits fluctuate around their final values and do not completely settle down until a sample size of approximately 1000. However, these confidence limits are associated with long travel times. In general, the shortest travel times are of interest. Shorter travel times, associated with the 50%, 90%, and 95% confidence limits, converge with very few samples and decrease with sample sizes larger than 100.

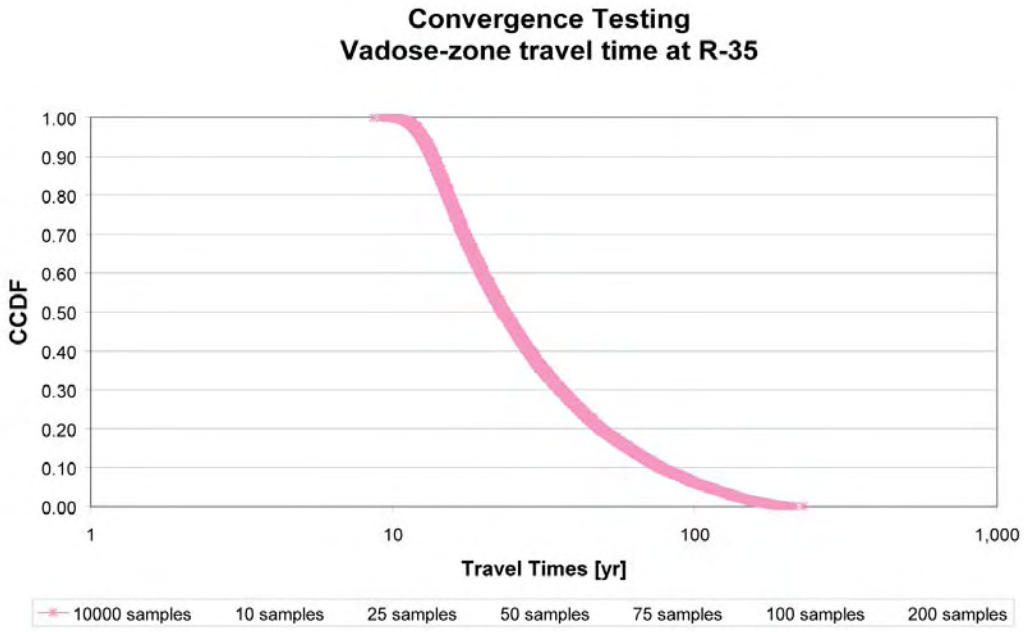

Figure F-1 Distribution of vadose-zone travel times for 10,000 realizations

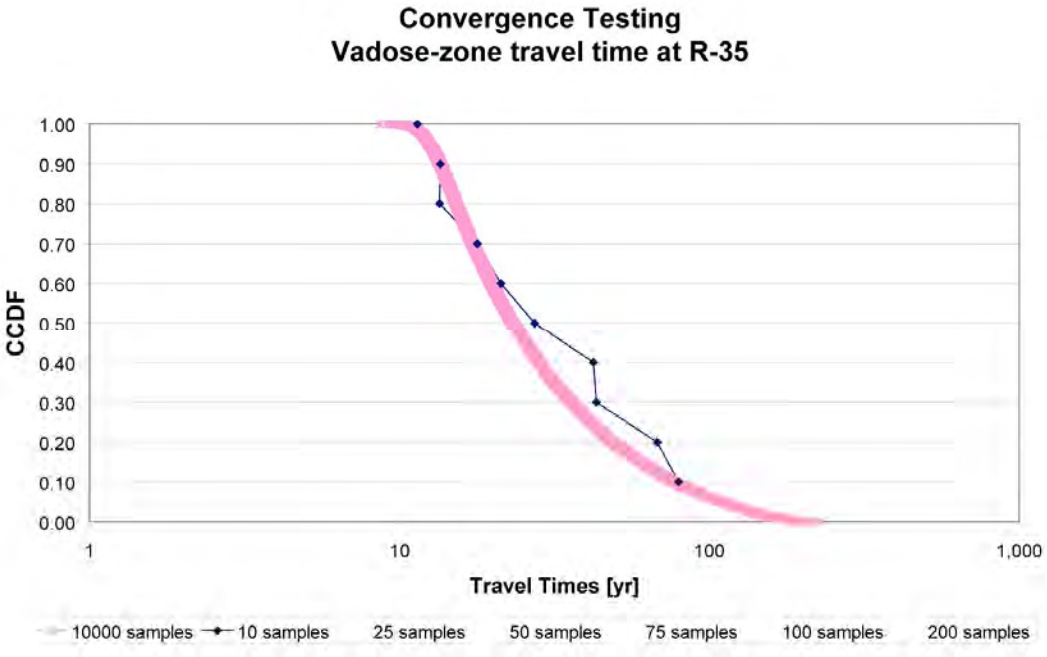

Figure F-2 Distribution of vadose-zone travel times for 10 and 10,000 realizations

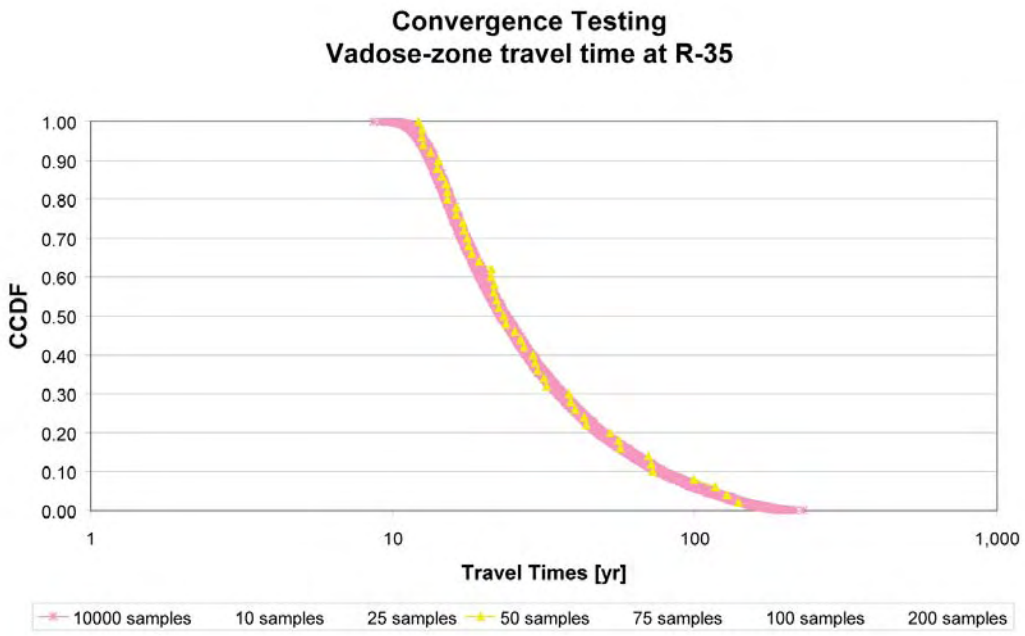

Figure F-3 Distribution of vadose-zone travel times for 50 and 10,000 realizations.

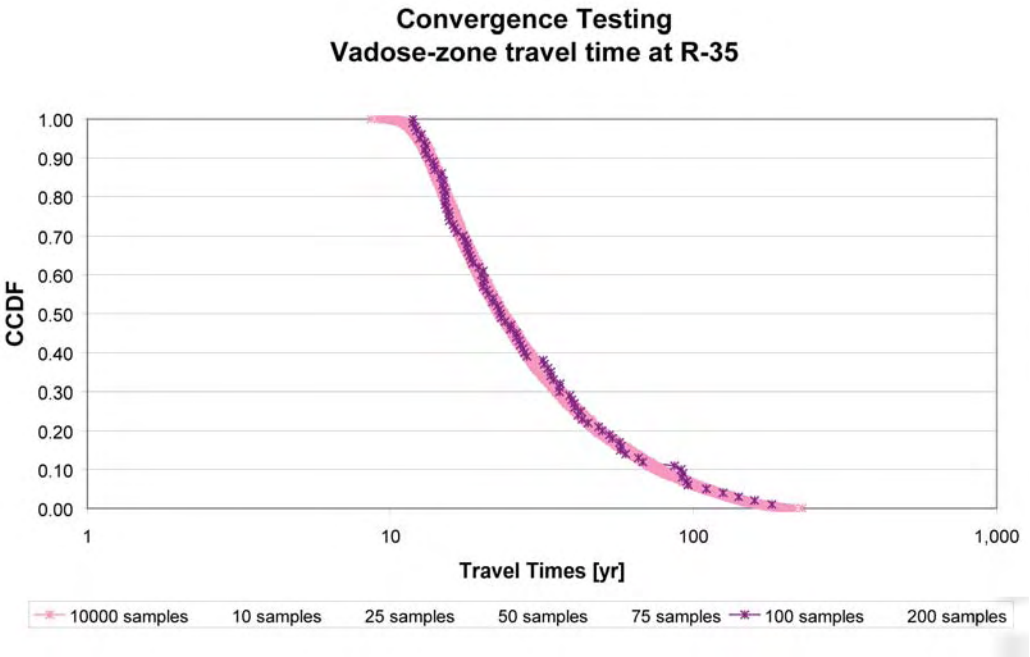

Figure F-4 Distribution of vadose-zone travel times for 100 and 10,000 realizations

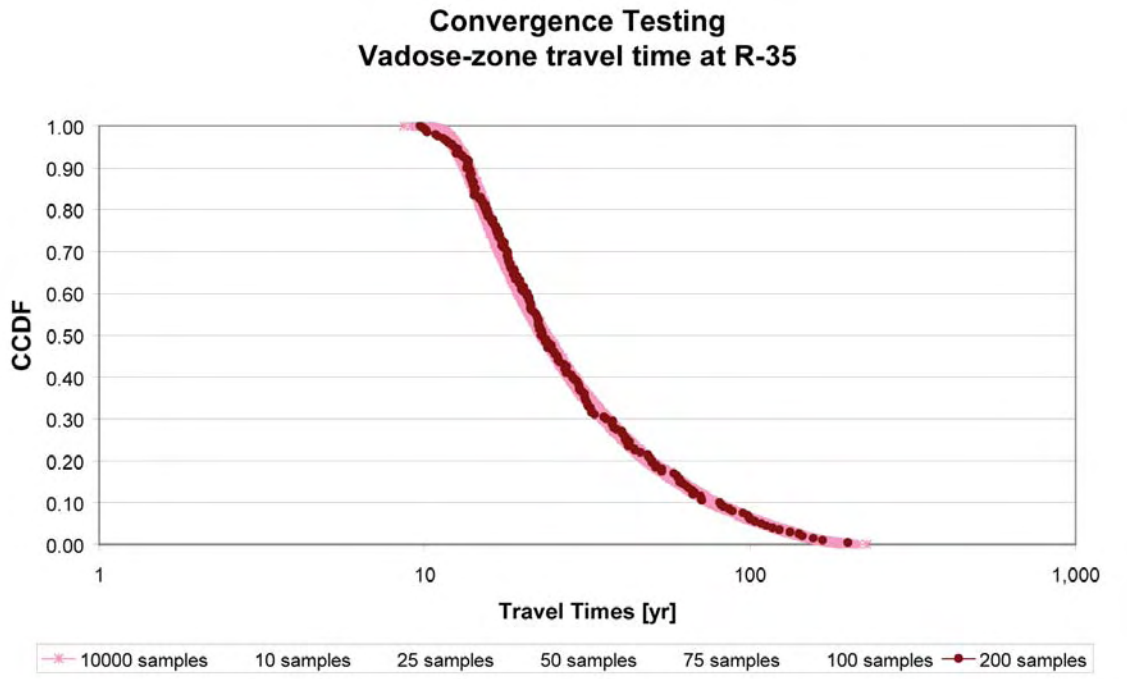

Figure F-5 Distribution of vadose-zone travel times for 200 and 10,000 realizations

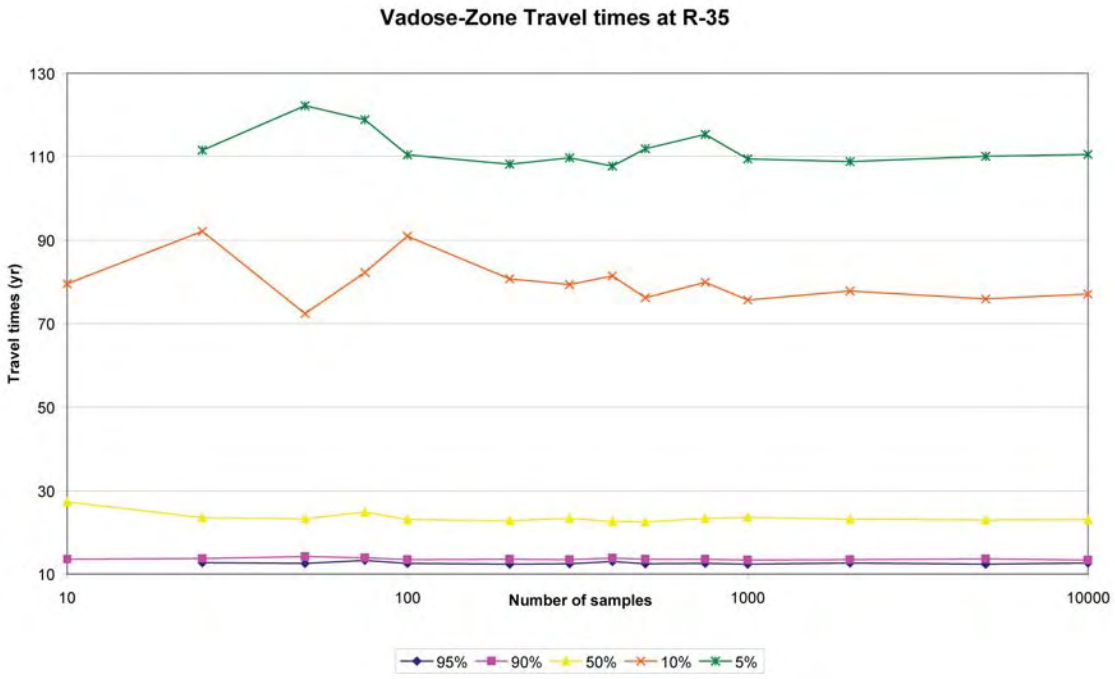

Figure F-6 Travel times versus sample size at a variety of confidence levels

Appendix G

Weighting Results of the Sandia Canyon Probabilistic Fate and Transport Assessment

G-1.0 INTRODUCTION

This appendix presents the approach used by Los Alamos National Laboratory (LANL or the Laboratory) for weighting probabilistic fate and transport results for Sandia Canyon based on how well the model results match measured contaminant concentrations for chromium (Cr) and molybdenum (Mo) contaminants at a number of locations in both the vadose zone and the regional aquifer.

The procedure used to generate parameter samples for the probabilistic Sandia Canyon fate and transport model, Latin Hypercube Sampling (LHS), results in each simulation having the same probability. The default weight of any one simulation is 1 divided by the number of simulations; therefore, with 100 samples, the probability of each simulation is 1/100 or 0.01. As an alternative to equal weighting, this appendix describes weighting the fate and transport results based on how well each simulation matches measured system data. The specific approach is to weight each simulation based on how well the simulation results match measurements of vadose zone and regional aquifer Cr and Mo concentrations. To yield a meaningful probabilistic distribution of model output (a cumulative distribution function [CDF] or a complementary cumulative distribution function [CCDF]), the weights assigned to each simulation must be dimensionless, range from 0–1, and the sum of the weights equal 1. To be consistent with the approach of weighting the results based on how well the results match the measured data, the weights should also decrease as the fit between model and data decreases.

In general, the weighting of simulation results may be considered in several ways, based on their fitness or closeness to measured data. For example, one simulation may be chosen as the most fit or best simulation and all weight given to that simulation. However, such an approach seeks an exact or very close match with measured data. Simulation results are not expected to provide exact matches to all field data because of inherent uncertainties in field measurements, the inability to directly measure some model parameters, and the differences in scales between model cells and effective volumes sampled by field measurements. Another approach is to define a region of calibration space, that is, an envelope (see Figure G-1) where all simulations are considered “calibrated” and given an equal weight and all simulations whose results fall outside of that region are given a weight (and probability) of 0. This approach requires normalization (0–1) of probability space of the simulations that “fit” and perhaps a second set of Monte Carlo simulations constrained to the calibration space to yield sufficient samples for estimating fate and transport and performing decision analysis. The third and the chosen method also defines a region or envelope within which all simulations are defined as displaying an adequate fit to the data. All simulations in this envelope receive equal weight. However, simulations with results falling outside this envelope do not receive 0 weight as in the example above. Instead, each simulation outside the accepted region receives a weight that (a) is less than the weight of a simulation whose results fall inside of the accepted region and that (b) decreases with distance away from the accepted region.

G-2.0 DEFINITIONS OF METRICS AND ENVELOPE

The following section provides metrics and the equations used in weighting simulation results. The Laboratory team selected two general types of metrics for weighting Sandia Canyon simulation results. Each of these metrics and the envelope of accepted results for each of these metrics are discussed below.

G-2.1 Metric 1: Vadose Zone Contaminant Concentrations

The first metric is based on Cr and Mo concentrations in the vadose zone. An envelope for a contaminant distribution in the vadose zone is defined by specifying a minimum and maximum acceptable concentration at a sequence of depths below the ground surface. For convenience, these depths are taken to be the nodal depths associated with the vadose-zone model.

Only the vadose zone beneath surface water Reach 4 (SW4, discussed in Appendix D) has measurements of Cr and Mo contamination. All core data for this reach were combined to define envelopes of equally likely concentrations. The profiles corresponding to upper and lower limits for both Cr and Mo are shown in Figures G-2 and G-3.

G-2.2 Metric 2: Regional Aquifer Contaminant Concentrations

Concentrations of Cr and Mo, taken from the average concentrations for 2006, are the metrics for the regional aquifer. At selected wells in the regional aquifer, a range of equally likely values is specified. The wells considered for this computation and the upper and lower acceptable limits for Cr concentrations for each well are presented in Figure G-4. To date, Mo did not reach the regional aquifer.

G-2.3 Calculation of Probabilities Associated with Single Metrics for Individual Contaminants at Specific Locations

General Methodology

The calculation of weights begins with an error calculation for each simulation. For the distribution of contamination in the vadose zone, this error is the ratio of the area of simulation results that lie outside the acceptable envelope (Figure G-5) to the total area of the envelope (AE).

The error is calculated as follows:

Equation G-1

$$\text{Area of the envelope} = AE = \Sigma\,(Cmax\text{-}Cmin)_d$$

Where the summation is taken over the depths ($_d$) associated with each vadose zone model node or layer.

If $C_{id} > Cmax_d$, then

Equation G-2a

$$E_{id} = C_{id} - Cmax_d \qquad \textit{(positive value [, } +\infty\textit{])}$$

If $C_{id} < Cmin_d$, then

Equation G-2b

$$E_{id} = Cmin_d - C_{id} \qquad \textit{(positive value [0, } Cmin_d\textit{])}$$

If $C_{id} >= Cmin_d$ and $C_{id} <= Cmax_d$, then

Equation G-2c

$$E_{id} = 0$$

Where the error for simulation i = E_i

(Note: concentration values can be replaced by log concentration values. This alternative had been considered and also applied.)

and the total error for simulation i, TE_i is given by:

Equation G-3

$$TE_i = [\Sigma E_i/AE] + A \qquad \textit{(these values are between [A, +}\infty\textit{])}$$

Where the summation is taken over the depth (d).

In case a curve falls entirely into the envelope area, then TE_i = A, where A is called the "total error additive term" or "additive parameter for total error." A value of 0.01 was established for A after sensitivity analysis previously done for the decision analysis study for Mortandad Canyon (LANL 2005, 091696).

Dividing by AE yields a dimensionless number not affected by the magnitude of the measurements. Therefore, the error estimate is independent of the units of measurement.

The constant A is added to the total error to avoid problems associated with later normalization of the error for simulations that fall completely within the envelope.

For any other metrics (peak concentration, depth to peak, concentration at a given time, etc.), the error is the difference between the simulated concentration (or depth) and the edge of the range of defined values where are all values inside the range are assumed to be equally likely (see Figure G-6 for examples). The arrival time is used as an example in illustrating how the error calculation is done when a range is defined. All other remaining error terms are calculated in the same manner. Note that these metrics are included in the code that calculates simulation weights but are not employed in this Sandia Canyon work.

The error associated with the concentration at year j is given by

error for simulation i = E_i

If $C_{ij} > Cmax$, then

Equation G-4a

$$E_i = C_{ij} - Cmax \quad \text{(positive value [0,+}\infty\text{])}$$

If $C_{ij} < Cmin$, then

Equation G-4b

$$E_i = Cmin - C_{ij} \quad \text{(positive value [0, Cmin])}$$

If $C_{ij} >= Cmax$ and $C_{ij} <= Cmin$, then

Equation G-4c

$$E_i = 0$$

Where Cmax is the upper limit of the range of user-defined concentration for year j

Cmin is the lower limit of the range of user-defined concentration for year j

C_i is the concentration associated with simulation i for year j

(Note: Concentration values could be replaced by log concentration values. This alternative had been considered and applied.)

and the total error for simulation i, TE_i is given by

Equation G-5a

$$TE_i = [E_{ip}/ Cmax] + A \quad \text{if } C_i > Cmax$$

Equation G-5b

$$TE_i = [E_{ip}/ Cmin] + A \quad \text{if } C_i < Cmin$$

Equation G-5c

$$TE_i = A \quad \text{if } C_i >= Cmin \text{ and } C_i <= Cmax$$

Where TE_i is the total error in concentration for year j associated with simulation i

Note that the remaining metrics are all also defined in terms of ranges of acceptable or equally likely values. Therefore, the procedure for calculating the associated TE_i values is the same for each. Following the above steps for all metrics and all contaminants provides a set of total errors (TE_i) for each metric and each contaminant at each measuring location (vadose zone boreholes and regional wells).

Next, a relative error (RE_i) that ranges from 0–1 is calculated by dividing each total error, TE_i, by the maximum total error for all simulations for each metric and location:

Equation G-6

$$RE_i = [TE_i/ \max(TE_i)] \ (<=1)$$

RE is an error term that increases as model results get worse and is not a probability to be used in weighting results; as such, a probability should increase as the model results get better.

To correct for this problem and yield probabilities that decrease as the error gets worse, the following equation is used:

Equation G-7

$$W_i = 1 - RE_i + B$$

Where W_i is the weight for simulation i and there is one W_i for each metric

B is called “weight additive term” or “additive parameter for weight”; this value is added to the weight to avoid later normalization problems. A value of 0.01 was adopted after a sensitivity analysis previously done for the decision analysis study for Mortandad Canyon (LANL 2005, 091696)..

For these weights to be used as probabilities, they must range from 0–1, and sums to 1. This normalization is performed in the following manner:

Equation G-8

$$P_i = [W_i/\Sigma W_i]$$

Where P_i is the probability associated for simulation i for a given simulation and a given metric

ΣW_i is the sum of the weights of all simulations for a given metric and location

This resulting probability may be used to weight simulations results if only one metric is used, for example, peak concentration for one contaminant at one location. However, as described above, a number of metrics are to be used. Therefore, the probabilities for each metric (fitness to the concentration profile in the vadose zone for Cr and Mo, arrival time at wells in the regional aquifer, and contaminant concentrations at regional aquifer wells averaged over the last four quarters [corresponding to years 2006 and 2007], and each location) and each contaminant need to be combined into a single overall probability to be associated with each simulation.

The assumption in the development of this overall probability is that all metrics, each contaminant, and each measurement location should have the same weight. Employing these assumptions yields the following equation:

Equation G-9

$$P_{if} = P_{im}/\Sigma\, P_{im}$$

Where P_{if} is the final probability to be associated with simulation i

$P_{im} = \Sigma\, P_i$ summed over all metrics, contaminants and locations for simulation i, and

$\Sigma\, P_{im}$ is the sum of P_{im} over all simulations

This process yields probabilities for each simulation that include all metrics and contaminants, range from 0–1, all sum to 1, and increase with increasing model fitness to data.

G-3.0 APPLICATION TO SANDIA CANYON

The methodology described above was applied to the probabilistic modeling of the fate and transport of Cr and Mo contaminants resulting from discharges in Sandia Canyon. The following sections provide a description of the results of the weighting calculations and an analysis of those results.

G-3.1 Probabilities for Each Simulation for the Vadose Zone

Chromium and Mo simulations for conceptual model 1, CM1, were used in computing weights. Column 14 (or column SW4-5) was used to compare results. Calculated weights for each simulation are presented in Figure G-7.

Using the weights of either the standard or logarithmic methods would achieve the desired results. In this case, the majority of the simulations receive a slightly higher than default (0.01) weight, and about 20% receive a much lower weight because they show poor agreement to the measured values.

The statistics for those weights are as follows:

Weights	Standard	Logarithmic
Maximum	0.01167	0.011469
Minimum	0.00522	0.004823
Average	0.01	0.01
Standard Deviation	0.00146	0.001422

The maximum weight for both methodologies corresponds to simulation #34, and the worst of the 100 simulations is #95 for the standard method and # 2 for the logarithmic method. Simulations with weights near the average are #60 and #41. The results for those simulations are compared with the corresponding envelopes shown in Figures G-8 and G-9. Simulation #51, which also has a large regional aquifer weight, is also shown.

Both sets of curves show good agreement with the envelopes that are defined by the measured concentrations for the majority of simulations and results outside of the measured values for the "worst" cases.

G-3.2 Probabilities for Each Simulation for the Regional Aquifer

Chromium simulations for vadose-zone model CM1 were used as input to the regional aquifer. The associated regional aquifer simulated concentrations were then used in weighting the probabilities of each simulation. Concentrations in wells R-1, R-2, R-4 to R-28, and R-31 to R-34 were used in computing weights (Figure G-10).

The statistics for those weights are as follows:

R.A. Weights	Standard	Logarithmic
Maximum	0.010391	0.0141975
Minimum	0.008027	0.0066687
Average	0.01	0.01
Standard Deviation	0.000497	0.0012

The maximum weight for the standard method corresponds to simulation #51 and for the logarithmic method #70. The minimum weight is for simulation #1 for the standard method and # 55 for the logarithmic method. Simulations with weights near the average are #15 and #98 for the standard and logarithmic methods, respectively. The results for these simulations are compared with the corresponding envelopes: simulation #34 (best for vadose zone) was also included and is presented in Figure G-11.

For most wells the simulation results are outside the envelopes defined by the measured concentrations even for the "best" simulations. In addition, the relative magnitude of simulated concentrations is inconsistent with measured values for a number of wells (see, for example, the best simulations for R-11 and R-28).

G-3.3 Combined Probabilities for Each Simulation Using Vadose Zone and Regional Aquifer Metrics

The combined weights, the vadose zone and regional aquifer, were computed for vadose zone Cr and Mo concentrations for column 14 and regional aquifer (wells R-1, R-2, R4 to R-28, and R-31 to R-34) Cr concentrations with the standard and logarithmic methodology (Figure G-12).

Summary statistics for the combined vadose zone and regional aquifer weights are as follows:

Weights	Standard	Logarithmic
Maximum	0.010431	0.01400
Minimum	0.008151	0.00692
Average	0.01	0.01
Standard Deviation	0.000471	0.00113

When those weights are considered, the best simulations are #51 and #72, and the worst simulations are #1 and #55 for the standard and logarithmic methods, respectively.

It should be noted that two contaminants at 1 location for the vadose zone and 31 locations for one contaminant for the regional aquifer are equally weighted. Weighting each of these metrics equally yields final weights that are dominated by the regional aquifer simulations.

Most important, however, is the systematic overestimation of concentrations by the regional model and the inconsistent relative concentration between concentrations simulated at the different R-wells. Because of these problems, the fate and transport modeling requires refinement before individual simulations are weighted.

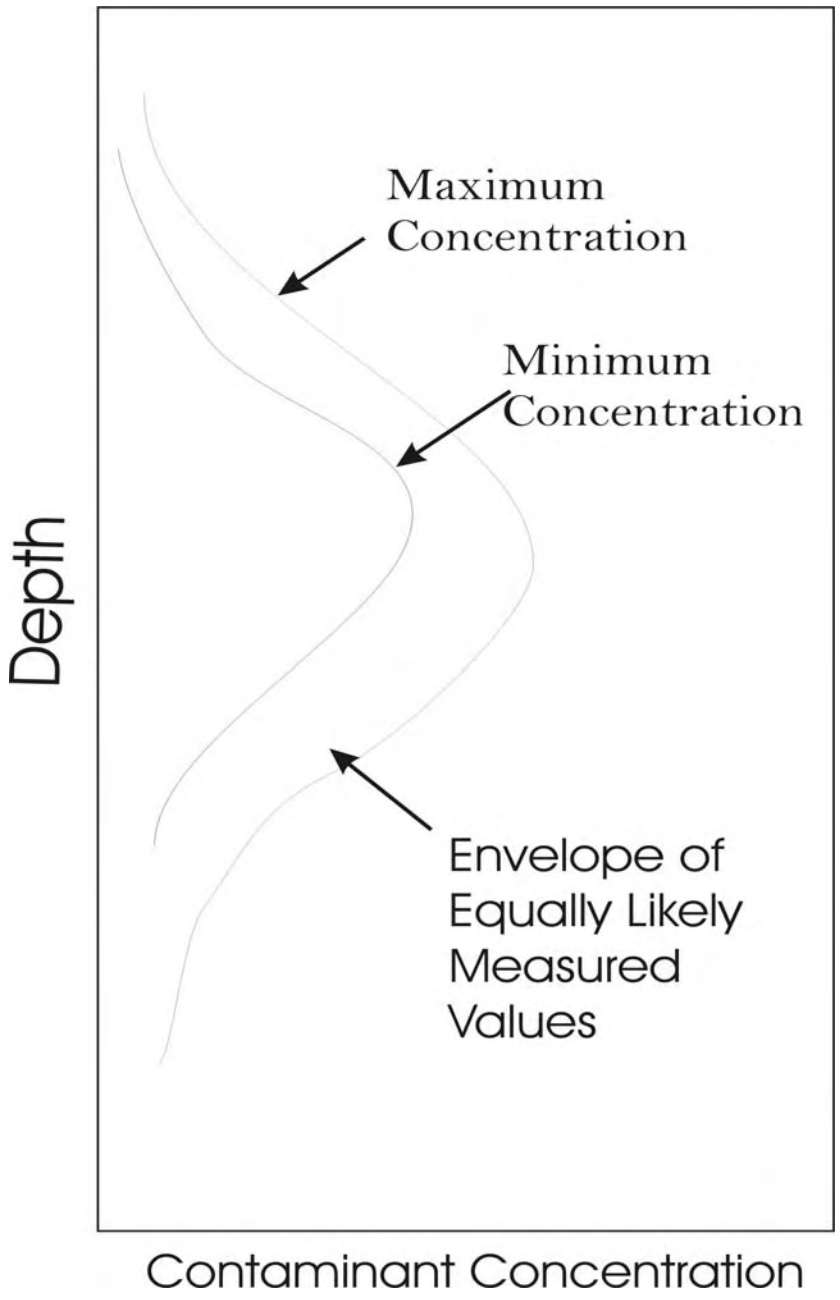

Figure G-1 Envelope of equally likely measured values

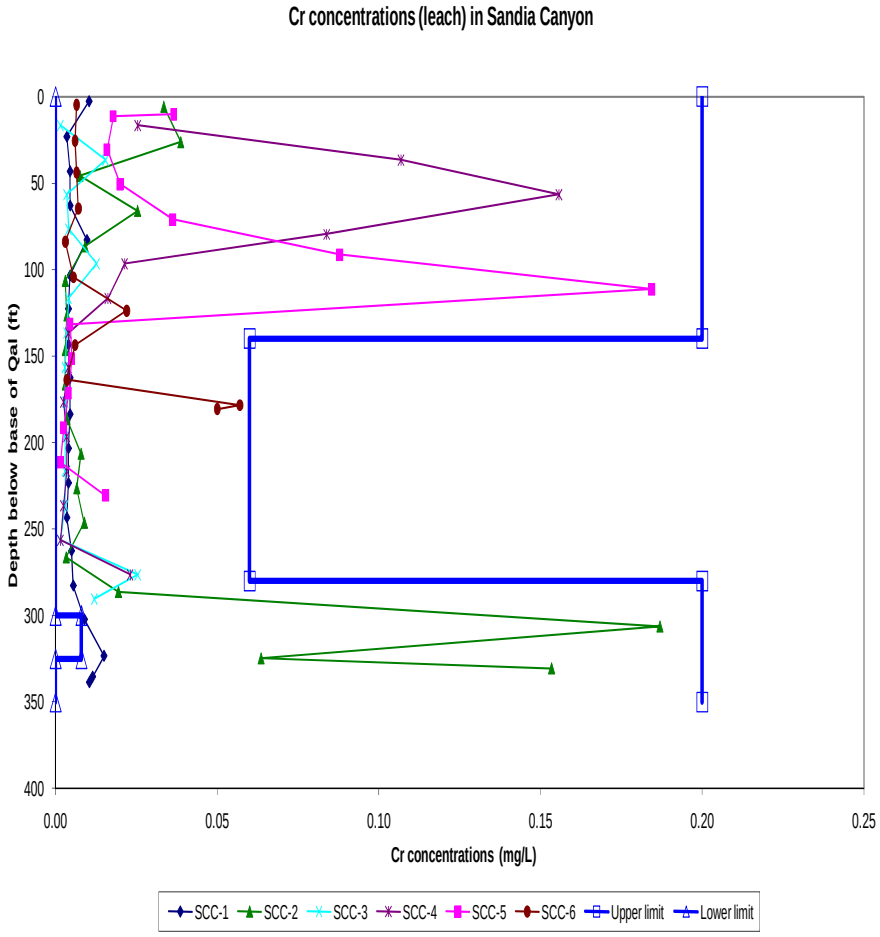

Figure G-2 Chromium concentrations and an acceptable envelope

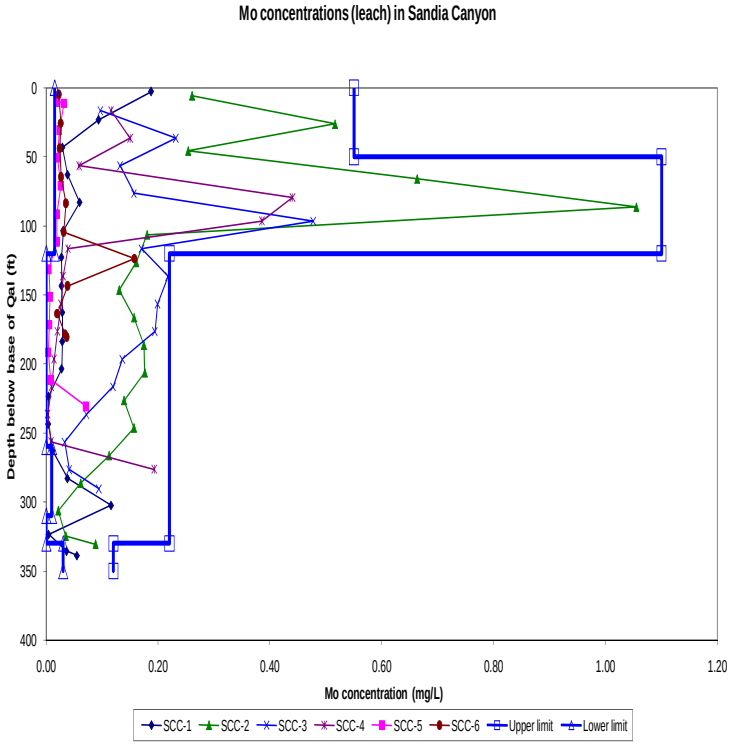

Figure G-3 Mo concentrations and an acceptable envelope for model comparison and weighting

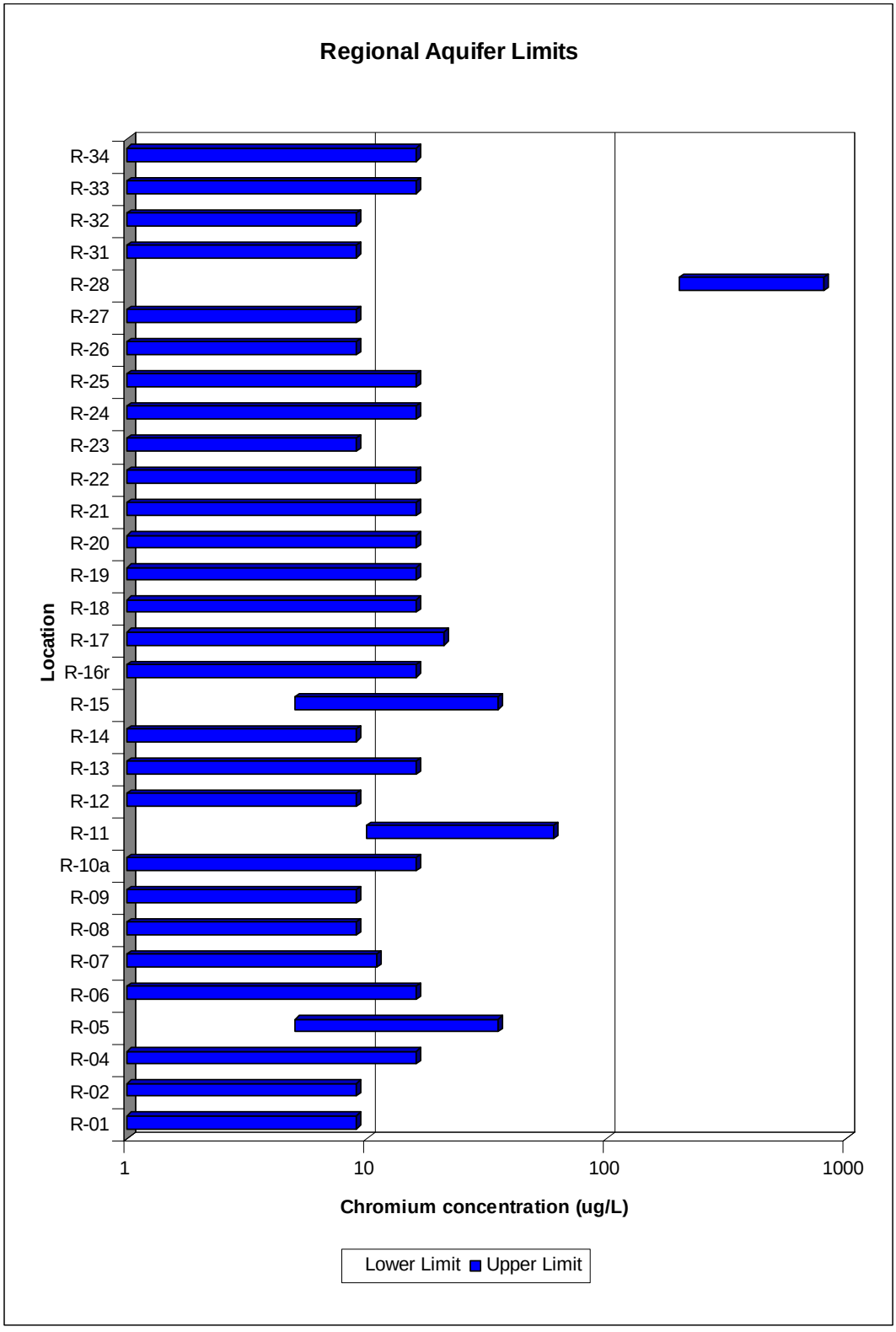

Figure G-4 Range of acceptable Cr concentrations for the regional aquifer wells

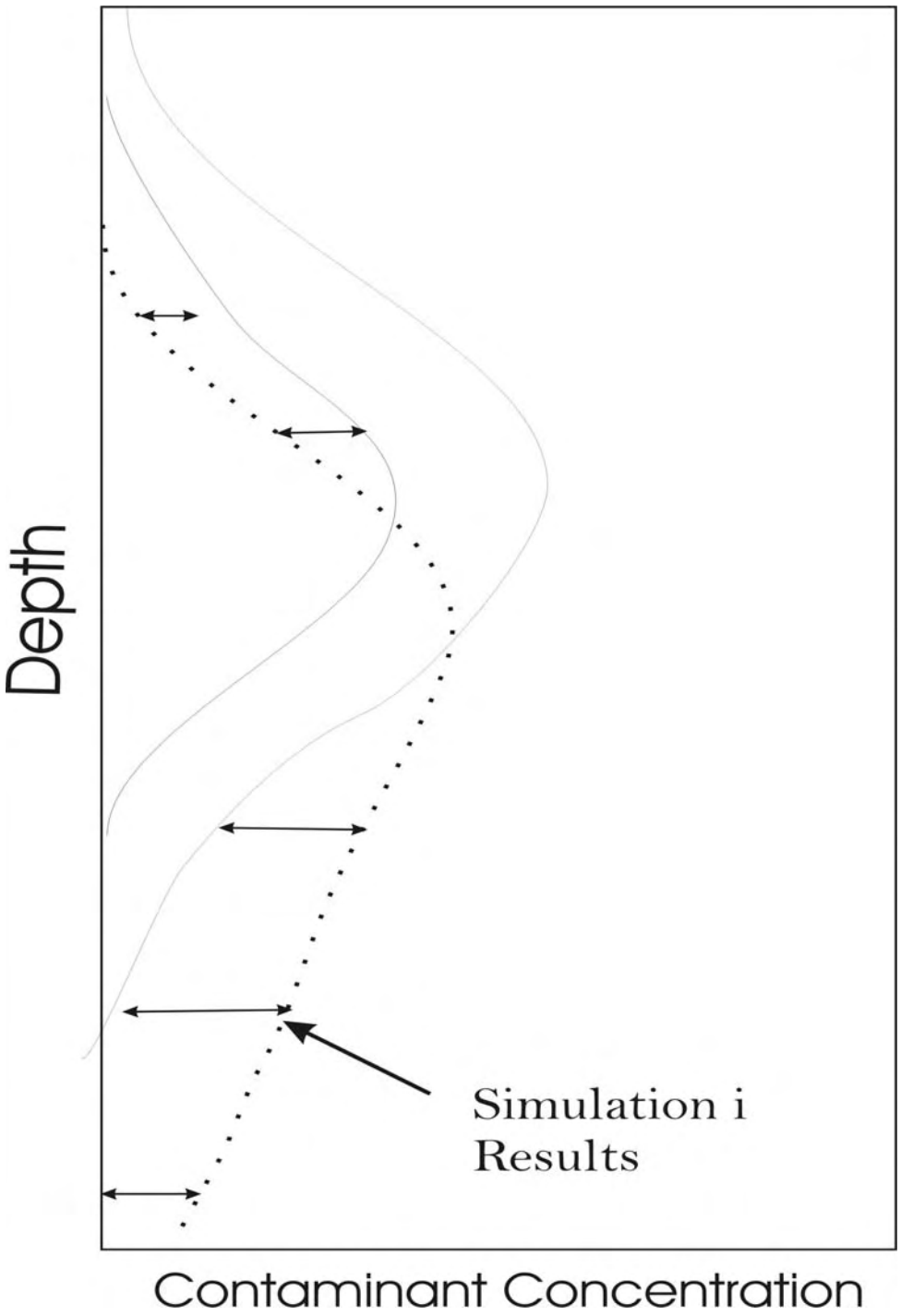

Figure G-5 Comparison of model results to envelope of equally likely values

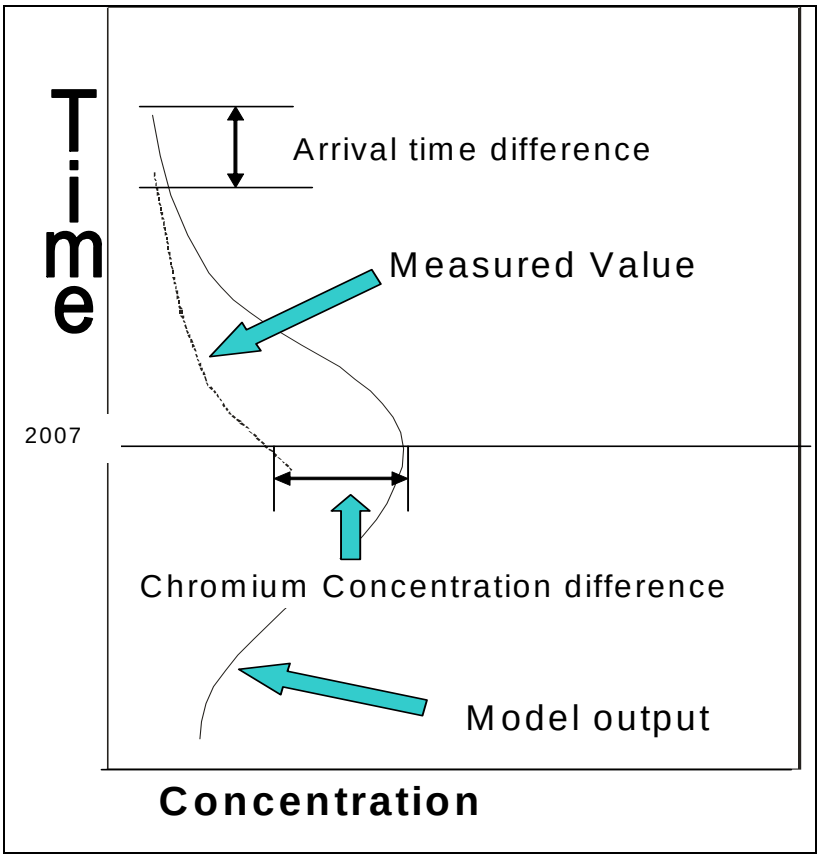

Figure G-6 **Comparison of time of arrival and concentration at year 2007 for the regional aquifer**

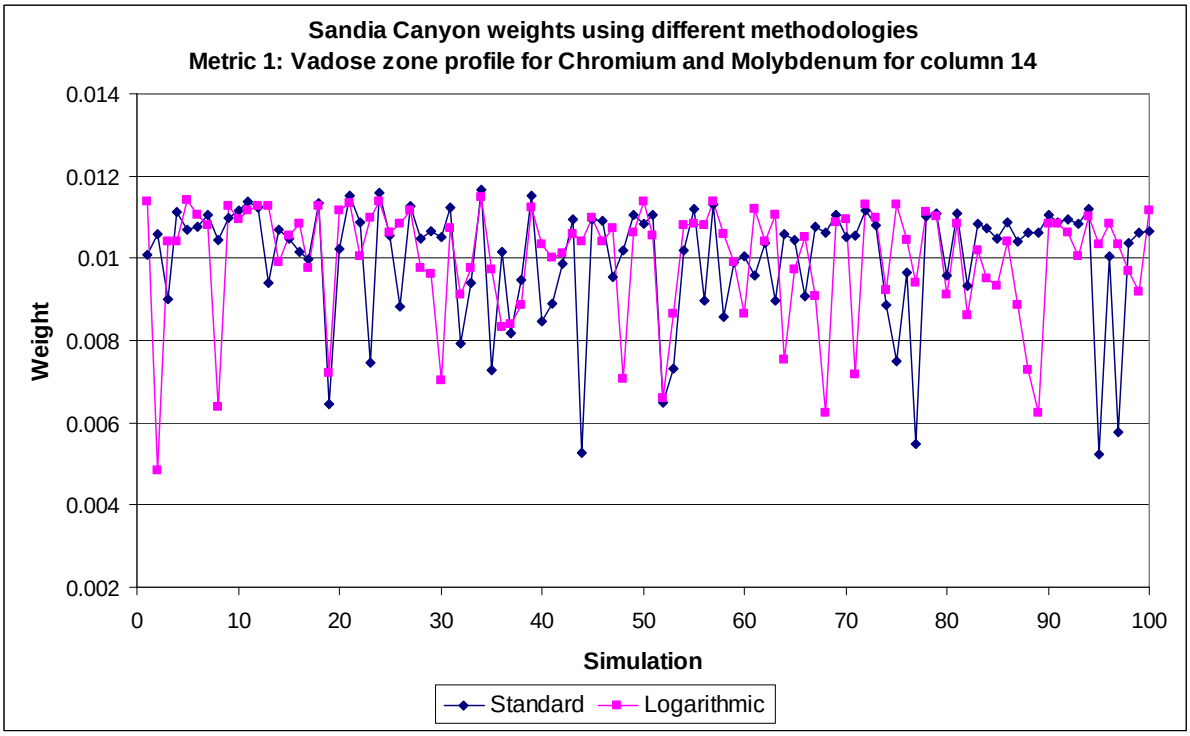

Figure G-7 Weights for the vadose zone for Cr and Mo at column 14

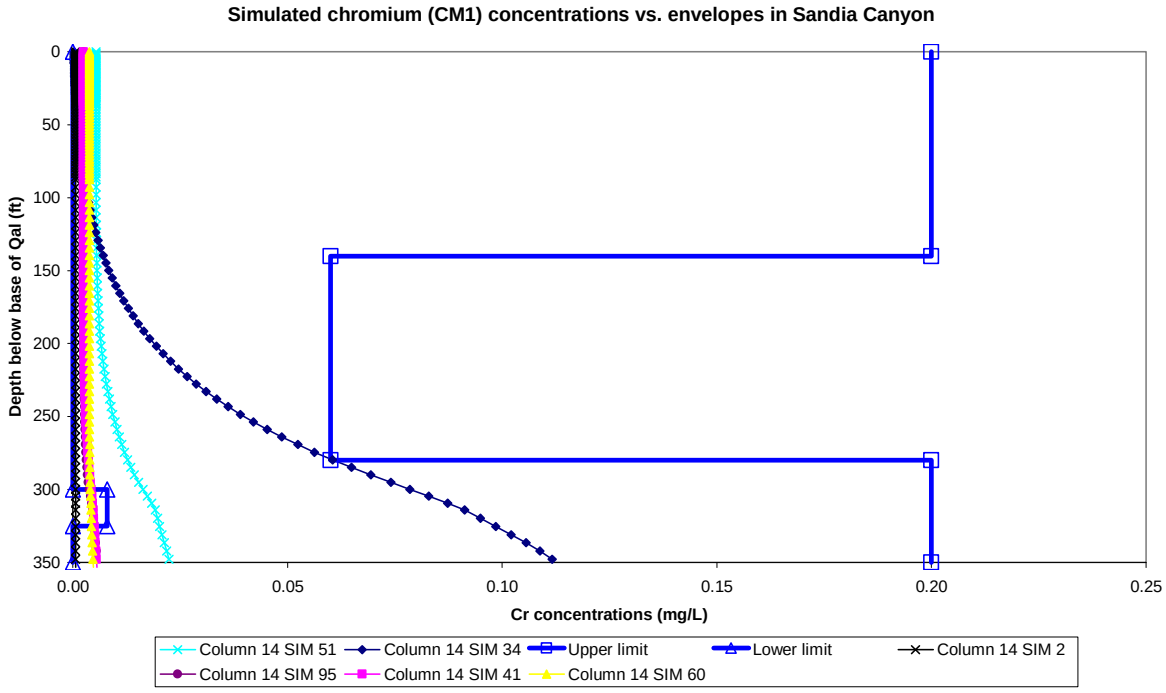

Figure G-8 Comparison between Cr concentrations and envelopes for the best (#51, #34), worst (#95, #2), and average (#60, #41) simulations

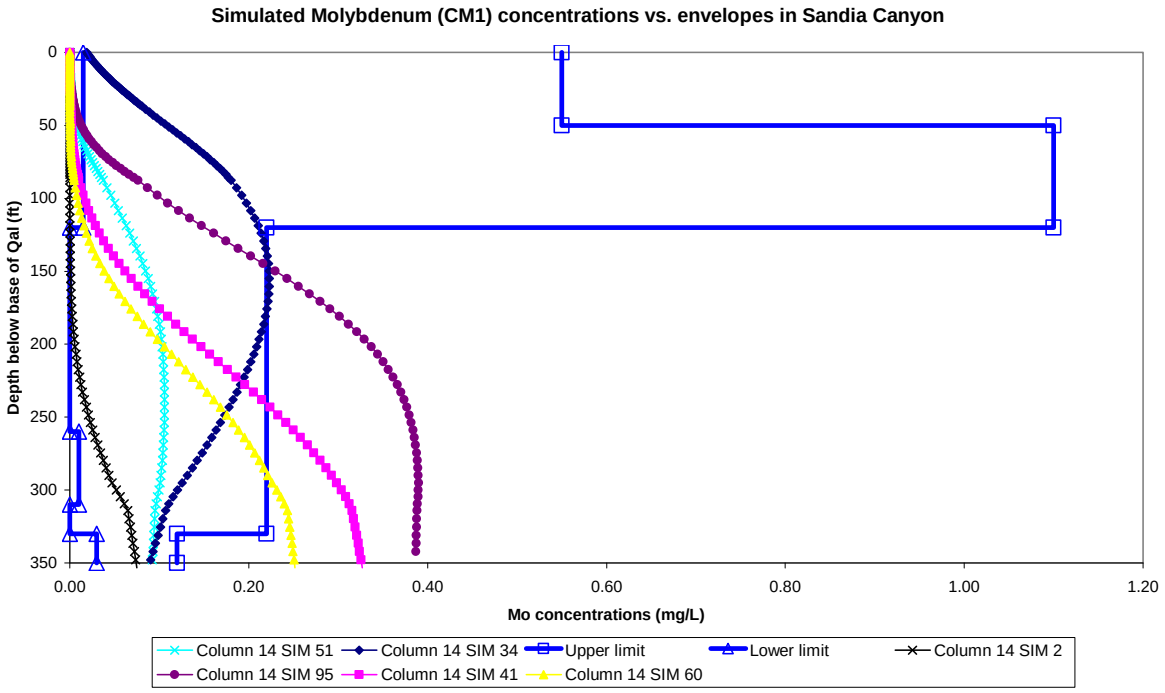

Figure G-9 **Comparison of Mo concentrations with envelopes for the best (#51, #34), the worst (#95, #2), and the average (#60, #41) simulations with respect to weighting of results**

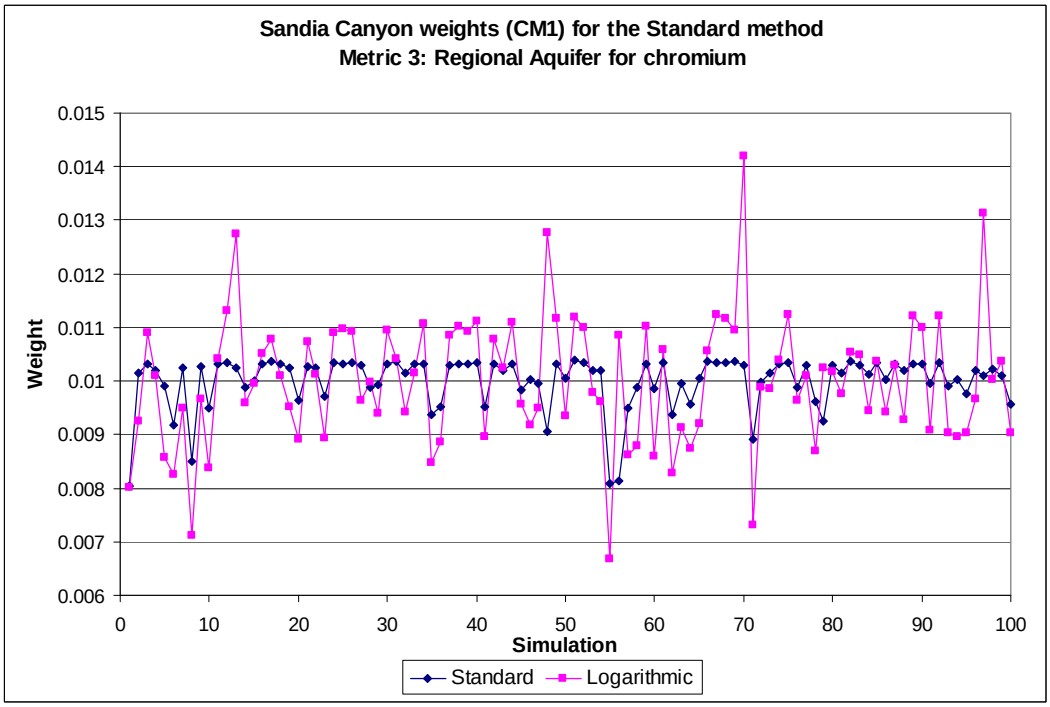

Figure G-10 Weights computed using regional aquifer Cr concentrations at R-wells

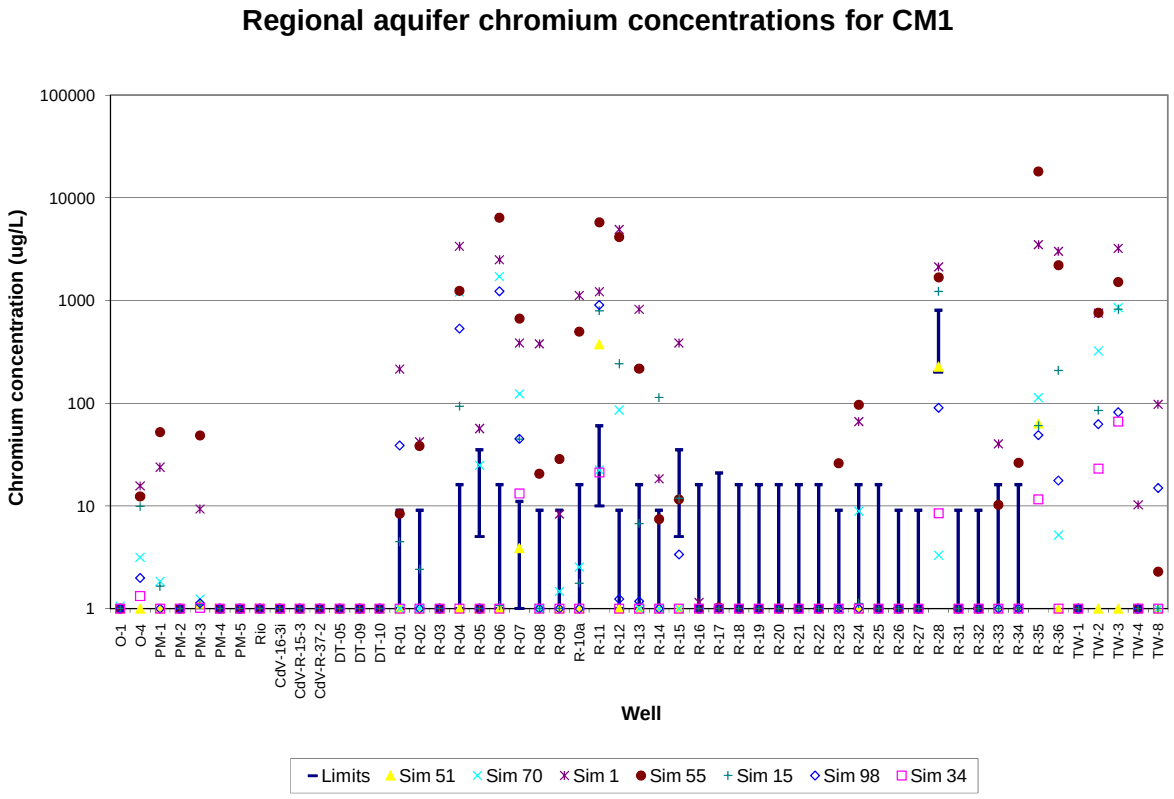

Figure G-11 Comparison of Cr concentrations with envelopes at the regional aquifer for best (#51, #70, #34), worst (#1, #55), and average (#15, #98) from the weighting results.

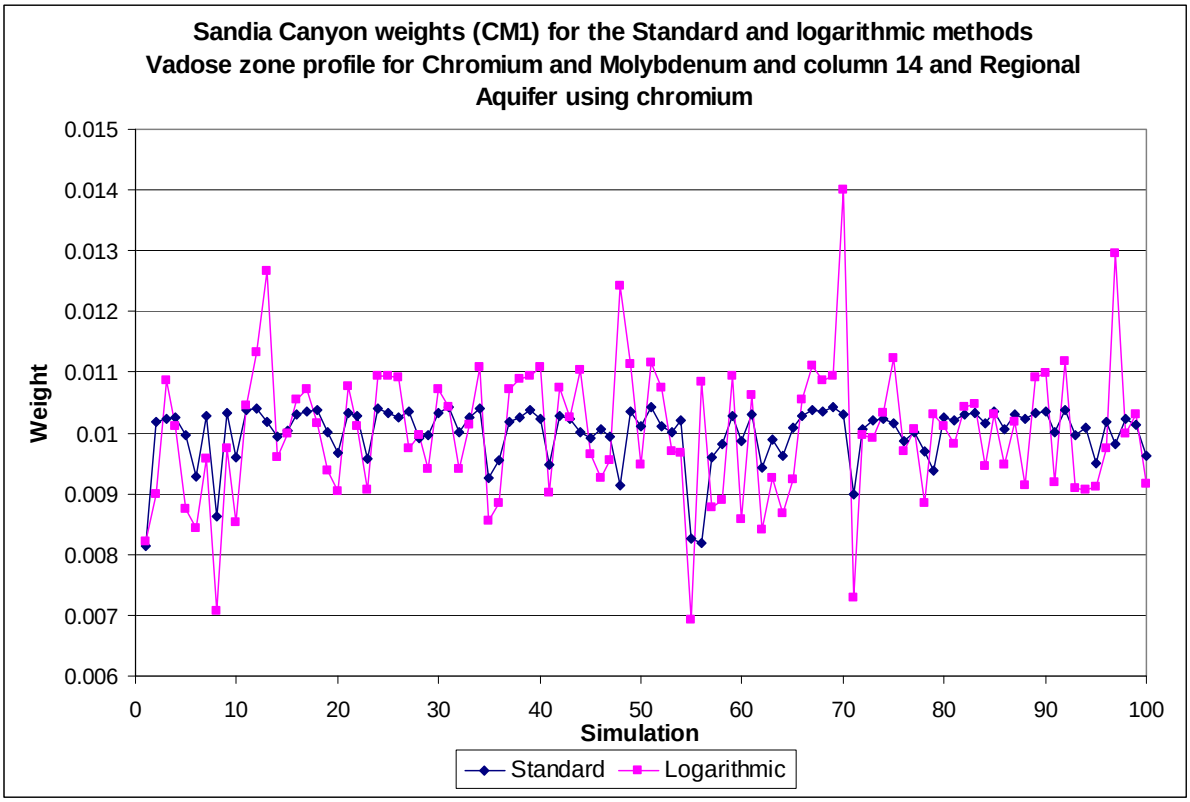

Figure G-12 Weights computed using vadose-zone metrics for Cr and Mo for column 14 and regional aquifer Cr concentrations at R-wells

Appendix H

Potential Diversion of Vadose Zone Water at Geologic Contacts and by Intraformational Horizons and Structures

H-1.0 INTRODUCTION

Dipping strata may divert moisture along geologic contacts or internal bedding features as water travels through the vadose zone, possibly affecting the distribution of contaminants in the vadose zone and the location of the entry point of contaminants into the regional aquifer. These geologic features may have hydrologic significance because of the juxtaposition of different lithologies with strongly contrasting hydrologic properties. Partially saturated groundwater flow through vadose zone may be perching or laterally diverted along the contacts regardless of the contact type: more permeable unit over less permeable unit, and vice versa. These contrasts may be further emphasized by differences of retention properties between the adjacent units. The geologic contacts discussed below are those associated with occurrences of perched groundwater in nearby areas, and they may divert moisture laterally under both saturated and unsaturated conditions beneath Sandia Canyon. The geometry of the geologic contacts was assessed using the structural contour maps taken from the 2005 site-wide, three-dimensional geologic model (Cole et al. 2006, 095079). The structure contour maps were modified to incorporate new corehole data for Sandia Canyon that are described in the "Interim Measures Investigation Report for Chromium Contamination in Groundwater" (LANL 2006, 094431).

The Guaje Pumice Bed, an important host rock for perched water in Los Alamos Canyon, is a pumice fall deposit that mantles the pre-Bandelier landscape throughout the region (Broxton and Vaniman 2005, 090038). A prominent feature of this landscape was a broad drainage system that drained the Pleistocene Los Alamos Canyon southeastwards before turning south-southwest in the vicinity of Sandia Canyon, about 500 m west of SCI-1 (see Figure H-1). The axis of this drainage parallels the southeasterly course of Sandia Canyon before turning south-southwest, crossing Mortandad Canyon near well R-15. The basal contact of the Guaje Pumice Bed dips south to southwest beneath the zone of maximum infiltration in Sandia Canyon. The pumice bed overlies generally impermeable silt-rich deposits of the Puye Formation. Diversion of water along this contact might be towards the axis of the paleodrainage system (south or southwest) before infiltrating into deeper portions of the vadose zone. The SCC-series coreholes in Sandia Canyon showed increased moisture content in the Guaje Pumice Bed without evidence of saturation (LANL 2006, 094431).

The upper contact of the Cerros del Rio basalt acts as a perching horizon at MCOI-4 and MCOBT-4.4 in Mortandad Canyon. This contact represents the eroded surface of a thick stack of basaltic lava flows that were erupted from vents now buried beneath the eastern part of the Pajarito Plateau by the Bandelier Tuff and in places by the Puye Formation. The number and locations of these vents is not known, but the sequence of basalts in the Sandia and Mortandad Canyon areas show a predictable sequence of tholeiites overlying alkalic basalts. The upper surface of the Cerros del Rio basalt beneath the area of maximum infiltration in Sandia Canyon dips primarily to the west, but this surface is modified by erosion and may contain a small southwest-draining channel that heads near SCC-6 and PM-3 (see Figure H-2), although the upper contact of the Cerros del Rio showed no evidence of perched water in either SCC-6 (LANL 2006, 094431) or in R-35a,b. Small amounts of perched water were noted in SCC-1, -2, -3 and -4, with a screen emplaced in this perched zone at SCC-1 (LANL 2006, 094431). Further study is needed to determine whether perched saturation may have occurred in the past at this horizon in the vicinity of SCC-6, and whether the perched saturation at SCC-4, -3, -2, and -1 is evidence of diverted flow beyond Sandia Canyon.

The individual flows making up the base of the Cerros del Rio basalt were deposited over a south to south-southeast dipping surface developed on top of the Puye Formation in the Sandia Canyon area (see Figure H-3). Fractures and rubble zones at the base of basaltic lava flows host perched groundwater at MCOI-5 and MCOI-6 in Mortandad Canyon. The nature of the perching horizon is poorly understood but may include relatively impermeable sedimentary rocks of the Puye Formation and clay altered flow-base

volcanic sediments at the base of the Cerros del Rio. Beneath the area of maximum infiltration in Sandia Canyon, water diverted at the basal Cerros del Rio contact would be expected to move in the down dip direction along this surface. The base of the Cerros del Rio basalt dips south to south-southeast beneath the inferred zone of maximum infiltration beneath Sandia Canyon and Mortandad Canyon. Although evidence of perched water within the Cerros del Rio is well established in drill holes MCOI-4, MCOBT-4-4, MCOI-5, and MCOI-6 in Mortandad Canyon, no equivalent deep-well data from Sandia Canyon in the vicinity of coreholes SCC-1, -2, -3, and -4 is as yet available. (Available data from the base of the Cerros del Rio farther east show no perched saturation at R-11 or R-34a and -34b, although a well-developed perched system exists near the base of the Cerros del Rio at R-12 that may have a source in Los Alamos Canyon.)

While the upper and lower contacts of the Cerros del Rio basalt may act as important hydrologic pathways, it should be noted that water movement in the interior of the Cerros del Rio basalt could follow significantly different and largely unpredictable flow paths. The entire basalt sequence is comprised of laterally and vertically stacked flows whose thicknesses and distributions vary as a function of vent type (e.g., cinder cones versus fissure flows), volume of basaltic magma erupted, distance from the vent area, and fluidity of the lavas. The topography onto which the lavas were erupted played a particularly important role in shaping the distribution of individual flow units. Basalts behave like other fluids, flowing through existing drainages and ponding in low-lying basins. If the topographic relief is subdued or if the eruptions are voluminous enough, the basaltic lava flows may fill in low-lying areas before spreading out as more predictable sheet-like bodies. Nevertheless, the sequence of tholeiites overlying alkali basalts throughout much of the Sandia and Mortandad Canyon areas suggests that these flows form sheet-like bodies. These stacked lavas consist of multiple flow units that are generally separated by interflow breccias. Flow interiors are made up of dense, variably fractured impermeable rock. Under saturated conditions, groundwater flow in these lava interiors is controlled by fractures, with hydraulic conductivity determined by aperture dimensions, fracture density, interconnectivity, and the presence of fracture-filling minerals. Porous flow is expected to dominate groundwater flow in the interflow zones that are made up of highly porous breccias, clinker, cinder deposits, and sedimentary deposits. Both nonfractured flow interiors and clay-filled fractured zones are expected to have very low permeability; zones with significant connected open fractures, lava tubes, and interflow zones are expected to have higher permeability and low porosity, a combination of properties which can lead to very fast travel times. Flowpaths within these basalts are highly uncertain because the complex internal stratigraphy of these rocks.

H-2.0 REFERENCES

The following list includes all documents cited in this appendix. Parenthetical information following each reference provides the author(s), publication date, and ER ID number. This information is also included in text citations. ER ID numbers are assigned by the Environmental Programs Directorate's Records Processing Facility (RPF) and are used to locate the document at the RPF and, where applicable, in the master reference set.

Copies of the master reference set are maintained at the New Mexico Environment Department Hazardous Waste Bureau; the U.S. Department of Energy–Los Alamos Site Office; the U.S. Environmental Protection Agency, Region 6; and the Directorate. The set was developed to ensure that the administrative authority has all material needed to review this document, and it is updated with every document submitted to the administrative authority. Documents previously submitted to the administrative authority are not included.

Broxton, D.E., and D.T. Vaniman, August 2005. "Geologic Framework of a Groundwater System on the Margin of a Rift Basin, Pajarito Plateau, North-Central New Mexico," *Vadose Zone Journal,* Vol. 4, No. 3, pp. 522–550. (Broxton and Vaniman 2005, 090038)

Cole, G., J.W. Carey, L. Burnette, and T. Miller, 2006. "The 2005 Three-Dimensional Geologic Model of the Pajarito Plateau," Los Alamos National Laboratory document LA-UR-06-3060, Los Alamos, New Mexico. (Cole et al. 2006, 095079)

LANL (Los Alamos National Laboratory), November 2006. "Interim Measures Investigation Report for Chromium Contamination in Groundwater," Los Alamos National Laboratory document LA-UR-06-8372, Los Alamos, New Mexico. (LANL 2006, 094431)

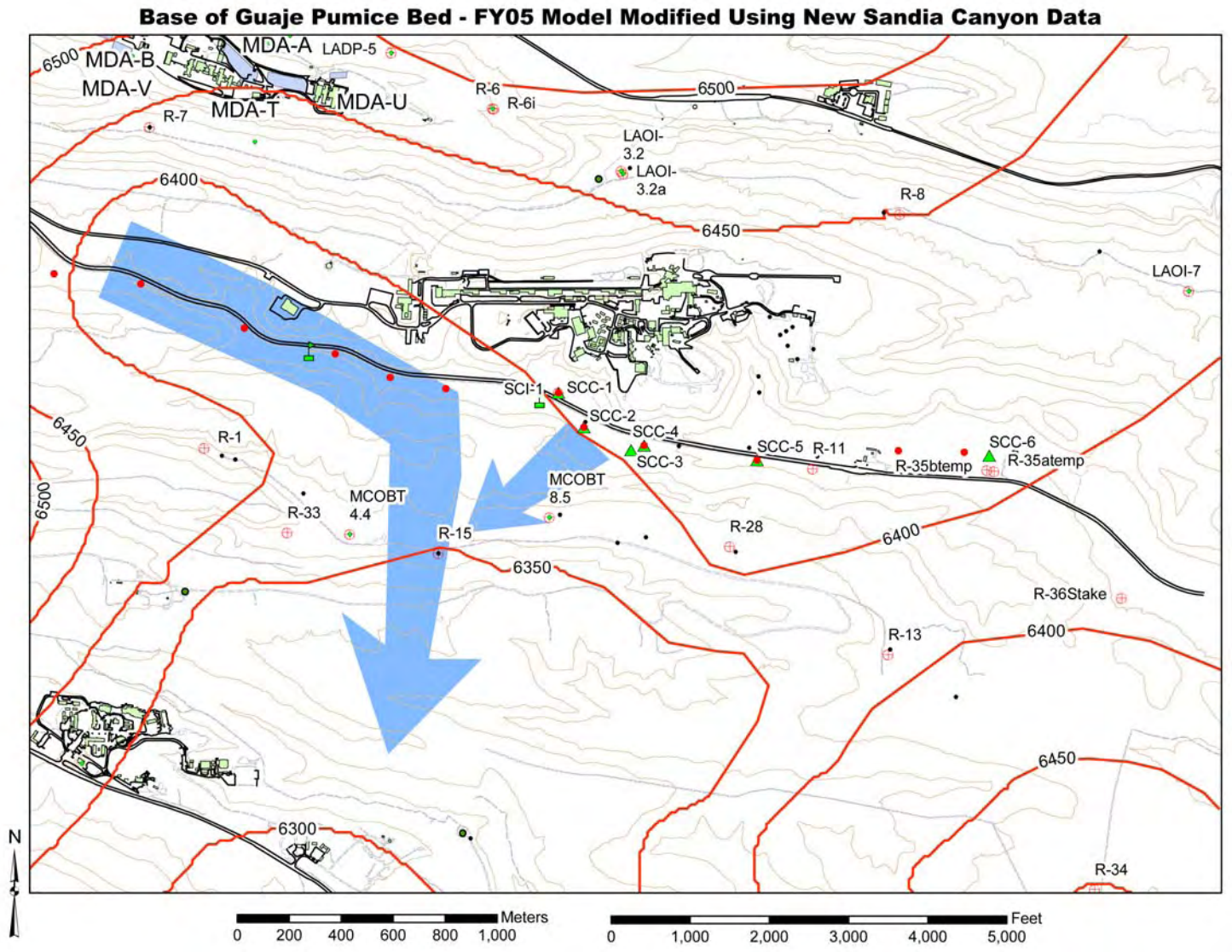

Figure H-1 **Structure contour map for the base of the Guaje Pumice Bed in the vicinity of Sandia Canyon. Arrows show inferred direction of movement for water diverted along this contact.**

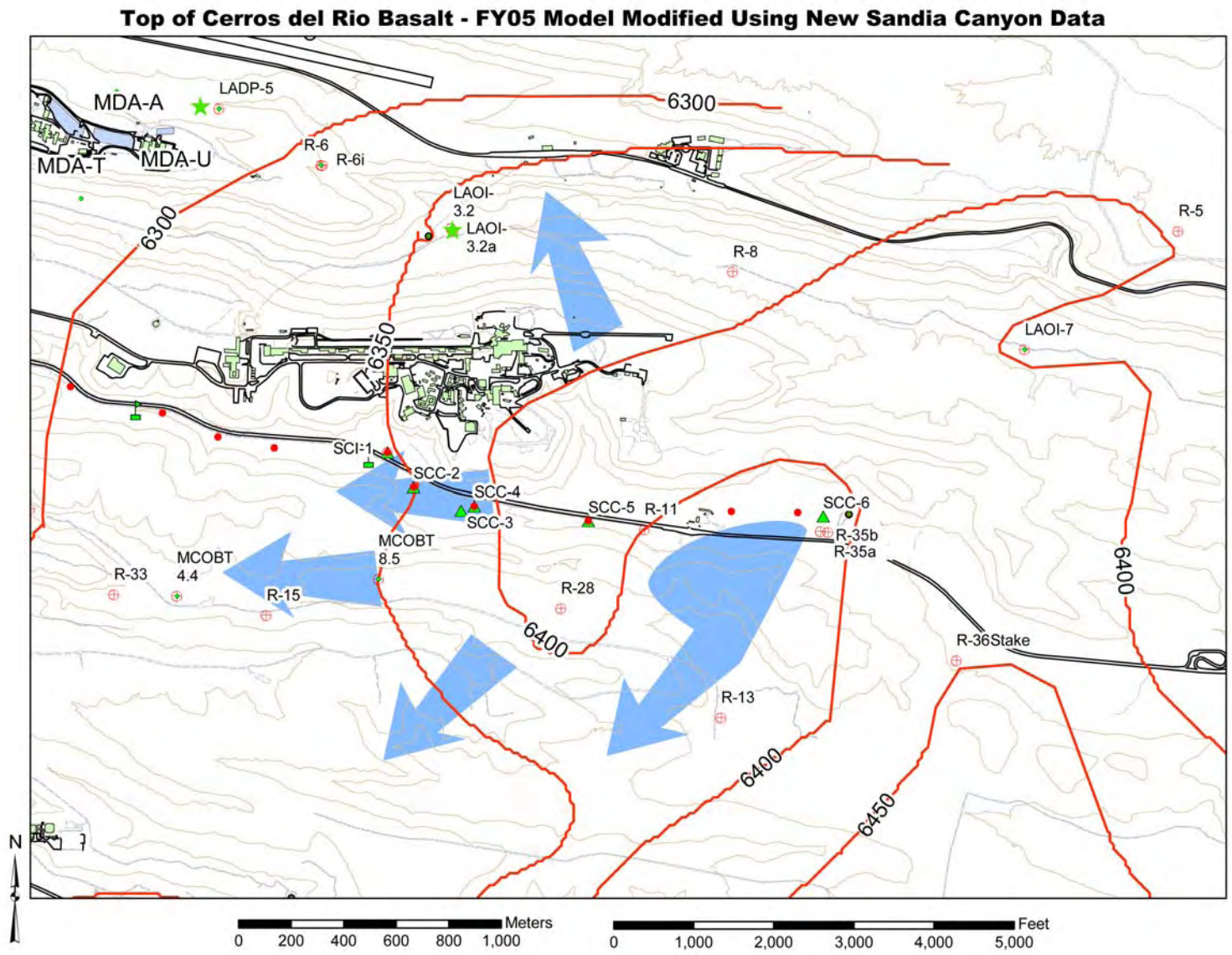

Figure H-2 **Structure contour map for the top of the Cerros del Rio basalt in the vicinity of Sandia Canyon. Arrows show inferred direction of movement for water diverted along this contact.**

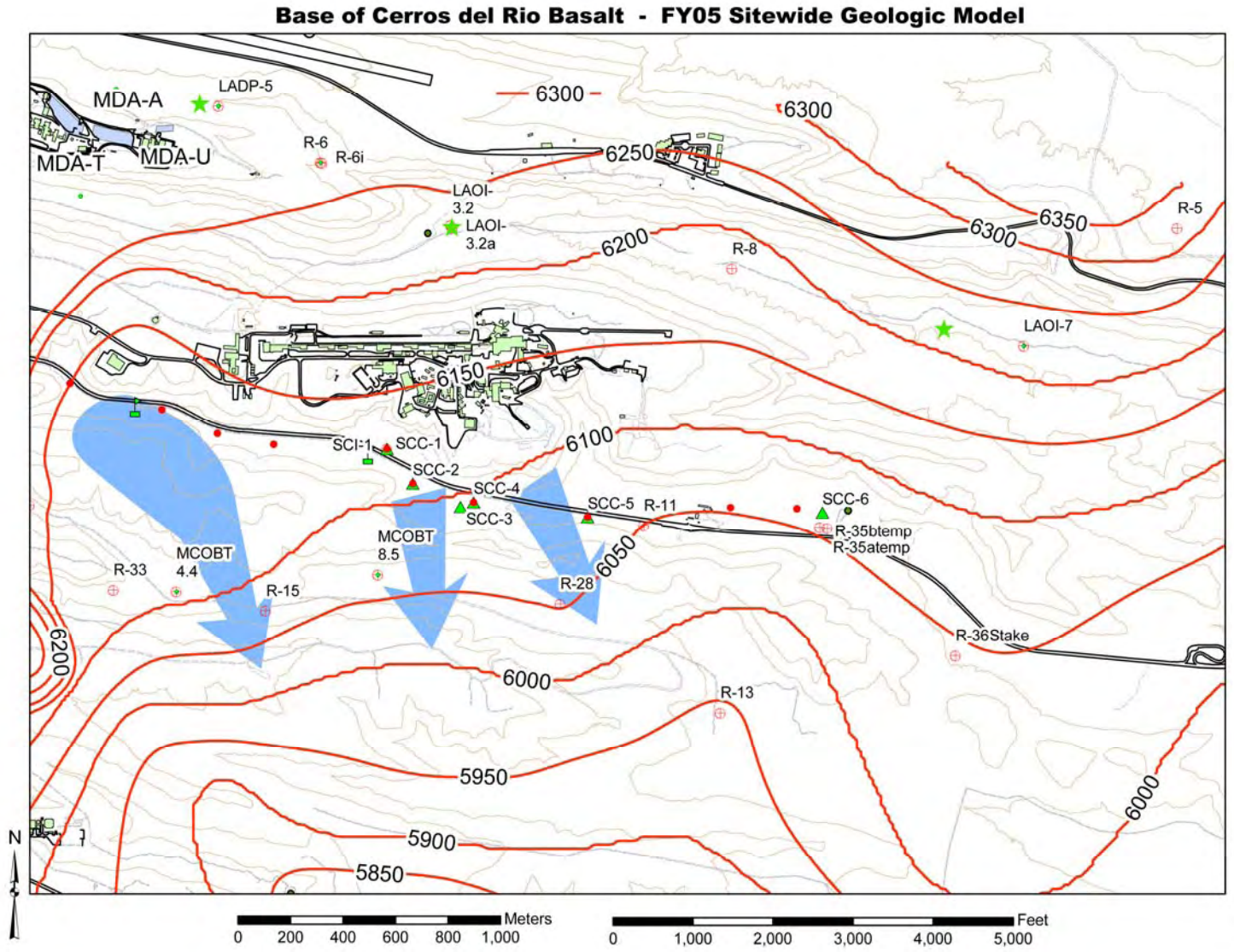

Figure H-3 **Structure contour map for the base of the Cerros del Rio basalt in the vicinity of Sandia Canyon. Arrows show inferred direction of movement for water diverted along this contact.**